# A 20th Century Pollution History Reconstruction Using Lake Sediments From Cajas National Park, South Central Ecuador

**Master Thesis**

Faculty of Science, University of Bern

Presented by

**Lea Alina Fränkl**

Oeschger Centre For Climate Change Research

**2016**

Supervisor:
**Prof. Dr. Martin Grosjean**
Institute of Geography and Oeschger Centre For Climate Change Research

Advisors:
**Tobias Schneider, Dr. Benjamin A. Musa Bandowe, Dr. Adrien Mestrot**
Institute of Geography and Oeschger Centre For Climate Change Research

Lake systems in Cajas National Park, eastern side (photo credit: Wojciech Tylmann, 2015)

Lake systems in Cajas National Park, eastern side (photo credit: Wojciech Tylmann, 2015)

Cajas National Park, western side (photo credit: Wojciech Tylmann, 2015)

Core collection in Cajas National Park (photo credit: Wojciech Tylmann, 2015)

## ABSTRACT

The sedimentary geochemical profile of pollutants in lake sediments reflect past changes in emissions from human activities and are therefore a proxy for reconstructing past anthropogenic activities. They preserve and provide a quantitative archive of long term data on past pollution emissions, allowing for the reconstruction and interpretation of local, regional, and global pollution histories. South America is particularly appropriate for paleo-reconstructions as it is the only continuous landmass in the southern hemisphere and, while many pollution reconstructions exist for northern hemisphere sites, data is sparse and less extensive for the southern hemisphere. Furthermore, South America is of significant interest due to its rapidly growing economy and consequent increasing emission rates.

This thesis presents a reconstruction of anthropogenic pollution for the 20$^{th}$ century from sediment cores taken from Lake Fondococha and Lake Llaviuco in Cajas National Park, Ecuador. The remote, high altitude lakes in Cajas National Park are removed from the influence of intense anthropogenic activities and as such should be pristine. The pollution signal in the lake sediments will thus reveal long-distance atmospheric transport from sources on a local to global scale, as well as depositional mechanisms influencing the high elevation lakes systems. A chronology was established for the past ca. 150 years for the cores by $^{210}$Pb dating using the Constant Rate of Supply (CRS) model. The sediment cores were analysed for Polycyclic Aromatic Compounds (PACs), mercury (Hg), copper (Cu), zinc (Zn), lead (Pb) and chromium (Cr), all of which are ubiquitous in the environment and serve as a proxy for human industrial and mining activities. PACs were measured in the sediments using pressurized liquid extraction and Gas Chromatography Mass Spectrometry (GC-MSD). Hg and heavy metals were analysed in the sediments using microwave assisted chemical digestion and Iductively-Coupled Plasma Mass Spectrometry (ICP-MS).

A chronology was established for Lake Fondococha which dated back to 1885. A diagnostic increase from natural background levels of all pollutants (PACs, Hg, heavy metals) around 1958 clearly indicates that the sediments of Lake Fondococha have recorded the emission history of Ecuador's industrialization (beginning in the 1960s), urbanization and petroleum exploration. The atmospheric depositional flux rate and profile of pollutants in the sediments of Lake Fondococha are concurrent with values found in other South American lake sediments. Although pollution levels are low and the lake can be considered as relatively pristine, the presence of all forms of pollutants in the sediments clearly indicates the influence of long-range atmospheric transport and wet depositional processes impacting the remote lake. Pollution sources in the sediments stem from vegetation fires/biomass burning, but with increasing inputs from fossil fuel combustion sources in recent times. The chronology for Lake Llaviuco dates back to 1969, accordingly the onset of Ecuador's industrialization is not recorded. However, levels of pollutants in the sediments of Lake Llaviuco far exceed those of Lake Fondococha and other South American lakes. Despite its location in a natural protected area, flux rates of all pollutants were found to be higher even than pollution records in sediments from lakes located in urban and agricultural regions. The high levels of contaminants in Lake Llaviucu are attributed to local sources, namely, its closer proximity to Cuenca (Ecuador's third largest city) and settlements bordering the national park, its proximity to major roads and higher levels of anthropogenic activities in (fisheries) and around (grazing) the lake compared to remote Lake Fondococha. This study presents the first long-term pollution history from a paleo-archive in Ecuador.

## TABLE OF CONTENTS

## LIST OF FIGURES

**APPENDIX**

## LIST OF TABLES



**APPENDIX**

# ACKNOWLEDGEMENTS

First and foremost I would like to thank Danae Motta and Stéphanie Arcusa for their all-encompassing and ceaseless support over the past year. The trail that began in Ecuador will continue for many years to come. I am further indebted to my friends (Jacqui, Marlena, Simon) and family (my parents, grandparents, Gion, Andri, Patick and Senta) for their unwavering support and ability to lift my spirits at any time.

Many thanks go out to all my colleagues at the labs - Christoph B, Christoph D, Tobs, Steph, Ivan, Raphi, Denis, Manuel and Nils - for the long discussions and advice over many wonderful coffee breaks. I am further indebted to Dr. Daniela Fischer and Michael Wendler for all their help with lab work over the past year, and to Dr. Wojciech Tylmann for his help in the field and with the $^{210}$Pb measurements. Thanks to Pablo Mosquera and Don Simon for their guidance in Cajas National Park and all the superb local legends and histories they shared with us on our long hikes through the páramo.

I would like to especially thank my advisors Dr. Bejamin Bandowe for all things PAC-related and Dr. Adrien Mestrot for all things Hg and heavy metal-related. I am indebted to them for their guidance, advice and absolute patience with me while I learned new lab techniques. I would also like thank Tobias Schneider, my PhD advisor, for his persistent optimism and advice in the field and in the labs.

Finally, I would like to thank my supervisor, Prof. Dr. Martin Grosjean, for giving me the opportunity to undertake this master thesis in the Paleolimnology Group, and for the incredible field work in the Ecuadorian Andes. It was an outstanding experience from start to finish.

# CHAPTER 1: INTRODUCTION

## 1.1 RESEARCH MOTIVATION

Anthropogenic activities and emissions of pollutants have significantly impacted the climate, the environment and human civilization since the start of the industrial revolution in the late 18th century (von Gunten et al., 2009; Smol, 2008). A fundamental issue arises when attempting to quantify past impacts of anthropogenic activities, namely, a lack of long term observational data for pollution deposition. Lake sediments, however, preserve past pollution and act as an archive for the reconstruction and interpretation of local and regional pollution history (Biester et al. 2007; von Gunten et al. 2009). Limnic sediments are described as one of the most valuable and powerful archives of catchment, fluvial system and atmosphere processes. These sediments mirror temporal changes in contamination sources as well as variations in the transport path regimes (von Gunten et al. 2009). Lake sediments have been particularly useful to document historic deposition of pollutants and contaminants, assisting scientists to better understand both anthropogenic and naturally sourced emissions since pre-historic times (Bandowe et al. 2014; Biester et al. 2007; Cooke et al. 2009; von Gunten et al. 2009; Lamborg et al. 2002; Lockhart et al. 2000; Outridge et al. 2005).

While many studies on pollution reconstruction from lake sediments exist, the majority focus on sites located in the northern hemisphere. In the southern hemisphere, the data is sparse and less extensive, and gaps appear in the pollution history data. South America is of significant interest because of its rapidly growing economy, emissions and pollution rates (von Gunten et al. 2009). It is therefore necessary to work towards filling the gaps in pollution data. In order to do this, this thesis focuses on investigating the sedimentary geochemical record of anthropogenic pollutants from two lake sediment cores taken from Cajas National Park, Ecuador, an area which, as far as reviewed research indicates, there has been no reconstructed pollution record.

The remote, high altitude location of Cajas National Park will indicate whether such seemingly pristine lakes are immune to long-distance atmospheric deposition of pollutants. Cores from these lakes will be analyzed for several toxic environmental pollutants. Firstly, polycyclic cromatic compound (PACs) content in the lake sediments will be used as a proxy for anthropogenic activity, especially emissions associated with industrial activities (e.g. the switch from coal to modern oil and gas burning) over the past century (Bandowe et al. 2014). Secondly, mercury (Hg) content within the cores will be examined. A threefold increase in Hg emissions has been observed in both hemispheres since pre-industrial times (Lamborg et al. 2002; Sprovieri et al. 2010) and rapidly increasing Hg emissions in both hemispheres are associated with significant increases in anthropogenic emissions. Coupled with this, gold and silver mining in South America is also known to have been a key source of Hg pollution, dating back to pre-industrial times (Cooke et al. 2009), thus the Hg profile revealed in the sediments is indicative of not only modern Hg emissions, but also historic trends in South American mining activities. In addition to investigating Hg, the content of several heavy metals - copper (Cu), zinc (Zn), lead (Pb) and chromium (Cr) – similarly associated with anthropogenic emissions and mining, will be reconstructed.

### 1.1.1 Pollutants in Remote High Altitude Regions

Studying the concentration of organic contaminants at high altitudes is particularly important because of the potential risk that these pollutants pose. Firstly, to humans living in or depending on resources coming from mountainous regions. Mountains represent the water towers of the world, and supply water both directly and indirectly to lowland regions. Pollutants deposited in alpine lakes thus have the potential to contaminate drinking and agricultural water supplies. Secondly, the terrestrial and aquatic ecosystems in alpine areas often support unique plant and animal communities of great ecological value. Lastly, understanding the transport and consequent fate of organic and inorganic contaminants in mountainous regions is valuable in itself (Daly and Wania 2005). High altitude, remote locations are ideal settings to study contaminant transport and behavior along steep environmental gradients on a small spatial scale. How different pollutants are distributed and behave on altitudinal gradients provides insight on how environmental and climate factors influence chemical behavior. Mountainous regions across the globe are highly diverse, yet they share some core characteristics which influence the environmental behavior of contaminants. These include low daytime air temperatures, higher precipitation rates, higher wind speed and radiation flux, and lower atmospheric pressure (Daly and Wania 2005). As many mountainous regions, including Cajas National Park, are not impacted by intense anthropogenic activities, it makes them appropriate locations to study the effect of atmospheric transport of contaminants of anthropogenic origin to supposedly pristine locations such as natural protected areas.

The question of how PACs, organochlorine compounds (OCs), Hg (which exhibits similar global dispersal properties as OCs) and other pollutants settle in high altitude, remote locations, such as lakes in the Ecuadorian Andes, is an important one. It runs parallel to how the Arctic, as one of the most remote regions on the planet, and the people who live there, have recorded alarmingly high levels of OCs, despite these compounds never having been used in these regions. Wania and Mackay (1993) developed the global distillation and cold condensation hypothesis. They hypothesized that the physical and chemical properties of OCs, most notably their volatility, together with typical environmental characteristics for cold regions (ambient temperatures), contribute considerably to the transport of OCs to polar and alpine regions. The process follows the temperature-dependent separation of organic compounds, which is greatly related to vapor pressure, and varies from compound to compound. Wania and Mackay (1993) hypothesized that global fractionation could be happening as OCs are separated at varying latitudes and condense at different temperatures, depending on their volatility. The result follows that OCs with rather low vapor pressure tend to accumulate in colder, more remote regions, which end up acting as ‘sinks’ for many of these compounds, whereby warmer regions act more as ‘sources’ of the compounds.

### 1.1.2 Atmospheric Pollutant Transport

It is rare for intense industrial or agricultural activity to exist in mountainous areas. While small settlements, traffic arteries, tourism and resource industries may be cause for local contaminant sources within mountains, most pollutants reach high altitude locations via atmospheric transport and deposition. Cajas National Park is situated 30 km west of Cuenca, Ecuador’s third largest city, in the InterAndean Valley and about 185 km east of Cajas NP sits Guayaquil, Ecuador’s largest city (see chapter 2). Cajas NP is remote and situated high in the Andes, yet despite its position, it is expected that a pollution signal will be found in the lake sediments. Calamari et al. (1991) first

noted the phenomenon of higher OCs concentrations at higher elevations on a global scale, and since then there have been numerous studies on the concentration gradients of OCs and other anthropogenic organic contaminants increasing with elevation (Daly and Wania 2005; Daly et al. 2007; Wania et al. 2008) There are several mechanism at play that facilitate the transport and deposition of pollutants in mountainous regions, known as orographic or mountain cold trapping.

Firstly, two main types of winds influence mountainous regions: (1) terrain-forced flows which are produced when high/low pressure systems and modified by underlying mountain ranges; (2) diurnal mountain winds are produced by temperatures differences within mountains or between mountains and surrounding plains. This results in diurnal winds carrying air into the mountains at low levels during the daytime and taking air out of the mountains during the night (Daly and Wania 2005). For contamination of mountain lake sediments to occur deposition of pollutants must take place which depends on air-surface exchange along elevation gradients. Deposition is favoured by low temperatures, high precipitation rates and high surface roughness, whereas evaporation favours high temperatures and low capacity of the surface for the contaminant. This results in the following mechanism at work, depicted in Fig. 1.1. Air rising from the lowlands cools and condenses forming precipitation heavy clouds which cause precipitation rates to increase with elevation (Daly and Wania 2005). The opposite occurs when air masses sink, warm and consequently cloud dissipate. In the daytime, high temperatures favour the evaporation of pollutants in the lowlands, whereby the contaminants are transported with up-slope winds to higher, cooler elevations where precipitation is more probable and thus deposition is enhanced. At night, cooler temperatures halt the evaporation of chemicals, and the down-slope wind systems carry less contaminated air back into the lower elevation valleys, ultimately creating a steady transfer of chemicals up-slope (Fig. 1.1) (Daly and Wania 2005).

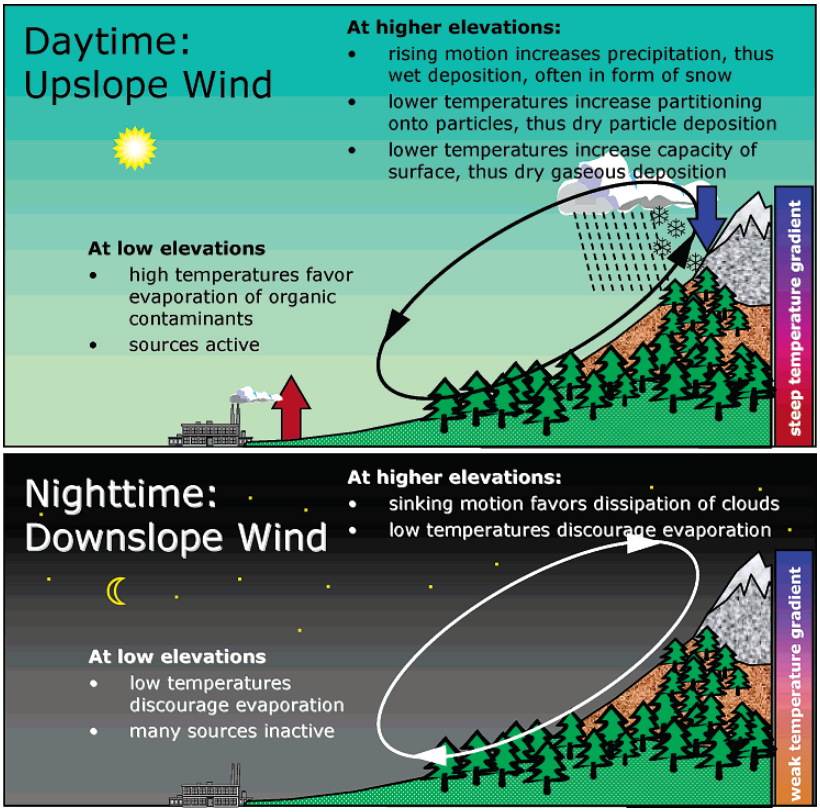


*Fig 1.1. Mechanisms influencing the distribution of pollutants along a mountain slope in terms of daytime and night-time conditions concerning wind direction, temperature gradients with elevation and source activity (from Daly and Wania 2005).*

### 1.1.3 Pathways of Pollutants to Alpine Lakes

High elevation alpine lakes are usually situated above the treeline and form the headwater catchments of water supplies (Daly and Wania 2005). The aquatic ecosystems of alpine lakes are often oligotrophic with a low content of suspended organic matter (Vilanova et al. 2001). Pollutants can enter alpine lakes either via atmospheric deposition or runoff. Because their catchments often have only thin soils and sparse vegetation cover they are especially sensitive to airborne pollutants as they are unable to act as a filter preventing contaminants from reaching surface waters (Vilanova et al. 2001).

#### 1.1.3.1 Deposition Processes

In terms of wet deposition, fog and snow also play an important role alongside rain scavenging. Not only do mountains generally have higher precipitation rates, fog and snow represent forms of precipitation that are more efficient at scavenging certain pollutants (Daly and Wania 2005; Daly et al. 2007). Fog is a common form of ground-based cloud in Cajas NP, and forms when a decrease in temperature causes an increase in relative humidity beyond the dew point (Whiteman 2000). As fog droplets are smaller than rain droplets, they have a higher surface-to-volume ratio which can lead to substantial enrichment of surface-active organic chemicals in fogwater, thus suggesting that fog can be an important mechanism for contaminant deposition in mountain regions. Most importantly, fog can indicate towards differences in contaminant concentrations within mountains if occurrence and frequency of fog is localised (Daly and Wania 2005). Wet deposition is generally more important for water-soluble and low-volatile organic compounds.

Dry deposition of gases tends to be higher at lower temperatures, as well as the association of organic compounds with particles in the atmosphere, and particles generally deposit at a faster rate than gases. Further, as dry deposition also increases with wind speed, and higher elevations tend to experience higher wind speeds and lower temperatures, it can be said that dry deposition of both gases and particles (and their bound organic pollutants) is enhanced in mountainous regions (Daly and Wania 2005).

Temperature inversions, described as increases in temperature with elevation, influence the behaviour of pollutants as they can affect the frequency and elevation of fogs and clouds and thus wet depositional processes. For example, surface-based inversions form at night or in winter when the ground loses heat via long-wave radiation. This inversion breaks-up during the day as up-slope air movement removes air from the valley (Whiteman et al. 1999). Inversions therefore resist vertical movement of air masses and result in contaminants becoming trapped during inversions and this limits the transport of pollutants along elevation gradients (Daly and Wania 2005).

#### 1.1.3.2 Mountain Cold-Trapping

Wania et al. (2008) hypothesize on the main mechanism responsible for mountain cold trapping. They claim that it is the temperature-driven difference in the efficiency of precipitation scavenging between lowlands and mountains that cause the phenomenon. Chemicals which have higher concentrations at higher elevations are not as efficiently scavenged by precipitation falling at temperatures which occur at lower elevations. Instead, they are those whose rate of wet deposition increase as an orographically lifted air mass cools. The theory behind it goes as follows.

The ratio of a chemical's concentration in precipitation to its concentration in air is called the scavenging ratio, $W_{tot}$. If the $W_{tot}$ of a chemical is below approximately 3000 it is not efficiently scavenged by precipitation, thus dry deposition is the dominant mode of transfer to the surface. If a chemicals $W_{tot}$ is greater than 300,000 it is rapidly scavenged from the atmosphere with a precipitation event and wet deposition is thus the primary mode of transfer to the surface (Lei and Wania 2004; Wania et al. 2008). Wet deposition is much faster than dry deposition, therefore if a shift in importance of dry to wet deposition occurs, then also an increase in the overall deposition rate takes place. In the range between the thresholds (3000 – 300,000), wet deposition is sensitive to $W_{tot}$, which in turn is a function of temperature, and in general it increases as temperatures decrease (and vice versa).

However, precipitation rates also play an important role, especially if variations in the rate of wet deposition are at the core of the mountain cold-trapping mechanism. Changes in precipitation rate with altitude have a significant influence, specifically increases in precipitation with elevation enhances the process. Increased precipitation with elevation would provide an explanation for mountain cold-trapping of compound whose $W_{tot}$ is not influenced by temperature and elevation, e.g. contaminants that are particle bound at all temperatures within the lapse range of a mountain slope (Wania et al. 2008). Precipitation does not always increase towards the summit of a mountain, instead it varies greatly with elevation, as shown from a global survey of vertical precipitation profiles from 1300 long-term meteorological stations (Lauscher 1976). What Lauscher (1976) discovered was that only mid-latitude mountains experience an increase in precipitation with elevation. Tropical mountains within 10° and 20° N and S show a precipitation maximum around 1 – 1.5 km, and areas situated within the equatorial zone (within 10° of the equator), such as Ecuador, can even display a decrease in precipitation with elevation. Seasonality is also a consideration, especially in our study area where a wet and dry season occur. The lapse rate during the wet season is likely to be more significant in terms of the rate of pollutant wet deposition than in the dry season (Wania et al. 2008). Following this, we would expect a higher amount of contaminant deposition in humid mountains with high precipitation rates, and in mountains with the largest lapse range (e.g. the highest temperature difference between valley and summit).

#### 1.1.3.3 Physicochemical Properties of Compounds

The behaviour of many natural and anthopogenic compounds is dynamic in the environment and is strongly influenced by the compounds physicochemical properties (e.g. water solubility, vapour pressure) and the tendency to partition to sorbents (particulate matter, organic mater, minerals). Henry's Law Constant (HLC) is important in understanding the tendency of a chemical to volatilize from water to air, especially with regard to the air-water partitioning of chemical compounds that are scavenged from the atmosphere by rain, clouds and fog (Mackay and Shiu 1981). Many pollutants move as vapour between atmosphere and land/water bodies. They volatize from their sources or depositional surfaces and are transported in the atmosphere to different locations where they are re-deposited. The processes of wet and dry depositon, as well as volatilization, are all influenced by HLC. If a chemical has a low HLC then its ability to persist in the environment tends to be greater, and the higher HLC is, the more volatile the chemical. A knowledge of the air-water partition characteristics of a compound can provide insight into where certain compounds will tend to accumulate (Mackay and Shiu 1981). Table A.1.4 in Annex 1 displays some of the physiochemical properties of the PACs analysed in this study.

Mackay et al. (1995) classify organic pollutants into three classes based on their vapour pressure:

1. **Low volatility**. Compounds with a low vapour pressure (log $P_L$ at 25°C < -4). These are generally associated with particulates in the atmosphere and are deposited by wet and dry deposition fairly close to their sources (within 1000 km). This would include high-molecular-weight hydrocarbons such as benzo(a)pyrene.
2. **Intermediate volatility**. These compounds can change from gas to particulate phase within the global environmental temperature range (-40°C to +40°C). They can therefore have a far reaching transportation range, but tend to condense out of the atmosphere at a critical temperature point. They can be classed as having **relatively low volatility** (-2 > log $P_L$ at 25°C > - 4) or **relatively high volatility** (0 > log $P_L$ at 25°C > -2).
3. **High volatility**. Compounds with high vapour pressures (log $P_L$ at 25°C > 0), which exist in the atmosphere primariy in the gas phase at all environmental tempatures. They are transported globally and tend to be homogenous in concentration in the atmosphere. This would include persistent volatile organic compounds (e.g. HCB), and also mercury.

### 1.1.4 Polycyclic Aromatic Compounds

Polycyclic Aromatic Compounds (PAC) are ubiquitous environmental pollutants. Typically, these compounds contain two to eight aromatic rings. They are found in uncombusted petroleum and are also produced during the combustion of biomass and fossil fuel . PACs display a wide range of physical-chemical properties (see table A.1.4, Annex 1). Their varying physical-chemical properties (e.g. molecular weight, vapor pressure and water solubility) also explain their volatility, hydrophobicity, sorption, partition and ultimately determine their transport, fate, behavior and effects in the environment (Barra et al. 2006; Heim and Schwarzbauer 2013). They are toxic to all living organisms, and are classed as human carcinogens and mutagens. The U.S. Environmental Protection Agency and the European Community both list PAHs as priority pollutants (Bandowe and Wilcke 2010; Bandowe et al. 2014; Barra et al. 2006; Quiroz et al. 2005; Tobiszewski and Namieśnik 2012). Despite the major source of anthropogenic PACs being urban/industrial regions, PACs often occur in rural and remote areas as a result of their capacity to be transported long distances and from local vegetation burning (Barra et al. 2006; Van Drooge et al. 2011; Lima et al. 2005; Quiroz et al. 2005; Usenko et al. 2007). Remote high mountain lakes have been reported (Fernández et al. 2000; Vilanova et al. 2001) to act as natural traps for atmospherically transported PACs and while this phenomena has been well documented in the northern hemisphere, only one region in Chile has been described in terms of PAC signals in lake sediments in the southern hemisphere (Barra et al. 2006; Quiroz et al. 2005).

#### 1.1.4.1 Formation of PACs

PACs are a class of organic chemcials with at least 2 fused benzene rings. As a result of combustion processes, the organic compounds present in fuel sources are fragmented into free radicals that react (via several different mechanisms) to produce the first aromatic ring (Richter and Howard 2000). This first armocatic ring then further reacts with other small molecules, such as 2 to 3 ring carbons, which causes the aromatic ring to grow and form larger, more stable multi-ring structures (as seen in Fig. 1.2).

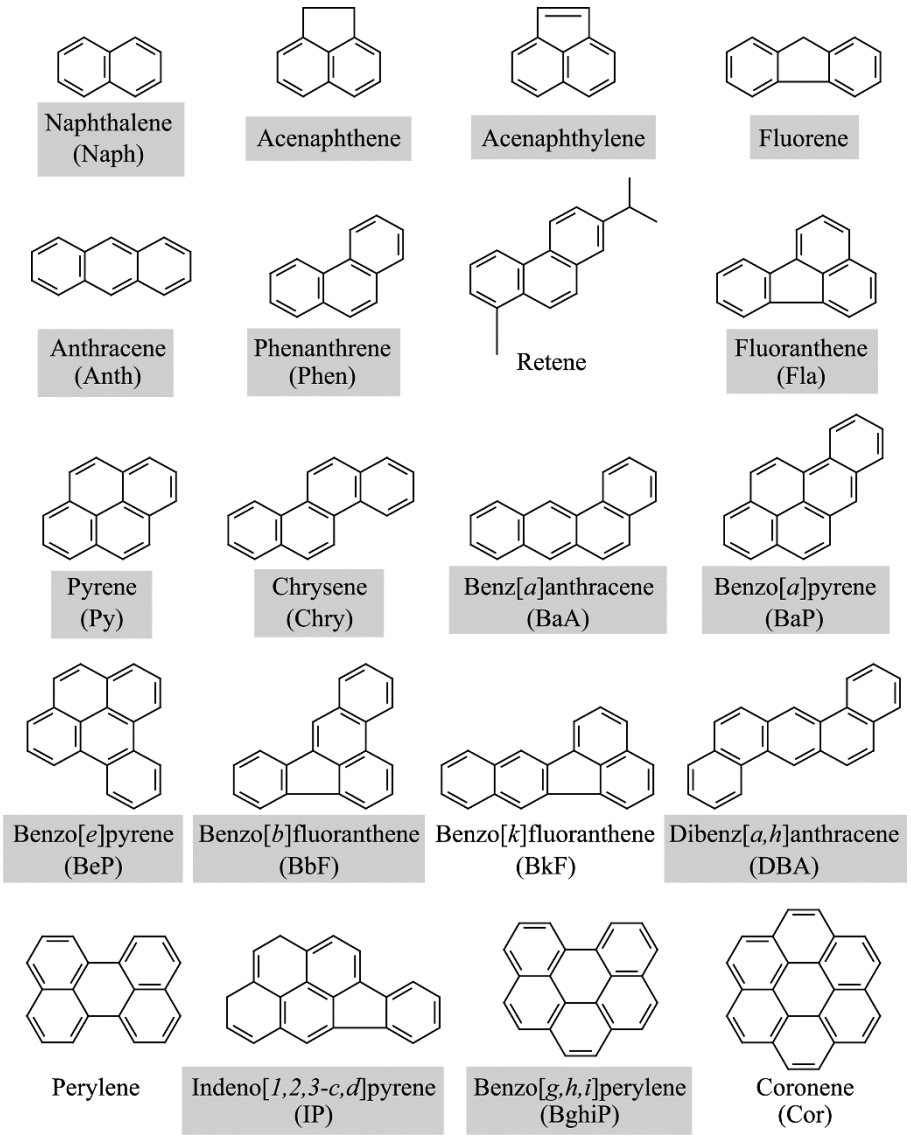


*Fig 1.2. The structure of selected PAHs. Those highlighted belong to the Environmental Protection Agency (EPA) list of 16 priority PAHs (from Lima et al. 2005).*

Polycyclic aromatic hydrocarbons (PAHs) are the best known subgroup of PACs. The assemblage of PAHs that are emitted from different sources varies only slightly, but the burning condition under which the PAHs are formed has a significant influence on the amount of each type of PAH that is produced (Lima et al. 2005). The PAH emission profile for a given source depends then on the processes that produced the PAHs (Manoli et al. 2004). For example, during low temperature processes, such as wood burning, low molecular weight PAHs are formed. Low temperature processes have been known to generate mixtures that are enriched in alkyl-substutued PAHs, whereas higher temperature burning fosters the formation of parent-PAHs (Blumer 1976, as read in Lima et al. 2005). High temperature processes (e.g. the combustion of engine fuels) emit higher proportions of high molecular weight PAHs (Lima et al. 2005; Mostert et al. 2010; Richter and Howard 2000).

Different PAH sources provide different molecular distribution patterns resulting from the variety of substrates, pathways and conditions of PAH formation (Yan et al. 2005). Gernerally, PAHs which have three or more rings have low solubility in water, a lower vapour pressure and are less volatile (Maliszewska-Kordybach 1999). These would include PAHs such as benzo(a)pyrene (B(a)P),

which has 5 rings (Fig. 1.2), and its notable for being the first chemical carcinogen discovered (Ravindra et al. 2008). Light PAHs (low-molecular-weight) exists almost exclusively in the gas phase. The heavier the PAH (high-molecular-weight) the more likely it is to be totally adsorbed on to particles (Ravindra et al. 2008). As the molecular weight of PAHs increases, the carcinogenicity increases and acute toxicity decreases. Combustion processes (especially high temperature combustion) mainly produce unsubtituted PAHs (four- to seven-ring parent PAHs) high-molecular-weight PAHs, and are generally associated with particles such as black carbon and soot (Lima et al. 2005). Petroleum-related PAHs are mostly alkylated homologues and low-molecular-weight PAHs (two- to three-ring parent PAHs) (Yan et al. 2005).

Perylene is a five-ring nuclear polycyclic aromatic hydrocarbon (see Fig. 1.2) which has been extensively found in both marine and freshwater sediments. Perylene is believed to differ from combustion-derived PAHs in that the major source of perelyne is natural *in situ* formation in sediments (Silliman et al. 2001; Silliman et al. 1998). In oxic conditions, perylene is either absent or present in only minor concentrations, thus it is rarely found in significant concentrations in surface sediments (Silliman et al. 2001; Wakeham et al. 1980). High concentrations of perylene are usually found only in deeper sediments – a pattern which contrasts that of anthropogenic PAHs. As concentrations tend to increase with depth, it is evident that perylene formation occurs under anoxic conditions (Garrigues et al. 1988). Perylene is believed to form microbiologically from non-specific biological precursors of either terrestrial and aquatic origin. However, while a variety of precursor materials have been suggested, none have been confirmed and so the origin of perylene continues to be an organic geochemical enigma (Silliman et al. 2001).

Retene (see Fig. 1.2) can form within the lake itself from biological transformations of precursor compounds, such as the needles from coniferous trees, or it can be deposited from emissions of biomass burning (Bandowe et al. 2014; Wakeham et al. 1980; Wania and Mackay 1993; Yunker et al. 2002). Retene is a PAH which thus acts as a marker for conifer-derived organic matter (Buggle and Zech 2015). By measuring retene as part of the target compounds it can be used to infer whether some sources of PAH originate from the combustion of local biomass as a result of slash and burn techniques used in the region (Hansen et al. 2003).

PACs also include the groups oxygenated PAHs (OPAHs, Fig. 1.3) and nitrogen-heterocyclic polycyclic aromatic hydrocarbons (azaarenes, AZAs, Fig. 1.3). OPAHs and AZAs may be similarly or even more toxic than PAHs, and some OPAHs have been found to exist in even higher concentrations in soils than their related parent-PAHs (Bandowe and Wilcke 2010; Bandowe et al. 2011). OPAHs are PAHs which have a minimum of one hydrogen on a benzene ring substituted with oxygenated organic functional groups (e.g. carbonyl, hydroxyl, carboxyl, anhydrides). Bandowe and Wilcke (2010) found a close correlation between PAH and OPAH concentrations in soils, which would suggest that they stem from similar sources (e.g. incomplete combustion of fossil fules) or from the transformation of PAHs in the atmosphere (photochemical and biological) and in soils/sediments (biological and abiotic) (Wilcke et al. 2014). Azaarenes contain one nitrogen atom in place of a carbon atom in the aromatic structure of a PAHs, and are formed and released into the environment from sources similar to PAHs (e.g. incomplete combustion of organic matter and fossil fuels and petrogenic sources) (Bleeker et al. 2002; Wilcke et al. 2014). Similar to the PAHs, OPAHs and AZA in the environment are mainly derived from combustion of fossil fuels and biomass. However, OPAHs can also be formed from post-emission transformation reactions (biological and abiotic) of PAHs (Wilcke et al. 2014a; Lundstedt et al., 2007).

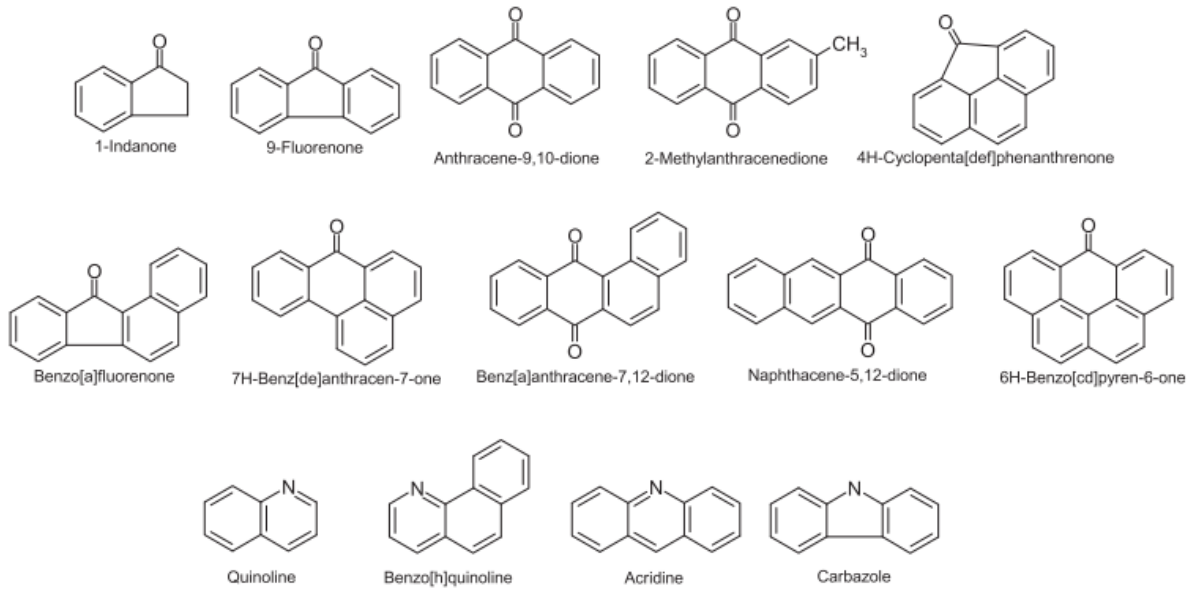


*Fig 1.3. Chemical structures of selected OPAHs and AZAs (from Lundstedt et al. 2014)*

### 1.1.4.2 Fate in the Environment

**ATMOSPHERE**

The fate of PAHs, OPAHs and AZAs in the atmosphere is very much influenced by their partitioning between the free gas phase and particulate matter. How the compounds partition between these two phases depends on the volatility of the compound, their moleculr weight, the ambient temperature and the concentration of particles in the atmosphere. The physicochemical properties of PACs (found in Table A.1.4, Annex 1) greatly influences their behavior in the environment (Lima et al. 2005). Usually, the higher the molecular mass of the compound, the lower its vapor pressure and solubility. How PACs are distributed in the atmosphere between gas and particulate phase and different particle sizes is determined by vapour pressure, and molecular weight. Thus PACs with 2-3 rings exist in the atmosphere in the gaseous phase and are highly mobile in the atmosphere and can therefore be globally distributed. Semi-volatile 4-ring PACs (e.g. phenanthrene, pyrene) can be found in both phases, whereas PAHs that have more than 5 rings are almost exclusively found in the particle phase (Fraser et al. 1998) and are classified with low mobility (rapid deposition and retention close to the source) (Maliszewska-Kordybach 1999). In general, PAHs tend to have low water solubility, yet the differences in water solubility between individual PAHs is substantial enough to impact how they are distributed in the environment. OPAHs and AZAs are typically characterized with higher molecular weight and lower vapour pressures compared to their related PAHs. Thus, the polar derivaties (OPAHs and AZAs) are more likely to sorb onto particulates, and because of their strong association to atmospheric particles and higher water solubility, OPAHs and AZAs should be removed faster from the atmosphere by depostition (Albinet et al. 2008).

PACs in the atmosphere are susceptible to both chemical oxidation (OH, $NO_3$, $O_3$) and photochemical alterations, however, they tend to degrade much faster when exposed to sunlight, which suggests that photochemical induced decay plays a more important role than chemical oxidation (Albinet et al. 2008; Lima et al. 2005). Photoloysis plays a relevant role for PAHs sorbed on to particulate matter, and degradation is usually much slower than in the gas phase. For PAHs

in the gaseous phase, OH radial-initiated reactions (daytime) and $NO_3$ radial-initiated reactions (nighttime) play an important role in PAH transformations (Vione et al. 2004).

Removal of PACs from the atmosphere occurs by either wet or dry deposition (see section 1.1.3.1). Typically, PAHs present in the gas phase dissolve within clouds and into raindrops (Offenberg and Baker 2002), whereas PAHs bound to particles tend to be washed out from the atmosphere via precipitation (Lima et al. 2005) and gravitational settling (Maliszewska-Kordybach 1999). Dry depsition can occur by direct fallout of PAHs that are adsorbed to larger particles. Total scavenging ratios of both gas and particle vary greatly amoung individual PAHs (by more than 3 orders of magnitude), however in general it can be said that the less volatile the compound (thus more likely to be associated with particles), the larger the scavenging ratio (Offenberg and Baker 2002). As PAHs are hydrophobic compounds, they have a predisposition to associate more with particles than to dissolve in water. Thus, PAHs that are depositied into lacustrine environments tend to associate with settling particles (Lima et al. 2005).

**SEDIMENTS**

In sediments PAHs can be degraded by microbial communities in the top sediments. Anoxic conditions in deeper sediment layers leads to the preservation of the molecules (hence the suitability of sedimentary archives for historical reconstructions). Low-molecular-weight PAHs (LMW) are more likely to experience microbial degradation within the sedimentary profile than high-molecular-weight (HMW) PAHs, and it is said that susceptibility to biodegration decreases as the number of fused rings in a PAH increase (see ring structures in Fig. 1.2 and 1.3). This could be as a result of particle-bound pyrogenic PAHs being less available for dissolution than un-bound PAHs in the water phase (Lima et al. 2005). Microbial transformation of PAHs to OPAHs in soils and sediments is related to biological activity (which in turn is driven by climate and soil fertility), but in general the higher the biological activity, the higher the concentration of OPAH (Wilcke et al. 2014). OPAHs and AZAs have higher water solubility than their related parent-PAHs which can result in their higher partition from sediment into water phase (surface water and pore water). OPAHs are also formed and accumulate in the environment as PAHs are degraded. Levels of OPAHs can increase at the same time that PAHs are decreasing through degradation (Lundstedt et al. 2007).

#### 1.1.4.3 Historic Trends In PACs

The PAC signal in lake sediments can be used as a proxy for anthropogenic activity over the past century. Natural, technological, social, economic and political events have influenced sedimentary geochemical signatures, thus resulting in lake sediments providing excellent archives of environmental and anthropogenic changes throughout time (Bandowe et al., 2014). Variations in the intensity and type of anthropogenic activity in historic time periods can be differentiated by the profiles of PAHs in sediment cores. This is related to the fact that changes in population size, industrial or agricultural activities, type of fuel that is being utilized, implementation of environmental protection measures, science and technological innovation and climate forcing as well as natural disasters and political/socio-economic events often impacts the amount and composition of PACs that are emitted and deposited in sediments (Bandowe et al. 2014).

PAHs are emitted from the incomplete combustion of carbon-containing compounds, e.g. fossil fuels, and also from naturally occurring forest/bush fires (Wilcke 2007). The main source of PAHs

in modern times is anthropogenic combustion. In historic periods strongly influenced by anthropogenic activities, the PAH record reflects emissions associated with industrial activities or population changes, for example, the switch from charcoal to modern heavy industry. However, the historical record of PAHs in the sediment record can be used not only to identify periods of anthropogenic-induced combustion, but also for pre-industrial periods as a proxy for the frequency and size of natural fires related to either climatic conditions or human activities (Bandowe et al., 2014; Lima et al., 2003). The pattern of PAHs in the sediment core reflects changes that occur in the combustion conditions and type of fuel, thus PAHs can also be used to identify sources and combustion temperature (Yunker et al. 2002).

Studies of PAHs in sediment cores from the east coast of the USA (Gschwend and Hites 1981) show a gradual increase in PAH concentrations from around the 1880s, which coincides with the onset of the Industrial Revolution in western countries, reaching a maximum at around the 1950s. Mostly we see these changes in the sediment PAH flux as a result of predominate use of coal for energy production. The substitution of coal with cleaner-burning fuels such as oil and natural gas is often apparent in the PAH profile of sediment cores as a steady decrease from the 1960s onward. The increased implementation of catalytic converters in motor vehicles and stricter environmental control measures, as well as the increase use of methane meant that the decline in PAH concentrations often persists throughout the 1970s and 1980s. This is a typical PAH trend found in sediment cores from many northern hemisphere, industrialised, western locations (Bandowe et al. 2014; Lima et al. 2003; Usenko et al. 2007). For example, the trend is clearly seen in Fig. 1.4 from Lone Pine Lake, located in the remote high altitude Rocky Mountains, USA. In the study conducted by Usenko et al. (2007), they found an initial flux input in 1870, which would be indicative of the start of the Industrial revolution, with flux values peaking in 1949 and gradually decreasing from 1967.

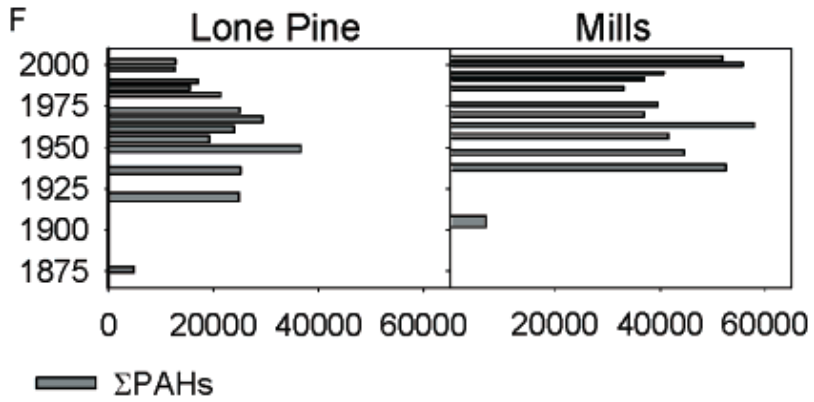


*Fig 1.4. Flux (ng m$^{-2}$ year$^{-1}$) (x-axis) profiles with age (years A.D.)(y-axis) of ∑PAHs in Lone Pine Lake (west, 3024 m) and Mills Lake (east, 3030 m) sediment cores (from Usenko et al. 2007)*

However, as seen in Mills Lake from the same study (Usenko et al. 2007), not all PAH profiles in sediment cores follow the afore mentioned trends. In Mill Lake, despite only a 10 km distance from Lone Pine Lake, the authors found that, apart from a small influx of PAHs in 1905, PAH levels only increased in 1938 and peaked in 1963. While PAH levels did begin to decrease, they then began increasing again in the 1990s, and still continue to increase. The authors attributed this second increase to a growth in population to the east of the Rockies (location of Mills Lake). Accordingly, the location and physical parameters (elevation, situation, wind, precipitation etc.) of each lake will greatly influence the flux of PAHs seen in the sediment core. Van Metre et al. (2000) also found a change in the decreasing PAH trend from the 1960s. Their study found that from all 10 of their study sites in the United States PAH emissions were increasing again, most

notably in locations close to urban centres, indicating a parallel between the increase in motor vehicle usage and PAH emissions. For regions globally that did not experience the western Industrial Revolution in the 1880s, PAH profiles in sediment cores tend to differ. For example, in sediments cores from Chile the initial increase in PAH concentrations begins only in the 1960s, and in China in the 1950s (Barra et al. 2006; Han et al. 2016). In the lake sediments from this study, we will investigate how and why the PAH signal in sediments from South America differ from those in the northern hemisphere.

#### 1.1.4.4 Molecular Diagnostic Ratios

The ratios of the concentrations of specific PAHs (often called molecular diagnostic ratios) can present an important tool for identifying emission sources of the PAHs in the sedimentary profile. PAHs are always emitted as mixtures, and it is often assumed that the relative molecular concentration ratios are characteristics of a given emission source. The majority of diagnostic ratios include PAHs that should have experienced similar environmental fate processes as a results of having the same molar mass and similar physiochemical properties. The analysis of PAHs in sediment cores and the subsequent calculation of their diagnostic ratios can supply information on the historical trends of the activities of PAH pollution sources (Tobiszewski and Namieśnik 2012).

A range of parent to alkyl-substituted PAHs can be used as markers for the ratio of industrial to vegetation burning or the dominance of combustion sources, for example, Naphthalene/2-Methylnaphthalene, Naphthalene/1-Methylnaphthalene, Naphthalene/1,3-Dimethylnaphthalene and Phenanthrene/1-Methylphenanthrene. Parent to alkyl-substituted PAHs provide some of the most definitive and ubiquitous tracers of organic material in aquatic systems (Yunker et al. 2002). It has been shown that that low energy biomass burning/petroleum sources result in a ratio where the alkalated PAH is greater than the parent PAH, and vice versa for high energy combustion sources (parent PAH > alkalated PAH) (Bandowe et al. 2014; Han et al. 2015; Tobiszewski and Namieśnik 2012; Yunker et al. 2002). Jensen and Hites (1983) found an inverse correlation between the concentration of alkylated PAHs which were produced by diesel engine exhaust and its temperature. They found that as the temperature of the exhaust decreased, the quantity of alkylated PAHs increased, thus the ratio of alkylated-to-parent PAHs also increased.

LMW-PAHs (as well as alkylated PAHs) are characteristic of emissions from low temperature combustion of biomass, vegetation and wood (agricultural and forest fires). LMW-PAHs also dominate in environmental archives that receive their PAHs depositions from long range atmospheric transport sources. HMW-PAHs or combustion derived PAHs (COMB-PAHs) dominate during the high temperature combustion of fossil fuels such as petroleum/coal (vehicles, power plants, industries) and deposition from point combustion sources (Lima et al. 2005; Tobiszewski and Namieśnik 2012). Parent PAH ratios have also been used to detect COMB-PAHs (Yunker et al. 2002, 2014). The ratio of ΣCOMB-PAHs/ΣParent-PAHs indicates the relative contribution of high temperatures combustion sources to the PAH mixture in the sediment profile (Yunker et al. 2002). The ratio between LMW-PAHs and HMW-PAHs is commonly used to distinguish between combustion and petroleum sources (Tobiszewski and Namieśnik 2012; Yunker et al. 2002). The ratio of ΣLMW-PAHs/ΣHMW-PAHs in the core is indicative of pyrogenic (<1) sources (e.g. the incomplete combustion of wood or fossil fuels), or petrogenic (>1) sources (e.g. stemming from petroleum products).

Besides their direct emissions (together with PAHs) from combustion processes, OPAHs can also be formed by the transformation of PAHs by photolysis, photochemical degradation and biological degradation of PAHs (Lundstedt et al. 2007). It is assumed that PAHs in the lakes from this study are mainly from atmospheric deposition due to their remote location. Thus, it is an assumption of this study that the OPAHs to PAH concentration ratios in sediments could be used as an indicator of ageing (travel distance) of the air mass (Han et al. 2015, 2016; McKinney et al. 1999). The longer the air mass has been travelling, the longer the PAH has spent in the atmosphere before deposition occurs. Thus, it is expected that a higher ratio of transformation product (OPAH) to parent-PAH will result from longer air mass travel (Jones and Voogt 1999; Lima et al. 2005). If secondary (photo)chemical transformation plays a role, then OPAH to related parent-PAH concentration ratios should increase with increasing transportation distance from the source (Wilcke et al. 2014). AZAs and OPAHs are also more water soluble than their related PAHs (Table A.1.4 in Annex 1). Therefore, wet deposition should lead to higher OPAH/parent-PAH and higher AZA/PAH ratios than in periods dominated by dry deposition. In this study, it will be attempted to use these ratios as indicators of wet/dry periods in this area.

### 1.1.5 Organochlorine Compounds (OCs)

Persistent Organic Pollutants (POPs) are organic substances that are characterized by high persistence, high bioaccumulation abilities, toxcitiy and long-range transport properties (Stockholm Convention). POPs are often defined as a pollutant with a half-life in water or sediments of more than 8 weeks. The range of POPs that damage the environment is vast, with some 500 to 1000 newly synthesized organic compounds being developed every year (Smol 2008). Organochlorine compounds (OCs) have been used in the past as pesticides for agriculture and for the control of disease vectors. Their characteristics of being persistent and capable of long range transport have enable many OCs to accumulate in the environment and in remote locations. Several OCs are classed as Persistent Organic Pollutants (POPs) under the Stockholm Convention (www.pops.int). Many POPs are effectively sorbed onto particles and accumulate in sedimentary records. As such, paleolimnological approaches are important as sediments, and other proxy records, are often the only way to reconstruct past POP trajectories (Smol 2008).

Certain POPs, such as Dichlorodiphenyltrichloroethane (DDT) and Polychlorinated biphenyls (PCBs), are often referred to as “legacy” (Smol 2008) or “common” (Heim et al. 2004; Warren et al. 2003) POPs. These contaminants can be detected in sediments from a time period from about the late 1950s and early 1960s, but mostly decrease in concentration up to present day as many were phased out of legal use as a result of increasing environmental awareness in the 1970s to 1980s in industrial countries. These legacy OCs include DDT, endrin, dieldrin, aldrin and lindane (ɣ-HCH) (Warren et al. 2003). However, new compounds are constantly being developed, and these new OCs are refered to as either “emerging” (Smol 2008) or “modern” POPs (Heim et al. 2004; Warren et al. 2003). Modern compounds tend to show maximum concentrations in the late 1980s, and these include chemicals such as polybrominated diphenyl ethers (PBDEs), which is a flame retardant for everyday products such as carpets or even children’s sleepwear (Smol 2008). As a result of this, “legacy POPs” can often be used as chronostratigraphic event markers in sediment cores to constrain dating methods, as it is known when they were put in use and when they were banned. Table 1.1 provides years in which cetain legacy POP began being used.

PCBs have been used extensively since 1930 in a variety of industrial activities such as paint additives, in electric transformers and large capacitors and in plastics (Smol 2008). Heim et al.

(2004) found that PCBs reached a maximum in sediment contamination at the beginning of the 1980s, which was followed by a distinct decrease up to present day. The authors associate the reduction with a gradual replacement of PCBs with tetrachlorobenzyltoluenes (TCBTs). It is possible to observe a distinct increase in sediment TCBT contamination since 1980. However, authors have noted from various locations that the decline of PCBs occurs within the range of 70-80% in between the 1960s and 1990s (Heim et al. 2004).

DDT, which breaks down into DDD and DDE, both of which have the capability of persisting longer than their parent compound DDT, is a very well known OC. It was first synthesized in 1874, and has been used as an insecticide since 1939. As a result of the overwhelming health and environmental concerns over the use of DDT, it was banned in most industrial countries in the 1970s (Smol, 2008). DDT was first used in Ecuador in 1946 in order to control rural and sylvatic plague caused by flea infested rodents (Saenz Vera 1953). The usage of DDT at the time was wide-spread and excessive, and its continued use was a means to control malaria until the year 2000 when it was finally phased out (Berg 2008). Grimalt et al. (2004) conducted a study of OC concentrations in high altitude mountain lake sediments from the Pyrenees and the Tatra Mountains. They found concentrations of DDTs (4,4-DDE + 4,4-DDT) increased after the Second World War, and peaked in 1976 (Fig. 1.5), after which there is a significant decline in concentrations between 1978 and 1990. There is a second peak of DDTs between 1992 and 1997, indicating either a renewed period of DDT use in some parts of Europe, or a remobilization of these compounds in the environment. After 1997 there is a strong decline in the concentrations of DDT (Grimalt et al. 2004).

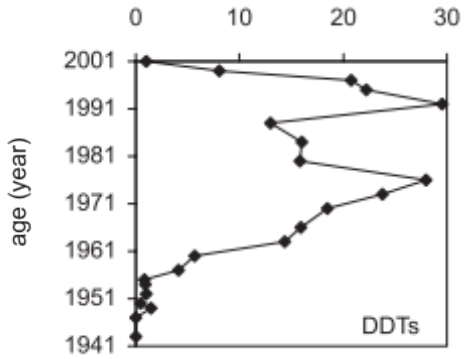


*Fig 1.5. Time scales of the concentration (ng $g^{-1}$)(x-axis) of DDTs (4,4-DDE + 4,4-DDT) from the sediment core of a high altitude European mountain lake, Lake Ladove (Tatra Mountains) (Grimalt et al. 2004)*

Hexachlorobenzene (HCB) was first introduced in 1945 to treat seeds, as a pesticide to kill crop fungi, and is also a byproduct of certain industrial chemical manufacture (Bailey 2001). Rapaport and Eisenreich (1988) wrote about the historical atmospheric deposition rates of HCB from ombrotrophic peat bogs in eastern North America. They reported low rates of HCB deposition up to the 1940s, thereafter an increase until rates peaked in the 1960s, where after rates began to decline. A study carried out in Sweden by Bignert et al. (1998) looked at time trends of organochlorine pollution since the 1960s, and reported similar declines in HCB rates since the peak in the 1960s.

Endofulfan is an OC that has been in use since 1954. It is a pesticide that is effective against a wide range of insect pests and mites, and thus is applied to a vast range of crop types globally. As a result of its semi-volatility and persistence, endosulfan is one of the most ubiquitous OC pesticides

in the air (Weber et al. 2010). However, unlike most legacy POPs, endosulfan does not show a declining trend in concentrations, indicating that its usage is still ongoing. While endosulfan usage appears to have declined slightly in the Northern Hemisphere from 1996 – 2004, use of the pestiside increased in the Southern Hemisphere over the same time period (Weber et al. 2010).

*Table 1.1. Potential POPs for chronostratigraphic markers to validate $^{210}Pb$ radiometric data*

| POP | EVENT MARKER | REFERENCE |
|---|---|---|
| PCBs | In use since 1930, peak at beginning 1980s, decline to present | Heim et al. 2004 |
| DDT | In use since 1939, banned in industrial countries in 1970s | Smol 2008; Grimalt et al. 2004 |
| DDT Ecuador | In use since 1946, banned in 2000 | Vera 1953; Berg 2008 |
| Endosulfan | In use since 1954 | Weber et al. 2010 |
| HCB | In use since 1945 | Rapaport & Eisenreich 1988; Bigert et al. 1998; Bailey 2001 |

### 1.1.6 Mercury

Mercury (Hg), while classed as a metal, has many properties that are akin to POPs. It has an ability, like POPs, to biomagnify in food chains and to be transported over long distances. The consequences of mercury pollution are vast, and its toxicity for organisms dire (Smol 2008). Mercury is a natural element found ubiquitously in the Earth's lithosphere. It is emitted naturally from the lithosphere to the atmosphere as gaseous elemental $Hg^0$ from sources such as geological deposits, volcanic eruptions, forest/vegetation fires and volatilization from the oceans (Michelazzo et al. 2010; Streets et al. 2011). Key anthropogenic sources of mercury come from burning coal and the combustion of other fossil fuels, alkali and metal-processing industries, incineration of waste, the paper and pulp industry, and the mining of gold/silver and mercury (Fig. 1.6, a) (Smol 2008). In South America, stationary combustion (31 tons), non-ferrous metal production (25.4 tons), mercury production (22.8 tons) made up the largest sources of anthropogenic Hg emissions in the year 2000 (Pacyna et al. 2006). Human activities have greatly altered the natural flux of Hg from the lithosphere to the atmosphere, and from the atmosphere to the surface environment. Current anthropogenic Hg emissions have been estimated to be around 2000 Mg $yr^{-1}$ (megagram per year), compared to 500 Mg $yr^{-1}$ from natural geogenic emissions (Streets et al. 2011). As far back as 5000 years ago, humans have unceasingly disrupted the natural Hg cycle in the pursuit for energy and precious metals by digging into the lithosphere to extract gold, copper, silver, coal and other materials, all of which come hand-in-hand with releasing Hg into the natural environment. Thus, the accumulation of Hg in environmental archives, such as lake sediments, represents the legacy of historical Hg emission trends (Fig. 1.6, b) (Streets et al. 2011).

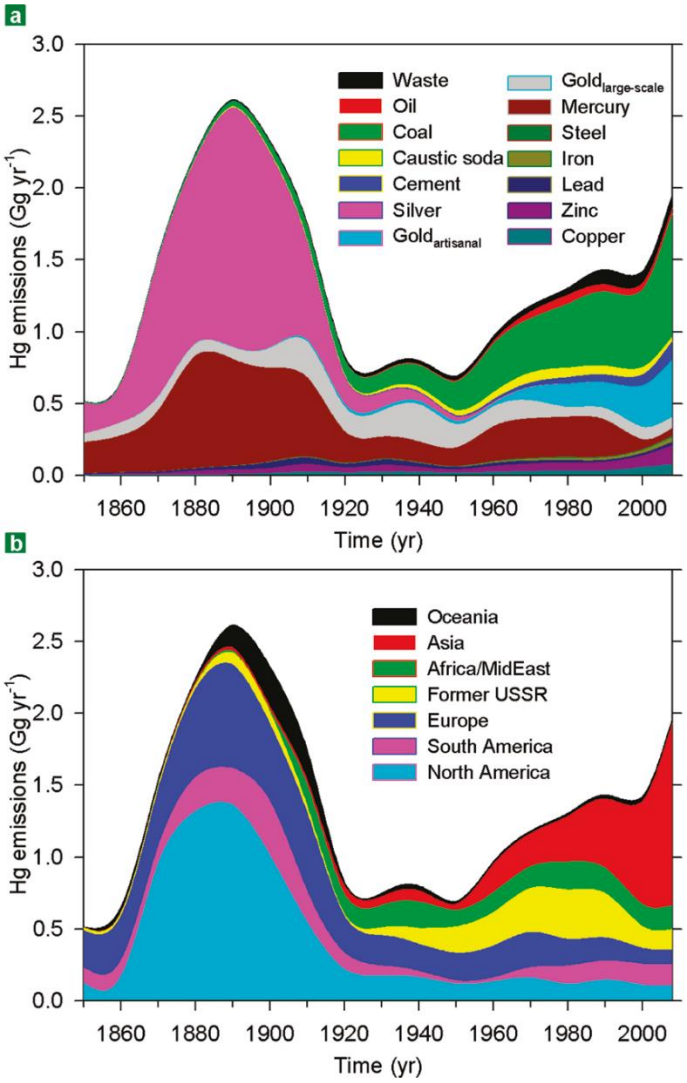


*Fig 1.6. Trends in Hg emissions by source type (a) and world region (b) (Streets et al. 2011)*

The atmosphere offers a key environmental pathway for the redistribution of Hg globally (Sprovieri at al. 2010), and atmospheric depositional fluxes of Hg at any given location is generally an indicator of sources on a large and small spatial scale (Lamborg et al. 2002). However, difficulties exist in analyzing global long-term trends of Hg in the atmosphere, and this is predominantly due to a lack of a coordinated monitoring network and scarce representation of measurements from the Southern Hemisphere (Sprovieri et al. 2010). Given the global scale prospective of Hg dispersion, it is fundamental to understand the secular change of Hg deposition in both hemispheres (Lamborg et al. 2002).

Slemr et al. (2011) present concentrations of Hg in air, which have been monitored since 1995 at a number of sites in the northern hemisphere, but only one site (Cape Point, South Africa) in the southern hemisphere. They found a decreasing trend of 1 – 1.5% per year in concentration of Hg in air, which they claim (by combining new and old data) can be considered representative of trends in the southern hemisphere. The homogeneity of Hg concetrations in the southern hemisphere is expected given that anthropogenic emissions contribute only a small fraction of all Hg emissions in the southern hemisphere. Sources that dominate emissions stem from oceanic emissions and emissions from biomass burning, e.g. forest burning in the Amazon (Michelazzo et al. 2010; Obrist et al. 2008; Slemr et al. 2011). In general, however, Hg concentrations are slightly lower in the southern hemisphere that the northern (Pirrone et al. 2010). This has been attributed

to greater industrial activity in the northern hemisphere ad the atmospheric lifetime of Hg which, although long enough for the hemispherical distribution of Hg, is not long enough to survive the long time needed for cross-equator transport (Pirrone et al. 2010). Relatively few observations of atmospheric Hg have been made in Central and South America, and most of the existing studies are carried out in close proximity of major emission sources, such as mines (Barros de Oliveira et al. 2012; Cooke et al. 2009; Malm 1998; Nriagu 1994). As far as reviewed literature has indicated, there have been no studies concerning Hg deposition in lake sediments from Ecuador. Studies located in Ecuador focused on mercury concentrations in the air around mining sites (González-Carrasco et al. 2011) and on metal contamination of river cathchments (Tarras-Wahlberg and Lane 2003).

#### 1.1.6.1 Fate of Mercury in the Environment

**ATMOSPHERE**

Mercury exists in the atmosphere in two states: elemental mercury, $Hg^0$, and oxidized mercury, Hg(II). $Hg^0$ and Hg(II) are found in the gaseous state, associated with particulate matter and in the aqueous phase (in clouds and rain). Both forms of Hg have differing physiochemical properties that influences their behavior (Pirrone et al. 2010). Elemental Hg ($Hg^0$) is the dominant chemical form found in the atmosphere (see Fig. 1.7), contributing to 53% of total Hg emissions (Pacyna et al. 2006). It is less reactive, more volatile and, most importantly, less soluble than Hg(II). These properties of Hg are key in determining its long atmospheric residence time of 0.5 to 1 year (Schroeder 1998). This makes it possible for $Hg^0$ to be transported tens of thousands of kilometers through the atmosphere. It is the reason for high levels of $Hg^0$ in remote locations, making $Hg^0$ the most important Hg species on a global scale.

The main property influencing the fate of Hg in the atmosphere is its redox chemistry. Hg(II) is more likely to deposit and remain in ecosystem compartments compared to $Hg^0$, thus is it important in the Hg biogeochemical cycle. $Hg^0$ is much less likely to be deposited or to be scavenged by water/cloud droplets and is thus reposnsible for Hg long-range transport in the atmosphere (Pirrone et al. 2010). As a result of mercury's geographical and vertical homogeneity in the atmosphere of the northern (up to several km altitude) and southern hemisphere, decadal scale reductions and increases in emissions are very likely to be reflected throughout the lower troposphere (Outridge et al. 2005; Schroeder 1998; Slemr et al. 2011). Owing to its volatility and chemical persistence, $Hg^0$ already mobilized in the environment can easily be recycled in air-surface exchange, which results in the dispersion of $Hg^0$ on regional, continental and global scales (Schroeder 1998). The global scale redistribution of emitted Hg is spurred by its exchange between various environmental compartments. Hg present in the atmosphere can be deposited in the oceans or land (soil, vegetation, aquatic bodies), and then re-emitted into the atmosphere hours, weeks or decades later (Pirrone et al. 2010).

**SEDIMENT**

Hg can be be oxidized, transported and depositied by wet or dry deposition in regions far away from where it was originally emitted. Hg in lake sediments is likely bound to reduced sulfur groups of organic matter or precipitated metacinnabar (HgS), the solubility of which is very low and therefore diffusion of Hg within the sediment is negligible (Biester et al. 2007). Inorganic Hg is known to be stable within the sediments. This has been shown by the temporal consistency of Hg increases seen in multiple lake sediment cores globally, the preservation of distinct Hg peaks in

lake sediments and the absence of Hg redistribution in experimental cores (Biester et al. 2007; Cooke et al. 2009; Lamborg et al. 2002; Lockhart et al. 2000).

Lake sediments are important areas of Hg methylation as they are influenced by both atmospheric deposition and runoff from the surrounding catchment. The Hg cycle in lake environments is complex and methylation of Hg can be influenced by sediment type, dissolved organic carbon content, pH, iron and sediment type and structure (Pirrone et al. 2010). If part of the deposited Hg transforms into highly toxic methyl mercury it can bioaccumulate in food chains to concentrations that are adverse to ecosystems and human health (Slemr et al. 2011). For this reason many developed countries have substantially reduced their Hg emissions since the 1980s (Sprovieri et al. 2010). Yet these emission reductions are offset by rapid industrialisation in many developing regions of the world (Slemr et al. 2011).

#### 1.1.6.2 Historic Trends In Mercury

Globally, historic trends in Hg emissions from 1850 to 2008 are shown in Fig. 1.7. Streets et al. (2011) calculated that global Hg emissions peaked in the 1890s at 2600 Mg $yr^{-1}$, and attributed this peak mainly to gold and silver production which uses Hg in the extraction processes (see section 1.1.7). Thereafter emissions declined rapidly and remained relatively constant around 700 – 800 Mg $yr^{-1}$, however after 1950 emission grew again, attributed to growth in coal combustion and artisanal gold production, rising to 2000 Mg $yr^{-1}$ in 2008. While regional emission trends (Fig. 1.6, b) point towards North America and Europe as dominant emission regions in the 19$^{th}$ century, the emphasis in the 20$^{th}$ century shifted initially to Russia, and then swiftly to Asia after 1950. It has been estimated that Asia is responsible for 64% of global Hg emissions in 2008 (Streets et al. 2011).

Streets et al. (2011) developed speciated emission trends for Hg (Fig. 1.7). The share of $Hg^0$ in total Hg emissions was shown to have declined from 80% in 1850 to 55% today. Contrasting this, $Hg^0$ emissions have actually been growning in the modern era (from 420 Mg $yr^{-1}$ in 1950 to 1080 Mg $yr^{-1}$ in 2008) as a result of global economic and industrial development. Slemr et al. (2011) attributed that this could be due to declines in the re-emission of Hg from surface ocean and soil reservoirs. A further suggestion by Streets et al. (2011) is that production of commercial products containing legacy Hg (such as batteries, thermometers etc.) peaked around the 1970s and has been declining ever since. They postulate that this Hg eventually enters the environment through incineration, waste water or leakage from landfills.

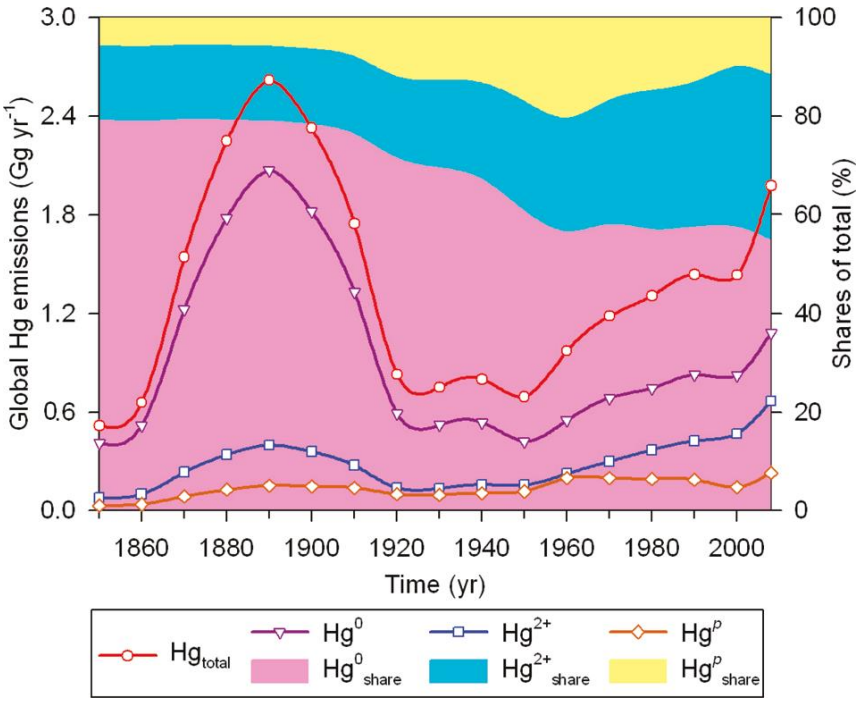


*Fig 1.7. Global trends in speciated emissions of Hg. Absolute magnitude (lines) and shares of total (shading) (Streets et al. 2011)*

Anthropogenic emissions of Hg have been investigated in various studies of lake sediments, ice cores and peat bogs from both hemispheres, all of which have observed a 3 to 5 fold increase in Hg deposition since pre-industrial times (Biester et al. 2007; Lamborg et al. 2002; Lindeberg et al. 2006; Pirrone et al. 2010; Sprovieri et al. 2010). The timing and sharp increase in Hg concentrations around the Industrial Revolution is indicative of the significant impact anthropogenic activity has on the global Hg cycle (Lamborg et al. 2002). Furthermore, the timing and shape of modern Hg emission rates is very similar to that of $CO_2$, implying that the combustion of fossil fuels are perhaps the primary cause for global increase in Hg emissions (Hudson et al., 1995; Lamborg et al., 2002). Fast developing countries such as India, China and Brazil show rapidly increasing Hg emissions due to a rapid increase in energy production from coal combustion (Pirrone et al. 2010).

Studies show that Hg deposited in lake sediment layers has increased in the last century when compared with deeper, older layers (Biester et al. 2007; Lamborg et al. 2002; Lockhart et al. 1998). Cooke et al. (2009) investigated Hg pollution in three lake sediment cores from the central Peruvian Andeas. They found that the natural, background Hg in their lakes was ca. 6 – 7 µg $m^2$ $yr^{-1}$, a range which is consistent with other lake-sediment reconstructions of pre-anthropogenic Hg deposition globally (Biester et al. 2007; Bindler et al. 2001; Lindeberg et al. 2006; Lockhart et al. 1998). Two of the lakes they investigated were in the vicinicty of some of Peru's largest mines, while a third lake was considered remote and removed from direct mining influences. The remote lake recorded a factor increase of Hg in modern times of 4.6 compared to natural background Hg levels. This is consistent with studies globally that suggest an average increase of global Hg deposition rates of 3 – 5 times above background values (Biester et al. 2007; Lamborg et al. 2002; Lindeberg et al. 2006; Pirrone et al. 2010; Sprovieri et al. 2010). The two lakes that were impacted by mining showed factor increases of 105 above background levels. The high Hg flux rates of these lakes reflects the legacy of > 3'5000 years of regional Hg pollution as a result of mining which still resides within their catchment (Cooke et al. 2009).

#### 1.1.6.3 Mercury Mining in South America

Mercury mining in South America began first around ca. 1400 BC, an era which predates the earliest complex Andean society. At this time, cinnabar (HgS) was the main source for mercury and its pigment, vermillion, was used extensively in Andean societies as body paint or for ceremonial objects (Cooke et al. 2009). Large scale mining began during the colonial era (ca. 1532 – 1900 AD) with the invention of Hg amalgamation, the dominant silver processing technique. It has been estimated that colonial Hg emissions averaged at around 600 tons per year (Nriagu 1994). However, this estimate represents rather the minimum of Hg emissions during colonial times, as it only represents state-registered Hg emissions from silver processing. Actual Hg emission are unknown (Cooke et al. 2009), but it is estimated that the South and Central American mining activities (from 1570 – 1900, especially Peru and Mexico) released far larger amounts of Hg to the environment than North American mining activities, but at a much lower rate. If these South and Central American Hg emissions had been spread evenly over the globe, it would have resulted in an increase of 0.8 μg $m^{-2}$ $yr^{-1}$. No global signal associated with South American mining activities has been reported, and this may be explained by Hg being deposited locally around mining areas and remaining unavailable for re-emission, rather than being removed globally (Lamborg et al. 2002).

Huancavelica, situated in the central Peruvian Andes, was the largest Hg mine supplying Hg to all of South America's silver mines during colonial times. Accordingly, it served as a key source of pre-industrial Hg pollution in the Andean region (Cooke et al. 2009). Cooke et al. (2009) reconstructed the history of mining in Huancavelica from three lake sediment cores in the region. Two lakes were situated in close proximity to the mine, the third ca. 225 km away. They found that there was significant Hg pollution occurring in the Andes already prior to Peruvian industrialization. Their results suggest that pre-Inca Hg emissions differed from colonial Hg emissions. The dominant form of Hg in pre-Inca times was a coarse particulate form, such as cinnabar dust. This dominated in areas near Hg point-sources and Hg pollution was mostly being deposited in the local environment. During this time there were high levels of Hg in the lake sediments close to the mine, and an apparent lack of Hg pollution in the lake further away. However, with colonialism and the Spanish invention of amalgamation, Hg emissions were no longer only local. Vaporisation during the smelting process yielded gaseous $Hg^0$ and thus long-range transport of Hg occurred, apparent in increasing Hg pollution in the lake situated 225 km away, suggesting that over the past ca. 550 years, emissions of Hg have been transported longer distances.

The use of mercury to extract gold in Ecuador volatises 300 tons of Hg directly into the atmosphere, while 700 tons are discharged in mine tailings, polluting rivers, lakes and soils, every year (González-Carrasco et al. 2011). Given the severe environmental damange caused by mining and its consequent release of Hg into the atmosphere, it is of interest to investigate whether the impact of mining in Ecuador, and more specifically the mining regions surrounding Cajas NP, will leave a pollution signal in the remote lake sediments of Cajas NP.

### 1.1.7 Heavy Metals

Heavy metals have been described as the best characeterised anthropogenic contaminants used for monitoring human activities in history, with their predominant sources from mining,

industrial usage or from petroleum additives (Heim and Schwarzbauer 2013). Natural sources of heavy metals come from soil dust, sea spray, volcanic avtivity and the Earth's crust (Morselli et al. 2003). Metals enter lake systems from various sources. This can be either from runoff and groundwater inflows that scavenge metals from the catchment lithology, or from the atmospheric fallout of metals emitted into the atmosphere. Enhanced anthropogenic activities since the beginning of the Industrial Revolution have accelerated the supply of metals to freshwater systems. Some heavy metals are required by biota in small quantities for physiological processes. However, when concentrations of metals exeed a certain threshold they can become harmful to organisms and even toxic (Smol 2008). Technological advancement throughout history has often been the driving force behind our ability to extract and use metals, and as populations have grown the demand for metals has increased leading to many parts of Earth being extensively mined for metals (Smol 2008). Humans have undoubtedly become the most important factor in the global biogeochemical cycling of trace metals with millions of tons of metals extracted annually from mines or emitted from industry, and their consequent redistributed in the biosphere (Nriagu 1988).

#### 1.1.7.1 Fate of Heavy Metals in the Environment

Metals are deposited on the water surface by wet or dry atmospheric depositional processes or they can enter the lake directly from the catchment (from the weathering of rocks or from previously deposited industrial sources) via runoff. Once they are in the water column they are scavenged by particles and deposited in the sediment (Smol 2008). Sedimentary records of certain heavy metals are considered good qualitative sources of pollution history trends. However, not all metals in a lake's water column will be archived in the sediment. Nriagu and Wong (1986) estimated that just 40 – 60% of pollutant metals in their lake study were actually retained in the sedimentary record. Post-burial remobilization of metals results from diagenesis, e.g. compaction, bioburbation and (in environments with very low sedimentation rates) diffusive migration of dissolved metals as a result of redox-related concentration gradients (Boyle 2001; Outridge et al. 2005; Zan et al. 2011). Elements that are known to undergo redox-mediated migration in lake sediments include As, Co, Cr and V, and it is undecided whether other elements such as Hg, Cd, Cu, Pb and Zn are also affected (Boyle 2001), although Pb is unlikely to ungergo diagenetic degradation (Cooke et al. 2008). Lakes that have low sediment accumulation rates and low organic matter content (ogliotrophic) often favour metal remobilization (Outridge et al. 2005). Diagenetic and post-deposition mobility must be taken into consideration when studying metal records in sediments.

#### 1.1.7.2 Historic Trends in Trace Metals

Natural archives such as lake sediments are useful to document the timing and relative magnitude of atmospheric Pb, Cu, Zn and Cr deposition. Fossil fuel combustion is considered the major source of Hg and Cr, while non-ferrous metal production is known to be the largest source of atmospheric Cu and Zn (Pacyna and Pacyna 2001). The flux of Pb to lake sediments can be used as a proxy for various anthropogenic activites as it has the advantage of not undergoing diagenetic degradation in sediments. Pre-industrial Pb pollution is associated with metallurgical activity at local and regional scales, and since industrialization key anthropogenic sources of Pb are the combustion of leaded gasoline, mining, metallurgical processing and coal burning (Cooke et al. 2008). Similar to mercury emission trends, historical records of environmental lead contamination comes from both global and local sources. With lead, it is possible to distinguish several time steps in

emissions. For example, until ca. 1900 emissions of Pb can be associated with the smelting of indigenous Pb ore and coal burning, as well as an increase in industrial activities at the beginning of the 20th century, until about 1930. Introduction of leaded gasoline in the 1920s led to a period of unchecked global Pb emissions, which led to dramatically increased Pb levels in the atmosphere. It is estimated that in 1983 the global Pb emissions from gasoline reached about 248,000 tons (Eichler et al. 2015). In 1970s there occurred a Pb gasoline phase-out as a result of environmental strategies such as low-leaded and unleaded gasoline, which often leads to a Pb maximum in sediment cores around the 1970s. This facilitated a reduction in global Pb emissions to ca. 90,000 tons by 1995 (Eichler et al. 2015). After this, a decline in Pb values can be observed as a consequence of reducing car-exhaust emissions and the use of unleaded petrol (Heim and Schwarzbauer 2013). This is a trend that can been seen in Fig. 1.8 below.

A study by von Gunten et al. (2009) looked at copper deposition from lake sediments in central Chile. The three lakes included in the study were situated in different regions (close proximity to mines or not), yet all observered a general positive trend in Cu concentrations during the 20th century. This increasing trend is further seen in Fig. 1.8 which depicts the production of copper in Chile, Bolivia and Peru since the 1920s. Lakes impacted by pollution from mining showed a clear trend in Cu deposition. This trend followed Cu production numbers and mining activity from the nearby mines, as well as reductions in Cu deposition as a result of the implementation of technological measures to reduce Cu emissions. Increases in Cu in the lake sediments was additionally attributed to agricultural activities in the region surrounding the lake as Cu compounds were often used to control plant disease in this region. von Gunten et al. (2009) stress that catchment configuration (geochemistry of the bedrock and land use) as well as sediment dynamics (bioturbation, redox changes) are fundamental to understand the suitability of a sediment core as an archive.

Between 1930 and 1985 global production from mines of chromium, copper, and zinc increased by 18, 5 and 4-fold respectively (Nriagu 1988). From the end of the 19th century onward, South America became an important global producer of nonferrous metals (including Zn, Ag, Au, Cu, Pb, Cd). In 2013, Andean countries held approximately 40% of global copper and silver reservers (Eichler et al. 2015). Thus, mining in South America has a high impact on the amount of copper, zinc, lead, chromium and other heavy metals in the environment. The timing of initial and peak smelting activities tends to be asynchronous between different mining centres (Cooke et al. 2008) which suggests a unique history of development for metal pollution depending on the region. Lakes are common across the Andean landscape and thus offer an independent method for local to regional scale reconstruction of heavy metal producing activities, be it mining or industrial, in the 20th century. Data from atmospheric archives for heavy metals are few for South America. There exist some studies of heavy metals from Bolivian ice cores (Eichler et al. 2015; Hong et al. 2004), copper in lake sediments from Chile (von Gunten et al. 2009), trace metal loads in lake sediments from Brazil (Barros de Oliveira et al. 2012) and studies based around mining regions (Cooke et al. 2008; Cooke et al. 2009).

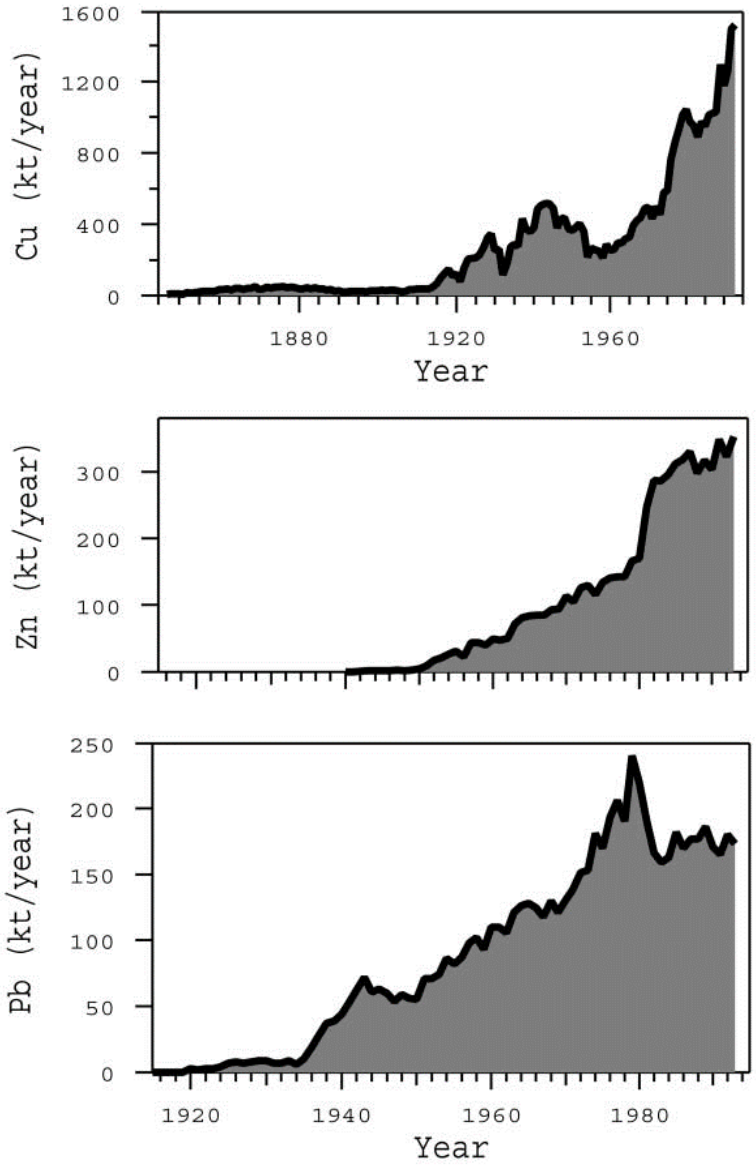


*Fig 1.8. Changes in Cu, Zn and Pb production (kilotons per year) in Chile, Bolivia and Peru since the 1920s (Hong et al. 2004)*

## 1.2 PROJECT AIM

### 1.2.1 Research Questions

The presented master thesis project will focus on reconstructing past (20th century) anthropogenic pollution from the sediments of two remote, high altitude lakes in Cajas National Park, Ecuador. The concentrations and fluxes of PACs, OCs, Hg and heavy metals (Cu, Zn, Pb, Cr) will be analysed in sediment cores from Laguna Llaviuco (low elevation) and Laguna Fondococha (high elevation). Several previous studies have demonstrated that the emisson of these pollutants (PACs, OCs, Hg, and heavy metals) into the environment from anthropogenic sources has sharply increased since the start of the Industrial Revolution. The main objectives and research questions for this Masters thesis are:

1. Can OCs, PACs or Hg signals in the sediment cores be used as event markers to **validate the $^{210}$Pb chronology**?

2. Does **elevation** impact the deposition of PACs, Hg and heavy metals?

3. Does the **depositional flux rate** of atmospherically transported pollution in the lakes of Cajas National Park class them as pristine?

4. Do the **pollution inventories** of PACs and Hg in southern hemisphere sediments follow global (northern hemisphere) patterns?

5. Do the PACs concentration ratios (**molecular diagnostic ratios**) indicate the origin of an air mass?

6. Do the levels of Hg, Pb, Cu, Zn and Cr in the lake sediments indicate pollution from **mining activities**?

### 1.2.2 Project Design

To achieve the objectives of this thesis and to answer the research questions, the MSc Thesis project was designed as follows:

- **SAMPLING:**Sediment cores were collected from Cajas National Park in June 2014 and July 2015. Cores were sampled from the deepest point of each lake using an UWITEC gravity corer with a 6 cm diameter.

- **DATING**: $^{210}$Pb dating of the cores to provide a ca. 150 year chronology for the sediment cores. Peaks in the usage and ban of OCs are to be used as event markers to constrain the $^{210}$Pb models.

- **LABORATORY ANALYSIS:** Laboratory analysis of total organic carbon, nitrogen, OCs, PACs, Hg, in sediment cores from the 2 lakes using digestion/extraction methods and measurement with elemental analyzer (EA), GC-MSD and ICP-MS.

- **CALCULATIONS AND STATISTICS:** Correlation Analysis and Principal Component Analysis of all groups of pollutants will compare and provide information on the relationships between, and origins of, various researched components in each lake.

# CHAPTER 2: STUDY SITE

## 2.1 GEOGRAPHY

### 2.1.1 Ecuador

Ecuador is located in western South America (see Fig. 2.1). The country is divided into three regions: el Oriente to the east, which is mainly dominated by Amazonian rainforest; the central la Sierra, made up of the Andean Cordillera; la Costa to the west, which is Ecuador's coastal region. It is bordered by Peru to the south-east and Colombia to the north-east (CIA, 2014). The country is climatologically interesting and the Andes especially have a very complex spatial precipitation pattern, being influenced by both the Pacific and the Amazon basin in the east (Vuille et al., 2000). However, it is also affected by the weather phenomenon El Niño Southern Oscillation. El Niño is undoubtedly the dominant precipitation signal and can cause landslides and flooding (Vuille et al. 2000). Ecuador is a volcanically active country, with a corridor of volcanoes concentrated along the Andes Mountains. Cotopaxi, located ca. 50 km south of the capital Quito, is the highest active volcano in the world (CIA, 2014).

### 2.1.2 Cajas National Park

The research sites (lakes) are located in Cajas National Park (2° 50′ 0″ S, 79° 10′ 0″ W), situated in the south central Ecuadorian Andes (ca. 4000 m.a.s.l). Cajas National Park (Cajas NP) is located ca. 30 km west from the Andean city of Cuenca in the Province of Azuay (see Fig. 2.1). Cajas NP was acknowledged a national park in 1996, but the areas itself was already declared a National Area of Recreation in 1977, and consists of 285 $km^2$ of protected land. With 1.4 lakes per $km^2$, Caja NP has one of the highest densities of lakes in the world (Girón and Peñaherrera n.d.). The park itself was sculpted by glaciers and boasts moraines, U-shaped valleys and over 800 glacial lakes as part of its landscape (Goodman, 1996, as read from Hansen et al. 2003). Cajas NP has a mountain ecosystem within the watersheds of the rivers Balao and Cañar, which flow into the Pacific Ocean, and the Paute river, which flows to the Atlantic ocean (Girón and Peñaherrera n.d.). Neighboring city Cuenca (population ca. 350'000) obtains about 60% of its drinking water from the lakes of Cajas NP (Michelutti et al. 2015).

There have been some studies conducted in the lakes of Cajas National Park. These have focused on pollen-based climate reconstruction (Colinvaux et al. 1997; Hansen et al. 2003) or the impact of El Nino-Southern Oscillation (Moy et al., 2002; Rodbell et al., 1999), and changing climate in the Andes (Michelutti et al. 2015). However, no studies to date have investigated limnological changes associated with anthropogenic pollution transitions throughout the 20$^{th}$ century in this region of the Andes.

## 2.2 GEOLOGY

### 2.2.1 Ecuador

The Andes exist because the subduction of the Nazca plate under the lighter, continental South American plate. The consequent subduction zone that was formed 60 million years ago during the alpine/cascadic orogenesis is still the cause of active volcanism in the region. Ecuador hosts several volcanic arcs consisting of many active and potentially active volcanoes. Since 1999, four

of these volcanoes have erupted (Parque Nacional Cajas, 2009; Hall et al. 2008). Ecuador is divided by the north-south direction of the Ecuadorian Andes, a 650 km-long and 150 km-wide segment of the great Andean mountain chain. In northern Ecuador, this mountain chain is divided into two parallel mountain ranges, the Western or Cordillera Occidental and the eastern or Cordillera Real (Fig. 2.2). Together, the Cordilleras have an average elevation of 3500 to 4000 m above sea level and are home to most of the volcanoes that summit up to 6000 m. The Cordilleras are separated by a 20 – 30 km-wide, 300 km-long depression known as the InterAndean Valley. Situated around 2000 – 3000 m in elevation, the InterAndean Valley hosts a number of large cities, over 3 million inhabitants and major transportation networks (Hall et al. 2008).

The western and eastern flanks of the Andes descend steeply to the coastal plain in the west, and Amazon basin in the east. The Orient, consisting of the upper Amazon Basin, comprises of a large area of low relief, covered in dense tropical jungle (Hall et al. 2008). Beneath the rainforest lies a series of Tertiary sedimentary fan deposits overlying late Cretaceous marine and subaerial sedimentary units (CODIGEM-BGS, 1993, as read in Hall et al. 2008). Parallel to the eastern flank of the Andes run low mountain ranges ("serranías"), which have been the site of recent active volcanism. Between the western flank of the Andes and the Pacific Ocean lies the coastal plain, a relatively flat region apart from two low mountain ranges along the coastline, underlain by Eocene to Miocene marine sediments and Post-Miocene subaerial sedimentary units. The coastal basin consists of Lake Cretaceous Piñón-Pallatanga oceanic volcanic sequences (Reynaud et al. 1999).

### 2.2.2 Cajas National Park

Cajas National Park sits on the sedimentary and basic to intermediate volcanic deposits of the Cordillera Occidental from the Paleocene-Eocene age (Monzier et al. 1999). Overlying these deposits are rocks that come from the Tarqui formation (IGM, mapa geologico del Ecuador, 1976), which is the most widespread late Miocene volcanic series in southern Ecuador (Monzier et al. 1999). More than 80% of the park area stems from the Tarqui formation, made up of various parent material which can be roughly categorized into three strata: (I) dark and fine-grained andesitic layer, (II) an overlying layer of tuff with a ryolitic to dacitic composition, and (III) an uppermost layer of homogeneous ryolitic medium grained material which forms visible hills within the park. Tillite is a former till that has been compacted and lithified to form a hard sedimentary rock. It can be found around depressions, such as the lakes, in Caja NP and has its origin from the last glacial period. After the last ice age Cajas NP was covered in a coating of ash, most likely coming from the eruption of the Sangay (110 km northeast of Cajas NP) or the Tungurahua (130 km northeast of Cajas NP) volcano around 3000 years ago (Parque Nacional Cajas 2009). As a result of its location, Cajas NP is not at immediate risk of volcanic eruptions, however, volcanic ash (tephra) from various Ecuadorian volcanic eruptions have been found in the lake sediments of Cajas NP (Arcusa 2016; Moy et al. 2002).

The Pleistocene experienced several glacial/interglacial periods during the last ice age (Schubert and Clapperton 1990). Of the most recent glacial extensions in Ecuador, the oldest occurred ca. 13,000 to 16,000 years BP. Following that, there were two further glacial extensions, all of which are responsible for the highly irregular surface of the park, which is cause for the high density of wetlands that exist(Parque Nacional Cajas, 2009). The advance and retreat of glaciers left its footprint in the form of U-shaped valleys, moraines and cirque lakes which are typical for the

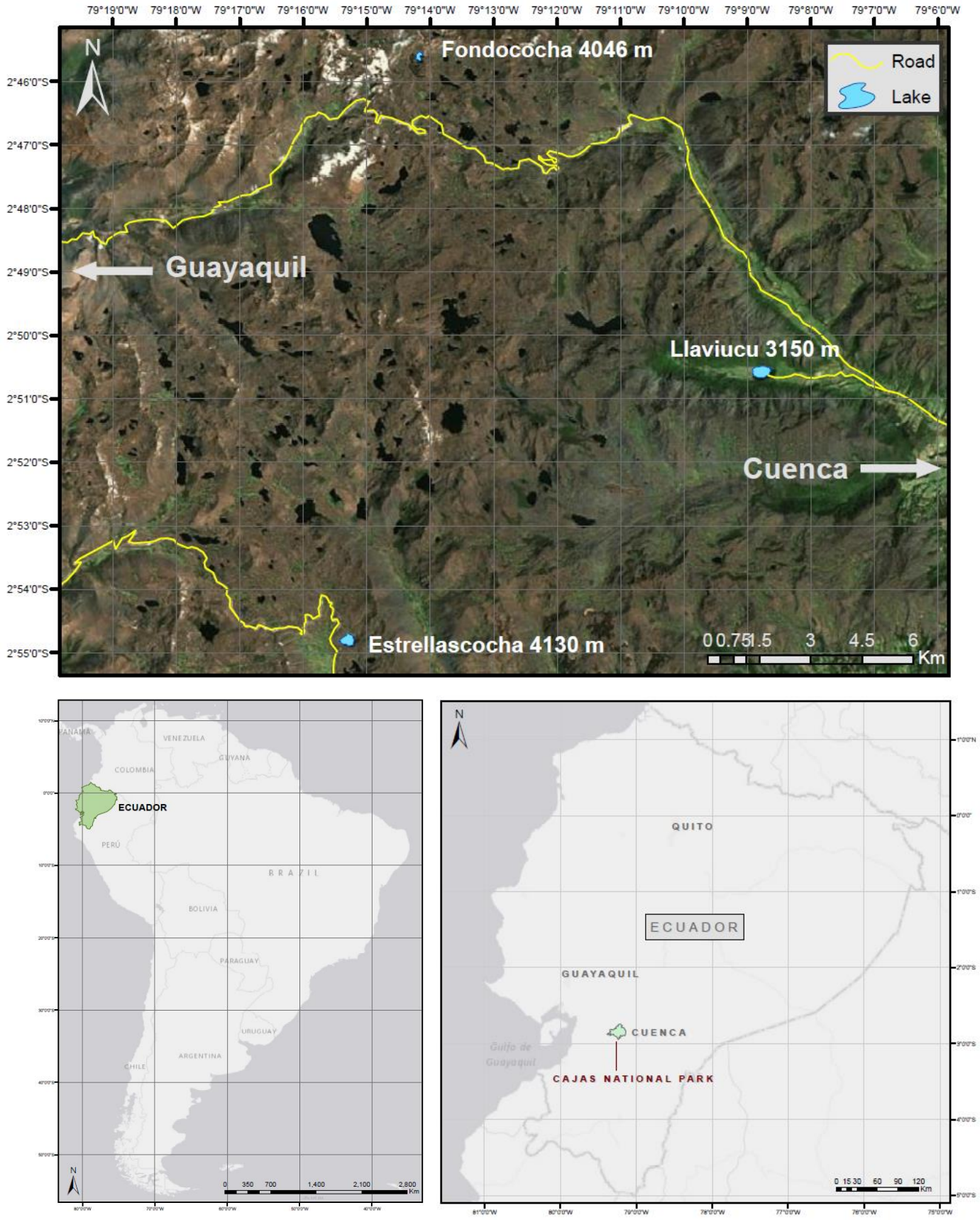


*Fig 2.1. Overview map of the study site. Location of Ecuador in South America (bottom left), location of Cajas National Park in Ecuador (bottom right), and location of the two lakes within Cajas National Park (top)*

landscape found in the park. For example, the Mamamag-Llaviuco transect, a large U-shaped valley that divides two entirely different ecosystems (grassland and forest) within only 1.3 km (Girón and Peñaherrera n.d.).

## 2.3 CLIMATE

### 2.3.1 Ecuador

Climate in the tropical Andes has been highly dynamic over the Holocene and is closely moderated by the Pacific Ocean (Michelutti et al. 2015). The climate of the region is influenced by various and contrasting atmospheric and topographic mechanisms, resulting in complex phenomena and varying levels of variability, and Ecuador is affected by (1) the migration of the Intertropical Convergence Zone (ITCZ); (2) trade winds; (3) the influence of the Hadley and Walker circulations; (4) moisture advection from the Amazon basin and (5) topographic uplift of air masses from the Andes (Morán-Tejeda et al. 2016). However, the main driver for climate variability in the tropical Andes is El Niño Southern Oscillation (ENSO), which is characterised by periodic fluctuations in sea surface temperature (SST) and subsequent anomalies in surface air pressure over the Pacific Ocean. ENSO stimulates inter-annual climate variability with warm (El Niño) and cold (La Niña) phases, and is the cause for extreme climatic events such as floods and droughts. A further important influence on climate variability is the Pacific Decadal Oscillation (PDO), which induces a shift between warm and cool phases at inter-decadal timescales of surface waters in the Pacific Ocean.

Ecuador is climatologically very interesting because of its exposure to the Pacific Ocean and the direct effects of ENSO. The Ecuadorian Andes are temperature-sensitive to the Pacific and precipitation-sensitive to both the Pacific and the Atlantic (Vuille et al. 2000). The Andes act as a barrier and are likely to modify the ENSO signal which Morán-Tejeda et al. (2016) found to have a strong relationship between precipitation variability in Ecuador. The InterAndean valleys situated between the eastern and western Cordillera experience a varying influence of both oceanic and continental air masses (Fig. 2.2) and have two rainy seasons (from February – May and from October – November) and two dry periods, the first of which (June – September) is much more pronounced than the second one in December. The Andes of Ecuador exhibit extreme heterogeneity of spatial and temporal precipitation distribution, and there is no single mechanism of rain formation for any given region (Rollenbeck and Bendix 2011). Several processes interact, for example: small and large scale convective cloud systems, local and regional valley/mountain breeze systems and terrain-lines for moisture transport. All of these processes interact to create highly complex patterns of precipitation in time and space (Rollenbeck and Bendix 2011). In general, air masses tend to lose much of their humidity on the flanks of the Andes, consequently precipitation in the InterAndean valleys is lower (ca. 800 – 1500 mm $yr^{-1}$) (Vuille et al. 2000) but with a long duration (Rollenbeck and Bendix 2011).

### 2.3.2 Cajas National Park

The lakes in Cajas NP are mainly fed by precipitation (Michelutti et al. 2015). Cajas NP receives within 829 and 1343 mm of annual precipitation (Girón and Peñaherrera n.d.). Fog and rain are recurrent above 3000 m, and below an elevation of 3600 m there exists a persistent fog belt on the western side flank of the Andes. Precipitation on the western flank is also much more seasonal. Fig. 2.2 shows the location of L. Llaviuco, a lake in this study, on the eastern flank of the western

Cordillera. Average annual temperatures in Cajas are around 7°C. Temperatures show very little seasonal variation, but have strong diurnal changes, with average daytime temperatures between 12 – 18 °C, and average nighttime temperatures of -8 °C (Hansen et al. 2003). The southern Ecuadorian Andes are subject to warm humid winds of the El Nino current as it is situated in a transition zone between the humid north and the dry south. Clouds from the Pacific Ocean and the Paute river basin in the east rise up to the highest peaks in Cajas NP, leaving very humid conditions in their wake. This humidity eventually finds its way into the soil and to the many streams and lakes in the park (Girón and Peñaherrera n.d.).

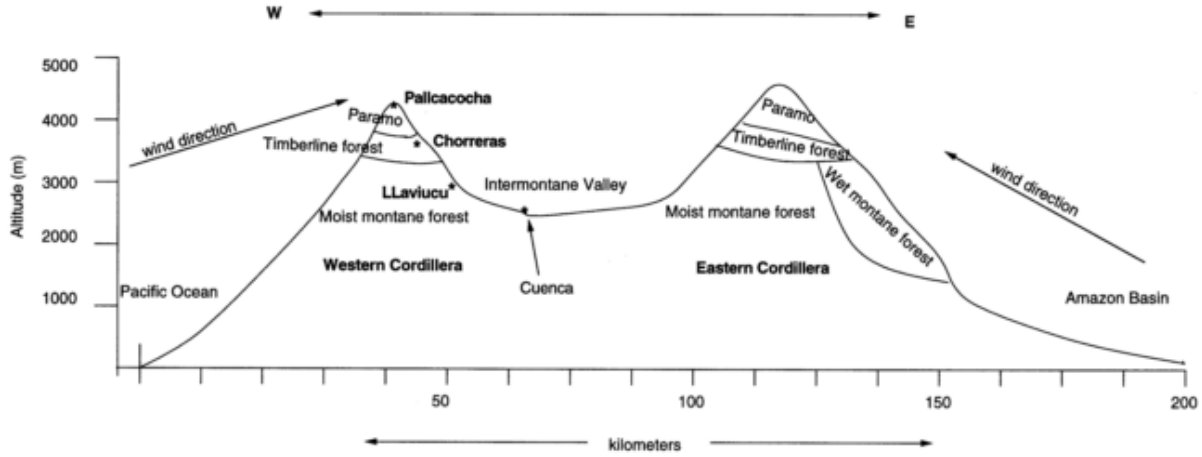


*Fig 2.2. Cross-section of the eastern and western Cordillera showing prevailing wind patterns and vegetation zones at the latitude of Cuenca, Ecuador. Three lakes from CNP are depicted on the diagram, one of which (L. Llaviuco) is part of this study (Hansen et al. 2003)*

## 2.4 VEGETATION & SOIL

### 2.4.1 Vegetation in Cajas

Vegetation types at a given elevation are influenced by several factors: (1) temperature lapse rates and moisture; (2) topographic position (soil depth/moisture); (3) exposure to regional wind patterns and (4) historical and present day land use (Hansen et al. 2003). Páramo is a neotropical alpine ecosystem situated between the continuous forest border (ca. 3500 m asl) and the eternal snow line (ca. 5000 m asl). Páramo coves over 75,000 km$^2$ of the northern Andes of Colombia, Ecuador, Venezuela and Peru, and more than 10 million people in the Andean highlands depend on páramo for their water supply. The high water retention capacity of páramo is attributed to the underlying volcanic soils (Buytaert et al. 2006).

Vegetation in Cajas NP (vegetation zones depicted in Fig. 2.2) consists of páramo above 3500m which continues until the highest peaks at 4300 m (Hansen et al. 2003). The ecological conditions of páramo are as follows: low average temperature, large oscillations of diurnal temperature, more pronounced fluctuations in daily temperature than in annual temperature, frequent night frosts, high humidity (frequent fog) and large differences in irradiation and ex-radiation within twenty-four hours (Parque Nacional Cajas, 2009). Páramo above 4100 m is dominated by low-growing cushion plants (*Azorella*), forbs (*Chrysactinium*) and pteridophytes (*Asplenium*) (fig 2.3). Between 3500 to 4100 m the sub-páramo ecosystem beings where bunch grasses (*Calamagrostis*) and smaller herbaceous plants (e.g. *Bidens, Werneria*) dominate. Occasionally small woody plants

are present (such as *Arcytophyllum*). Poorly drained sites are home to wetland species including *Carex* and *Hyericum*. In Cajas it is also possible to see isolated patches of forest, often dominated by *Polylepis spp* and a few other species (Hansen et al. 2003). 26% of Azuay province is covered with páramo, and it is a particularly important source of water for agriculture and drinking water both within Azuay and for populations living/farming in the western Guayas Province on the coast (Moore 2006). The forest line begins around 3500 m, and this moist montane forest contains trees ranging from about 8 - 12 m in height (species include: *Hedyosmum scabrum, Miconia pustulata, Piper andreanum*). Lower elevations, for example around Laguna Llaviuco (Fig. 2.4), still host the remains of large stands of montane Andean forests that can reach heights of 15 – 20 m (Hansen et al. 2003), however the valley of Llaviuco is now mostly pastoral grassland (Colinvaux et al. 1997).

### 2.4.2 Soils in Cajas

The underlying volcanic soils of the southern páramo of Ecuador are extremely porous, with an open soil structure and very high water retention capabilities. The páramo is described as a global carbon sink. This is because organic carbon sequestration is enhanced by a low redox potential due to high soil water content and a wet climate (Buytaert et al. 2006). Volcanic ash deposits in the soil further increase the organic matter accumulation within the soils, with up to 44% organic carbon content in the dark, humic soils. Buytaert et al. (2006) classified soils from the rio Paute basin, situated in the vicinity of Cajas NP, as Aluandic or Silandic Andosols and with strong Hydric and Histic properties with a low volcanic glass content. A further property of southern Ecuadorian páramo soils is homogeneity. Any differences in soil properties between the two Cordilleras is as a result of climatic differences, rather than variations in the parent material of the bedrock. The water retention of the soils in Cajas NP is 52 million $m^3$, with an annual drainage of 6 million $m^3$ (Girón and Peñaherrera n.d.).

## 2.5 LAKE SYSTEMS OF CAJAS NATIONAL PARK

The majority of lakes in Cajas NP are remote and accessible only by hiking trail. Mining activity has been conducted in the vicinity of Cajas NP (see below), and L. Llaviuco housed a fish hatchery during the 20$^{th}$ century which has closed since the founding of the national park (see below). Of the two lakes investigated in the study, L. Llaviuco has been part of previous studies (Colinvaux et al. 1997; Hansen et al. 2003; Michelutti et al. 2015).

Laguna Fondococha (Fig. 2.3) is a small (34,109 $m^2$) open system lake with a high (4046 m) elevation and a shallow depth of 9.9 m. Laguna Llaviuco (Fig. 2.4) is an open system lake and has an elevation of 3150 m, a depth of 16.5 m, and an area of 142,512 $m^2$. Both Laguna Llaviuco and Fondococha are situated on the eastern flank of the western Cordillera. L. Llaviuco was formed by the damming of a terminal moraine, and sits within the moist montane forest vegetation zone (see Fig. 2.2) (Hansen et al. 2003). High altitude L. Fondococha sits within the páramo to sub-páramo grassland ecosystems and is oligotophic with very low productivity, and accordingly receives very little terrestrial vegetation input. L. Llaviuco, as a result of its surrounding vegetation, is mesotrophic with a higher terrestrial vegetation input (ECOLAP & MAE, 2007).

*Fig 2.3. Laguna Fondococha (Wojciech Tylmann, 2015)*

*Fig 2.4. Laguna Llaviuco (Wojciech Tylmann, 2015)*

## 2.6 ANTHROPOGENIC IMPACTS

### 2.6.1 Industry and Agriculture in Ecuador

Agriculture was the main stay of Ecuadors Economy in the past. Manufacturing, petroleum, mining industries and services have grown in the past 30 years and become a major part of Ecuador's economy. The agricultural sector currently accounts for about 14% of the GDP and 30% of the labor force in Ecuador. Bananas are its largest export, closely following this, coffee, cocoa and sugar cane are the next big agricultural sectors. Large-scale industry was first introduced in Ecuador in the 1950s (Nations Encyclopedia, 2016). It currently makes up ca. 36% of the GDP and about 25% of the total labor force. Principal industrial exports include petroleum, shrimp and metals from mining, with oil coming in as Ecuador's top export. Ecuador is a member of OPEC (Oil and Petroleum Exporting Countries) since the 1970s and exports ca. 60% of the oil it produces, most of which comes from the Amazon basin. Export of primary commodities (agricultural/fishing, oil and precious metals) is a major component of Ecuador's Economy. In 1998 a drastic drop in oil prices coincided with a deadly shrimp virus that caused Ecuador's economy to severely shrink in 1999 (Nations Encyclopedia, 2016).

### 2.6.2 Mining Around Cajas National Park

Ecuador has abundant deposits of gold, silver, lead, copper and zinc (Nations Encyclopedia, 2016). Artisanal and small-scale gold mining in Ecuador is an important economic activity and the main source of Hg pollution (González-Carrasco et al. 2011). Globally, 10 – 15 million artisanal gold miners release on average 640 – 1350 tons of mercury into the environment in the gold extraction process, accounting Hg in the use of artisanal gold mining one-third of all global anthropogenic Hg consumption (González-Carrasco et al. 2011). Mining exists in the region of Cajas NP to exploit deposits of gold and silver which were discovered between 1994 and 1997. Fig. 2.5 depicts active mining sites around Cajas NP. The province of Azuay, within which Cajas NP is situated, is part of a cluster of six provinces in south and south-central Ecuador which are major players in metal mining development. The largest concentration of mining industries is grouped around the ca. 10,000 ha Quimsacocha Project in the Western Cordillera of the Andes, about 40 km southwest of Cuenca. Adjacent to Quimsacocha, are two further mineral concession covering an area over 45,000 ha (Moore 2006).

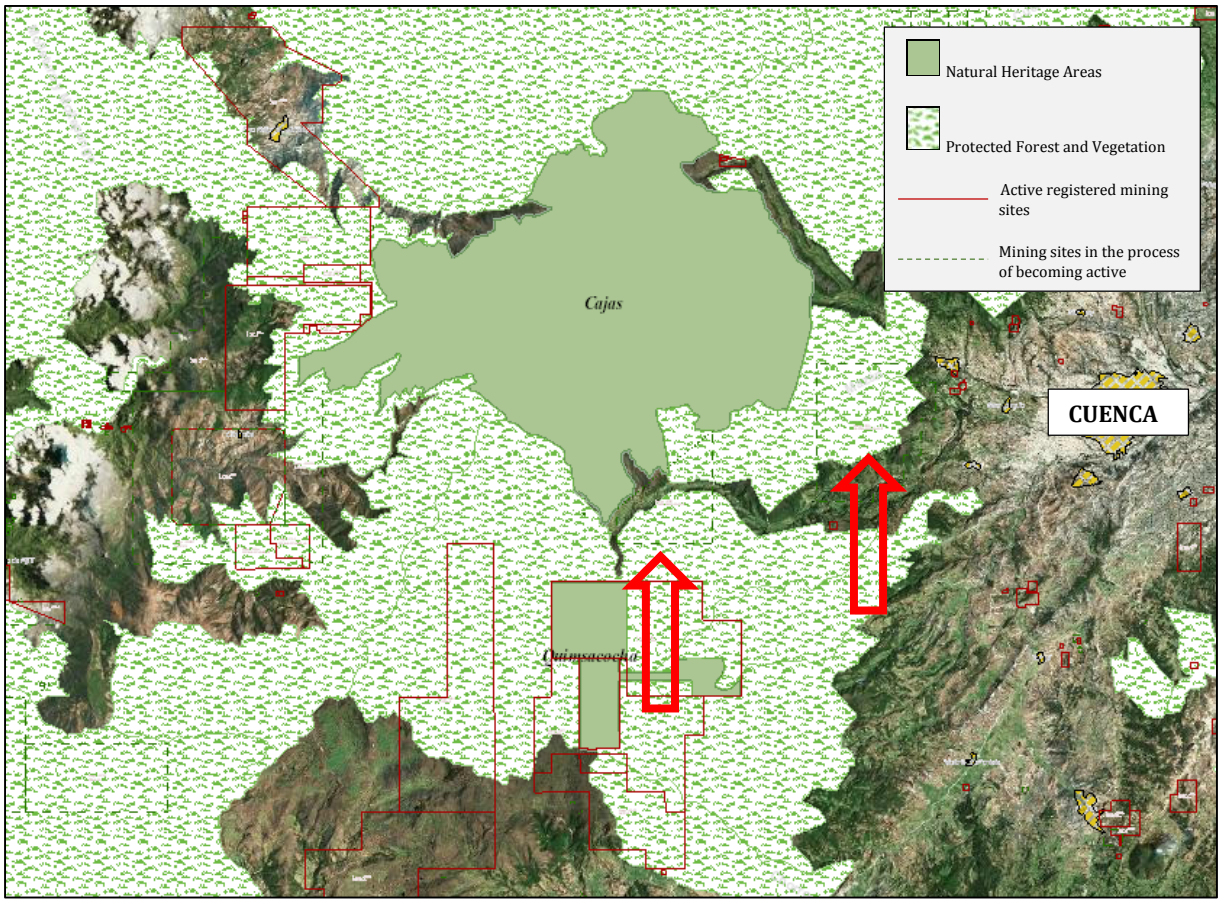


*Fig 2.5. Cajas National Park and surrounding protected forest/vegetation, the red arrows indicate two regions in the buffer zone of the national park which are in the process of becoming mining sites. Red boxes indicate active registered mining sites around Cajas NP (modified from the National Mining Authority (ARCOM).*

Until 2009, the mining industry exploited up to 29.7% of the area of Macizo del Cajas, a greater páramo area which includes Cajas NP and its buffer zone (Velástegui 2010). A further cluster of mining industy is situated on the western flank of the Western Cordillera and borders Cajas NP (Fig. 2.5). The gold-silver Río Blanco Project, covering 5800 ha, borders Cajas NP in the rural parish of Molleturo, and is located in the transition zone of the national park. The project was

originally contracted to the Canadian firm International Mining Corporation (IMC) in 1999. Copper Mesa Mining, covering over 3000 ha with its Chaucha Project, and AndeanGold which hopes to expand to cover 48,000 ha of mineral concessions in Molleturo, are both situated nearby Cajas. The Río Blanco Project is estimated to contain 605,000 ounces of gold and 4.30 million ounces of silver. There are four further mineral concessions which overlap with the Molleturo-Mollepungo Protected Forest and are within the buffer zone of Cajas NP (Fig. 2.5) (Moore 2006). In 2008 a constitutional mining mandate was passed in Ecuador that should have revoked IMC's contract as the mining zone overlaps with protected forest and the buffer zone of Cajas. However, despite the mandate, mining has continued as a result of a pro-mining government (Environmental Justice Atlas, 2014).

### 2.6.3 Fishing Industry in Cajas National Park

Around 1951 there began a practice in Ecuador of stocking high Andean lakes with rainbow trout (Bondad-Reantaso 2007). Laguna Llaviuco was not immune to this practice and from 1978 to 1998 there was an intensive fishing industry evolving within the lake. In these two decades it is estimated that 15.6 million fish were raised in cages within L. Llaviuco. Concerns raised on the quality of the water after such intensive farming resulted in the monitoring of L. Llaviuco from 1995 onwards by ETAPA (Barros and Carrasco 2006). In 1998 ETAPA had found a deterioration of the water quality of the lake which resulted in the banning of the fishery. Fish cages directly release large amounts of nutrient-rich waste such as feces, unconsumed feed, and metabolic products into the water and underlying sediments. If concentrations become high enough, this can drastically alter the quality of the water (Temporetti et al. 2001). In L. Llaviuco, the fishery had caused a change in the lakes' trophic state from mesotrophic to eutrophic over the course of two decades (Barros and Carrasco 2006). As a result of L. Llaviuco's high turnover rate of 17 days, the lake was able to restore itself to an oligo-mesotrophic state by the 2000s.

### 2.6.4 Human Activity in Cajas

There have been 28 archaeological sites recorded within the limits of Cajas NP and its immediate surroundings, all dating from the pre-Incan Era to the Incan Era (ca. 1800 BC to 1532 AD). During this time and subsequent colonial and republican Eras, the park was mostly used as a trade route to connect Andean towns such as Cuenca with coastal cities such as Guayaquil (Girón and Peñaherrera n.d.). Nowadays, there are no communities living within the park's borders, however, the busy Cuenca-Molleturo-Naranjal highway passes from east to west across 15 km of páramo ecosystem in the northern section of Cajas NP (see Fig. 2.1). The road is over 40 years old and has been reconstructed several times. Improvements in road infrastructure over the past 10 years have resulted in an increase in vehicular traffic through the park (Rodríguez 2008).

Since the founding of the national park in 1977, there has been little human activity occurring in Cajas, thus reinforcing the hypothesis that the lakes should be pristine. Boats are prohibited to the public, and fishing is only permitted from the lake shore. Tourism in the park includes hiking and horse trails which lead to many of the lakes. There are no settlements/development within the catchments, with the exception of L. Llaviuco, which has small dirt road leading to it along with two small buildings (one abandoned) which are seldom used (Michelutti et al. 2015). Around L. Llaviuco there is evidence of fire regimes, grazing and deforestation in spite of park restrictions (Sarmiento 2002). As a result of this deforestation, there are only fragments of the moist Andean forest left surrounding L. Llaviuco, as most of the valley is now pastoral grassland. The presence

of an Inca road in the valley would suggest that this area has infact been managed as pasture since prehistoric times (Colinvaux et al. 1997). Modern communities that surround Cajas National Park still use the high elevation areas for grazing cattel, despite this being technically forbidden since the establishment of the park. Locals continue the tradition of burning the paramo in order to stimulate regrowth of grasses for fodder for their cattle (Hansen et al. 2003).

# CHAPTER 3: MATERIALS AND METHODS

## 3.1 FIELDWORK

Fieldwork for the sampling of cores from the lakes in NP Cajas (Fig. 2.1) took place in July 2014 and 2015. Cores were retrieved from the deepest point of each lake using an UWITEC gravity corer with a 6 cm diameter. Sediment cores from L. Llaviucu and L. Fondococha were retrieved in July 2014, and a second set of sediment cores were retrieved from the above mentioned lakes in July 2015. The cores were sealed and stored for transport back to Switzerland, where they were analysed in the laboratories of the Geography and Geology Institutes of the University of Bern. Bathymetric maps of both lakes with the specific coring locations within the lake are shown in Fig. 3.1 and 3.2. Further details on the lakes are found in section 2.5 and Table 3.1.

*Table 3.1. Specific coring location and depths of cores used in this study.*

| Lake | Core Name | Location | Water Depth (m) | Core Length (m) |
|---|---|---|---|---|
| **FONDOCOCHA** | FON-14-1 | 2°45'36.6"S 79°14'11.1"W | 9.8 | 1.37 |
| | FON-14-2 | 2°45'36.6"S 79°14'11.1"W | 9.8 | 1.25 |
| **LLAVIUCU** | LLA-14-1 | 2°50'33.84"S 79° 8'43.15"W | 15 | 1.12 |
| | LLA-14-2 | 2°50'33.84"S 79° 8'43.15"W | 15 | 1.15 |

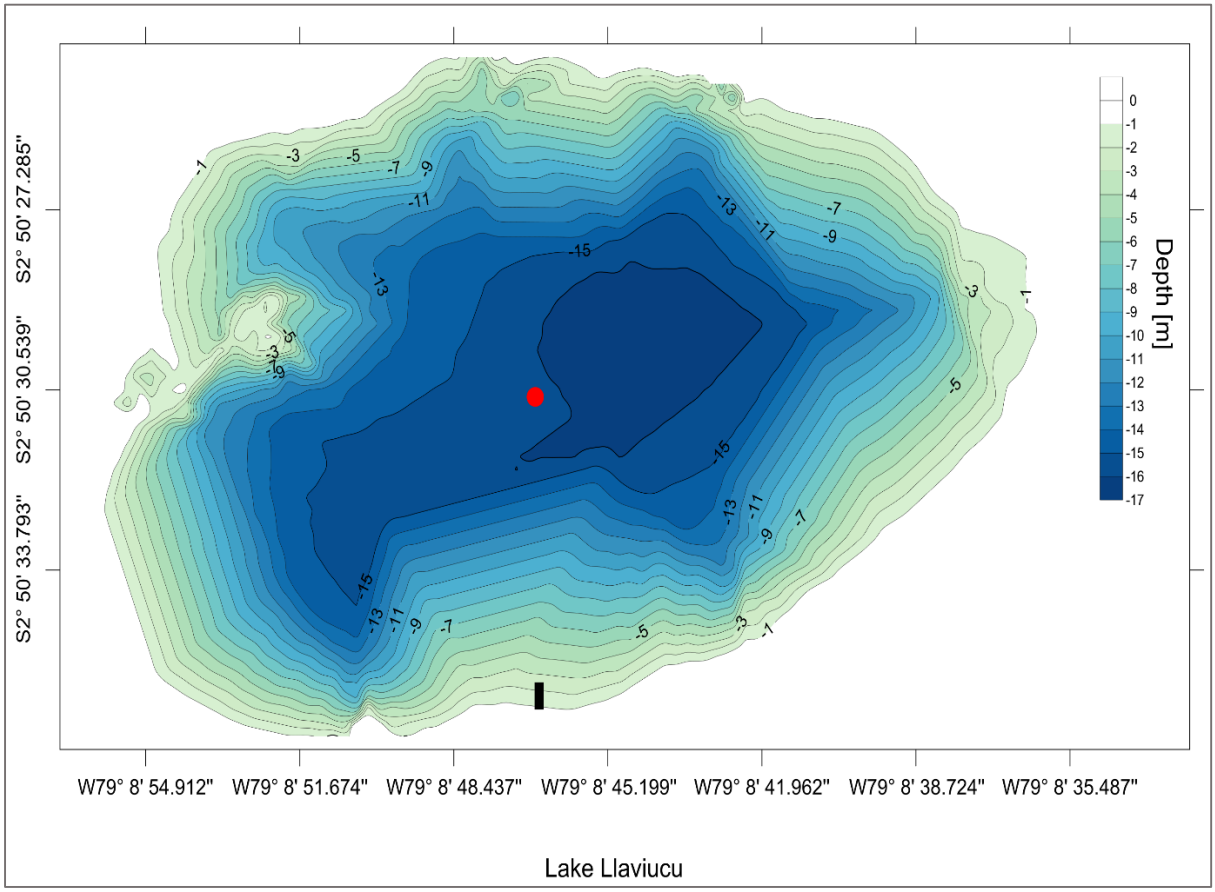


*Fig 3.1 Bathymetric map of Laguna Llaviuco. The red dot indicates the specific coring location, the black line indicates the location where the boat entered the lake (created by Pablo Mosquera, ETAPA).*

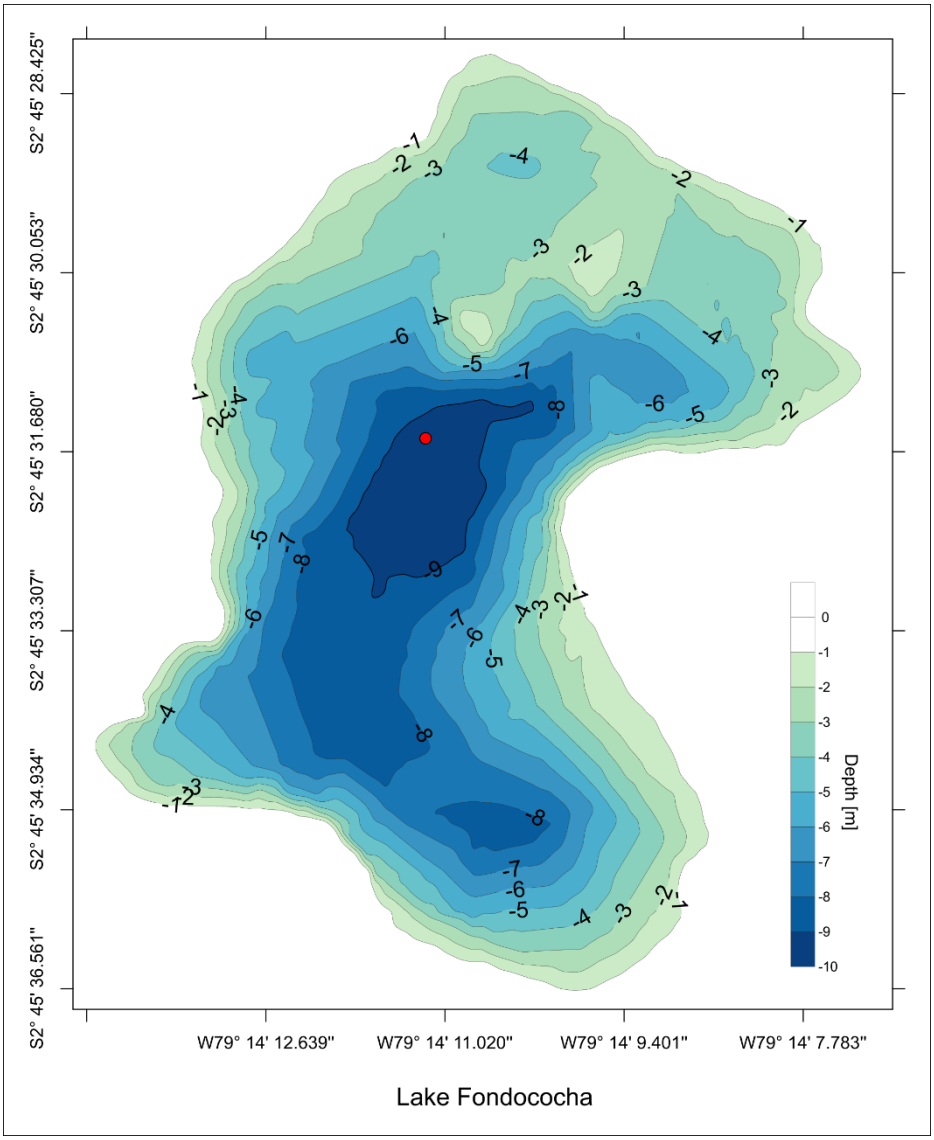


*Fig 3.2 Bathymetric map of Laguna Fondococha. The red dot indicates the specific coring location (created by Pablo Mosquera, ETAPA).*

## 3.2 CORE ANALYSIS

The Paleolimnology Research Group at the Institute of Geography, University of Bern (M. Grosjean) provides a high level of expertise in the analysis of lake sediments for high quality climate and environmental reconstructions. In a first step, unopened cores were scanned using a Multi-Sensor Core Logger (MSCL), after which the cores were opened, wrapped in plastic film and stored in a cold room at 4 ° C.

### 3.2.1 Core Description

Each sediment core underwent a detailed stratigraphic and sedimentological description once it had been opened. The description was based on the classification scheme of Schnurrenberger et al. (2003). This scheme is based on the observation of visual macroscopic features. Four criteria were used to describe the sediment cores.

1. The core is divided into units. These units are based on either core colour, which was identified using a Standard Munsell soil colour chart (Munsell Colour Company 1994), or by structural changes within the core.
2. Lithology is examined. The sediment is classed as either gravel, sand/detrital, silt/clay/detrital, carbonate, evaporates, peat/organic or volcanic ash. Hydrochloric acid (HCl) was added to sediment samples at regular intervals along the core as a test for the presence of carbonates.
3. The contact of different units is looked at. The contact could be classed at sharp (less than 2 mm), gradual (between 2 and 10 mm), wavy or erosional.
4. The texture of the sediment is the last criterion. This looks at whether the core is laminated, banded, massif/granular, porphyric, platy, 'mottled flames', graded, reworked or bioturbated.

### 3.2.2 Sediment Dating

#### 3.2.2.1 $^{210}$Pb Radiometric Data

In order to interpret pollution signals in the sediment cores, an accurate and reliable sediment chronology is needed. Lead-210 ($^{210}$Pb) dating is a highly resolved (up to annual resolution) and precise method of dating sediment cores. $^{210}$Pb is a natural radioactive isotope of lead and has a short half-life of only 22.3 years. Because of its half-life, $^{210}$Pb can be used only to date sediments back to approximately 150 years (Cohen 2003). It is therefore justified to use $^{210}$Pb dating for this study as the last 150 years encompasses the period of interest for a 20$^{th}$ century pollution history reconstruction, namely, it is applicable to the environmental changes that occur as a result of industrialization. Goldberg (1963, from Putyrskaya et al., 2015b) was the first to use the radioactive decay of $^{210}$Pb to date ice from a glacier. Since then, the method was refined by Krishnaswamy et al. (1971) who applied it to lake sediments, resulting in various empirical models being developed over the following years that assumed deposition rate, sedimentation rate and other processes that effect $^{210}$Pb behavior in the environment. Three different age models were tested in order to discover which one produced the most accurate $^{210}$Pb based chronology. These were: (1) CRS model (Constant Rate of Supply), (2) CIC model (Constant Initial Concentration) and (3) SIT model (Sediment Isotope Tomography).

#### 3.2.2.2 $^{210}$Pb Radionuclide-Dating

The $^{210}$Pb radionuclide originates naturally from the $^{226}$Ra (Radium-226, half-life 1600 years) decay chain, which in turn is originally derived from the $^{238}$U (Uranium-238, half-life 4.5 $10^9$ years) decay series (Fig. 3.3) (Putyrskaya et al., 2015). A disequilibrium occurs between $^{210}$Pb and its parent isotope $^{226}$Ra as a result of the diffusion of trace amounts of $^{226}$Ra, which is naturally present in bedrock and soils. $^{226}$Ra decays to the gaseous isotope $^{222}$Rn (Radon-222) and escapes to the atmosphere where it rapidly decays to $^{210}$Pb and is consequently removed from the atmosphere via precipitation or dry deposition as it is deposited onto land surfaces or into lakes/oceans. $^{210}$Pb that falls directly onto a lake is scavenged from the water column and deposited on the bed of the lake in the sediments (Appleby 2001; Cohen 2003).

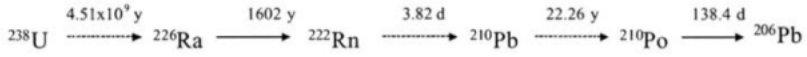


*Fig 3.3. $^{238}$U decay series depicting the foremost radionuclides concerned with producing $^{210}$Pb, together with their radioactive half-lives (Appleby 2001).*

It is usually assumed that atmospheric fallout of $^{210}$Pb at any given site is constant. The flux, however, can vary spatially and this is dependent on factors such as rainfall and geographic location (Appleby 2008). $^{210}$Pb that has been transported to the lake bed becomes incorporated in the sedimentary record, and as older sediments get buried, their unsupported $^{210}$Pb then acts as a natural clock by recording the time since it was originally deposited on the bed of the lake (Appleby 2008). The total $^{210}$Pb activity in sediments is twofold: *supported* $^{210}$Pb, which is derived from the in situ decay of the parent radionuclide $^{226}$Ra; and *unsupported* $^{210}$Pb, which is delivered to the lake sediment from the lake surface and the surrounding catchment by atmospheric deposition. Unsupported $^{210}$Pb is determined by subtracting supported activity from total activity, and it is the unsupported $^{210}$Pb that is used to determine age and sedimentation rate (Putyrskaya et al. 2015). The supply of $^{210}$Pb to sediments on the bed of the lake is influenced by various factors, namely: the atmospheric flux; the rate of transport from the catchment; the water residence time; the fraction of the radionuclide attached to settling particles; the mean particle settling velocity; post-depositional transport processes (e.g. mixing). Atmospheric flux is the most significant factor influencing $^{210}$Pb supply, and understanding processes which cause deviations in the atmospheric flux can be beneficial in resolving dating issues. For example, higher $^{210}$Pb supply rates could be caused by catchment inputs or sediment forcing, whereas low $^{210}$Pb supply rates are indicative of sediment erosion (Appleby 2008).

#### 3.2.2.3 Measurement Method

Sediment cores from Laguna Fondococha and Laguna Llaviuco were sampled for $^{137}$Cs, $^{226}$Ra and $^{210}$Pb. The top 20 – 30 cm for each core was sub-sampled as it is expected that this section will encompass the lead-210 lifespan. Samples were taken at a resolution of 0.5 cm, weighed (wet), frozen, freeze-dried, re-weighed (dry) and then homogenized and submitted to Dr. Wojeciech Tylmann at the Uniwersytet Gdański, Poland, for $^{210}$Pb measurments. The samples were stored for a minimum of three weeks in glass measurement containers to obtain secular equilibrium of radon and its short-lived daughter products with $^{226}$Ra. $^{137}$Cs and $^{226}$Ra activity was determined with gamma-ray spectrometry. Because of the relatively low mass of sediment available (and thus high uncertainty of results), activity of total $^{210}$Pb was determined indirectly by measuring its daughter product $^{210}$Po (half-life 138 days) using an alpha spectrometry. A detailed description of the procedure can be found in Tylmann et al. (2016).

#### 3.2.2.4 Constraining the $^{210}$Pb Model

It is rare to find a perfect exponential decrease in the $^{210}$Pb activity concentration with depth. This is only observed if the flux of unsupported $^{210}$Pb to the sediment surface along with the sediment accumulation is constant and no mixing or redistribution processes have occurred (Putyrskaya et al. 2015). Thus, situations arise where none of the afore mentioned assumptions are valid, and fluctuations can be seen in the vertical $^{210}$Pb sediment profile. This can be caused by surficial mixing of the sediment via physical (unstable sediments, chemical remobilization) or biological processes (bioturbation), or by variations in the $^{210}$Pb supply (Appleby 2001). Factors which can complicate or distort the CRS model, for example, are short water residence time, bioturbation, discontinuous or disturbed sedimentation and sediment resuspension (Oldfield and Appleby 1984). Because of this, it is important to validate the $^{210}$Pb dates by using an independent chronological marker. The artificial radionuclide $^{137}$Cs (Cesium-137) is often utilized as an independent dating technique in sediment records. Global atmospheric fallout from high-yield thermonuclear weapons testing began in 1954 and peaked in 1963, shortly after a test-ban treaty

was implemented. Furthermore, fallout from the Chernobyl reactor accident has been widely utilized to identify the depth at 1986. If there is a good qualitative record of these atmospheric fallout events available in the sediment, these specific events can be used to validate the $^{210}$Pb dating (Appleby 2001). Specific anthropogenic markers preserved in the lake sediments can also be used as independent event markers. The chemical signature of certain organic compounds, such as insecticides or other organochlorides, can be used to determine independent dates against which to assess the $^{210}$Pb chronology. For example, the insecticide DDT was first used in Ecuador in 1946 (Saenz Vera 1953). Thus, sediments post-1946 are expected to contain a DDT signal. For further examples see Table 1.5. Peaks and declines in the sediment profiles of mercury and lead are often associated with mid-19$^{th}$ century industrialization and can also be used as markers to constrain the $^{210}$Pb models (Smol 2008).

#### 3.2.2.5 CIC Model

The Constant Initial Concentration model has the assumption of a constant initial concentration of $^{210}$Pb from the atmosphere to the top bed of the lake's sediments (Krishnaswamy et al. 1971). $^{210}$Pb activity varies directly in proportion to the sedimentation rate (Appleby 2008). The model follows the assumption that no post-depositional migration of $^{210}$Pb has ensued (Cohen 2003; Putyrskaya et al. 2015), and thus calculates the age of the sediment *t(x)* in years using the following formula:

$$t(x) = \frac{1}{\lambda} \cdot \ln \frac{C(0)}{C(x)},$$

*Fig 3.4. Formula to calculate age in years for CIC model (from Putyrskaya et al., 2015)*

In Fig. 3.4, $\lambda$ is the radioactive decay constant of $^{210}$Pb in yr$^{-1}$, *C(0)* and *C(x)* are the initial and present activity concentrations of the unsupported $^{210}$Pb in the layer at depth *x* in Bq g$^{-1}$. In order to eliminate the influence of sediment compaction with depth, the unsupported $^{210}$Pb activity concentration is plotted over the cumulative weight. While the CIC model is simple, this method is unequivocal for lakes that have a constant sedimentation rate and/or the core site has been impacted, e.g. by an episodic slump event or changes in the pattern of sediment forcing (Appleby 2008; Cohen 2003; Smol 2008).

#### 3.2.2.6 CRS Model

The CRS model is based on the "constant rate of supply" of unsupported $^{210}$Pb. The methodology was developed by Krishnaswamy et al. (1971) in the original paper for dating lake sediments using $^{210}$Pb and there are three main assumptions that the model is based upon: (1) the rate of unsupported $^{210}$Pb deposited from the atmosphere is constant; (2) $^{210}$Pb in fresh water is rapidly removed from solution to particulate matter, thus ensuring that unsupported $^{210}$Pb activity in lake sediments is originating from atmospheric fallout; (3) initial $^{210}$Pb activity at the bed of the lake is not redistributed due to post-depositional processes and decays exponentially over time (Appleby 2001). The CRS model was developed by Appleby & Oldfield (1978) and assumes deposition of the same amount of unsupported $^{210}$Pb on sediments per time interval and a variable sedimentation rate (Putyrskaya et al. 2015), which results in lower $^{210}$Pb concentration when sedimentation rates are higher (Cohen 2003). When calculating the sediment age at a certain depth, the cumulative unsupported $^{210}$Pb below that depth must be compared to the total unsupported $^{210}$Pb in the core. To calculate age vs. depth the following formula can be used:

$$t(x) = \frac{1}{\lambda} \cdot \ln \frac{C_r(0)}{C_r(x)} = \frac{1}{\lambda} \cdot \ln \frac{\int_0^{\infty} \rho_b(x) C(x) \mathrm{d}x}{\int_x^{\infty} \rho_b(x) C(x) \mathrm{d}x},$$

*Fig 3.5. Formula to calculate age vs. depth for the CRS model (from Putyrskaya et al., 2015)*

In Fig. 3.5, *Cr(0)* represents the total cumulated unsupported $^{210}$Pb in the sediment core in Bq cm$^{-2}$. *Cr(x)* is the residual (cumulated) unsupported $^{210}$Pb in the sediment below the depth *x* in Bq cm$^{-2}$; $\lambda$ is the radioactive decay constant for $^{210}$Pb in yr$^{-1}$; $\rho_b(x)$ is the bulk density of sediments in g cm$^{-3}$; *C(x)* is the activity concentration of the unsupported $^{210}$Pb at depth x in Bq g$^{-1}$. At sites where sedimentation rates vary significantly, the CRS model is proved to be a reliable option when coupled with a chronostratigraphic marker as a reference point (Appleby 2008).

#### 3.2.2.7 SIT Model

The Sediment Isotope Tomography method was developed for more complex cases where the sedimentation rate and fluxes of unsupported $^{210}$Pb vary over time (Carroll and Abraham 1996; Putyrskaya et al. 2015). The method uses a frequentative approach to determine model parameters that mimic the radionuclide concentration with the depth profile. Further, the model does not require *a priori* knowledge for the exact cause of variation in radionuclide concentration with depth (Carroll and Abraham 1996). The vertical distribution of $^{210}$Pb activity concentration *C(x)* with depth *x* in a sediment profile is shown as:

$$C(x) = C(0)\exp\left[-\lambda \cdot x_{\max} \bar{S}\left(\underbrace{z + \sum_{n=1}^{N} \frac{a_n}{n\pi} \sin\left(\frac{n\pi x}{x_{\max}}\right)}_{\text{Sedimentation term}}\right) + \underbrace{\left(\sum_{n=1}^{N} \frac{b_n}{n\pi}\left(1 - \cos\left(\frac{n\pi x}{x_{\max}}\right)\right)\right)}_{\text{Source term}}\right],$$

*Fig 3.6. Formula for calculation of $^{210}$Pb activity concentration with depth (from Putyrskaya et al., 2015)*

where *C(x)* is the unsupported $^{210}$Pb activity concentration at depth *x* in Bq cm$^{-3}$; *C(0)* is the initial unsupported $^{210}$Pb activity concentration in Bq cm$^{-3}$; $x_{max}$ is the greatest depth of the measurement in cm; *S(x)* is slowness in cm yr $^{-1}$:($S = 1/v$), where *v* is the sedimentation speed in cm yr$^{-1}$; $\bar{S}$ is the average slowness; *z* is a relative depth: $z=x/x_{max}$; $a_n$ and $b_n$ are the unknown Fourier series coefficients. The age *t(x)* in year in this case is determined as:

$$t(x) = x_{\max} \cdot \bar{S}\left[z + \sum_{n=1}^{N} \frac{a_n}{n\pi} \sin(n\pi z)\right].$$

*Fig 3.7. Formula for calculation of age in years (from Putyrskaya et al., 2015)*

The SIT model is made up of two main components. Firstly, the sedimentation term and, secondly, the source term (see Fig. 3.6). The sedimentation term (represented by Fourier sine series) describes non-exponential changes in unsupported $^{210}$Pb activity concentration as a result of sedimentation processes. The source term (represented by a Fourier cosine series) shows changes resulting from varying unsupported $^{210}$Pb input into the sediment. The SIT model is able to estimate both the $^{210}$Pb supply during sediment deposition and the systems properties by adding the Fourier series function to the data, which means that no *a priori* system data is required. No need for any required assumptions on sedimentation regime is a big advantage of the SIT method (Putyrskaya et al. 2015). Results from the SIT model must always be constrained

with independent event markers (Carroll and Abraham 1996). As with all models, the SIT has its limitations. The model cannot always be used to reconstruct sediment accumulation history, and most importantly, the model is invalid if sediments have been subject to mixing (physical or biological) over short time scales which are relative to sediment accumulation rates as this erases the radioactive decay signal within the sediment (Carroll and Abraham 1996).

### 3.2.3 Elemental Carbon and Nitrogen

Total organic carbon (TOC) and total nitrogen (TN) concentrations were measured in each sample from each lake. TOC is an indicator for lake productivity, and TOC measured in the sediment samples is considered to be proportional to the organic matter in the lake sediments (Cohen 2003). TOC and TN values are used to calculate C/N ratios. The C/N ratio is an indicator of the origin of the TOC. C/N ratios that have high ratios (>20) indicate allochthonous sources of TOC, such as vascular plants (grasses, trees, shrubs), whereas a ratio <10 is indicative of autochthonous sources of TOC (e.g. non-vascular aquatic plants). Values between 10 and 20 indicate a mixture between the two sources (Meyers and Teranes 2001;Meyers 1994). The concentrations of TOC and TN in sediments were determined with an Elementar Analyser (Vario EL III, Elementar Anlysensystem, Hanau, Germany)

### 3.2.4 Pollution Reconstruction

#### 3.2.4.1 Polycyclic Aromatic and Organochlorine Compounds

The top ca. 15 cm of each sediment core half was subsampled at 0.5 cm resolution. The samples were freeze-dried and stored in a desiccator until analysis. Sediments were anaylsed for 26 polycyclic aromatic hydrocarbons (PAHs), 15 oxygenated PAHs (OPAHs), 4 azaarenes (AZAs) and 22 organochlorine compounds (OCs). The methods applied for the analysis of target compounds (Tables A.1.1, A.1.2, A.1.3 in Annex 1) are slight modifications of previous methods published by Bandowe and Wilcke (2010),

**Extraction of Samples**

Samples were prepared for the Accelerated Solvent Extractor (ASE), as seen in Fig. 3.8. A filter was placed at the bottom of the ASE cell and about 1/3 of the cell was filled with inert bulk and drying material (Isolute HM-N, Biotage, Upsalla, Sweden). About 1 g of crushed (for homogenization) sample material was mixed with bulk HM-N and transfered into each cell. Samples were then spiked with 50 µl of 7-deuterated PAHs mix (10 µg/ml each of naphthalene-D8, acenaphthene-D8, phenanthrene-D10, pyrene-D10, chrysene-12, perylene-D12 and benzo[ghi]perylene), 40 µl of 2-deuterated-OPAH (10 µg/ml benzophenone-D5, 9,10-anthraquinone-D8, 40 µl of Carbazole-$D_8$ (10 µg/ml) and 50 µL of deuterated-organochlorine mix (5 µg/ml each of alpha-HCH-D6, 4,4-DDT-D8, Endosulfan-D4) which serve as internal standards for the quantification of PAHs, OPAHs, AZAs and OCs, respectively. These deuterated compounds have similar physico-chemical properties as the compounds under investigation but are not naturally present in samples. The extra space in each cell was filled with bulk "HM-N", another filter was added on top, and the cells were sealed shut. For each sequence of samples prepared, 3 blanks (made of Isolute HM-N) were included.

Each sample, blank and reference material filled into the ASE extraction cell (Fig. 3.8) was extracted twice by pressurized liquid extraction (Björklund et al. 2000) using an ASE-200 (Dionex,

Sunnyvale, CA, USA). The first extraction uses dichloromethane (HPLC grade) and the second extraction was with acetone: dichloromethane: 1% trifluoroacetic acid (250: 125: 1% v/v/v). The 1 % trifluoracetic acid was prepared in acetonitrile as specified by US-EPA method 3545A (US-EPA 2007). For each extraction cycle the ASE was operated with the following instrumental parameters (pressure: 14 MPa, temperature: 120°, heating time: 6 mins, static cycle: 5 mins, flush volume: 60%, purge time: 1.5 mins, gas: $N_{2,}$) (Bandowe and Wilcke 2010).

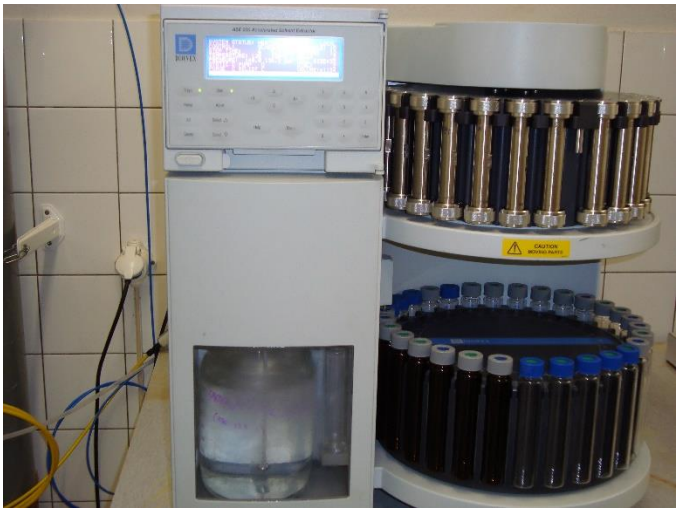

*Fig 3.8. Accelerated Solvent Extractor (ASE)*

In a next step, the two extracts from each sample were combined, spiked with hexane (10 ml) and concentrated (to a volume of ca. 1 ml) using a TurboVap® II concentration evaporator workstation (Charlotte, NC, USA) (Fig. 3.9). The water bath ran at temperature of 36°C with a pressure of ca. 8 – 15 psi. Once extracts have been evaporated to below 1 ml, another 5 ml of hexane was added, and the evaporation process repeated again till 1 ml. This process ensures that the remaining extract is completely dissolved in hexane, the solvent which is compatible with the procedure to be adopted in the next step (column chromatography).

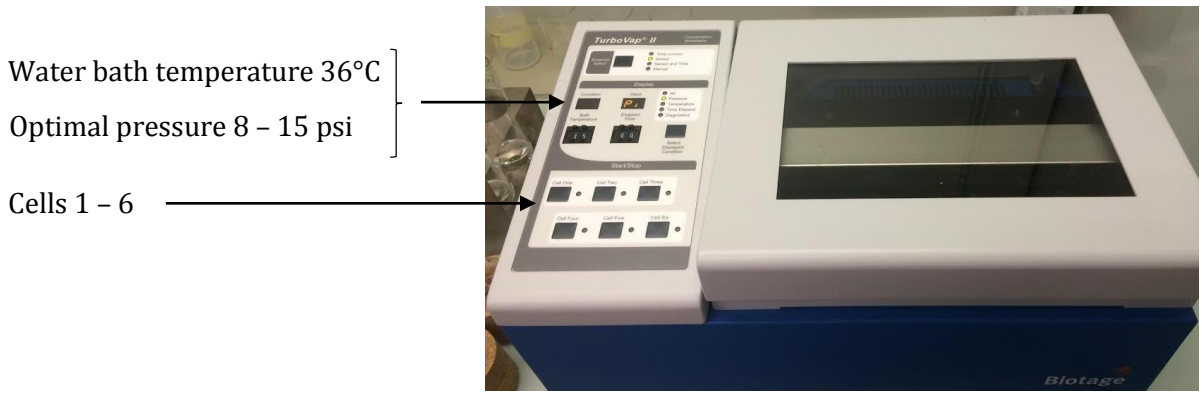


*Fig 3.9. TurboVap® II*

**Extract Clean up by Column Chromatography**

Silica gel (10% deactivated) was used as the sorbent during column chromatography. Silica gel was baked at 250°C in a clean-oven for ca. 12 hrs. The baked silica gel was then allowed to cool to room temperature, deionized water (10% of the total mass) was then added, placed on an overhead shaker and completely mixed.

An 8 mL borosilicate glass column (J.T. Baker, Deventer, The Netherlands) was filled with 3g of silica gel (10% deactivated) in between two tufts of glass wool. The columns were then conditioned with hexane. Extracts were then added to the column and subsequently eluted with (a) 15 mL of hexane/dichloromethane (5:1, v/v), and (b) 20 mL of dichloromethane. The eluents from each sample were collected together in a 50 ml glass flask (Fig. 3.10). The column chromatography extracts the target compounds from the many other organic compounds present in the matrix. All compounds have different retention times as they partition between solvent (mobile phase) and silica gel (stationary phase) which determine how long a compound remains in the stationary phase before being eluted. These solvents will elute the cleaner PACs and OCs from the column. The target compounds are separated from the matrix in order to reduce interference in the GC output.

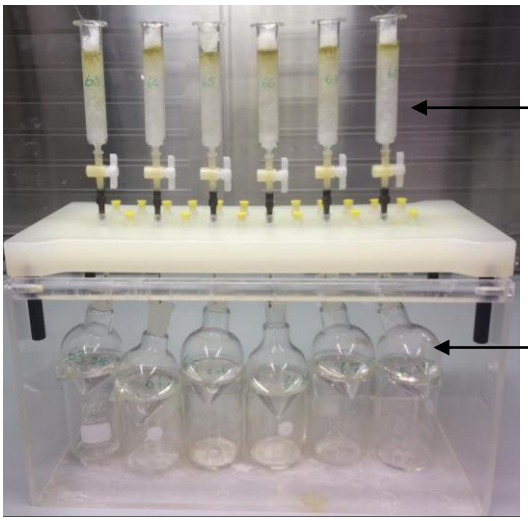


*Fig 3.10. Column chromatography*

Hexane (10 ml) and 3 drops of toluene (as keeper) were added to eluates from each sample to ensure that extracts do not evaporate to dryness. Each eluate was then concentrated in a Turbo Vap® II (at 35°C) to ca. 1 ml, 25 µL of fluoranthene-D10 (22 µg/ml) was added (Fig. 3.11), then transferred to a 1.5 mL GC glass vial ready for the measurement of target organic compounds using gas chromatography-mass spectrometry (GC-MSD).

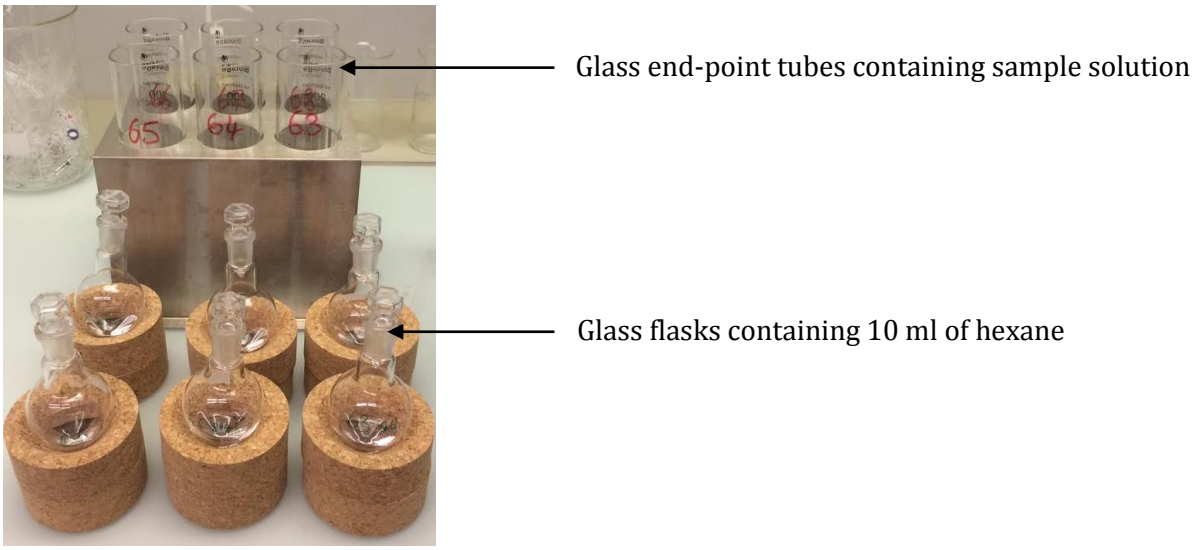


*Fig 3.11. Sample preparation for second evaporation*

**Gas Chromatography Mass Spectrometry (GC-MSD)**

Gas Chromatography Mass Spectrometry (GC-MSD) (Fig. 3.12) was used to measure the contents of PACs, and OCs in extracts from samples. The GC-system is made up of a carrier gas supply, an injector, an oven, the column and a detector. The column is placed in the oven and runs on a specific temperature programme which allows the separation of compounds to take place. For example, compounds with high boiling points elute late at low temperatures and show up as broad peaks in the chromatogram. The mass spectrometer (MSD) separates different ions according to their different mass-to-charge-ratios (m/z). First, the analytes are converted to ions, then the ions are separated, detected and the mass spectrum (relative abundance plotted as a function of the m/z ratio) is calculated in the data system.

A 7890A gas chromatograph coupled to a 5975C inert mass selective detector (MSD) with triple axis detector (Agilent Technologies) was used in all analyses. The GC-MSD was equipped with an autosampler, split/splitless injector, an interchangeable electron impact ionization ion source (EI) and a negative chemical ionization (NCI) source. The GC was equipped with a fused silica capillary column (30 m x 0.25 mm i.d. x 0.25 µm film thickness), with helium (He) as the carrier gas. Instrumental control, data recording and processing were done with Agilent Chemstation software. PAHs, OPAH+AZAs and OCs in extracts were measured from separate injections using different GC-MSD instrumental parameters.

To measure PAHs, OPAHs + AZAs and OCs, aliquots (3 µL) of extracts were injected into the GC-inlet in the splitless mode. Injected extracts were volatilized in the GC inlet (with a temperature of 300°C). Helium was used as a carrier gas with a constant flow rate of 1.2 mL $min^{-1}$. Oven temperatures of PAH measurements started at 80 °C (for 4 mins) and increased to 160 °C at a rate of 14 °C $min^{-1}$, hold time 1.5 min, then increased to 225 °C at a rate of 5 °C $min^{-1}$, hold time 5 min, and a final increase in temperature to 300 °C at a rate of 5 °C $min^{-1}$, hold time 11 min. For OPAH + AZA measurements, oven temperatures started at 80 °C (for 6 mins) and increased to 145 °C at a rate of 5 °C $min^{-1}$, hold time 3 min, then increased to 200 °C at a rate of 5 °C $min^{-1}$, hold time 7 min, and a final increase in temperature to 300 °C at a rate of 15 °C $min^{-1}$, hold time 5 min. Instrumental parameters for OCs extraction were as follows: oven temperature started at 100 °C and increased to 290 °C (10 min hold time) at a rate of 4 °C $min^{-1}$. The injector and detector temperatures were maintained at 250 °C and 300 °C respectively (following the method of Cheng et al. 2014). The MSD was operated in the EI mode (70 eV), with selected ion monitoring (SIM) for each compoundduring the measurement of PACs, and in the negative chemical ionization (NCI) mode with methane was used as a reagent gas during the measurement of OCs (Bandowe and Wilcke 2010). For each target compound or internal standard the ions that were monitored are shown in Tables A.1.2 - 4 (Annex 1). Calibration standards were prepared and filled with toluene up to 1 ml and measured in the GC-MSD.

*Fig 3.12. Gas Chromatography Mass Spectrometry (GC-MSD)*

### 3.2.4.2 Analysis of Mercury and Heavy Metals in Sediments

**Microwave Assisted Chemical Digestion**

Sediment cores were subsampled to a depth of ca. 12.5 cm at 0.5 cm resolution and freeze-dried. Teflon vessels (to be used during digestions) were placed in a bath of nitric acid ($HNO_3$) overnight (minimum 4 – 6 hours). After a rinsing with deionized water the vessels were then placed in a hydrogen chloride (HCl) bath again overnight or for 4 – 6 hours. The vessels were rinsed again with deionized water and placed under a fume hood. Freeze-dried sediment samples were grinded very fine in a mortar to homogenize them. About 100 mg of ground sample was added to a labeled Teflon vessel. One blank vessel and one vessel containing reference material (2709a, San Joaquin Soil, (Mackey et al. 2010)) were added to each run for quality control.

To each vessel 8 ml of Nitric Acid ($HNO_3$) 69% "super pure" was added, followed by 2 ml of Hydrogen Peroxide ($H_2O_2$) "super pure" which oxidises any organic matter (digestion) in the sample. The samples were placed into microwave carousels, sealed shut and placed in the microwave (Ethos contFLOW 1600, Milestone, Shelton CT, US). The vessel containing the blank was attached to a temperature sensor. Instrumental parameters for the digestion were as follows: microwave temperature 120 °C, held for 5 min (300 W power), then 200 °C for 10 min (700 W power), followed by 200 °C for 30 min (450 W power). Once digested, each sample was brought to 20 mL in labeled glass vials with ultrapure water (18.2 MΩ, MilliQ, Merck Millipore, Germany).

**Inductively-Coupled Plasma Mass Spectrometry (ICP-MS)**

An ICP-MS (Agilent Technologies, Santa Clara, US) was used to measure the concentration of trace metals and Hg in digests of all samples. The ICP-MS is sensitive in the ppt range and can measure 85% of all elements in the periodic table at the same time, and is shown in Fig. 3.13. The samples first enter the sample introduction system, where the sample is generated into a fine aerosol via a nebulizer and a spray chamber. From the spray chamber the sample aerosol become ionised by an argon gas plasma (5000-6000 °K) which breaks all chemical bonds. This ensures that the total concentration of an element in a sample is analysed independently of its chemical form or species (Ammann 2007). The plasma dries the aerosol, dissociates the molecules and removes an electron from the components, in so doing forming singly-charged ions in an excited state. These ions are directed into the mass spectrometer (MS), which scans the mass range, one mass-to-charge ratio

at a time. When exiting the MS, the ions hit a dynode of an electron multiplier. This acts as a detector, and the impact of the ions leads to a flow of electrons which are amplified until they become a measurable pulse (Thomas 2001). Rhodium (100 µg/L) and indium (10 µg/L) are used as internal standards as they are naturally not present in the sediment samples.

For the measurement of trace metals, 0.25 ml of sample digest solution was diluted with 4.75 ml of 1% nitric acid dilution solution and placed in the ICP-MS for measurement. A multi-element standard (IV-ICPMS-71A, inorganic ventures) was used to prepare a calibration curve (ranging from 0 to 500 µg/L). After every 20 samples measured by the ICP-MS, a rinse was run (1% $HNO_3$) followed by a low standard (0.5 µg/L), a high standard (100 µg/L) and another rinse (1% $HNO_3$). Multi-element analysis was performed in the "No Gas" and "He" mode. Operating parameters for multi-element analysis on the ICP-MS can be found in Table 3.2.

*Table 3.2. Operating parameters for the ICP-MS in the "no gas" and "He" mode for mercury and multi-element analysis*

| | MULTI-ELEMENT | | MERCURY | |
|---|---|---|---|---|
| | **No Gas mode** | **He mode** | **No Gas mode** | **He mode** |
| **Rf Power** | 1550 W | 1550 W | 1550 W | 1550 W |
| **Carrier Gas Flow Rate** | 1.05 L/min | 1.03 L/min | 1.05 L/min | 1.05 L/min |
| **Nebulizer Pump (revolutions per second)** | 0.1 rps | 0.1 rps | 0.1 rps | 0.1 rps |
| **Spray Chamber Temperature** | 2 °C | 2 °C | 2 °C | 2 °C |
| **Make Up Gas** | 0 | 0 | 0 | 0 |
| **LENCES** | | | | |
| **Extract 1** | 0 | 0 | 0 | 0 |
| **Extract 2** | -180 V | -200 V | -180 V | -160 V |
| **Omega Bias** | -95 V | -100 V | -95 V | -95 V |
| **Omega Lens** | 9.3 V | 10 V | 9.3 V | 8.4 V |
| **Cell Entrance** | -30 V | -40 V | -30 V | -40 V |
| **Cell Exit** | -50 V | -60 V | -50 V | -60 V |
| **Deflect** | 14.2 V | 1 V | 14.2 V | 2.2 V |
| **Plate Bias** | -40 V | -60 V | -40 V | -60 V |
| **CELL** | | | | |
| **He Flow** | 0 | 4.3 mL/min | 0 | 4.3 mL/min |
| **$H_2$ Flow** | 0 | 0 | 0 | 0 |
| **Octp Bias** | -8 V | -8 V | -8 V | -18 V |
| **Octp Rf** | 200 V | 180 V | 200 V | 190 V |
| **Energy Discrimination** | 5 V | 5 V | 5 V | 3 V |

Total Hg analysis requires different operating parameter from a multi-element analysis. For measurements of Hg, 0.5 ml of sample digest solution was diluted with 4.5 ml of dilution solution (consists of HCl 0.5% and $HNO_3$ 1%). A calibration curve was prepared using a highly concentrated mercury standard (10'000 µg/L Hg) for ICP (TraceCERT, Fluka). The standards were weighed rather than pipetted for higher accuracy. Seven standards were prepared, each diluted to between 0 – 2 µg/L of Hg. For every $10^{th}$ sample measured, the ICP-MS ran a rinse and measured two standards (0.1 and 0.2 µg/L) again (followed by another rinse) to ensure that the ICP-MS was measuring concentrations of Hg correctly. Hg was measured in the "No Gas" and "He" mode, and the operating parameters for total Hg analysis can be found in Table 3.2.

The 'stickiness' of Hg requires it to be run at low concentrations (high dilution), and also means that mercury is not analysed in the ICP-MS with other elements. A washout with HCL is needed between samples, and the cleaning agents for each rinse are:

1) EDTA, Triton X, $NH_4OH$: this solution has a very high pH, and used soap properties to clean the machine.
2) 5% $HNO_3$, 5% HCL: this solution changes the properties of the cleaning solution from alkaline to acid.

3) 1% $HNO_3$ and 0.5% HCL: this helps to stabilise the ICP plasma, and is the same as the dilution solution in the samples.

*Fig 3.13. Inductively-Coupled Plasma Mass Spectrometry (ICP-MS)*

**Quality Control and Assurance in Mercury and Metal Measurements**

Aliquots of the Standard Reference Materials (SRM 2709a: San Joaquin agricultural soil) from National Institute of Standards and Technology (Mackey et al. 2010) were analyzed together with samples. This provides data for method validation and quality assurance of the procedure adopted to determine trace metals and Hg in the samples. The average (*n = 14*) mass fraction of each trace metal and Hg measured in the reference material was compared to the certified value (Mackey et al. 2010, Table 3) and a recovery value was calculated. The measurement method (digestion and ICP-MS) for an element was deemed to be satisfactory if the recovery was between 70 to 130 %. Elements with a recovery < 70 % were re-checked with acid extractable amount content to see whether they fell within the range for the reference soil (Mackey et al. 2010, Table 4). This was done for Thallium, however, the recovery did not improve by much. Lutetium, Barium and Strontium were removed from the analysis as their recovery values were too low. Of the 32 elements measured, Cadmium and Selenium were the two elements with values below the limit of detection for the ICP-MS. From the certified reference material the average cumulative error for the whole procedure was calculated at 9.2% for heavy metal analysis and 8.4% for mercury analysis. The cumulative error is below 10% for both Hg and heavy metal analysis, which is considered good for a procedure involving digestion and extraction. Factors that could influence error are discussed below in the 'limitations' section.

For Hg measurements, duplicates were measured for five samples and triplicates for three samples from Laguna Fondococha. For Laguna Llaviuco one triplicate was measured. The number of duplicates and triplicates performed per lake was dependent on the amount of remaining material. The difference in re-measured samples was considered, and the relative standard deviation (RSD%) of those samples with the largest error was calculated to see how much those samples standard deviation varies when compared to the mean. The RSD on average was 2.5%, which is small and indicates that the repeated data values are precise. The recovery average for mercury extraction from the standard reference material is 0.9 ± 0.2 mg $kg^{-1}$ (Mackey et al. 2010, Table 3), and on average we found a Hg concentration of 1.06 mg $kg^{-1}$ in the SRM 1 – 14 (range

0.94 – 1.24 mg $kg^{-1}$), which is within the range of error. The average recovery is thus 117% (range 105 – 130% ± 23.5%), which again is within the acceptable mass fraction range of 70 – 130%.

**Limitations**

Contamination is a limitation that must be taken into consideration when using the ICP-MS. Even 0.5 ng of e.g. dust can influence the ICP-MS as it is extremely precise. Contamination of blanks can increase the lowest Hg or heavy metal detection by the ICP-MS. Further, fluctuations in pressure during the microwave process can influence values, as well as mistakes made for the calibration curve. Static conditions occur when weighing out 100 mg of finely ground sediment to place into Teflon vessels. The static causes a fine dust of sediment to stick to the sides of the vessel, which interferes with the highly precise weighing machine. Measures taken to counteract the static conditions include an anti-static mat under the weighing machine, and anti-static gun, and an anti-static wrist band. While these measures helped slightly in reducing the static, it was still not completely eliminated and could influence the weight of the sediment measured.

### 3.3 CALCULATIONS AND STATISTICAL ANALYSES

The sum of the concentrations of all analyzed PAHs and all non-alkylated PAHs are called ∑26 PAHs, and ∑parent-PAHs, respectively. The sum of all parent-PAHs with 2-3 benzene rings and 4-7 benzene rings are called low molecular weight-PAHs (LMW-PAHs) and high molecular weight PAHs (HMW-PAHs) respectively. The sum of the concentrations of PAHs that are deemed to be mostly originating from high temperature combustion (benzo[a]anthracene, chrysene + triphenylene, benzo[b+j+k]fluoranthene, benzo[e]pyrene, benzo[a]pyrene, indeno[1,2,3-cd]pyrene, dibenzo[ah]anthracene, benzo[ghi]perylene and coronene) are refered to as ∑COMB-PAHs. The sum of the concentration of all analyzed oxygenated PAHs and all analyzed azaarenes are refered to as ∑OPAHs and ∑AZAs, respectively.

Statistical analysis of the resulting data is used to compare and provide information on the relationships between various researched components in the sediment core. On each of the lakes, a principal component analysis (PCA) and a correlation analysis was performed on all examined components (concentrations of metals, Hg, PAHs, OPAHs, AZAs and C, C/N) using R (R Development Core Team). The data was first and foremost standardized (mean 0, standard deviation 1). The correlation analysis estimates the correlation coefficient, in our case this was the Pearson Product Moment correlation coefficient (*r*), between two variables. There can be a positive correlation (e.g. higher levels of one variable are associated with higher levels of the other) or negative (e.g. higher levels of one variable are associated with lower levels of another). The correlation coefficient ranges between +1 and -1 and quantifies the direction and strength of the linear association between two variables. The magnitude of the correlation coefficient indicates the strength of the association. Correlations close to zero suggest no linear association between two continuous variables. The correlation analysis will be used as a basis to explore which groups of pollutants and compounds correlate most significantly together.

PCA is a statistical technique used to analyse multivariate data sets by considering the linear combinations of the original variables that explain most of the variance and simplifies the interpretation of complex systems. PCA operates with no a priori assumption on data structure and thus highlights major underlying trends in large datasets by grouping variables that covary and samples that have similar variable compositions (Yunker et al. 2014). PCA will be used to identify different compositional assemblages in the sediment core, and to see which components

maximize the variance in the data set. The first two principle components (PCs) account for the largest percentage of total variance in a dataset. A PCA will be performed for each lake, and will take into account element heavy metal concentrations, mercury concentrations, as well as PAHs, OPAHs, AZAs concentrations, TOC and C/N ratios. Table 3.3 shows the grouping of compounds for statistical analysis.

*Table 3.3. Groups of compounds used in statistical tests for L. Fondococha and L. Llaviuco*

| Group | Compound Name | Abbreviation |
|---|---|---|
| **LMW-PAHs** | Naphthalene | NAPH |
| | 2-Methylnaphthalene | 2-MNAPH |
| | 1-Methylnaphthalene | 1-MNAPH |
| | Biphenyl | BP |
| | 1,3-Dimethylnaphthalene | 1,3-DMNAPH |
| | Acenaphthylene | ACENY |
| | Acenaphthene | ACEN |
| | Fluorene | FLUO |
| | Phenanthrene | PHEN |
| | Anthracene | ANTH |
| | 1-Methylphenanthrene | 1-MNAPH |
| | 3,6-Dimethylphenanthrene | 3,6-DMPHEN |
| **HMW-PAHs** | 4H-Cyclopenta[d,e,f]phenanthrene | CPHEN |
| | Fluoanthene | FLUA |
| | Pyrene | PYR |
| | Benzo[a]anthracene | B(A)A |
| | Chrysene + Triphenylene | CHRY+TRY |
| | Benzo [b+j+k] fluoanthene | B(BJK) |
| | Benzo[e]pyrene | B(E)P |
| | Benzo[a]pyrene | B(A)P |
| | Indeno [1,2,3-cd] pyrene | IND |
| | Dibenzo[ah]anthracene | DIBE |
| | Benzo[ghi]perylene | B(GHI) |
| | Coronene | COR |
| **Metals** | Mercury | Hg |
| | Copper | Cu |
| | Zinc | Zn |
| | Lead | Pb |
| | Chromium | Cr |
| **Bio-PAHs** | Retene | RET |
| | Perylene | PERY |
| **AZAs** | Quinoline | QUI |
| | Benzo[h]quinoline | BQI |
| | Acridine | ACR |
| | Carbazole | CBZ |
| **OPAHs** | 1-Indanone | 1-INDA |
| | 1,4-Naphthoquinone | 1,4-NQ |
| | 1-Naphthaldehyde | 1-NLD |
| | 2-Biphenylcarboxaldehyde | 2-BPCD |
| | 9-Fluorenone | 9-FLO |
| | 1,2-Acenaphthylenequinone | 1,2-ACQ |
| | 9,10-Anthraquinone | 9,10-ANQ |
| | 1,8-Naphthalic anhydride | 1,8-NAA |
| | 4H-Cyclopenta[def]phenanthrenone | CPHENone |
| | 2-Methylanthracene-9,10-dione | 2-MANQ |
| | Benzo[a]fluorenone | B(A)FLUone |
| | 7H-Benz[de]anthracene-7-one | BANTone |
| | Benz[a]anthracene-7,12-dione | 7,12-B(A)Dione |
| | Naphthacene-5,12-dione | 5,12-NACQ |
| | 6H-Benzo[cd]pyrene-6-one | BPYRone |
| **Carbon** | total organic carbon | C |
| | C/N ratio | C/N |

# CHAPTER 4: RESULTS

## 4.1 SEDIMENT CORE DESCRIPTION

### 4.1.1 Sediment Core Laguna Fondococha

The sediment cores from Laguna Fondococha were divided into eight units described below. None of these units reacted to HCl indicating a lack of carbonate material present in the sediment. The contact between all units was mostly sharp. Unit I encompasses the top ca. 14.5 cm of the cores. Fig. 4.1. shows a ture colour (RGB) image of unit I – the relavent unit for this study.

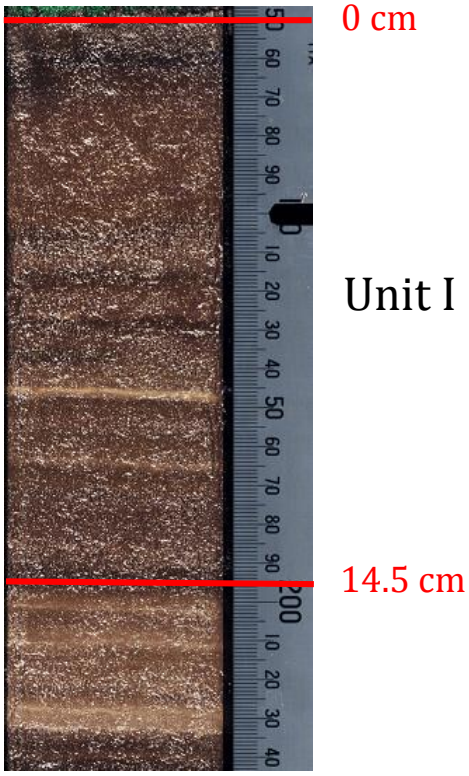


*Fig 4.1 RGB image of sediment core FON-14-1 showing unit I (0 cm – 14.5 cm)*

I. Brownish/black in colour (HUE 10 YR 2/1) at the top, fading to a dull yellowing brown (HUE 10 YR 5/4). Composed of very organic fine silt with mostly a massif structure, with two lighter bands. The contact to unit II is gradual.

II. Greyish/yellow (HUE 2.5 Y 6/2) to olive brown (HUE 2.5 Y 4/3). Slightly organic fine silt lithology. Slight lighter/darker banding.

III. Unit three is largely brownish/black in colour (HUE 10 YR 2/2 or 3/2) and consists of decomposed organic matter. The lithology is peaty/silty, with the majority of the unit being homogenous/massif in structure, with a few lighter/darker bands.

IV. This unit consists of volcanic ash. The tephra is very fine and homogenous, with a light grey colour (HUE 75 Y 7/1).

V. Unit five is a homogenous section of organic fine silt with a brownish/black colour.

VI. Lithologically consisting of organic fine silt, unit six is black in colour (HUE 5 Y 2/1) with fine lighter banding throughout the section.

VII. This small 0.5 mm unit consists of fine sand with a light grey colour.

VIII. The last unit was made up of black silty clay and contains fine lighter layers.

### 4.1.2 Sediment Core Laguna Llaviuco

The sediment cores for Laguna Llaviuco were composed of two units, described shortly below. A more detailed description of the cores can be found in Arcusa (2016). Neither of the units reacted to HCl, indicating a lack or carbonate material in the sediment. Unit I includes the top 15 cm of the core (which is relavent for this study), and true colour (RGB) and near infrared (NIR) images of unit I for various core halves is shown in Fig. 4.2.

I. Consists of a very fine organic silt, contains layers of macrofossils (rootlets). It is mostly massif with some very fine lighter layers. The colour ranges from olive yellow (HUE 5 Y 6/4) to brownish black.

II. Unit two begins with a sharp contact to unit 1 of a layer of rootlets, followed by a further band of macrofossils. The rest of the unit is made up of very fine, organic-rich silt (with a brownish/black colour), interspersed with dark and light banding. The darker layers consist of dense clay/silt layers with an olive gray colour (HUE 10 Y 6/2).

#### 4.1.2.1 Cross Core Correlation

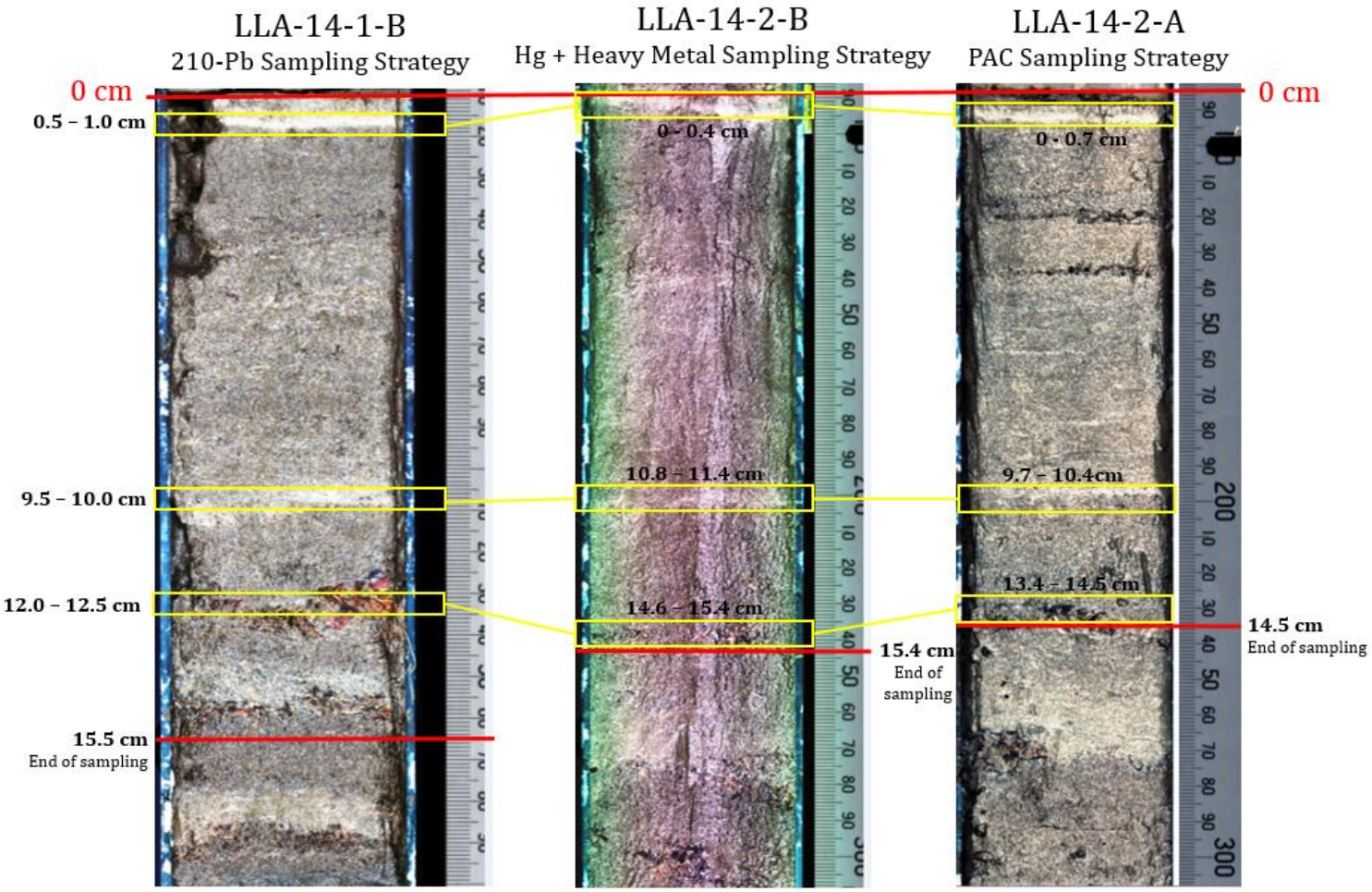


Fig 4.2. Cross core correlation between cores LLA-14-1-B (RGB) and LLA-14-2-A (RGB) + LLA-14-2-B (NIR)

Cross core correlation between the core LLA-14-1-B (sub-sampled for $^{210}$Pb dating) and the parallel core halves LLA-14-2-A and B (sub-sampled for PACs + OCs and Hg + heavy metals respectively) was carried out in order to establish a uniform chronology for all the cores based

on the sample depths of LLA-14-1-B. Cross core correlation was necessary as much material was required for the various analyses of this thesis, thus multiple cores from each lake were sampled. The sampling strategy differed between cores as it was attempted to incorporate certain layers within samples. The master core for the cross core correlation was LLA-14-1-B, which had a strategic sampling resolution of 5 mm, and for which we could calculate age per depth of sample. Three diagnostic layers were then selected (outlined in yellow in Fig. 4.2) which were clearly correlating between each three core halves. These three layers were used as reference layers to regularize ages and depths for LLA-14-2-A and LLA-14-2-B. The result was the accurate assigning of ages to sample from the two parallel core halves. Regularization is considered adequate as we have relatively regular sedimentation rates in LLA-14-1-B.

## 4.2 AGE/DEPTH MODELLING

### 4.2.1 Laguna Fondococha

$^{210}$Pb age-depth model for Laguna Fondococha was attempted using two different models: CRS, CIC (see Annex 2, Fig. A.2.1 for model comparisons). Supported $^{210}$Pb ($^{226}$Ra) values for Laguna Fondococha are stable at around 50 – 60 Bq kg$^{-1}$. Background unsupported $^{210}$Pb levels are reached at 8.75 cm depth in the core (Fig. 4.3). Total $^{210}$Pb values show stable values at the top of the core, followed by a sharp decrease at around 1.5 cm. From about 5.5 cm downward the lower values indicate a higher sedimentation rate, thus a higher material input (matrix effect). A dip occurs in total $^{210}$Pb at the sediment surface (0 cm) that is lower (443.2 Bq/kg) than the following value (450.7 Bq/kg) at depth 0.5 cm. To correct for this, surface activity was projected for point 0 cm by extrapolating the 3 data points below the first one. This resulted in a projected surface activity of 507.45 Bq/kg. Measured $^{137}$Cs activity was low, averaging 5.6 ± 3.0 Bq/kg, and thus the 1963 fallout peak could not be used as an independent chronomarker to constrain the CRS model.

Unsupported $^{210}$Pb activity distribution with depth indicates irregular sedimentation rates. The CIC model was discarded as it assumes a constant sedimentation rate throughout the period over which unsupported $^{210}$Pb is measurable. This is not the case in L. Fondococha (see Fig. 4.4) and the age reversals in the CIC model that occur at 0.75 cm, 3.25 cm and 5.5 cm depth (Annex 2, Fig. A.2.1) are a further indication that the assumption of constant initial $^{210}$Pb activity is not fulfilled. The mass accumulation rate (MAR) varies between 0.005 and 0.025 g cm$^{-2}$ yr$^{-1}$. An increase occurs in the MAR between ca. 1.5 cm and 4.5 cm depth in the core (Fig. 4.3 and 4.4). When examining the core photo (Fig. 4.1), it is evident that there is a change in colour occurring within the sediment (lightening) at ca. 5 cm, which gradually darkens again to about 1 cm depth. This layer could be indicative of increased erosion in the area, facilitating a matrix effect in the specific $^{210}$Pb activity in the lake sediments. This could explain the irregularities we see in the unsupported $^{210}$Pb activity between ca. 2.5 cm to 5 cm depth in the core. MAR stabilizes again between 1 – 1.5 cm, ca. in the 1990s. This coincides with the official declaration of Cajas as a National Park 1996. Prior to 1996 the region around the lake could have been used for grazing, thus increasing the erosion rate. Stricter regulations from 1996 onward could mean that grazing in the area no longer occured, resulting in a stabilizing of the MAR. In general, the CRS model shows low sedimentation rates for Laguna Fondococha, averaging at 0.014 g cm$^{-2}$ yr$^{-1}$.

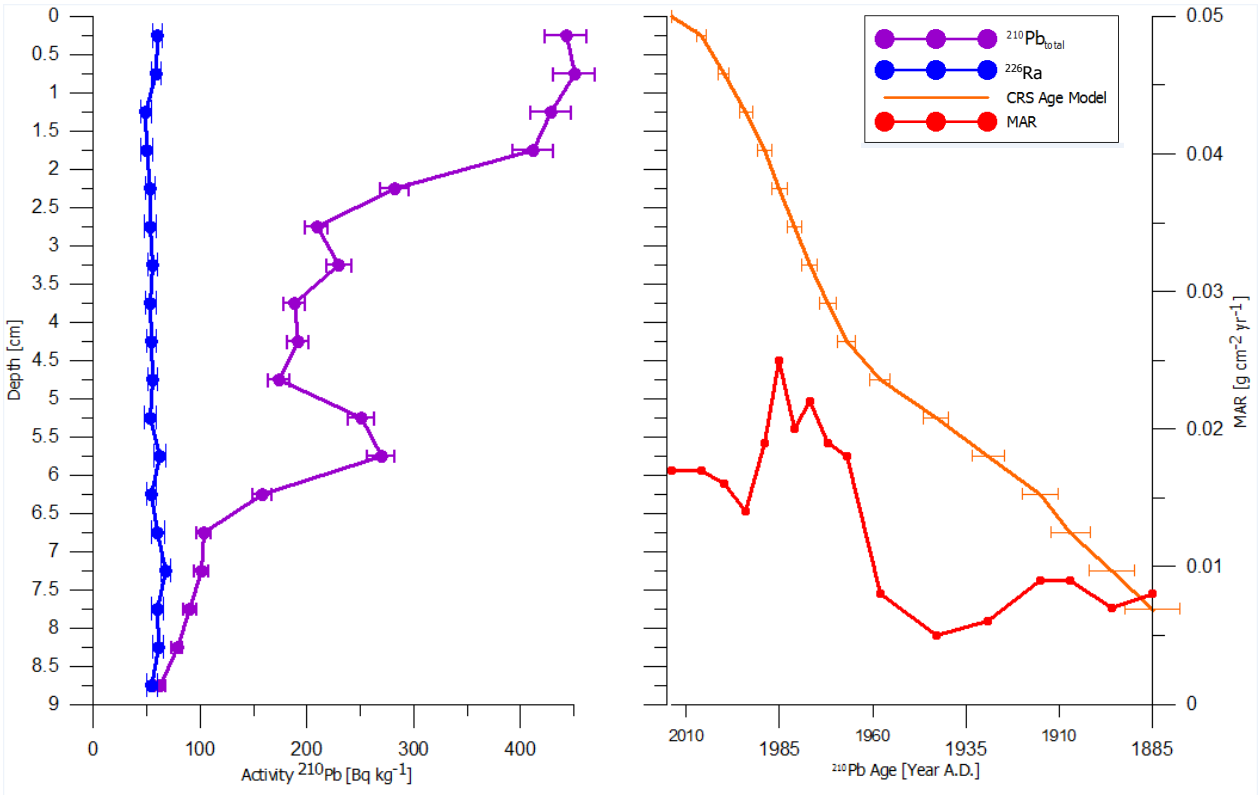


*Fig 4.3. CRS model corrected for missing inventories and projected surface activity for Laguna Fondococha showing Mass Accumulation Rate (g cm² yr⁻¹) in red; CRS age model (orange), supported ²¹⁰Pb (²²⁶Ra, dark blue); and total ²¹⁰Pb (purple).*

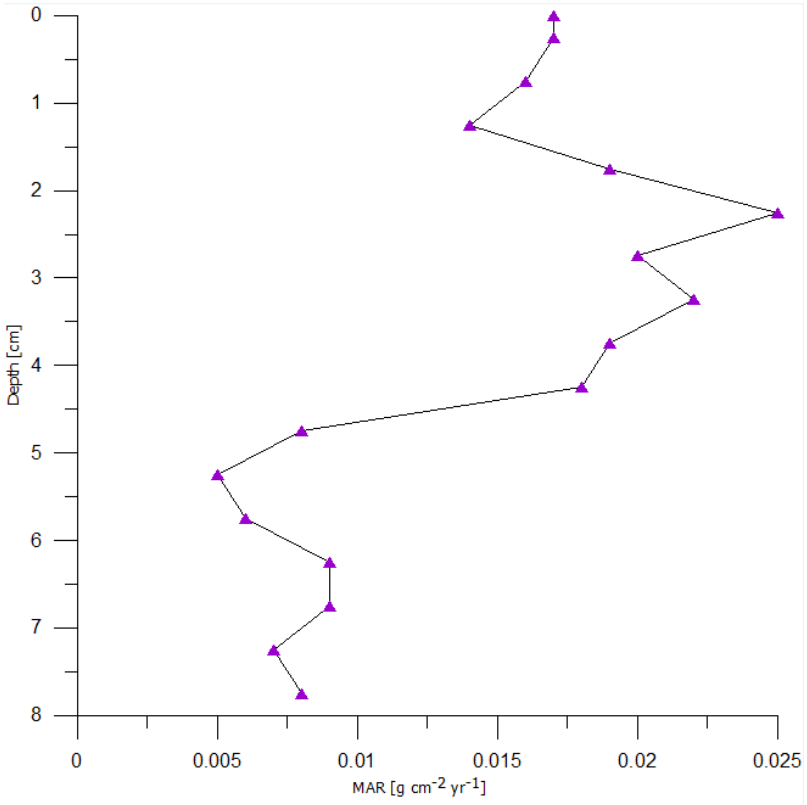


*Fig 4.4. Mass Accumulation Rate (g cm² yr⁻¹) vs. depth in Laguna Fondococha*

The CRS model was deemed to yield the most plausible results from all models, and as such it also underwent a missing inventory correction. The correction of 38.8 Bq/m$^{-2}$ was derived from an exponential trend over part of the $^{210}$Pb profile, following the procedure by Tylmann et al. (2013). There are a number of ways to calculate the missing inventory correction, which is applied to reduce the tailing effect, seen as an artifact of uncorrected CRS models. Which way the missing inventory is calculated has a large impact on calculated dates, especially in the lowermost part of the profile. Because of this, three different missing inventory values were tested in the CRS model for L. Fondococha. The corrections were added to the cumulative inventories of the CRS model where previously the model simply displayed 0 Bq/m$^{-2}$ (hence the 'missing' inventory). A missing inventory correction was calculated using the lower most values of cumulative dry mass and unsupported $^{210}$Pb from 5.25 cm depth to 8.75 cm (correction I). Correction II (values from 4.75 downwards), was calculated in order to include the bend that we see in all the CRS models starting at around 5 cm depth (Fig. 4.5). Correction III included all values from surface to 8.75 cm depth.

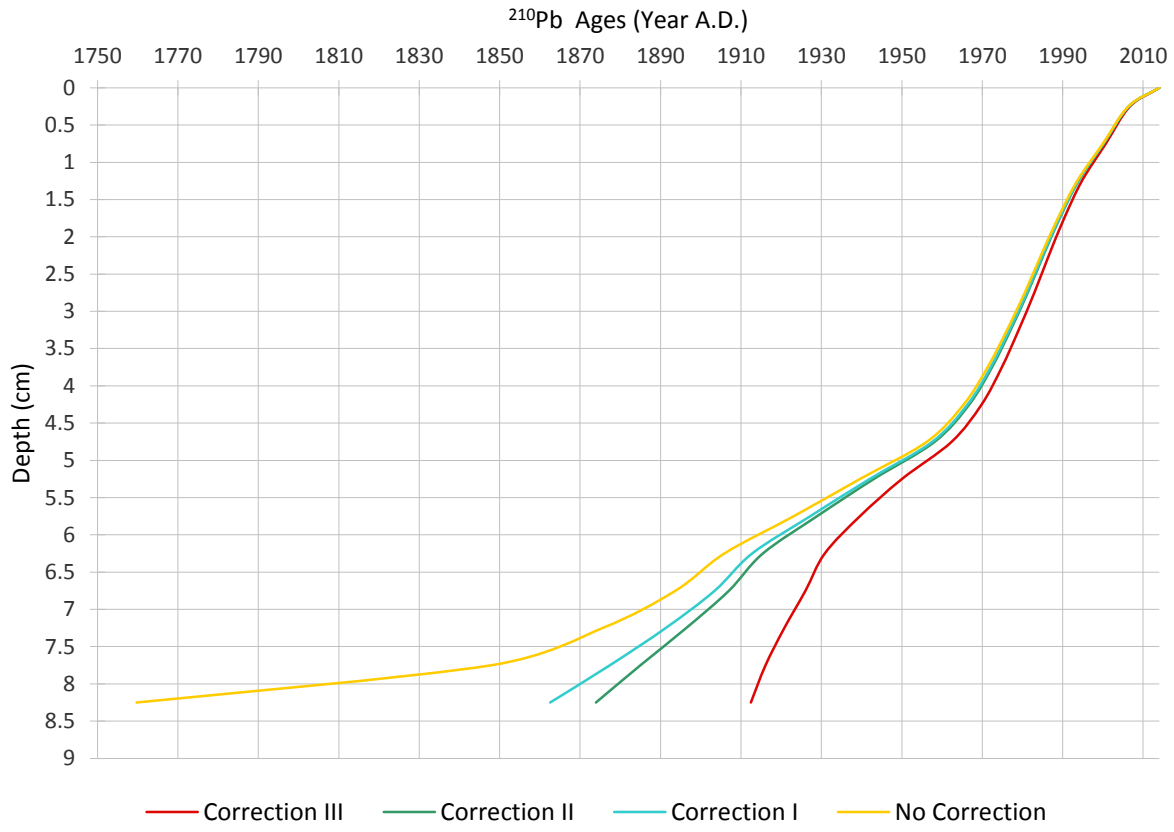


*Fig 4.5. CRS model ages calculated with varying values for missing inventory and without any missing inventory calculations for Laguna Fondococha.*

The higher the value of the correction, the bigger the shift to younger ages we experienced with the dating. Without any missing inventory calculations the CRS model gives values that are far too old (tailing effect seen in Fig. 4.5 with no correction). With all models, the first major spread that we see only occurs at 4.5 cm (Fig. 4.5), indicating that for the top section of the core, from ca. 1958 to 2014, we can say with a high degree of confidence that the calculated ages are accurate. For near-exponential $^{210}$Pb profiles is it suitable to use correction III (including all values from surface to 8.75 cm). However, because the $^{210}$Pb profile for Languna Fondococha is not regular, a correction value was calculated only from the lowermost part of the unsupported $^{210}$Pb profile

(correction II). The exponential equation for correction II was calculated from 4.75 cm to 8.75 and yielded an age of 1885 at 8.75 cm depth.

### 4.2.3 Laguna Llaviuco

The $^{210}$Pb age-depth model for L. Llaviuco was attempted using two different models, the CRS and CIC (see Annex 2, Fig. A.2.2 for model comparison). Supported $^{210}$Pb values ($^{226}$Ra) average at 29 ± 3.2 Bq/kg along the profile, with unsupported activity reaching background levels at 23.15 cm depth. MAR varies between 0.03 and 0.22 g cm$^{-2}$ yr$^{-1}$ with a sharp increase at 15 cm depth (Fig. 4.6). Down core from 15 cm we see the MAR fluctuate. The CIC model yielded age reversals at 0.25 cm, 1.5 cm, 2.75 cm and 4.25 cm depth (Annex 2, Fig A.2.2), which indicate non-constant sedimentation rates and resulted in the CIC model being disregarded in favor of the CRS model. A missing inventory correction was calculated for the CRS model following the procedure by Tylmann et al. (2013). The correction of 395.86 Bq/m$^{-2}$ was derived from an exponential trend over the whole $^{210}$Pb profile (correction III, see Fig. A.2.2, Annex 2 for model comparisons) to avoid the tailing effect of the CRS model. The correction yielded an age of 1969 at depth 23.15 cm. Measured $^{137}$Cs activity in the cores was low, averaging at 2.5 ± 1.1 Bq/kg, therefore, as in L. Fondococha, we are unable to use the 1963 cesium fallout peak to constrain the CRS $^{210}$Pb model.

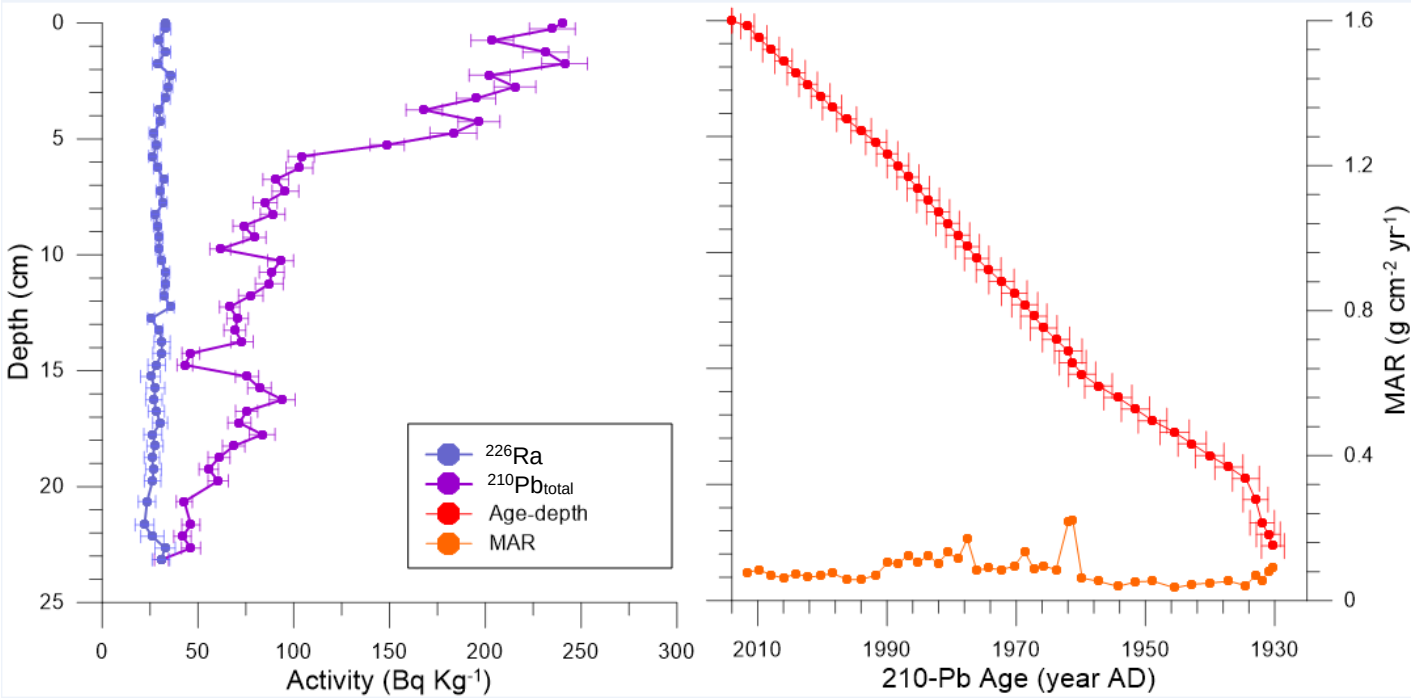


*Fig 4.6. CRS model for Laguna Llaviuco showing Mass Accumulation Rate (g cm$^2$ yr$^{-1}$) in orange; CRS age model (red), supported $^{210}$Pb ($^{226}$Ra, dark purple); and total $^{210}$Pb (light purple)*

## 4.3 METEROLOGICAL DATA

In order to investigate the effect of elevation on precipitation rates, annual precipitation (mm) was compiled from eight meterological stations surrounding Cajas NP for the years 2002 to 2008. The average annual precipitation rate for these eight years was calculated and plotted in Fig. 4.7 according to the elevation of the station. We see an increasing trend in precipitation rates with altitude, a relationship which was tested for its strength with a Pearsons Correlation Coefficient of 0.76 (*df =11; p < 0.01*), indicating a strong positive relationship exists between the two variables.

Fig. 4.7 shows average annual precipitation plotted against elevation and displays the coefficient of determination ($R^2$). $R^2$ tells us that 58% of the variation of y-values (precipitation) around the mean is explained by x-values (elevation), namely that 58% of the values fit the model. As this is testing values from the natural environment, 58% is strong enough to say that the relationship between elevation and precipitation in the region of Cajas NP is robust.

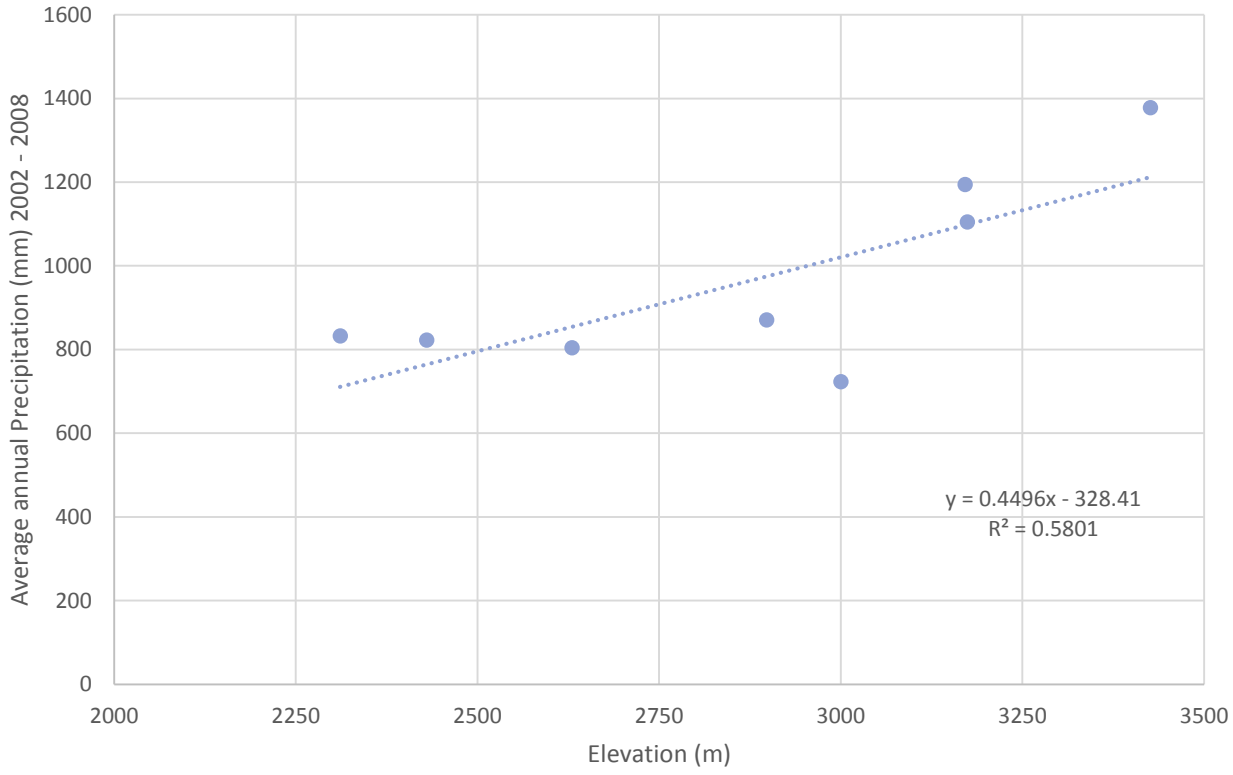


*Fig 4.7. Average annual precipitation (mm) for the years 2002 – 2008 by elevation (m) in the region of Cajas NP*

### 4.4 CARBON AND NITROGEN OF LAKE SEDIMENTS

Total organic carbon (TOC) ranged between 7.5 and 11% for L. Llaviuco, between 5 to 12.3% for L. Fondococha, and the profile for both lakes is shown in Fig. 4.8. From the two lakes, TOC was about equal for L. Fondococha and Llaviuco (on average 8.96% and 8.81% respectively). The average C/N ratio in L. Llaviuco and L. Fondococha was 12.72, 13.10 respectively. For both TOC and C/N ratios L. Fondococha display relatively stable values until ca. 1985 were values begin to increase. L. Llaviuco also exhibits relatively stable values until ca. 2000, whereafter a slight increase is seen. Total organic carbon values and C/N ratios for the lakes can be found in Annex 3, Table A.3.3.

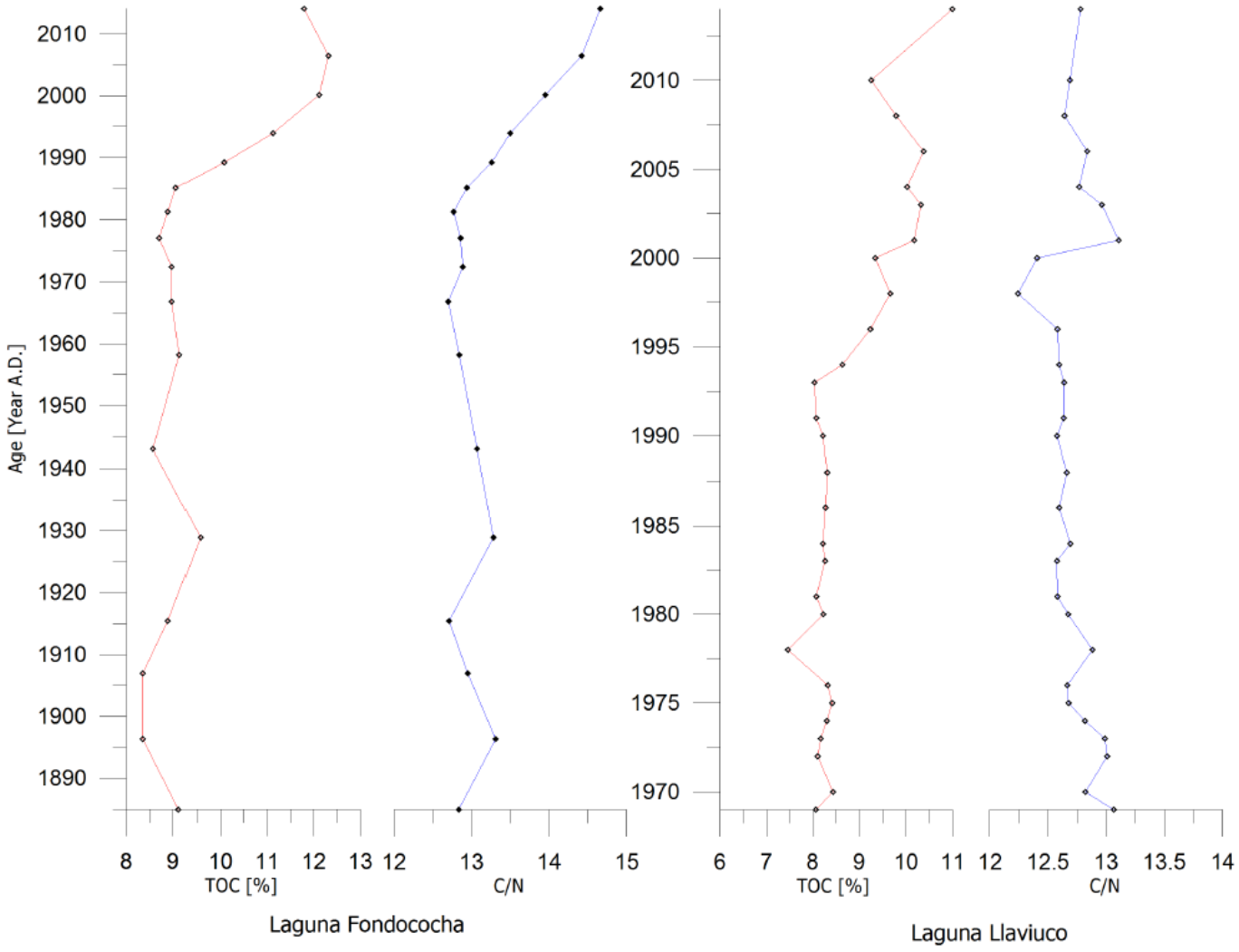


*Fig 4.8. Total organic carbon (%) and C/N ratio for Lagunga Fondococha and Laguna Llaviuco*

## 4.5 ORGANOCHLORINE COMPOUNDS IN LAKE SEDIMENTS

Tables on OC concentrations detected in both lake can be found in Annex 3, Tables A.3.1-2. In L. Fondococha, Hexachlorobenzene, Beta-HCH, Dieldrin and Endrin were detected (Fig. 4.9). The concentration of Hexachlorobenzene ranged between 0.01 and 0.04 ng $g^{-1}$ with the highest concentration 1981. Beta-HCH concentrations range between 0.11 to 1.79 ng $g^{-1}$ with a peak in 1972. After 1989 we no longer detect any Beta-HCH in the sediment samples. Dieldrin concentrations were detected beginning in 1915 and continue to be detected in the sediment until present day, with concentrations ranging from 0.08 to 1.06 ng $g^{-1}$ in 1915. Lastly, Endrin was also detected beginning in 1915 with the highest concentration of 0.73 ng $g^{-1}$, however past 2000 no more Endrin is detected in the samples.

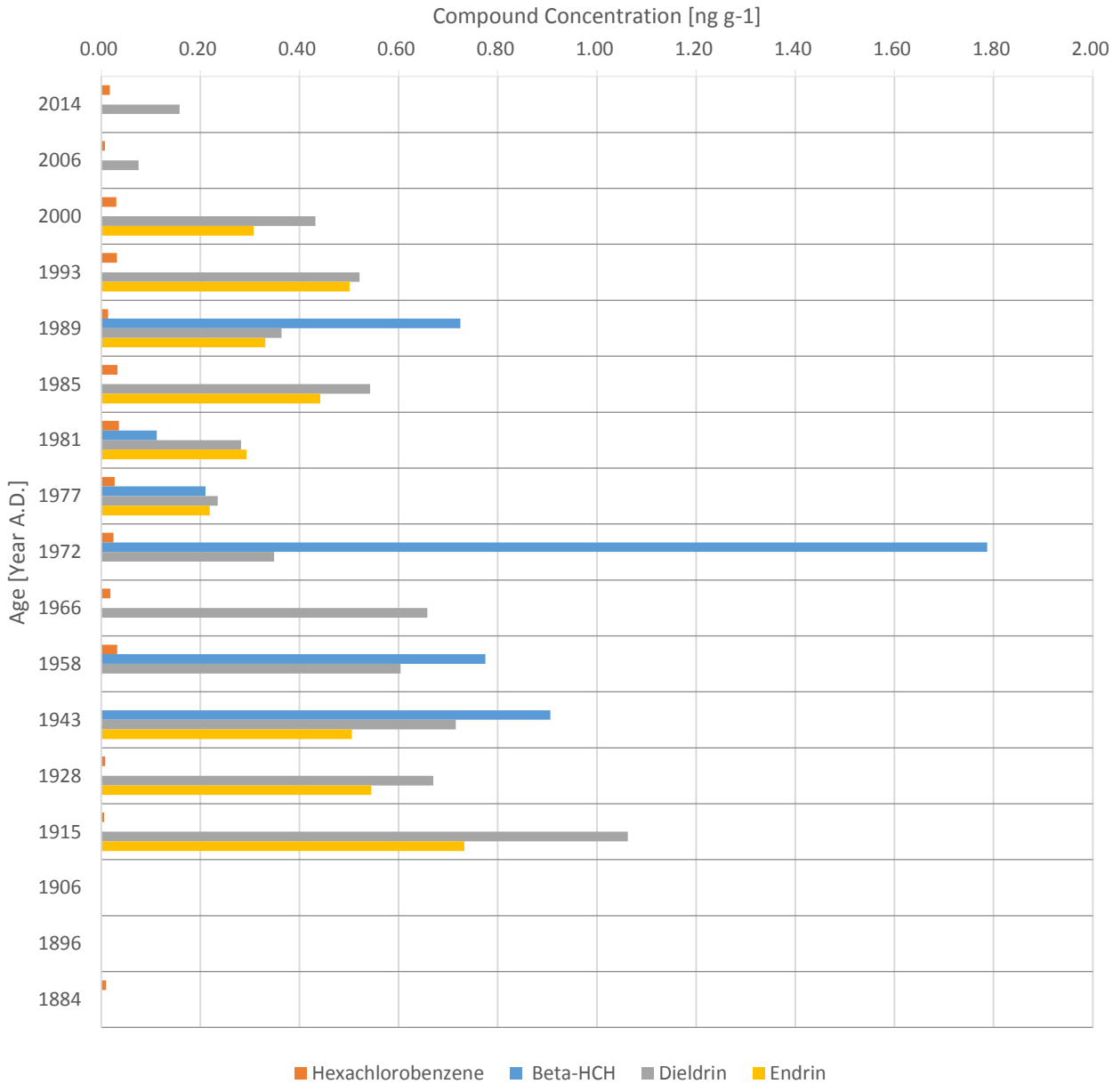


*Fig 4.9. Variations in the concentrations (ng $g^{-1}$) of OCs in the sediments of L. Fondococha*

In L. Llaviuco Methoxychlor was detected. Methoxychlor concentration remained below detection limits (Fig. 4.10) until depth of 3.95 cm (ca. 1998). The concentration of Methoxychlor ranged between 10.36 – 87.09 ng $g^{-1}$ from 1998 till 2009. The peak concentration of Methoxychlor is seen at a depth of 2.45 cm (ca. 2003). After 2010 the concentration of Methoxychlor concentration was again below detection limit until recent.

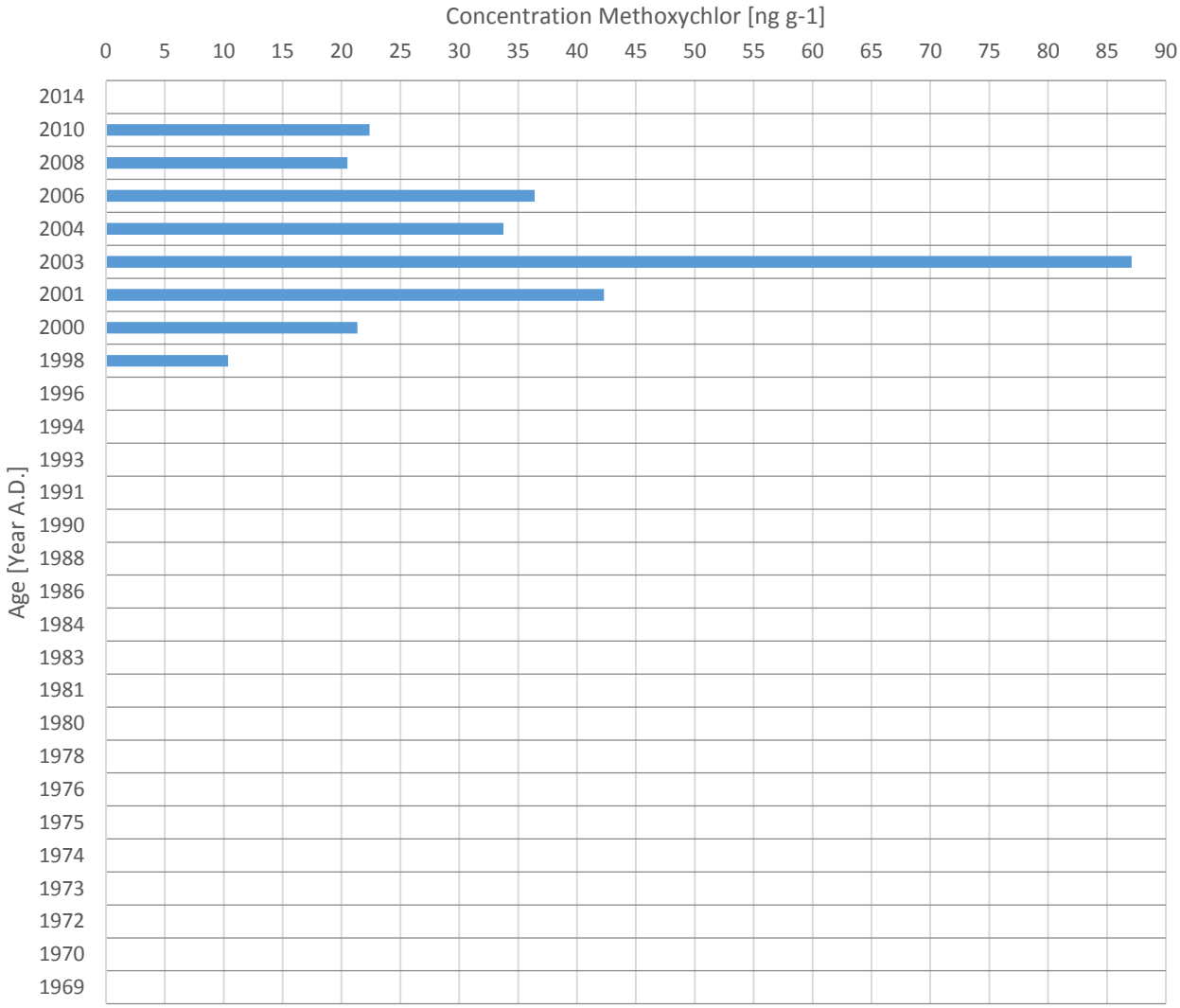


*Fig 4.10. Changes in concentrations of Methoxychlor (ng $g^{-1}$) in sediments of L. Llaviuco*

## 4.6 POLYCYCLIC AROMATIC COMPOUNDS IN LAKE SEDIMENTS

The contents of PACs in the lake sediments are presented as concentrations (ng per g of dry sediments), organic carbon normalized concentrations (ng per g of C in sediments) and fluxes (ng $cm^{-2}$ $yr^{-1}$). Carbon content is the sorbent of organic compounds, therefore, we normalize the PAC concentrations to carbon in order to account for 'real' changes in concentrations, and not changes resulting from higher/lower concentrations of carbon at one depth compared to another. Concentrations of PAC in the sediment also depend on sedimentation rates of clastic materials into the lakes. It is important to consider temporal variations in the sediment yields, as Fig. 4.11 and 4.12 show the difference in the profile of PAC concentrations (red dashed line) and the flux profile (grey shaded area). Flux is calculated by mass/time*area. To calculate the flux (ng $cm^{-2}$ $yr^{-1}$) from the CRS model, mass accumulation rate (g $cm^2$ $yr^{-1}$) was multiplied against the concentration of PACs in the sediment sample section.

### 4.6.1 Laguna Fondococha

The temporal variations in the flux and concentrations of PACs are shown Fig. 4.11 (table showing details of fluxes can be found in Annex 3, Table A.3.4). From 1885 – 1958 the fluxes of ΣPAHs did not change much (average: 1.86 ng $cm^2$ $yr^{-1}$, range: 1.02 – 2.76 ng $cm^2$ $yr^{-1}$). After 1958 the ΣPAHs fluxes increase by a factor of 2.37 with an average of 4.4 ng $cm^2$ $yr^{-1}$ for the period 1958 – 2014. The mean fluxes for the period (1958 – 2014) compared to background levels (1885 – 1958) was statistically tested using a two-sample t-test (*df* = 14; *p-value* < 0.01). This result shows that the difference in the pre- and post-1958 mean fluxes is statistically significant. From Fig. 4.11 we can identify three peaks in the ΣPAHs fluxes. The highest flux of ΣPAHs was in the 1980s (1981–1989), after which there has been consistent decreases until recent. The oldest peak occurs around 1907, after which fluxes decrease and stay low and invariant until the drastic and continuous increase in fluxes starting from 1958.

Retene, an indicator of biomass burning, only sees its first significant increase from background values in the 1960s (Fig. 4.11). Fluxes of retene peaked in the period between 1981 and 1989. Post 1958 fluxes of retene increases by a statistically significant factor of 3.04 (*df* = 10; *p-value* < 0.01) compared to the pre-1958 average flux. The temporal profiles of retene mirror that of the ΣPAHs.

The variations in fluxes of ΣLMW-PAHs (an indicator of low temperature/biomass combustion) mirror those of ΣPAHs and retene. The ΣLMW-PAHs fluxes stay low and invariant (ranging between 0.32 to 0.79 ng $cm^2$ $yr^{-1}$) from 1885 till 1958 when it begins to increase until its peak in 1980-1989. The post 1958 average flux increased by a factor of 2.41 (statistically significant with *df* = 12; *p-value* < 0.05) compared to pre-1958 fluxes. Since its peak value in the 1980s the fluxes have decreased until recent times. The temporal trends in ΣLMW-PAHs (including the periods of highest fluxes) are very similar to that of the ΣPAHs and retene.

The ΣCOMB-PAHs also remained low and largely invariant between 1885 and 1958, after which there is a large and steady increase in the flux levels from 1958 reaching its peak around 2000 before showing slight decreases until recent. The mean increases in fluxes of ΣCOMB-PAHs increase post-1958 by a factor of 5.8 compared to pre-1958 levels and a t-test showed that this increase is statistically strongly significant (*df* = 15; *p-value* < 0.01).

Perylene was the dominant individual PAH in most of sections of the sediment with fluxes ranging between 3.77 to 25.31 ng $cm^2$ $yr^{-1}$. The temporal variation in the fluxes of perylene was different from the other combustion derived PAHs demonstrating the well-known fact that perylene has non-combustion sources (Silliman et al. 2001, 1998) . The fluxes of perylene were high and stable between 1885-1915 followed thereafter by significant decreases until 1958. Large increases in flux are observed beginning in 1958, peaking in 1985 before decreasing till its lowest levels from 1990s until recent.

The variations in the fluxes of ΣOPAHs and ΣAZAs (Fig. 4.11) follow similar patterns as those of the ΣPAHs, retene, ΣCOMB-PAHs. ΣOPAHs flux ranges between 0.28 and 1.39 ng $cm^2$ $yr^{-1}$, while ΣAZAs ranges between 0.03 and 0.10 ng $cm^2$ yr-1. Both show relatively stable background fluxes from 1885 till 1958, before their dramatic increases by factors of 2.63 (OPAHs) and 1.99 (AZAs) post 1958. The post 1958 increase in fluxes was statistically significant (with $df = 11$; $p\text{-}value < 0.01$ and $df = 12$; $p\text{-}value < 0.01$ respectively). OPAHs and AZAs fluxes have decreased since their peak levels in the 1980s.

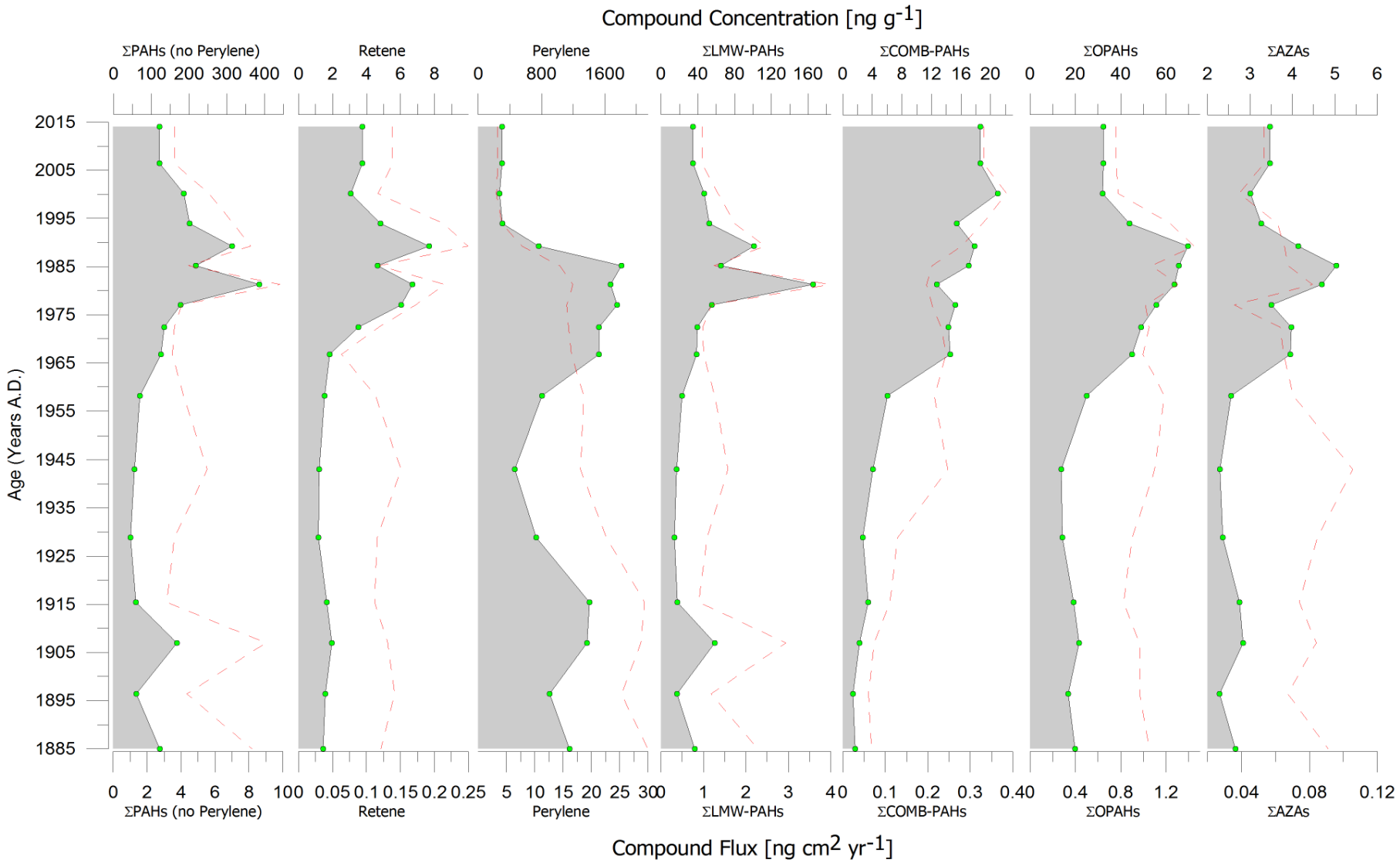


*Fig 4.11. From left to right: fluxes (grey) and concentration (red dashed line) of the sum of PAHs (no Perylene), Retene, Perylene, sum of Low-Molecular-Weight PAHs, sum of Combustion PAHs, sum of Oxygenated PAHs (OPAHs) and sum of Azaarenes (AZAs) in Laguna Fondococha. Green dots represent sample points.*

### 4.6.2 Laguna Llaviuco

Temporal changes in the flux of the ΣPAHs can be visualized in Fig. 4.12 and range from 16.37 (ca. 1969) to 52.51 (ca. 1996) ng $cm^2$ $yr^{-1}$, with the average flux of the ΣPAHs being 29.13 ng $cm^2$ $yr^{-1}$. A table of fluxes and averages for all PAHs for L. Llaviuco can be found in Annex 3, Table A.3.5. We can see three prominent peaks in the ΣPAHs which occur around 1973, 1996 and 2006. After the first initial peak in 1973, the flux of the ΣPAHs remains more or less stable until it dips in 1993 prior to rising to its largest peak in 1996. Thereafter fluxes decrease again, remain constant, and increase to the third peak in 1996. As a result of the age-depth model for L. Llaviuco, we cannot identify background levels of PAHs prior to an initial increase. The age-depth model provides ages until 1969, and although fluxes are generally lower for all measured PAHs, OPAHs and AZAs at 1969 compared to up-core fluxes, it cannot be assumed that we have reached background levels at 1969.

Retene remains relatively constant in the core profile ranging from 0.42 to 1.83 ng $cm^2$ $yr^{-1}$. In Fig. 4.12 we see two peaks, firstly in 1984 and secondly in 2014, neither of which are mirrored in other PAH profiles in L. Llaviuco.

ΣLMW-PAHs see an initial increase from 1969 to 1975, thereafter they fluctuate with small peaks and dips until ca. 2010 where a dramatic decrease occurs before increasing again to 2014. The average flux for the ΣLMW-PAHs is 8.04 ng $cm^2$ $yr^{-1}$ with the largest peak occurring in 1996.

ΣCOMB-PAHs also see an initial increase from 1969 to 1975, thereafter it remains more or less stable until 1993 where an increase by a factor of 1.2 (statistically significant with $df = 23$; $p\text{-value} < 0.01$) occurs. After the initial peak in 1996 the ΣCOMB-PAHs remain more or less constant.

Perylene remains relatively constant within the core profile until a clear peak occurs in 1996. Thereafter, post 2003, fluxes decrease by a factor of 2.2, which was found to be statistically significant with a t-test with $df = 18$ and $p\text{-values} < 0.01$.

ΣOPAHs and ΣAZAs follow similar profiles throughout the sediment core. OPAHs range between 5.38 and 8.25 ng $cm^2$ $yr^{-1}$ and exhibit a slight bulge in the profile between 1972 and 1986 (see Fig. 4.12). ΣAZAs similarly exhibits this bulge in its profile between 1972 and 1984. After this initial bulge, both OPAHs and AZAs remain relatively constant throughout the profile.

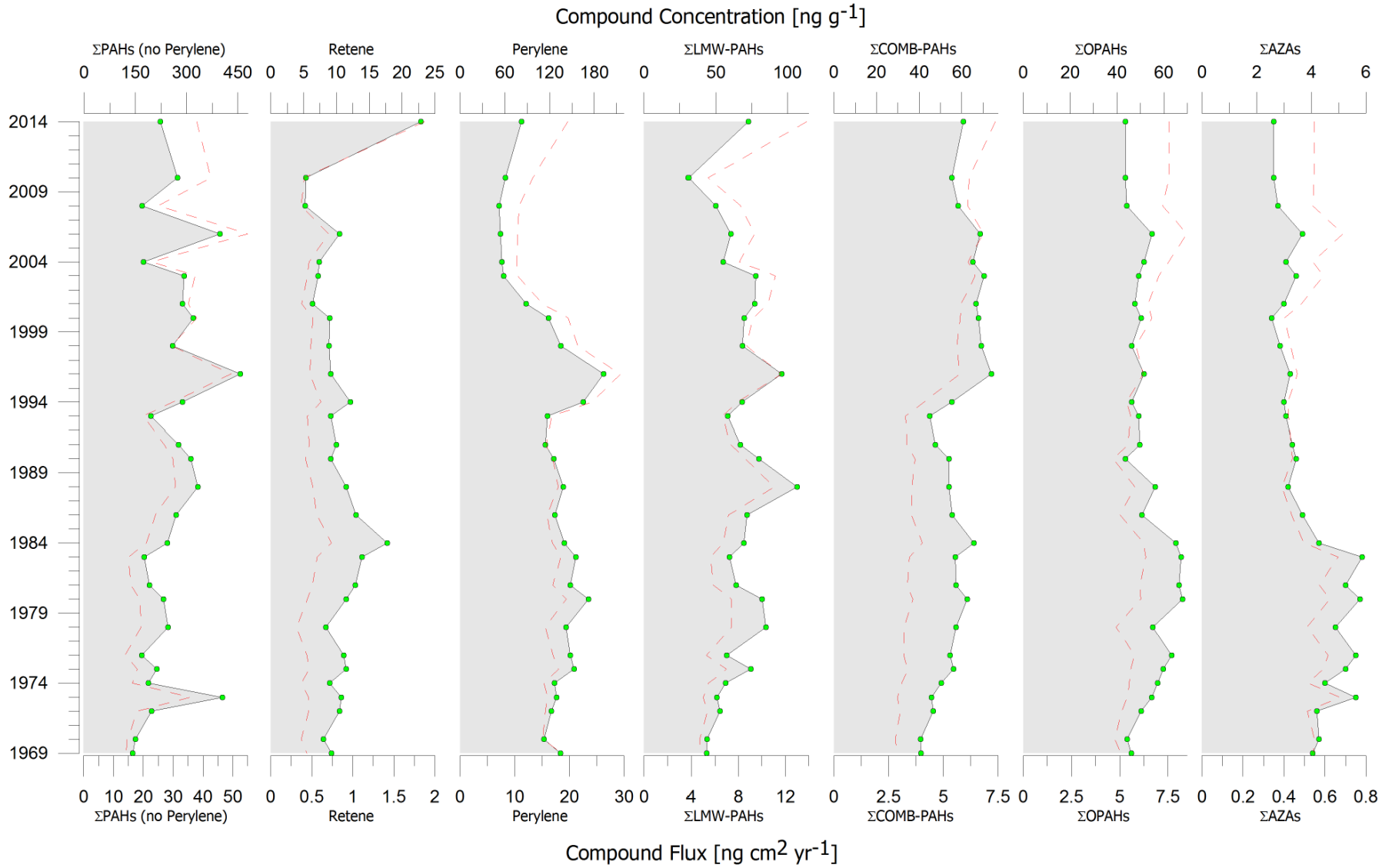


*Fig 4.12. From left to right: fluxes (grey) and concentration (red dashed line) of the sum of PAHs (no Perylene), Retene, Perylene, sum of Low-Molecular-Weight PAHs, sum of Combustion PAHs, sum of Oxygenated PAHs (OPAHs) and sum of Azaarenes (AZAs) in Laguna Llaviuco. Green dots represent sample points.*

### 4.6.3 Molecular Diagnostic Ratios

#### 4.6.3.1 Laguna Fondococha

In L. Fondococha, ΣLMW-PAHs/ΣHMW-PAHs ratio was >1 (highest > 4 from 1885 – 1907) and remained > 1 from the oldest sections until the early 21st century (ca. 2006), thereafter the ratio decreased to < 1. In Annex 3, Table A.3.8 shows absolute molecular diagnostic ratios for L. Fondococha. In Fig. 4.13 we see a decreasing trend to the top of the core. The ΣCOMB-PAHs/ΣParent-PAHs ratio was low until 1907 and then shows a progressive increase starting from 1915 and continuing until recent. The ratios of parent PAH/alky-PAHs (represented in Fig. 4.13 as NAPH/2-MNAPH) is gradually increasing over time, with their highest values occurring since 2006. For the ratio of ΣOPAH/ΣPAHs we cannot identify a trend, however, there is a slight increase in ratio values from 1958 to 1972. This could indicate a relatively higher deposition of OPAH than PAHs. This increase in the ratio could indicate towards air masses arriving from further distances or a period of intense precipitation. For the ratio of ΣAZA/ΣPAHs were fairly invariant. The ratio is slightly higher than background values between 1915 and 1929.

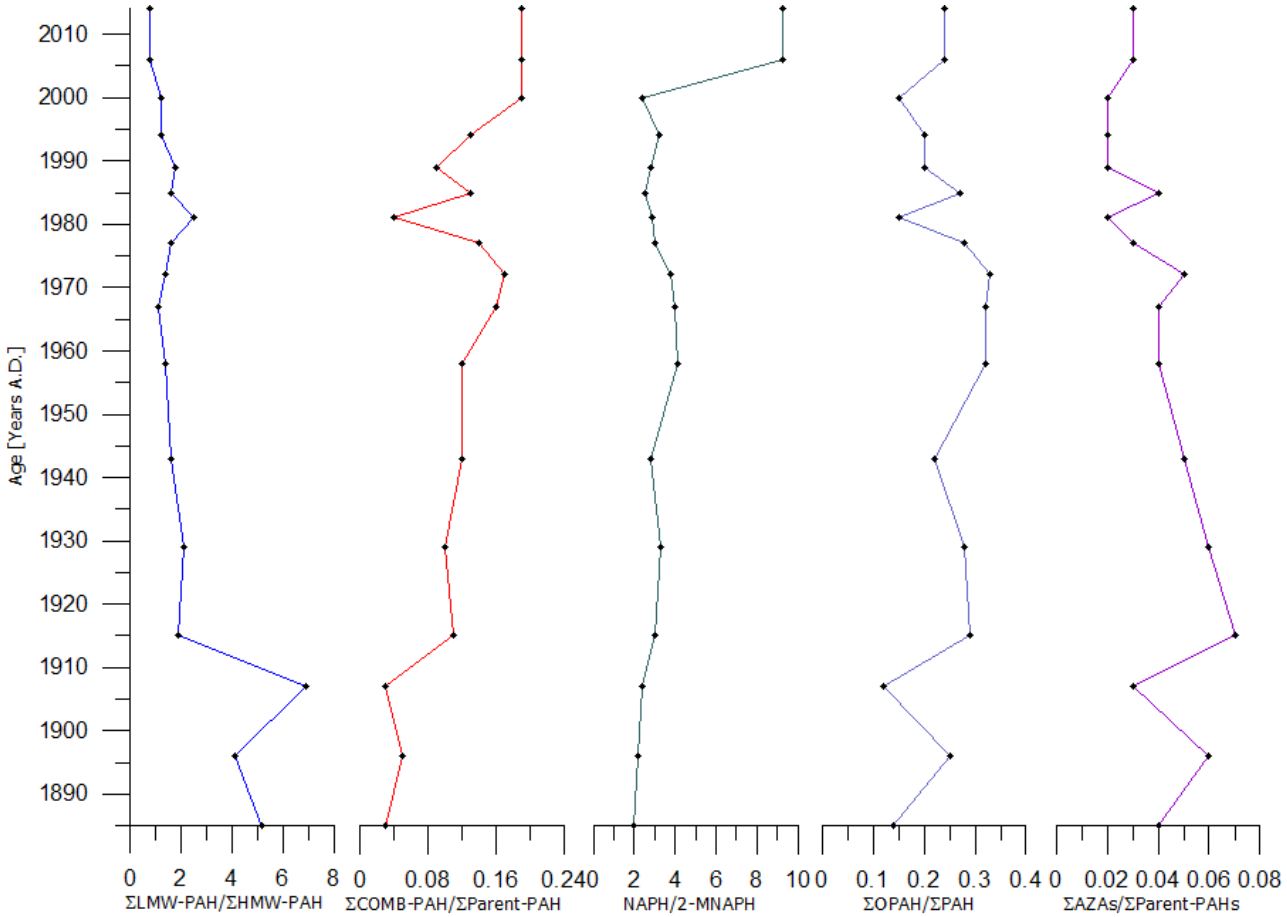


*Fig 4.13. PAH, OPAH and AZA molecular diagnostic ratios for L. Fondococha*

#### 4.6.3.2 Laguna Llaviuco

Table A.3.9 in Annex 3 displays the absolute molecular diagnostic ratios for L. Llaviuco. The ratio of ΣLMW-PAHs/ΣHMW-PAHs remains > 1 until 2003, where it shifts to < 1. The ΣCOMB-PAHs/ΣParent-PAHs ratio (Fig. 4.14 and Table A.3.9) remains relatively stable until 1988, thereafter there is a clear increase until present day. The parent to alkyl-substituted PAHs (represented in Fig. 4.14 as NAPH/2-MNAPH) shows a fluctuating index that remains > 1 until the early 2000s, after which it decreases dramatically (after 2006 < 1). ΣOPAH/ΣPAH and ΣAZA/ΣPAHs display similarly invariant profiles, with a strong decrease in index values at the top of the core.

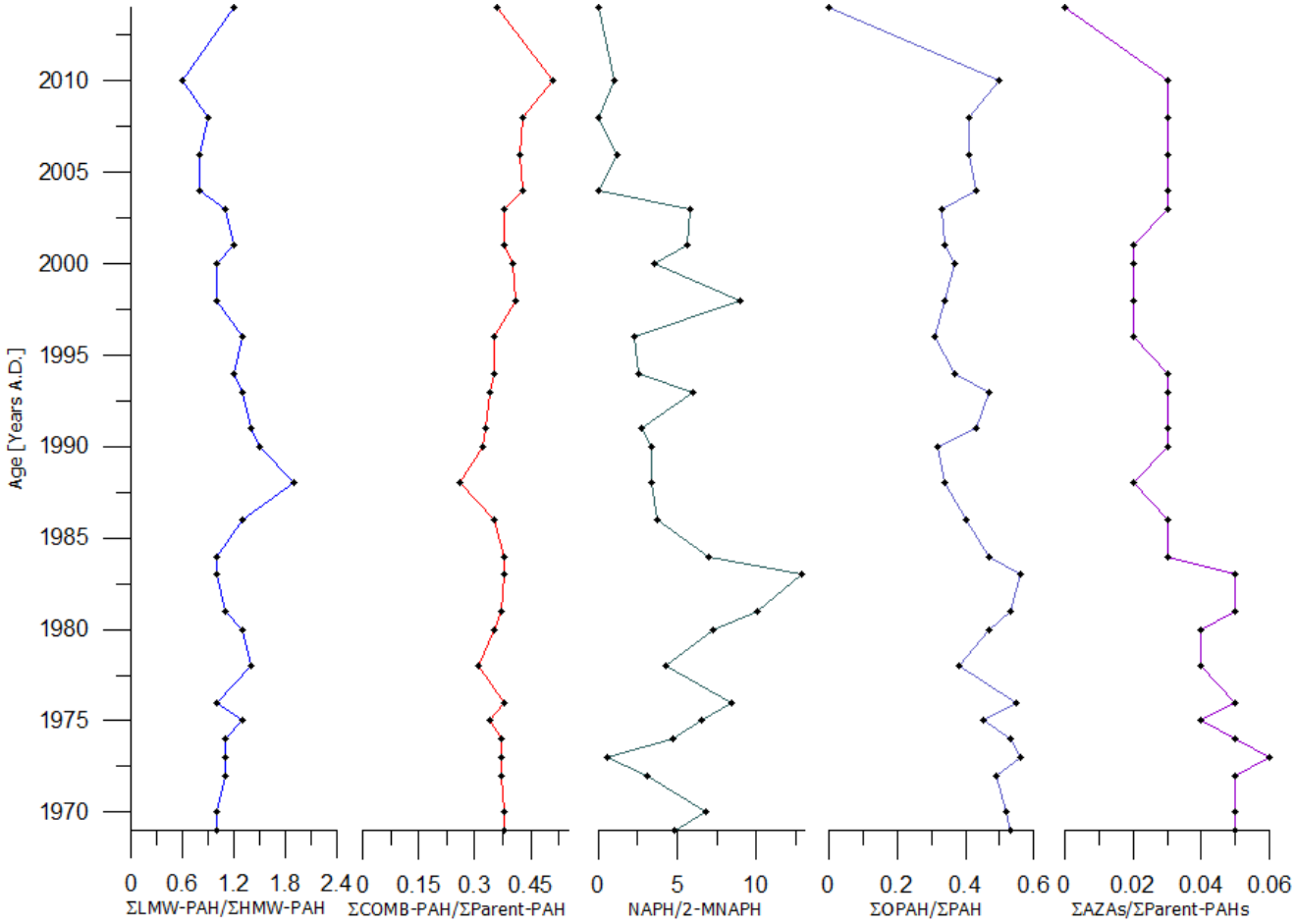


*Fig 4.14. PAH, OPAH and AZA molecular diagnostic ratios for L. Llaviuco*

## 4.7 MERCURY AND TRACE METALS IN LAKE SEDIMENTS

### 4.7.1 Laguna Fondococha

As seen in Fig. 4.15, temporal variations in the fluxes for Hg range between 0.68 (ca. 1896) to 4.17 (ca. 1985) ng $cm^2$ $yr^{-1}$, with an average Hg flux of 2.06 ng $cm^2$ $yr^{-1}$. In the profile of Hg, Cu, Zn, Pb and Cr we see the same initial increase in the pollution signal of the sediment profiles at ca. 1958 as we do in the profiles of the PACs. Pre-1958, the average flux of Hg to the sediment was 0.87 ng $cm^2$ $yr^{-1}$, which we can assume to be background fluxes of Hg. However, post-1958 the average flux of Hg increased by a factor of 3.32 to 2.06 ng $cm^2$ $yr^{-1}$. This increase in means was found to be statistically significant with a t-test (*df = 12*, *p < 0.01*). There is a clearly pronounced peak in the Hg profile of L. Fondococah which occurs in 1985 and indicates towards just over a decade (from ca. 1981 to 1994) of increased Hg deposition in the lake.

Copper sees a slight initial increase in its flux which facilitates a minor buldge in the profile from ca. 1896 to 1943, a buldge which is similarly mirrored in the profiles of Hg, Zn, Pb and Cr (see Fig. 4.15). The average flux of Cu pre-1958 is 174.97 ng $cm^2$ $yr^{-1}$, which increases by a factor of 2.6 post-1958 to an average flux of 448.25 ng $cm^2$ $yr^{-1}$ (statistically significant with *df = 13, p < 0.01*). Cu fluxes peak firstly in 1989, but we see the strongest increase in Cu flux in ca. the last decade with 719.7 ng $cm^2$ $yr^{-1}$ deposited in 2014.

Zinc, lead and chromium follow relatively similar profiles. They all experience the same slight bulge from ca. 1896 to 1943 and all have the same large initial increase around 1958 (see Fig. 4.15). Average flux values are 1035.35 ng $cm^2$ $yr^{-1}$ (Zn), 317.47 ng $cm^2$ $yr^{-1}$ (Pb), and 204.16 ng $cm^2$ $yr^{-1}$ (Cr), all of which experience a factor increase of over 2 (2.18, 2.29 and 2.14 respectively, all statistically significant with *df = 15, p < 0.01*) after 1958. From 1958 the three metals increase to a first small peak around 1977, followed by the largest peak in 1985. Thereafter all three metals decrease in flux values to 1994, afterwhich they stabilize to present day values. A table of fluxes for all trace metals can be found in Annex 3, Table A.3.6.

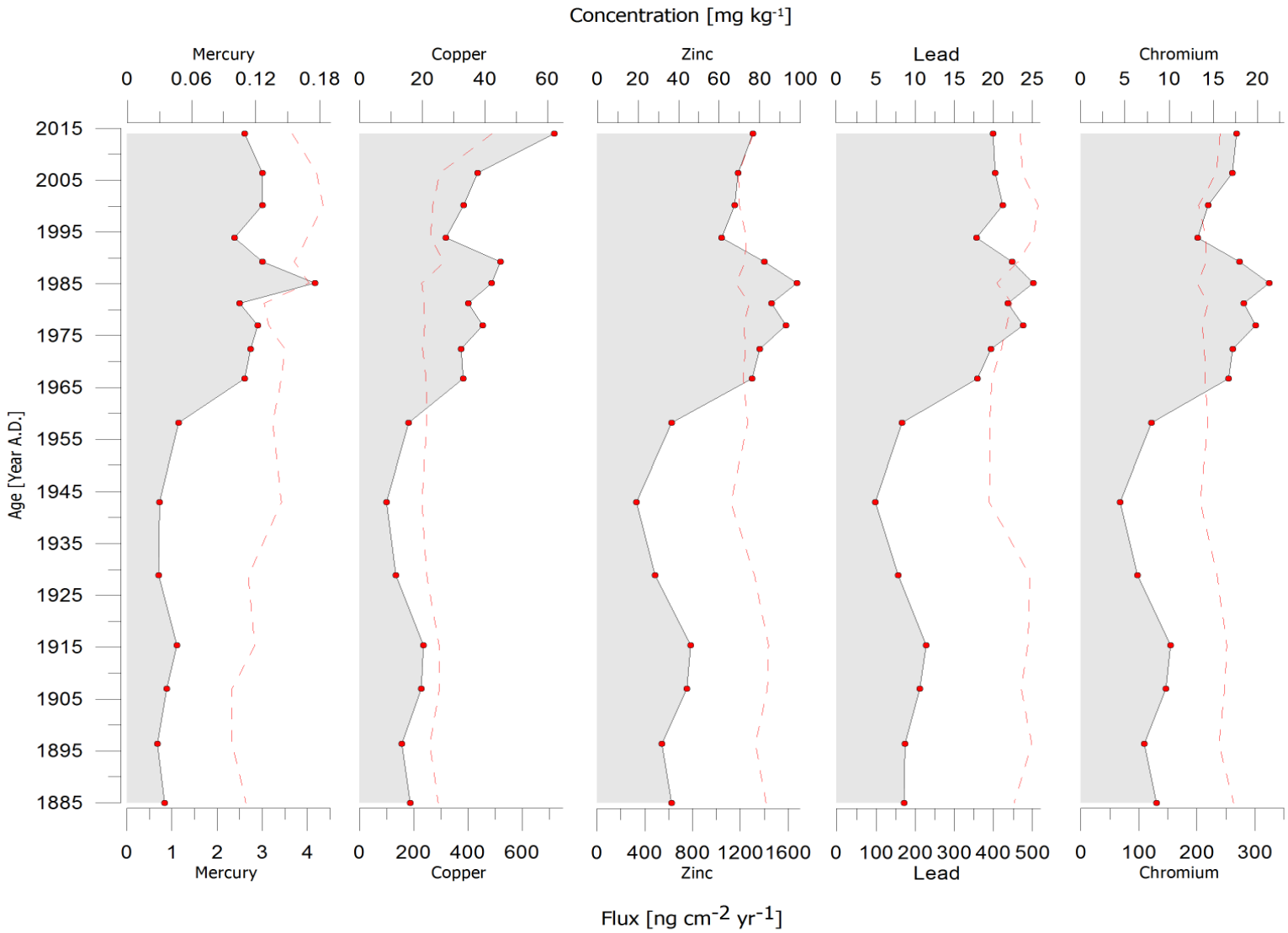


*Fig 4.15. Fluxes in ng cm$^{-2}$ yr$^{-1}$(grey shaded area) with measurement points (red dots); compound concentration in mg kg$^{-1}$ (red dashed line) for Hg, Cu, Zn, Pb and Cr in Laguna Fondococha*

### 4.7.2 Laguna Llaviuco

Fig. 4.16 shows the temporal vairations of Hg and heavy metals in the sediments of L. Llaviuco since 1969. As the background levels of these elements were not reached it is not possible to visualize the initial increae of these toxic pollutants. For Hg , the flux values range from 20.85 ng $cm^2$ $yr^{-1}$ (ca. 2014) to 48.18 (in ca. 1980), with an average flux of 33.72 ng $cm^2$ $yr^{-1}$. Starting from ca. 1973 there is an increase in Hg flux which reaches its maximum in 1980 and gradually decreases again to 1994. Fluxes remain constant until about the year 2000, where they decrease to 2005, increase again slightly till 2010, and from 2010 to 2014 we see a decrease in the flux of Hg in the sediment core. From 2005 – 2014 we see the lowest values of Hg since 1969.

The copper profile we see in Fig. 4.16 for L. Llaviuco is interesting as it remains relatively stable with the exception of one very large peak in 1975, which could be an outlier. On average, the flux of Cu (exluding the 1975 peak) is 7339.83 ng $cm^2$ $yr^{-1}$, which means that from 1974 to 1977 (the Cu 'peak') the Cu flux increased by a factor of 2.6 to 19,229.83 ng $cm^2$ $yr^{-1}$. Post 1978 we see a decreasing trend in Cu fluxes until its lowest value is reached in 2014.

Zinc and lead follow similar profiles, with average fluxes of 44,193.10 and 23,945.87 ng $cm^2$ $yr^{-1}$ respectively, and exhibit an increasing trend in flux values from about 1969 until they peak in 1978 with their largest depositional flux of 72,739.18 ng $cm^2$ $yr^{-1}$ (Zn) and 46,179.36 ng $cm^2$ $yr^{-1}$ (Pb). From the 1978 peak on towards present day we see a clear decreasing trend in both Zn and Pb flux in the sediment core.

Chromium also shows an increasing trend starting from 1969 and peaks in 1980 with a flux of 8276.84 ng $cm^2$ $yr^{-1}$, afterwhich there is a steadily decreasing trend until the lowest values in this section of the core are reached in 2014. Average flux for Cr in L. Llaviuco is 5788.73 ng $cm^2$ $yr^{-1}$. A table of fluxes for all trace metals can be found in Annex 3, Table A.3.7.

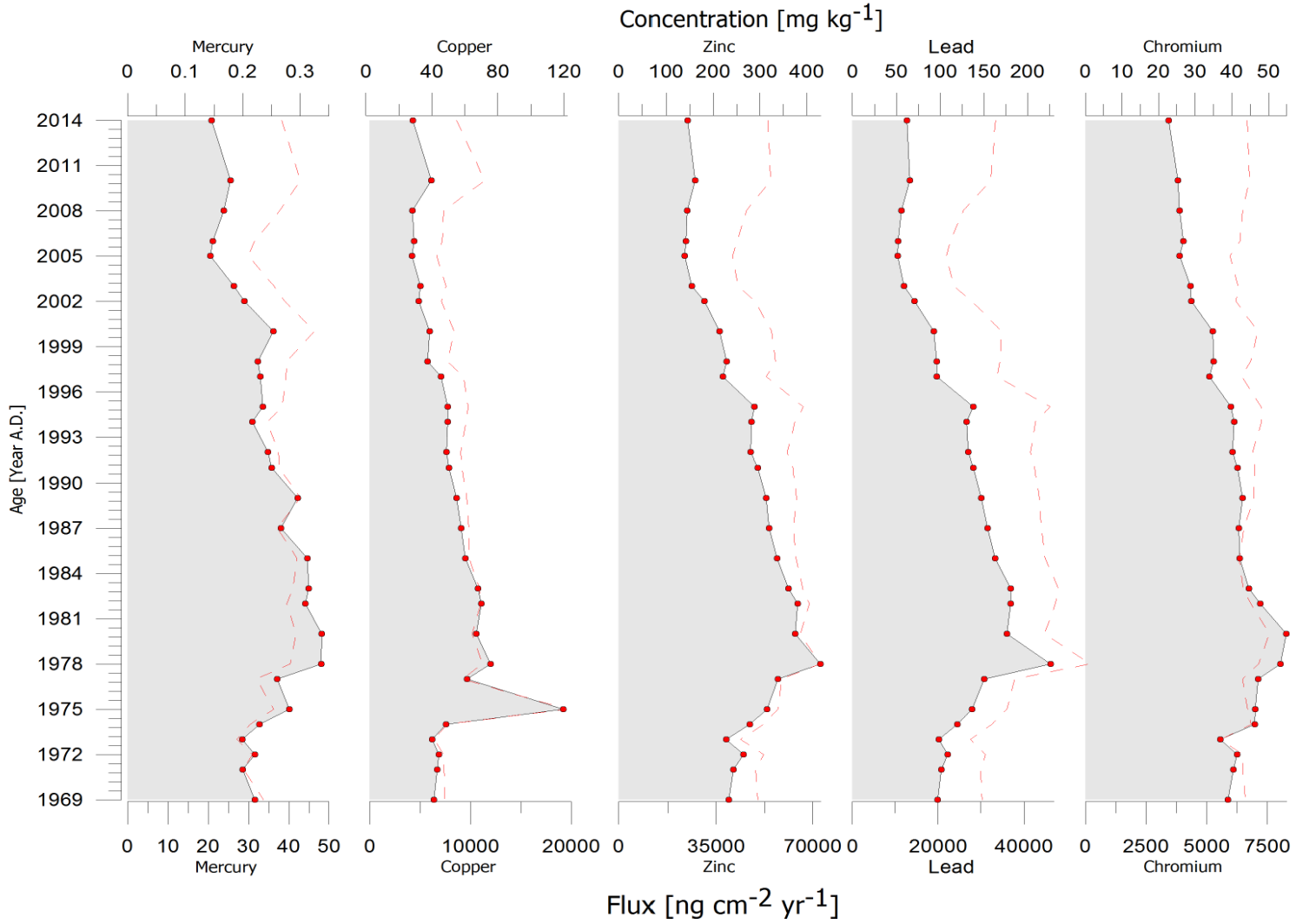


*Fig 4.16. Fluxes in ng cm$^{-2}$ yr$^{-1}$(grey shaded area) with measurement points (red dots); comound concentration in mg kg$^{-1}$ (red dashed line) for Hg, Cu, Zn, Pb and Cr in Laguna Llaviuco.*

## 4.8 RELATIONSHIPS BETWEEN SEDIMENTARY GEOCHEMICAL PROPERTIES

The relationships between PACs, heavy metals, C and C/N measured in the sediments were investigated using statistical approaches (correlation & principal component analysis). First and foremost a correlation matrix was used to investigate the dependence between multiple groups of variables at the same time. Variable groups in the correlation matrix are as follows: ΣLMW-PAHs, ΣHMW-PAHs, ΣCOMB-PAHs, PERY, RET, ΣOPAHs, ΣAZAs, C, C/N, Hg, Cu, Pb, Zn, Cr. In order to compute the correlation coefficients between each variable, the method of Pearson parametric correlation test was implemented which measures the linear dependence between two variables.

### 4.8.1 Laguna Fondococha

Table 4.1 shows that there are significant relationships between some of the variables. Firstly, it is clear that total organic carbon (C) and the C/N ratio are both strongly positively correlated with not only each other but also with ΣCOMB-PAHs. C correlates strongly with also Hg and ΣHMW-PAHs. Hg has significantly strong positive relationships with ΣHMW-PAHs and ΣCOMB-PAHs. Zn and Cr correlate strongly together. PERY has strong negative correlations with C, C/N, ΣCOMB-PAHs, Hg and ΣHMW-PAHs. Hg also experiences a strong negative correlation with Zn. ΣLMW-PAHs and OPAHs have a strong positive relationship, as do ΣOPAHs and retene. ΣAZAs seem to only correlate positively with PERY.

*Table 4.1. Correlation matrix for Laguna Fondococha of ΣLMW-PAHs, ΣHMW-PAHs, ΣCOMB-PAHs, PERY, RET, ΣOPAHs, ΣAZAs (ng g$^{-1}$), C (%), C/N and Hg, Cu, Pb, Zn, Cr (mg kg$^{-1}$). Correlation coefficients are coloured accourding to their significance (**green**: p < 0.05; **blue**: p < 0.01; **red**: p < 0.001)*

| | Hg | Cr | Cu | Zn | Pb | ∑LMW | ∑HMW | ∑COMB | ∑OPAH | ∑AZA | C | C/N | RET | PERY |
|---|---|---|---|---|---|---|---|---|---|---|---|---|---|---|
| **Hg** | 1.00 | **-0.81** | 0.17 | **-0.93** | -0.16 | 0.03 | **0.99** | **0.95** | 0.44 | **-0.65** | **0.87** | **0.75** | **0.70** | **-0.95** |
| **Cr** | **-0.81** | 1.00 | 0.41 | **0.94** | **0.58** | -0.40 | **-0.85** | **-0.62** | **-0.80** | 0.13 | -0.44 | -0.25 | **-0.75** | **0.59** |
| **Cu** | 0.17 | 0.41 | 1.00 | 0.12 | **0.59** | -0.73 | 0.08 | 0.43 | **-0.71** | **-0.72** | **0.59** | **0.75** | -0.25 | **-0.46** |
| **Zn** | **-0.93** | **0.94** | 0.12 | 1.00 | **0.46** | -0.15 | **-0.93** | **-0.81** | **-0.57** | 0.38 | **-0.67** | -0.53 | **-0.66** | 0.78 |
| **Pb** | -0.16 | **0.58** | **0.59** | 0.46 | 1.00 | -0.36 | -0.21 | 0.01 | -0.45 | -0.49 | 0.25 | 0.34 | -0.07 | -0.08 |
| **∑LMW** | 0.03 | -0.40 | **-0.73** | -0.15 | -0.36 | 1.00 | 0.17 | -0.26 | **0.81** | **0.55** | -0.38 | -0.52 | **0.59** | 0.24 |
| **∑HMW** | **0.99** | **-0.85** | 0.08 | **-0.93** | -0.21 | 0.17 | 1.00 | **0.90** | **0.56** | **-0.56** | **0.80** | **0.67** | **0.79** | **-0.90** |
| **∑COMB** | **0.95** | **-0.62** | 0.43 | **-0.81** | 0.01 | -0.26 | **0.90** | 1.00 | 0.17 | **-0.82** | **0.97** | **0.90** | 0.53 | **-1.00** |
| **∑OPAH** | 0.44 | **-0.80** | **-0.71** | **-0.57** | -0.45 | **0.81** | **0.56** | 0.17 | 1.00 | 0.24 | 0.01 | -0.21 | **0.83** | -0.18 |
| **∑AZA** | **-0.65** | 0.13 | **-0.72** | 0.38 | -0.49 | **0.55** | **-0.56** | **-0.82** | 0.24 | 1.00 | -0.91 | **-0.93** | -0.24 | **0.84** |
| **C** | **0.87** | -0.44 | **0.59** | **-0.67** | 0.25 | -0.38 | **0.80** | **0.97** | 0.01 | **-0.91** | 1.00 | **0.97** | 0.45 | **-0.98** |
| **C/N** | **0.75** | -0.25 | **0.75** | -0.53 | 0.34 | -0.52 | **0.67** | **0.90** | -0.21 | **-0.93** | **0.97** | 1.00 | 0.27 | **-0.91** |
| **RET** | **0.70** | **-0.75** | -0.25 | **-0.66** | -0.07 | **0.59** | **0.79** | 0.53 | **0.83** | -0.24 | 0.45 | 0.27 | 1.00 | **-0.56** |
| **PERY** | **-0.95** | **0.59** | -0.46 | **0.78** | -0.08 | 0.24 | **-0.90** | **-1.00** | -0.18 | **0.84** | **-0.98** | **-0.91** | **-0.56** | 1.00 |

Prior to running a PCA, a Detrended Correspondence Analysis (DCA) was run on the pollutant data from L. Fondococha. DCA is a similar method to PCA but it assumes a unimodal distribution model. DCA provides axes scaled in 'standard deviation units' (SD). As a rule of thumb, if the first axis is shorter that 2 SD (< 2), it suggests that the data can be successfully analysed using linear methods.

If the axis is longer than 3 SD (> 3) then a unimodal method is more effective. The length of the gradient for axis 1 for L. Fondococha, however, was very low (0.6 SD). For this reason, in a next step a PCA was run.

A PCA was run on L. Fondococha pollutant data that included all PAHs, OPAHs, AZAs, Hg, Cu, Pb, Zn, Cr as well as 23 further metals (PCA can be found in Annex 4, Table A.4.1). Some of the PAHs exhibit no concentration values with depth, therefore these values were removed from the PCA. The PCA resulted in 7 principle components (PCs) with an eigenvalue > 1 in all depths (*n = 17*). An eigenvalue > 1 indicates that PCs account for more variance than accounted by one of the original variables in the standardized data. It is common to use this as a cutoff point for which PCs are kept. Similarly, the number of PCs kept can be attributed to the number that accounts for a certain fraction of the total variance (usually ca. 80 - 90% of total variance explained). In L. Fondococha, the first 7 PCs explain 95% of the variability of the dataset. In order to extract the results of the PCA for all the variables (all pollutants), the correlation between the variables and the PCs was visualized as coordinates (Fig. 4.17). Fig. 4.17 shows us how much each individual variable (compound) correlates with PC 1 and 2, with the colour scale indicating the overall contribution (in %) of that variable (compound) to the PC.

PC 1 (dim1) explains 47.9% of the variance in the dataset. PC 2 (dim 2) explains 20.9% of the variance. The distance metric the PCA tries to retain in the ordination axes is the Euclidean distance. The angle from the origin (coordinate 0,0) to the position of the variable indicated the (dis)similarity in a distribution. Variables that are grouped together with small angles from the origin are positively correlated, and we can see when looking at Fig. 4.17 that most of the metals, with the exception of Ag, Hg, As, Cu and Pb, strongly correlate positively together along PC 1. Perylene also strongly correlates with these metals. Perylene is a PAH with natural origins, therefore PERY and many of the trace metals positively grouped together would be indicative of a strong natural background element to PC1, for example erosion processes taking place in the catchment. Hg exhibits a relatively strong negative correlation to the rest of the metals, and tends to group together with HMW-PAHs. PC2 displays variable at a 90° angle to PC1, indicating no correlation between the distributions of the compounds. Along the axis of PC2 we tend to see strong positive correlations of LMW-PAHs, OPAHs and Retene. The variance contribution of each component to the first 7 PCs can be found in Annex 4, Table A.4.1. A PCA was run again on L. Fondococha, however this time all metals apart from those considered as strong pollutants (Hg, Pb, Cu, Zn, Cr) were removed from the analysis, and total organic carbon (C, %) and the C/N ratio were added as variables. The biplot for PC1 and 2 of this PCA can be found in Annex 4, Fig. A.4.1, and it shows us that PC1 is now mostly dominated by strong correlations between LMW-PAH and OPAHs, while PC2 correlates strongest with HMW-PAHs and Hg. PERY, Cr and Zn again group together and contribute in variance to PC1, and we can see that carbon and C/N correlate most with HMW-PAHs, especially combustion PAHs.

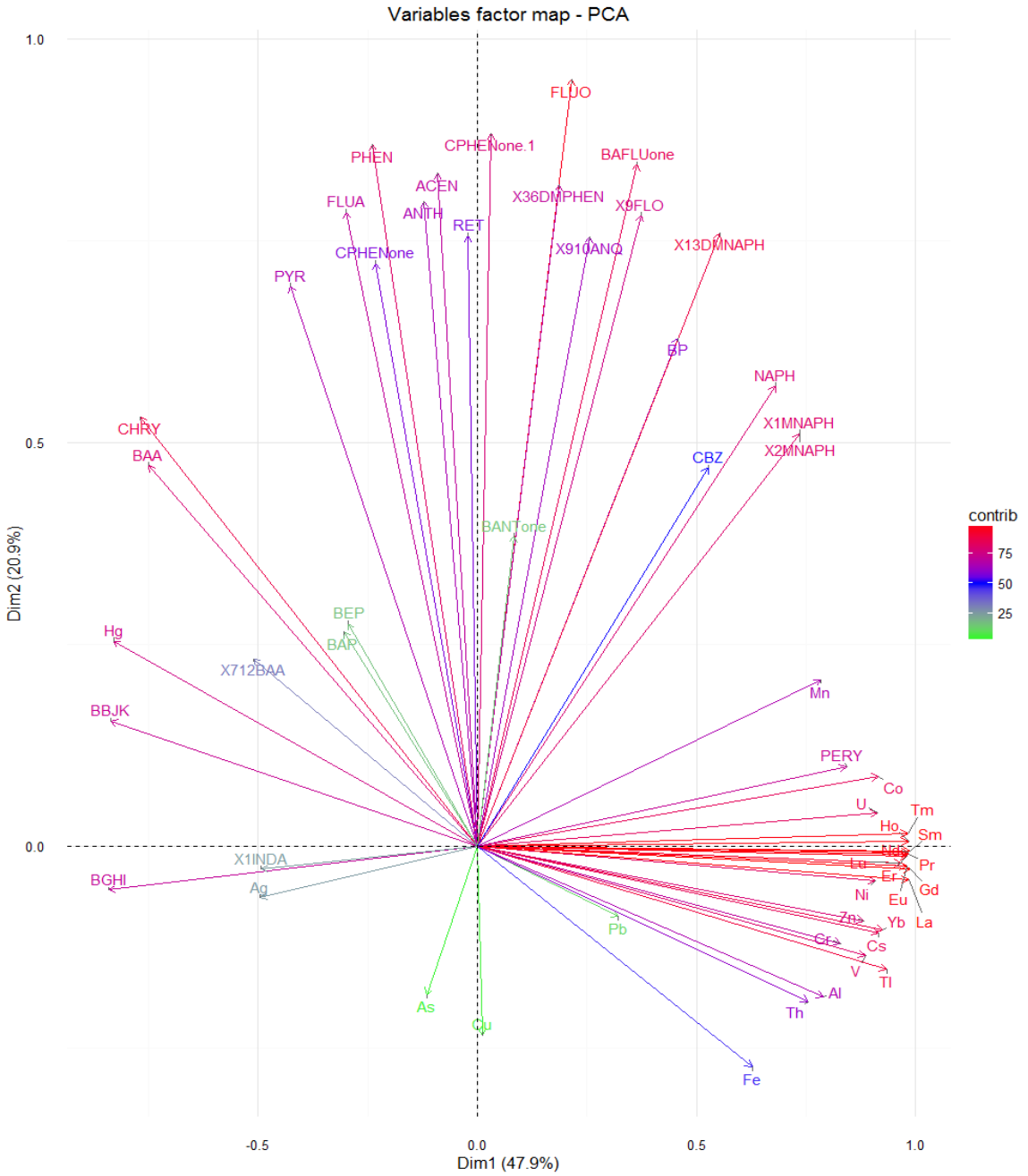


*Fig 4.17. Biplot for all measured elements in L. Fondococha for principal components 1 and 2 which includes all individual PAHs, OPAHs, AZAs, and metals. The colour gradient indicate the contribution (%) of individual variable to PCs.*

A last PCA was run on L. Fondococha in order to see how groups of pollutants were distributed. The ∑OPAHs, ∑LMW-PAHs, ∑HMW-PAHs, ∑AZAs, ∑COMB-PAHs as well as Cu, Pb, Hg, Zn, Cr, retene, perylene, C and the C/N ratio were plotted, as seen in Fig. 4.18. The first 3 PCs have an eigenvalue > 1 and explain 83% of the variance in the dataset. From Table 4.2, PC1 shows clearly the dominant compounds are Hg, HMW-PAHs and COMB-PAHs. While PERY and C also contribute a lot to the variance of PC1, in Fig. 4.18 you can see that the almost 180° angle between them indicates a strong negative correlation. COMB-PAHs correlate strongly with C and C/N. PC2 groups the LMW-PAHs, OPAHs, Cu and Cr together, and from Fig. 4.18 we can see that LMW and OPAHs correlate strongly together, but negatively with both Cu and Cr. PC3 clustered Zn, Pb, LMW-PAHs and retene together, and while a relationship may exist between RET and LMW, Zn and Pb both negatively correlate with retene and LMW-PAHs.

*Table 4.2. Contribution (%) of the variance of individual variables to the first three principle components (PCs) with eigenvalue > 1 in all depths (n = 17) using a PCA. Contributions ≥ 7% are highlighted in red.*

| | PC1 | PC2 | PC3 |
|---|---|---|---|
| **Hg** | 14.08 | 1.35 | 0.10 |
| **Cr** | 3.81 | 14.91 | 7.55 |
| **Cu** | 1.33 | 15.81 | 2.41 |
| **Zn** | 6.24 | 6.42 | 13.25 |
| **Pb** | 0.17 | 6.55 | 22.80 |
| **∑LMW** | 0.01 | 9.08 | 21.19 |
| **∑HMW** | 12.86 | 3.00 | 1.31 |
| **∑COMB** | 14.36 | 0.49 | 1.50 |
| **∑OPAH** | 1.03 | 17.83 | 7.61 |
| **∑AZA** | 4.24 | 6.73 | 0.67 |
| **C** | 12.90 | 3.75 | 0.28 |
| **C/N** | 9.91 | 8.70 | 0.12 |
| **RET** | 3.76 | 4.65 | 21.13 |
| **PERY** | 15.31 | 0.74 | 0.08 |

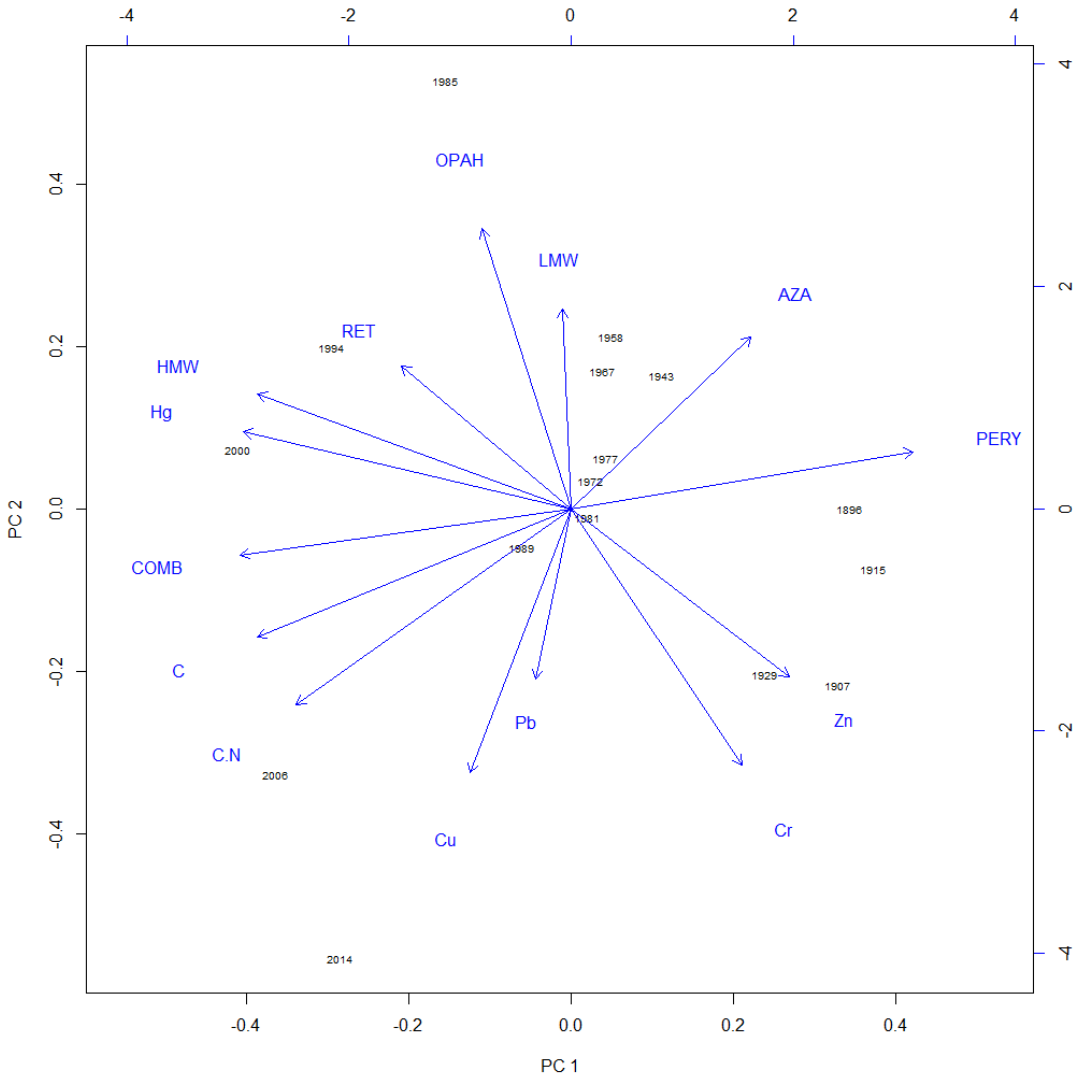


*Fig 4.18. Biplot of PC1 and PC2 showing pollutant group distribution of ∑OPAHs, ∑LMW-PAHs, ∑HMW-PAHs, ∑AZAs, ∑COMB-PAHs, Cu, Pb, Hg, Zn, Cr, retene, perylene, C and the C/N ratio for L. Fondococha from a PCA.*

### 4.8.2 Laguna Llaviuco

From Table 4.3 we see strong positive correlations again between Hg and ΣHMW and ΣCOMB-PAHs, as well as with C. Zn and Cr correlate strongly with each other, but Zn is negatively correlated with ΣCOMB-PAHs, Hg and ΣHMW-PAHs. ΣHMW-PAHs positively correlate with C and ΣCOMB-PAHs. ΣLMW-PAHs correlate positively with ΣOPAHs, which also correlate strongly with retene. ΣAZAs correlate positively only with PERY. The significant correlations in both L. Fondococha and Llaviuco are very similar, indicating that pollutants are interacting in the same way with each other in both lakes.

*Table 4.3. Correlation matrix for Laguna Llaviuco of ΣLMW-PAHs, ΣHMW-PAHs, ΣCOMB-PAHs, PERY, RET, ΣOPAHs, ΣAZAs (ng $g^{-1}$), C (%), C/N and Hg, Cu, Pb, Zn, Cr (mg $kg^{-1}$). Correlation coefficients are coloured accourding to their significance (**green**: $p < 0.05$; **blue**: $p < 0.01$; **red**: $p < 0.001$)*

| | Hg | Cr | Cu | Zn | Pb | ∑LMW | ∑HMW | ∑COMB | ∑OPAH | ∑AZA | C | C/N | RET | PERY |
|---|---|---|---|---|---|---|---|---|---|---|---|---|---|---|
| **Hg** | 1.00 | **-0.81** | 0.17 | **-0.93** | -0.16 | 0.03 | **0.99** | **0.95** | 0.44 | **-0.65** | **0.87** | **0.75** | **0.70** | **-0.95** |
| **Cr** | **-0.81** | 1.00 | 0.41 | **0.94** | **0.58** | -0.40 | **-0.85** | **-0.62** | **-0.80** | 0.13 | -0.44 | -0.25 | **-0.75** | **0.59** |
| **Cu** | 0.17 | 0.41 | 1.00 | 0.12 | **0.59** | **-0.73** | 0.08 | 0.43 | **-0.71** | **-0.72** | **0.59** | **0.75** | -0.25 | -0.46 |
| **Zn** | **-0.93** | **0.94** | 0.12 | 1.00 | 0.46 | -0.15 | **-0.93** | **-0.81** | **-0.57** | 0.38 | **-0.67** | -0.53 | **-0.66** | **0.78** |
| **Pb** | -0.16 | **0.58** | **0.59** | 0.46 | 1.00 | -0.36 | -0.21 | 0.01 | -0.45 | -0.49 | 0.25 | 0.34 | -0.07 | -0.08 |
| **∑LMW** | 0.03 | -0.40 | **-0.73** | -0.15 | -0.36 | 1.00 | 0.17 | -0.26 | **0.81** | **0.55** | -0.38 | -0.52 | **0.59** | 0.24 |
| **∑HMW** | **0.99** | **-0.85** | 0.08 | **-0.93** | -0.21 | 0.17 | 1.00 | **0.90** | **0.56** | **-0.56** | **0.80** | **0.67** | **0.79** | **-0.90** |
| **∑COMB** | **0.95** | **-0.62** | 0.43 | **-0.81** | 0.01 | -0.26 | **0.90** | 1.00 | 0.17 | **-0.82** | **0.97** | **0.90** | 0.53 | **-1.00** |
| **∑OPAH** | 0.44 | **-0.80** | **-0.71** | **-0.57** | -0.45 | **0.81** | **0.56** | 0.17 | 1.00 | 0.24 | 0.01 | -0.21 | **0.83** | -0.18 |
| **∑AZA** | **-0.65** | 0.13 | **-0.72** | 0.38 | -0.49 | **0.55** | **-0.56** | **-0.82** | 0.24 | 1.00 | **-0.91** | **-0.93** | -0.24 | **0.84** |
| **C** | **0.87** | -0.44 | **0.59** | **-0.67** | 0.25 | -0.38 | **0.80** | **0.97** | 0.01 | **-0.91** | 1.00 | **0.97** | 0.45 | **-0.98** |
| **C/N** | **0.75** | -0.25 | **0.75** | -0.53 | 0.34 | -0.52 | **0.67** | **0.90** | -0.21 | **-0.93** | **0.97** | 1.00 | 0.27 | **-0.91** |
| **RET** | **0.70** | **-0.75** | -0.25 | **-0.66** | -0.07 | **0.59** | **0.79** | 0.53 | **0.83** | -0.24 | 0.45 | 0.27 | 1.00 | **-0.56** |
| **PERY** | **-0.95** | **0.59** | -0.46 | **0.78** | -0.08 | 0.24 | **-0.90** | **-1.00** | -0.18 | **0.84** | **-0.98** | **-0.91** | **-0.56** | 1.00 |

For L. Llaviuco, a PCA was run that plotted the ΣOPAHs, ΣLMW-PAHs, ΣHMW-PAHs, ΣAZAs, ΣCOMB-PAHs as well as Cu, Pb, Hg, Zn, Cr, RET, PERY, C and the C/N ratio, as seen in Fig. 4.19. The PCA shows us that the first three PCs have eigenvalues > 1, however as they only explain 77% of the variance in the dataset, Table 4.4 portrays the first 4 PCs, which explain 84% of the dataset. In PC1 it is clear that ΣHMW-PAHs and ΣCOMB-PAHs dominate, along with C, Zn and Pb. Fig. 4.19 shows us that C, ΣCOMB- and ΣHMW-PAHs strongly correlate positively with each other, while they correlate negatively with Zn, Pb and Cr. PC2 favors Hg, ΣLMW-PAHs, ΣAZAs and RET. From Fig. 4.19 there is a clear positive correlation between retene and ΣLMW-PAHs, both of which correlate negatively with ΣAZAs. Hg tends to demonstrate no correlation between itself and RET/ΣLMW-PAHs, instead groups together positively with ΣHMW-PAHs and ΣCOMB-PAHs. For biplots of PC 2 + 3 and and PC 3 + 4 see Annex 4, Fig. A.4.2. PC3 is dominated by ΣOPAHs which correlate negatively with RET and positively with ΣAZAs. PC4 is dominated by Cu and PERY and there exists a strong negative correlation between the two compounds. C/N ratio also dominates in PC4 but has no correlation with either Cu or PERY.

*Table 4.4. Contribution (%) of the variance of individual variables to the first 4 principle components (PCs) explaining > 80% of the variance in all depths (n = 28) using a PCA. Contributions ≥ 7% are highlighted in red.*

| | PC1 | PC2 | PC3 | PC4 |
|---|---|---|---|---|
| **Hg** | 1.16 | 12.59 | 13.27 | 0.42 |
| **Cr** | 6.64 | 6.24 | 2.06 | 0.58 |
| **Cu** | 5.26 | 1.35 | 2.63 | 50.24 |
| **Zn** | 14.46 | 4.55 | 0.32 | 1.34 |
| **Pb** | 14.62 | 3.59 | 0.07 | 1.29 |
| **∑LMW** | 5.51 | 12.28 | 0.15 | 0.01 |
| **∑HMW** | 13.89 | 4.63 | 4.27 | 1.05 |
| **∑COMB** | 13.86 | 4.52 | 5.19 | 0.36 |
| **∑OPAH** | 0.50 | 6.04 | 36.02 | 0.34 |
| **∑AZA** | 0.37 | 16.37 | 10.31 | 1.09 |
| **C** | 16.71 | 2.50 | 0.98 | 0.23 |
| **C/N** | 1.76 | 6.73 | 11.80 | 11.76 |
| **RET** | 2.30 | 11.22 | 12.60 | 5.96 |
| **PERY** | 2.96 | 7.39 | 0.34 | 25.33 |

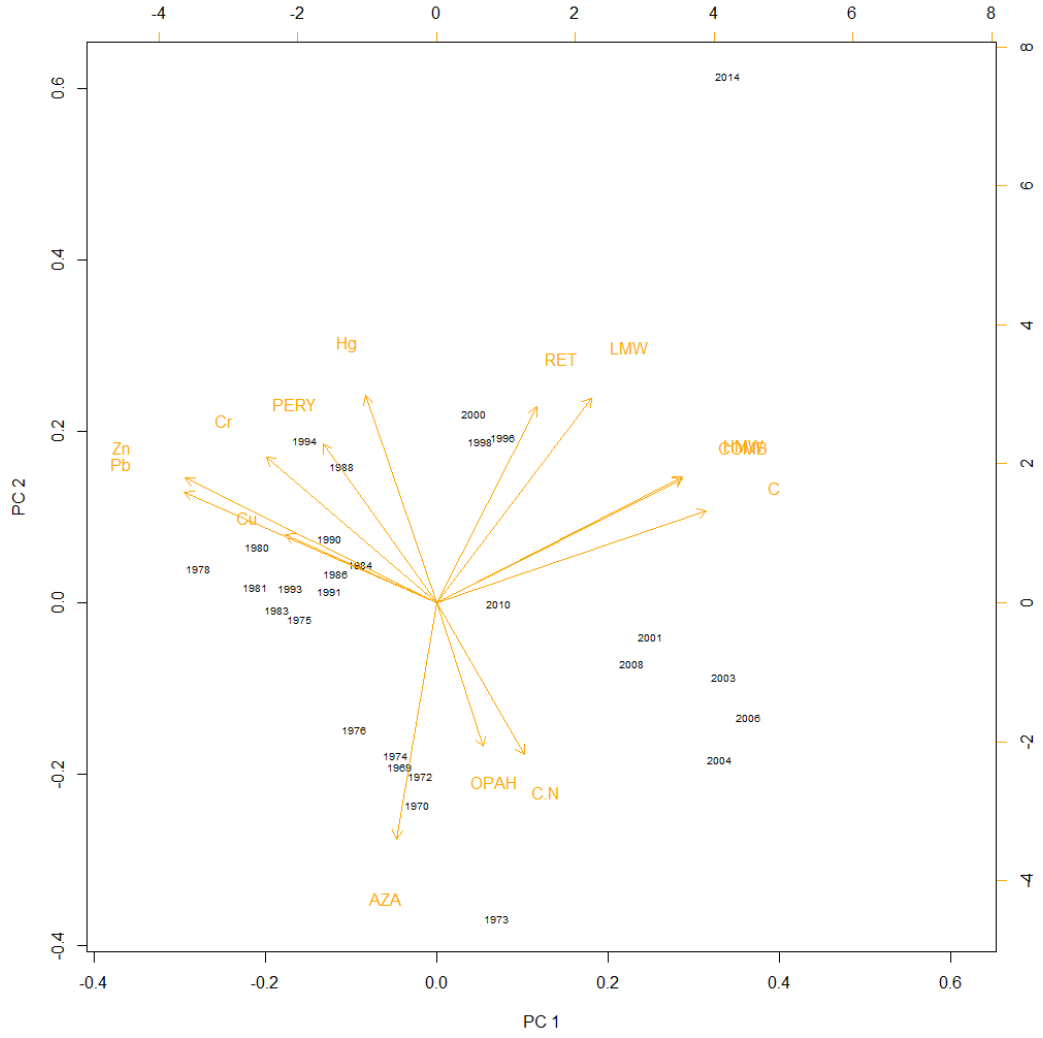


*Fig 4.19. Biplot of PC1 and 2 showing pollutant group distribution of ∑OPAHs, ∑LMW-PAHs, ∑HMW-PAHs, ∑AZAs, ∑COMB-PAHs, Cu, Pb, Hg, Zn, Cr, retene, perylene, C and the C/N ratio for L. Llaviuco from a PCA.*

# CHAPTER 5: DISCUSSION

## 5.1 AGE-DEPTH MODELS

$^{210}$Pb is a powerful technique for estimating the age of recently deposited sediments and applying modern sedimentation processes (Tylmann et al. 2013). When utilising any age-depth models the limitations of this model must always be taken into consideration. Most dating that is based on conceptual models, such as the CIC and CRS, generally provide acceptable results (Appleby 2008). However, these models have their limitations in that they do not always fulfill the asumptions and prerequisites required. If model restictions are not followed it can lead to significant errors in the $^{210}$Pb age of a sediment layer (Tylmann et al. 2013). Model choice can be subjective and for this reason stratigraphic markers are recommended to constrain the model.

### 5.1.1 Constraining the $^{210}$Pb Model

$^{137}$Cs values in the sediments were very low and sporadic, thus no reliable record of artificial $^{137}$Cs fallout was detected. Such low $^{137}$Cs concentrations could be an artifact of the location of Cajas NP within the InterAndean Cordillera corridor, or, on a larger scale, could be linked to its location in the southern hemisphere. Hancock et al. (2011) state that establishing chronostratigraphic horizons using $^{137}$Cs as a proxy age indicator is more problematic in the southern hemisphere as nuclear weapons fallout is roughly three times lower than in the northern hemisphere. This is attributed to the lower flux from atmosphere to land/lake as a result of the large ocean/land ratio in the southern hemisphere. The $^{137}$Cs peak is therefore more difficult to positively identify due to realtively high measurement uncertainties associated with low $^{137}$Cs concentrations (Hancock et al. 2002).

The majority of the 14 OCs measured in the sediment cores had concentrations below the limit of detection. This could be related to the remote nature of the location and/or the low mass of sediment available for extraction. Therefore, in the future, it would be advisable to increase the mass of the sediment in order to extract and detect more compounds. There were, however, a few OCs (at certain depths) that were detected, quantified and showed a slight trend. These included Methoxychlor in L. Llaviuco and Hexachlorobenzene (HCB), Beta-HCH, Dieldrin and Endrin, in L. Fondococha (see Annex 3, Tables A.3.1 and A.3.2 for concentrations). Of these detected OCs, HCB, Dieldrin and Endrin would have the most potential to be implemented as a chronomarker. They are known legacy POPs and have been detected in sediments from a time period of the late 1950s to early 1960s, whereafter they tend to decrease in concentration up to present day as a result of increased environmental awareness in the 1970s ad 80s in industrial countries (Warren et al. 2003). HCB has been in use since 1945 and as a result of its vapor pressue, water solubility and persistence in the environment, it is known for its long-range transport globally (Bailey 2001). These characeteristics would make it the most suitable OC that we detected for use as a chronomarker. However, the concentrations of HCB were detected in only one of three lakes measured beginning in ca. 1958 (Fig. 4.9, Table A.3.1). Furthermore, there are large uncertainities in HCB emission sources, especially in the concentration of HCB used in pesticides and chemical industries in developing countries (such as Ecuador), as well as from emissions of HCB from combustion and metal industries (Bailey 2001). Dieldrin and Endrin are first detected in 1915 and Endrin again in 1977. The legacy POPs detected in the samples tend not to follow known global emission trends, and thus the uncertainty of using them as independent event markers to

constrain the $^{210}$Pb models is considered too high. Exact dates of legacy POP implementation and useage in Ecuador would be beneficial to better interpret this data in the future.

### 5.1.2 Multi-Model Approach

As we are missing the presence of an independent marker to constrain the $^{210}$Pb model, multiple models (CIC, CRS) were tested in order to say with a certain degree of confidence that the chronology for each lake is accurate (Tylmann et al. 2013). The most appropriate model cannot be determined in advance and thus ages were calculated using all available models. The chronologies provided by the different models were diverse (see Annex 2, Fig. A.2.1 and A.2.2), which leads to the conclusion that no single model can provide a fully reliable $^{210}$Pb geochronology. However, with all the models tested on our lakes, it was clear that they all display similar trends until ca. 5 cm depth (L. Fondococha) and ca. 10 cm depth (L. Llaviuco), corresponding to ca. 1943 and ca. 1975 respectively. For this reason, any peaks and/or fluctuations in pollution proxies seen in the sedimentary profile of L. Fondococha in the past ca. 70 years can be considered true, and not an artifact of dating (and similarly for L. Llaviuco for the past ca. 40 years).

For both Laguna Fondococha and Llaviuco the CRS model was used to calculate an age-depth profile. Both models took into account a correction of the missing inventory (i.e. the amount of unsupported $^{210}$Pb contained in the lower section of a profile which is impossible to detect (Tylmann 2014)), and for L. Fondococha projected surface activity was also calculated. Without the missing inventory correction the CRS model often displays a tailing effect for the lower sediments (Fig 4.5). This distinct decrease with depth to minimum values in lower sections of the core are the result of age overestimations, which are attributed to an old-date error (Binford 1990; MacKenzie et al. 2011; Tylmann et al. 2013). For comparison, we look at the age-depth model that Michelutti et al. (2015) calculated for L. Llaviuco, also using the CRS model (see Annex 2, Fig A.2.2). The profile measured by Michelutti et al. (2015) is distinctively different from the profile presented in this study, and we attribute this difference to the fact that their model did not correct for the missing inventory. Consequently, the tailing effect is apparent starting around 6 cm depth in their age-depth profile. The tailing effect results from a systematic error occurring during the calculation of ages close to the end of the profile which causes an increasing divergence from the true age. Furthermore, non correction of the inventory of excess $^{210}$Pb in the core can foster an under-estimation of the predicted sedimentation rates (Binford 1990; Gharbi 2014; MacKenzie et al. 2011; Tylmann 2014; Tylmann et al. 2013).

For L. Llaviuco the correction of the missing inventory produced an age-depth model that reached an age of ca. 1930 at 23 cm of depth. In L. Llaviuco samples were measured for pollution proxies to a depth of 14.3 cm, which corresponds to the year 1969 from the corrected CRS age-depth model. The pollution history reconstruction for L. Llaviuco thus cannot extend past this point in time, and we do not reach background concentrations of pollution proxies either. It would be beneficial in the future to test the CRS model with various missing inventory corrections (i.e. correction calculations using only the lower values) and to measure pollution proxies further downcore. The CIC models for both lakes were disgarded as neither lake fulfilled the prerequisites (Appleby 2008; Cohen 2003). While it was attempted to calculate ages using the SIT model, programming issues with the model resulted in time constraints and unfortunately the model had to be disregarded for this study.

**Limitations**. A large amount of uncertainty exists in the dating of sediment cores. While using a multi-model approach can compensate for the lack of a useable independent marker, pin-pointing year by year differences and similarities between the lakes still hold a definite level of uncertainty which must be kept in mind when interpretations are made. Compounds measured in the lake sediments are measured as concentrations. The concentrations are measured relative to the sample mass, and are therefore not independent from each other, e.g. an up-core increase in concentration of an element could be explained either by an increase in its supply rates, or by a decrease in the supply rate of one or more of another component. It is for this reason that mass accumulation rate data is necessary from the $^{210}$Pb model, as it can unambiguously distinguish between these cases. However, it must be noted that $^{210}$Pb data is considerably less precise that concentration data, and thus presenting results as accumulation rates/fluxes may reduce precision. Further, where there are 'missing' accumulation or sedimentation rate values interpolation is required, which can add unknown biases to the data. It is also important to note that accumulation rates from any given core can differ greatly from the accumulation rate history of the lake as a whole, as local redistribution processes dominate accumulation rate history for any given region within the lake. Accordingly, measured accumulation rates in a core can be noisier than that of the entire lake (Boyle 2001).

## 5.2 POLLUTION HISTORY

### 5.2.1 Historic Variations of Polycyclic Aromatic Compounds

**South American Comparison.** On average L. Fondococha sees a flux of ΣPAHs (without perylene) for the years 1967 – 2014 of 4.4 ng cm$^2$ yr$^{-1}$, compared with L. Llaviuco which has an average flux of 29.12 ng cm$^2$ yr$^{-1}$ for the years 1969 – 2014. Fluxes of ΣPAHs larger by a factor of 6.6 for L. Llaviuco (*df = 33; p < 0.01*). For comparison with other lakes in the southern hemisphere, the study by Barra et al. 2006 and Quiroz et al. 2005 focuses on PAH fluxes in remote Lakes Laja and Galletue in the south central Chilean Andes (Table 5.1). Fluxes of ΣPAHs (without perylene) in these two lakes range from 0.8 to 19.6 ng cm$^2$ yr$^{-1}$, which is within the range of fluxes of PAHs that we find in L. Fondococha but generally lower than the range of PAHs levels in L. Llaviuco. Table 5.1 displays PAH flux trends from various remote mountain lakes and some industrial regions globally. When compared to fluxes of PAHs found in remote mountain lakes from Europe and North America, the fluxes of PAHs in lakes from South America are in the lower range (excluding L. Llaviuco). L. Fondococha can be considered relatively pristine as it has very low levels of PAHs when compared those found in the literature (Table 5.1).

**Industrial Increase.** The initial increase in the flux of PAHs that we see ca. 1958 in L. Fondococha is similarly experienced in Lake Galletue in 1963 and Lake Laja around 1960. Given dating uncertainties, the corresponding onset of the initial PAH increase in all three lakes from South America can be considered noteworthy. Similarly, the peak in ΣPAHs that we see in L. Fondococha in 1989 mirrors a peak in ΣPAHs fluxes found by Quiroz et al. (2005) in Laja Lake. All three South American lakes see peaks in the ΣPAHs fluxes in the late 1980s/90s, and a decrease in the levels of PAHs starting from the late 1980s/90s. L. Llaviuco follows a slightly different profile than the other lakes, only decreasing in PAH levels starting in 2006. However, L. Llaviuco is also the most polluted of all the South American lakes, which indicates that the source of pollution in the lake is local, and perhaps not solely atmospheric. The year of initial increase in PAHs in L. Llaviuco is unknown. Compared with sediments from the northern hemisphere, the sediments from South

America tend to follow a delayed trend. A PAH signal from the start of the western Industrial Revolution (usually seen in the late 1800s) is not evident in the sediments. The initial increases in PAHs occur almost simulateously in the late 1950s/early 1960s, which could be attributed to a delayed start in industrial activities in South America (see section 5.2.3.1). PAH maximums are reached in the 1980s/90s, instead of the 1950s/60s which we see in may industrialised western regions (e.g. Bandowe et al. 2014; Usenko et al. 2007; Muri et al. 2006). Levels of ΣPAHs show decreasing trends from the late 1980s/90s, rather than from the 1960s.

*Table 5.1. Comparison of ∑PAH depositional fluxes (fluxes in ng $cm^{-2}$ $yr^{-1}$) from lake sediments from different regions globally.* ***Note****: the number of PAHs included in the ∑PAHs differs for each study, but do not include perylene. The table should be used to provide an overview of profile trends, not absolute PAH levels.*

| Region | | Site | Elevation (m) | ∑PAH Flux (ng $cm^{-2}$ $yr^{-1}$) | PAH Maximum (Year) | PAH Initial Increase | PAH Initial Decrease | Reference |
|---|---|---|---|---|---|---|---|---|
| SOUTH AMERICA | REMOTE | Laguna Fondococha, *Ecuador* | 4046 | 1.02 – 8.6 | 1981 | 1958 | 1989 | This study |
| | | Laguna Llaviuco, *Ecuador* | 3150 | 16.4 – 52.5 | 1996 | - | 2006 | This study |
| | | Lake Laja, *Chile* | 1360 | 2.9 – 19.6 | 1989 | ~ 1960s | ~ late 1990s | Quiroz et al. 2005; Barra et al. 2006 |
| | | Lake Galletue, *Chile* | 1150 | 0.8 – 11.5 | 1999 | 1963 | ~ late 1980s | Barra et al. 2006 |
| EUROPE | REMOTE | Lake Jezero na Planini pri Jezeru, *Slovenia* | 1430 | 3 - 290 | ~ 1950s | ~ 1900s | ~ late 1950s | Muri et al. 2006 |
| | | Loch Coire nan Arr, *Scotland* | 125 | No flux values (ng $g^{-1}$) | 1920 - 1934 | 1860 - 1874 | 1920 - 1934 | Rose & Rippey 2002 |
| ASIA | INDUSTRIAL | Lake Huguangyan Maar, *China* | - | 4.7 – 35.0 | Increasing to present day | ~ 1950s | Still increasing | Han et al. 2016 |
| | | Lake Chaohu, *China* | - | 9.7 – 179.3 | Late 1990s | ~ 1900s | ~ 2000s | Han et al. 2016 |
| NORTH AMERICA | REMOTE | Lone Pine Lake, *USA* | 3024 | 0.48 (1870) – 3.66 | 1949 | 1949 | 1967 | Usenko et al. 2007 |
| | | Mills Lake, *USA* | 3030 | 0.69 (1905) – 5.8 | 1963 | 1938 | Still increasing | Usenko et al. 2007 |

**PAH Source Attribution.** The retene profile in L. Fondococha mirrors that of the ΣPAHs and the ΣLMW-PAHs in terms of initial increase, peaks and initial decrease (Fig. 4.11). Retene can be used as a proxy of wood and vegetation combustion (Fernández et al. 2000; Han et al. 2015, 2016) and similarly ΣLMW-PAHs indicate toward low-energy combustion processes such as biomass burning. Both of these molecular markers would suggest the dominance of low temperature biomass burning in the ΣPAHs profile for L. Fondococha. These PAHs could be originating from the local tradition of burning the páramo in order to stimulate the regrowth of grasses for cattle fodder (Hansen et al. 2003), as well as residential wood-burning from settlements surrounding

the national park. This conclusion is further supported by the ratio between ΣLMW-PAHs/ΣHMW-PAHs. For both L. Fondococha and L. Llaviuco the ratio remains > 1 until the year 2000 and 2003 respecively, where it then decreases to < 1 in both lakes (Fig. 4.13 and 4.14). A ratio > 1 can indicate that a lake is impacted by vegetation burning (and long-range transport) as LMW-PAHs dominate over HMW-PAHs. The ratio of < 1 after the year 2000 is suggestive of the dominance high temperature combustion sources (which release higher proportion of HMW-PAHs/COMB-PAHs, a trend which is clearly occurring from the steady increase in the ΣCOMB-PAH (Fig. 4.11) in the PAHs profile since 1958 in L. Fondococha (and 1969 in L. Llaviuco). The ratio of ΣOPAHs/ΣPAHs also sees an overall decreasing trend from bottom- to top-of-core in both L. Fondococha and Llaviuco (Fig. 4.13), which further supports the conclusion that the combustion of fossil fuel (which emits lower OPAHs-to-parent-PAH amounts compared to biomass combustion (Han et al. 2016) increased, especially after 1972 (in L. Fondococha) and since 1969 (in L. Llaviuco). Han et al. (2016) found a similarly decreasing trend in both ratios in Chaohu Lake, China, which they attributed to an increase in the contribution of fossil fuel combustion over time.

The ΣOPAHs and ΣAZAs profiles similarly follow that of ΣCOMB-PAHs and ΣLMW-PAH, showing a strong increase from 1958 onward, which can be explained by the fact that that OPAHs and AZAs have similar pyrogenic sources as PAHs (Han et al. 2015; Wilcke et al. 2014). Fluxes of OPAHs and AZAs both decrease around the year 2000 (L. Fondococha) which parallels with decreases in ΣLMW-PAH. The PCA and correlation analysis show strong positive relationships between OPAHs and LMW and retene in L. Fondococha and L. Llaviuco ($r = 0.8; p < 0.001$), a relationship similarly found by Han et al. (2015), which would indicate that non-industrial pyrogenic sources, such as fire, are the origin of OPAHs in the lakes. There is a lack of long-term OPAHs and AZAs inventories in South America and, as far as reviewed literature has indicated, our results provide the first historical record of atmospheric OPAH and AZA concentrations in this region.

As is common for perylene in sediments, the concentration tends to increase with depth, being the most abundant PAH in older sediment layers, and often contributing relatively insignificant levels to the total PAH mixture in surface sediments. In the lakes of Cajas NP this trend is also apparent as levels of perylene in the sediment of L. Fondococha and L. Llaviuco show dramatic decreases from 1985 and 1996 respectively until present. The predominance of perylene in older sediments is well documented in the literature (Bandowe et al. 2014; Barra et al. 2006; Fernández et al. 2000; Han et al. 2015, 2016; Quiroz et al. 2005), however, its precursor(s) still remain unknown. The perylene/TOC relationship has been described as a good indicator for the formation of perylene as a result of diagenesis by microbial activity in subsurface, anoxic sediments (Silliman et al. 2001). When we compare perylene with the TOC profile of both lakes we find a stark contrast between high perylene concentrations and low organic carbon concentrations (Fig. 4.8), a relationship that is similarly found by Quiroz et al. (2005) and Han et al. (2015). It is also supported by the correlation analysis and PCA conducted on the lakes, showing a strong negative correlation between perylene and TOC and C/N for both lakes, which would indicate that certain components of TOC are precursors of perylene formation. The origin of the organic matter is indicated by C/N index values which average around 13 for both lakes, which points to partly allochthonous (terrestrial) sources.

Perylene accounts for on average 86% (range 48 – 94%) of the total PAH mass in L. Fondococha. The characteristic for perylene to dominate in highland lakes is also a common phenomenon seen in European lakes, where perylene is known to account for 50 – 70 % of the total PAH mass (Fernández et al. 2000). In L. Llaviuco perylene accounts on average for 35% (range 14 – 53%) of

the total PAH mass, however, when compared with LMW-PAHs (18%) and HMW-PAHs (16%), perylene is still the dominant PAH within the sediment profile.

### 5.2.2 Historic Variations of Mercury and Trace Metals

**Industrial Increase**. In L. Fondococha there is the possibility to compare pre- and post-industialisation Hg, Cu, Zn, Pb and Cr levels in the core. Post-1958 there is an increase in Hg fluxes by a factor greater than 3 compared to pre-industrial levels, which is on par with the timing of increased industry in Ecuador (see section 5.2.3.1). This is compatible with the study by Lamborg et al. (2002) which found a similar mean factor of change of approximately 3x for post-industrial Hg deposition in cores from New Zealand. They compared their southern hemisphere cores with northern hemisphere cores (Novia Scotia, Canada), which has experienced a 5x increase in Hg levels post-industrialisation. These finding are in line with many Hg studies of lake sediments, ice cores and peat bogs from both hemispheres globally, all of which report a 3 to 5 fold increase in Hg deposition since pre-industrial times, with slightly lower concentrations in southern hemisphere archives (Lamborg et al. 2002; Lindeberg et al. 2006; Pirrone et al. 2010; Sprovieri et al. 2010). Other sites in South America record similar factor increses in Hg since pre-industrial times (Brazil > 2; Ecuador > 3; Peru > 4) (Table 5.3) (Barros de Oliveira et al. 2012; Cooke et al. 2009). All other measured metals show similar post-industrial increases by a factor greater than 2 in L. Fondococha. Barros de Oliveira et al. (2012) studied trace metal loadings in sediments from Lagoa Vermelha, a remote lake in southeastern Brazil. They found equally high surface enrichment factors of > 2 in their core for Hg, Pb and Zn, which they attributed to atmospheric deposition of pollutants from industrial activities in southern Brazil (Table 5.2). They found concentrations of Cr to be on par with geogenic origins. Interestingly, they found a strong positive correlation coefficient between concentrations of Zn and Pb in surface sediments ($r^2 = 0.58$), which we also see in L. Fondococha ($r^2 = 0.59$), which they attribute to smelter activities at the Pb-Zn-Ag mining district. Zn and Pb follow very similar profiles in L. Fondococha, and Ecuador is known to have abundant deposits of Pb, Zn and Ag (Nations Encyclopedia 2016). In  The scale of post-industrial increase in Hg and other heavy metals seen in L. Fondococha is similar to that of other South American sediment cores (Table 5.2 and 5.3) not influenced by mining, and indicate that atmospheric deposition is the driving force behind changes in metal pollution in the sediment.

*Table 5.2. Comparison of heavy metal concentrations (mg $kg^{-1}$) ranges from lake sediments from different regions. The range is indicative of natural background values (lowest values) and post-industrialization values (highest value), with the exception of L. Llaviuco, whose values explain the range in industrialization concentrations.*

| Site | Hg | Cu | Zn | Pb | Cr | Reference |
|---|---|---|---|---|---|---|
| Laguna Fondococha, *Ecuador* | 0.09 – 0.18 | 19.8 – 42.3 | 65.7 – 84.1 | 19.4 – 25.7 | 13.1 – 17.3 | This study |
| Laguna Llaviuco, *Ecuador* | 0.19 – 0.3 | 47.3 – 72.03 | 241.2 – 405.2 | 107.1 – 225.7 | 37.1 – 50.3 | This study |
| Lagoa Vermelha, *Brazil* | 0.04 – 0.102 | - | 39.6 – 85.9 | 7.7 – 18.7 | 10.6 – 57.4 | Barros de Oliveira et al. (2012) |
| Lake Chaohu, *China* | - | 20.4 – 29.9 | 38.4 – 185.8 | 21.1 – 54.3 | 36.4 - 67.8 | Zan et al. (2011) |

Differences exist in absolute values of fluxes and in the profiles between the lakes in Cajas NP. Biester et al. (2007) found that, on average, flux values of Hg for urban/agricultural regions range between 10 – 20 ng $cm^{-2}$ $yr^{-1}$, yet the flux values that we see on average in L. Llaviuco far exceed that (Table 5.3). Concentrations of heavy metals in L. Llaviuco also surpass those found by Zan et al. (2011), who studied heavy metal pollution in a eutrophic lake in China surrounded by agriculture and industry (Table 5.2). Reasons for such higher levels of heavy metals could be the result of in-basin difference in the lake systems. For example, differences in sedimentary patterns in-lake, upland Hg/heavy metal retention and local climatology can all explain lake-to-lake differences (Lamborg et al. 2002). It is imperative to define the severity of pollution by inventorying heavy metal concentrations and their spatial distribution in the sediment, as heavy metals in lake sediments can mobilise from sinks to sources (Zan et al. 2011). In eutrophic lakes especially, increased heavy metal concentrations from the remobilization of metals is closely related to the europhication process. Nutrients that are strongly adsorbed by metal oxides are released back into the water column as metals mobilise within the sediment (Zan et al. 2011). As L. Llaviuco was eutrophic from ca. 1978 to 1998 before it re-established itself as oglio-mesotrophic in the 2000s, heavy metal mobilization within the sediment would be a factor to considering when looking at the metal profiles. As we cannot calculate a factor increase for pre-industrialisation values of metals it is difficult to know whether L. Llaviuco was polluted already prior to increased major industry in Ecuador (e.g. from near by mining activities), or whether the high metal values have only occurred in modern times. Reasons for higher rates of all pollutants in L. Laviuco are discussed further in section 5.2.3.3.

*Table 5.3. Hg flux rates [ng cm-2 yr-1] from lake sediments from different regions of the world. Lakes from this study show average flux rates for pre-industrial (1885 – 1958) and industrial (1967/69 – 2014) time windows. For the Peruvian lakes factor increases (FI) of modern Hg levels compared to background Hg are supplied by the authors.*

| Location | Site | Lake | Pre-Industrial Hg Flux | Industrial Hg Flux | Reference |
|---|---|---|---|---|---|
| Ecuador | Remote | Llaviuco | - | 33.7 | This Study |
| | | Fondococha | 0.9 | 2.9 (FI = 3.2) | |
| Peru | Mining | Yanacocha1 | 0.6 – 0.7 | FI = 42 | Cooke et al. (2009) |
| | | Yanacocha2 | | FI = 105 | |
| | Remote | Negrilla | | FI = 4.6 | |
| Greenland | Remote | Søndre Strømfjord, 3 lakes | 0.1 – 0.3 | 0.5 - 1 | Bindler et al. (2001) |
| Canadian Arctic | Remote | Northen Territories & Hudson Bay, 7 lakes | 0.1 – 0.5 | 0.5 – 0.8 | Lockhart et al. (1995) |

**Mining Signal.** Evidence for the release of Hg to the atmosphere from mining sources prior to the initial increase in 1958 is limited in the sediment of L. Fondococha, despite the large amounts of Hg that South American mining activities are considered to have released to the environment (Cooke et al. 2009; Lamborg et al. 2002). Although the province of Azuay is a major player in metal mining, with the industry exploiting almost 30% of the greater Macizo del Cajas region (of which

Cajas NP is part of), there appears to be no clear mining signal in the sediment around the time (ca. in the late 1990s) when known mining projects in the region began (Moore 2006; Velástegui 2010). Two lake sediment cores analysed for historic trends in Hg from Novia Scotia, Canada, (Lamborg et al. 2002) found a similar story in their sediments: a dramatic increase in Hg around the time of the Industrial Revolution, but an apparent lack of enhanced Hg deposition as a result of gold mining activities in and around the National Park from where the cores were taken. The lack of a modern mining signal in the sediments may be explained by Hg being deposited locally around mining areas and remaining unavailable for re-emission. Local Hg losses would result from near-source deposition from the atmosphere (where it is released to the air from gold and silver recovery) or it is lost to local soils and water during the amalgamation process (Lamborg et al. 2002). This would indicate that the Hg and heavy metal signal in the lakes of Cajas NP follow regional/national atmospheric Hg and heavy metal deposition trends, rather than recording local mining signals.

In L. Fondococha, an peak from approximately 1981-94 is apparent in the sediment which is diagnostic of all trace metals (Fig. 4.15). In L. Llaviuco, although not as defined, it is fair to say that from the late 1970s to early 1990s there is also a 'peak' seen in heavy metal deposition (Fig. 4.16). South America experienced a modern-day gold rush in the 1970s as a consequence of increased gold prices by a factor of 8 to 10 (Malm 1998; Pfeiffer and Lacerda 1988). On a national scale, mining played a more significant role in the Ecuadorian economy in the 1980s when gold, largely forgotten since its early exploitation in the 16$^{th}$ century, grew again in importance (Flores and Merrill 1991). The peak that is diagnostic of all heavy metals in the 1980s in L. Fondococha could therefore be linked to an increase in gold mining and processing in Ecuador. Furthermore, data from the World Bank (World Development Indicators) show that Ecuador experienced a huge increase in the import (9.9% of all merchandise) and export (3.5% of all merchandise) of ores and metals in the 1980s as a result of the discovery of new gold deposits. Tentatively, it could be said that the peak that we see in all trace metals at this time could be a signal of the gold rush experienced in Ecuador. As a consequence of this, emissions of Hg and other metals mined in the region would have steadily increased over the next decade, further resulting in the increased export of ores and metals (and subsequent increased import from other South American countries experiencing the same gold rush).

**Modern Hg Decrease**. Both lakes experience decreases in Hg flux since the start of the 21st century (since 2010 for L. Llaviuco and since ca. 2006 in L. Fondococha). This would be in line with several studies that have reported decreasing trends in global Hg concentrations (Pacyna et al. 2006; Slemr et al. 2011; Streets et al. 2011). Slemr et al. (2011) claim a 30% decrease in global atmospheric Hg since 1995, a trend that cannot be explained by decreasing anthropogenic emssions (as emissions are increasing in Asia, Africa and South America), nor by increased oxidation of atmospheric Hg. They suggest that a changing climate, acidification of the oceans and, most importantly, the legacy of past Hg released into the environment all contribute to the current high levels of Hg in the environment. Pacyna et al. (2006) also speculate that the implementation of emission control devices in power plants of developing countries starting in the late 1990s is likely to play a role in the stabilizing of global Hg anthropogenic emissions. Deposition of Hg in the sediment core from L. Fondococha post-1958 is greater by a factor of 3.2 from pre-1958 values, suggesting that industrialization in Ecuador is a major player in the source emissions of Hg regionally. In L. Llaviuco, the high Hg values in the sediment would suggest other sources of Hg are also impacting the lake. If, as Pacyna et al. (2006) suggest, emission control devices have been

implemented since the 1990s, this would also explain the decrease in Hg we see from the 2000s onward in both lake sediments.

### 5.2.3 Pollution Signal Interpretation in Cajas National Park

#### 5.2.3.1 National: Industry in Ecuador

The pollution profile of L. Fondococha allows us to identify an initial increase in the year 1958 which is diagnostic of all measured pollutants, organic and inorganic. On a national scale, this initial increase can be attributed to Ecuador's industalisation which began after the 1950s (Flores and Merrill 1991). Prior to the 1950s, Ecuador's economic center was the Costa, with Guayaquil dominating in export and import affairs as a result of a booming cacao industry. The decline of the cacao industry in the 1930s and 40s (as a result of disease and loss of foreign markets to competitors) resulted in a weakening of the economy, however, government sponsored replanting efforts in the 1950s meant that by 1958 Ecuador was the world's sixth leading exporter of cacao. Ecuador's economy made great strides after 1950. Between 1950 and 1970 there was a slow and steady expansion of non-agricultural activities, and the 1960s saw rapid growth and diversification of the manufacturing sector (Flores and Merrill 1991). We attribute the initial increase of all pollutants in 1958 to this growth in industrial manufacturing in Ecuador.

In 1967 new petroleum fields were discovered in the Oriente which facilitated Ecuadors transformation to a world producer of oil. This brought with it large increases in government revenue in the early 1970s. Additionally in 1970 large natural gas deposits were discovered in the Gulf of Guayaquil. In 1978 the construction of the first large oil refinery was completed in Esmeraldas (Flores and Merrill 1991). In the production and refining of oil and gas, benzene (PACs have at least 2 benzene rings in the basic molecular structure) is one of the largest-volume petrochemical solvents used. Further oil processing by-products include pet coke, a heavy dust which contains toxic chemcials and heavy metals, including chromium (Lieber 2013). The peaks that we seen in the ΣLMW-PAHs and heavy metals in L. Fondococha in the 1980s could be suggestive of the opening of this first large refinery which would have released large amounts of petrogenic PAHs into the atmosphere and surrounding region. In L. Llaviuco especially there is a diagnostic peak in 1978 for all heavy metals (except Cu), and peaks in ΣLMW-PAHs in the late 1970s and 80s which could all be linked to the opening of refineries.

The production and export of oil that began in the 1970s led to unprecedented economic growth in Ecuador with the manufacturing sectors alone seeing an almost 13% increase from just 1975-77, and this growth in the Ecuadorian economy is mirrored in the sharp increase of all PACs and heavy metals in the sediment profile of both lakes. However, in the early 1980s a decrease in the price of petroleum coupled with a loss of forgein markets and dramatic climate changes (floods/drought) caused by El Niño lead to an faltering of the economy. The 1980s was a volatile decade for the Ecuadorian economy which ultimately lead to years of economic crisis as a result of fluctuating oil prices, inflation and debt (Flores and Merrill 1991). The faltering of the economy in the 80s left a defined signal in the lake sediments of Cajas. Across all anthopogenic pollutants in both lakes there is a general but significant decrease beginning in the late 1970s/ early 1980s, which only begins to recover again at the end of the 80s/ beginning of the 90s. Exceptions are the increasing trend of OPAHs and a peak in all heavy metals in L. Fondococha (and to a certain extent L. Llaviuco) around 1985, which could be accredited to an increase in gold mining in the 1980s (Flores and Merrill 1991).

A further noteworthy incident in Ecuador's modern history is the 1987 earthquake which destroyed up to 70 km of the Trans-Ecuadorian Pipeline and caused a six month suspension in crude oil production (Flores and Merrill 1991). Ecuador's petroleum sector was severly affected, but the impact to the environment was even more severe. 17,000 tons of crude oil were released in the Coca River and an additional 5,000 barrels were released into the surrounding areas (World Bank 1987). This incident would have released a huge amount of petrogenic PAHs into the atmosphere, and could be responsible for the 1988/89 peak we see in both lakes in LMW-PAHs. Ecuador's strong petroleum exploration and refining capacity can also be attributed to the trend (> 1) seen in the ratio between ΣLMW-PAHs/ΣHMW-PAHs for both lakes of Cajas NP until the 2000s. An index of > 1 can be associated with petrogenic sources, e.g. raw petroleum products.

Another severe financial crisis hit Ecuador in 1999 (again as a consequnce of El Niño and plummeting oil prices), but adopting the US dollar for official national currency in 2001 lead to modest recovery of the economy in the 2000s. The history of Ecuadors heavy industry, domestic fossil fuel comsumption and increased volume of motor traffic (spurred by government subsidies on domestic oil) are all significant sources of PAHs and heavy metals (Sadler et al. 2011), the signal of which we can certainly see in the emission inventories of the sediment cores from Cajas National Park. Decreases/stabilizing of emissions in the past decade can be attributed to slower economic growth and the implementation of technological measures to reduce emissions (e.g. catalytic converters in motor vehicles and stricter environmental control measures).

#### 5.2.3.2 Regional: Urban Sprawl

Neighbouring city Cuenca has experienced significant population increases from 1975 (110,000) to 2013 (over 350,000). This increase is associated with increasing anthropogenic activities and rapid growth in vehicles, with a yearly increase of 12% of non-commercial vehicles since 1975 (Sander et al. 2015). The increasing population of Cuenca comes hand-in-hand with an increase in combustion from residential wood stoves and fireplaces. These combustion processes are commonly incomplete due to insufficient access to air and slow, low-tempterature burning conditions (Lima et al. 2005) and could be contributing as a significant source of PACs to the lake sediments of Cajas NP. An increase in municipal waste incineration, regarded as a key source of Hg and other pollutants to the atmosphere (Pacyna et al. 2006), could also play a role in increased emission inventories seen in the lake sediments.

The steady rise that we see in the ΣCOMB-PAHs, mercury, lead and chromium (all originating from the combustion/incomplete combustion of fossil fuels) since 1958 in L. Fondococha, (and to a certain extent in L. Llaviuco) can be credited to population dynamics and increased vehicular usage on a regional scale. Eichler et al. (2015) found that anthopogenic Pb pollution levels from road traffic in South America now exceeds those levels of Pb from historical metallurgy in the last two millennia, even in regions with exceptional high local metallurgical activities. Eichler et al. (2015) found that the most pronounced enrichment factor of Pb in their ice core from the Bolivian Andeas for the last 2000 years occurred in the 1960s – parallel to increased use of leaded gasoline in South America. Pb deposition began decreasing in the 1980s after the introduction of unleaded gasoline in Brazil in 1975, with other South American countries following suit in the next decade. In our cores from Cajas NP we see strong increases in Pb depositional fluxes in both lakes from the 1960s, which peaks in the late 1970s before decreasing to current flux rates. The trend profile in both lakes for Pb is thus highly likely to be influenced by regional use of leaded and unleaded gasoline, and also likely to contain a imprint of South American traffic-related Pb emissions.

The transport sector has the highest fuel consumption in Ecuador, and within this sector road transport demands more than 80% of total energy. This energy demand in road transport has been steadily increasing inline with increasing population and economic dynamics (Cevallos Sierra 2016), and it is a trend we can see within our cores. The value range of the ratio ΣCOMB-PAHs/ΣPAHs shows the proportion of high-energy combustion derived PAHs in relation to the ΣPAHs (Tobiszewski and Namieśnik 2012). In both lakes we see a steady increase in the proportion of ΣCOMB-PAHs from ca. 1915 in L. Fondococha and since measurments start in 1969 for L. Llaviuco. This is consistent with findings from Van Metre et al. (2000) who studies the impact of urban sprawl on 10 lake sediments cores from urban regions in the USA. They found a change in the assemblage of PAHs towards those driven by combustion sources, as well as increases in concentrations of PAHs concurrent with increases in automobile useage. Other ratios, such as the parent-PAHs/alky-PAHs, which also indicate increasing proportion of the contribution of high temperature combustion processes to the PAH content in lakes sediments in modern times (also shown by the ΣLMW-PAHs/ΣHMW-PAHs), are in agreement with an increase of combustion derived pollution sources.

The major Cuenca-Molleturo-Naranjal highway that winds through the northern section of Cajas NP passes closer to L. Llaviuco (which also has a separate smaller road leading to the lake) than the isolated L. Fondococha. Traffic activities associated with the production of heavy metals include tire wear (Zn), fuel combustion (Pb), engine wearing and fluid leakage (Cu, Cr) (Zan et al. 2011), all of which show highly elevated levels in L. Llaviuco. The road was designed for 700 – 1500 cars per day (Flores 2013), however, it is estimated that an average daily traffic of 4000 vehicles passes through the park (Ramsar Bureau 2003). Infrastructure improvements over the past 10 years have resulted in an increase in vehicular traffic through the park (Rodríguez 2008) to current numbers of 934,230 annually in 2012 (ETAPA 2012). The highway presents numerous pathways for increased pollution within the park, namely water pollution from petroleum, an increase in the number of visitors to the area and an increase in waste (Ramsar Bureau 2003). Larger particles produced during fuel combustion tend to accumulate closer to the source (Lima et al. 2003) and could therefore be contributing to L. Llaviuco's combustion-PAH load in the sediment which is larger by a factor of 19.4 ($df = 27, p < 0.01$) for the years 1969 – 2014 than that of L. Fondococha for the years 1967 – 2014 (Table 5.4). PAHs could be entering L. Llaviuco from runoff as well as atmospheric deposition. Furthermore, construction of the inter-provincial highway also brought with it an extension of the farming frontier through slash and burn techniques in order to create new pasture for extensive grazing (Ramsar Bureau 2003). This could be a reason for the recent increase of retene and LMW-PAHs that we see in L. Llaviuco's profile (Fig. 4.12).

#### 5.2.3.3 Local: Lake Situation

**Laguna Fondococha.** The first PCA conducted on L. Fondococha contained all elements measured with the multi-elemental analysis using the ICP-MS, as well as all individual PACs. The first principal component showed a clustering of earth elements which would indicate that erosional processes in the catchment are the most important input in L. Fondococha. C/N ratios further indicate that organanic matter originates from terrestrial sources outside of the lake. In order to reduce the signal of natural background elements and evaluate sources of anthropogenic pollution in the lake, a further PCA was run with only anthropogenic pollutant groups as well as perylene and carbon. The first PC in L. Fondococha is dominated by perylene, which we know is the most

significant PAH in the sediment making up 84% of the ΣPAHs. PC1 is also dominated by Hg and HMW-PAHs, which group together, as well as COMB-PAHs and C. This would indicate an anthropogenic source (incomplete combustion of fossil fuels) of the PAHs in L. Fondococha, excluding the contribution of perylene which is most likely formed *in situ* within the lake itself. PC2 favours LMW-PAHs and OPAHs, which group together and exhibit a stong positive relationship. The strong correlation between LMW-PAHs and OPAHs could indicate similar environmental behaviour.

**Laguna Llaviuco.** The first principal component favoured Zn and Pb, which positively clustered together, and HMW-PAHs, COMB-PAHs and C which also positively clustered together. The two clusters negatively correlated together. This would indicate that Zn, Pb and combustion derived PAHs are released together into L. Llaviuco from nearby mines and/or vehicle emissions. The second PC favours Hg, LMW-PAHs and retene (which group together), perylene and AZAs. Perylene has no correlation with LMW-PAHs or retene, AZAs or Hg reinforcing its natural origin. Perylene contributes less to the ΣPAHs in L. Llaviuco than it does in L. Fondococha, hence its position in PC2. LMW-PAHs and retene have a strong positive relationship which indicates that they stem from similar sources, most likely biomass burning. Hg negatively correlates with AZAs, retene and LMW-PAHs, but from the correlation analysis we can see there is a strong positive correlation between Hg and HMW-/COMB-PAHs, indicating similar sources. C concentrations positively correlate with mostly HMW-PAHs, which has been related to the co-sorption of PAHs to carbonaceous matter. Futhermore, PAHs are co-produced together with some pyrogenic forms of C (Han et al. 2016).

Geophysical time series are often autocorrelated due to carryover processes in physical systems. This can complicate the identification of significant correlations between time series. All independent variables (PACs, Hg, heavy metals, TOC) in our pollution dataset are influenced by a common variable, namely the mass accumulation rate. Accordingly, they all follow the trend of an independent variable and therefore are not truly independent themselves. In the future to avoid this from occurring, p-values should be detrended and corrected for zero autocorrelation.

**Lake Comparison.** Flux rates for all measured organic pollutants and heavy metals are different for the two lakes, namely, L. Llaviuco sees fluxes which are several orders of magnitude higher compared to L. Fondococha. The exception is perylene, which is larger by only a factor of 1.2 in L. Llaviuco and is not considered statistically significant, which further justifies the conclusion of perylene's natural origin. Table 5.4 shows factor increase values for all pollutants for a comparable period of time. Reasons for the differences in flux rates between the two lakes could be a result of lake elevation, location, and/or different lake system processes. These factors are discussed in the following section.

*Table 5.4. Average flux rates for L. Fondococha and L. Llaviuco for all anthropogenic pollutants during a similar time period. Factor increase of fluxes was calculated between the two lakes. All factor increases between individual average lake fluxs were found to be statistically significant (df = 28; p < 0.01).*

| Average Flux [ng cm-2 yr-1] | L. Fondococha (1967 - 2014) | L. Llaviuco (1969 - 2014) | Factor Increase |
|---|---|---|---|
| **ΣPAHs (no PERY)** | 4.44 | 29.13 | 6.6 |
| **Retene** | 0.11 | 0.83 | 7.2 |
| **ΣLMW-PAHs** | 1.37 | 8.04 | 5.9 |
| **ΣCOMB-PAHs** | 0.29 | 5.57 | 19.4 |
| **ΣAZAs** | 0.07 | 0.51 | 7.8 |
| **ΣOPAHs** | 0.98 | 6.22 | 6.5 |
| **Mercury** | 2.89 | 33.72 | 11.7 |
| **Copper** | 448.3 | 7764.46 | 17.3 |
| **Zinc** | 1345.6 | 44,193.1 | 32.8 |
| **Lead** | 419.5 | 23,945.87 | 57.1 |
| **Chromium** | 264.5 | 5788.73 | 21.9 |

**Anthropogenic Activities.** L. Llaviuco is located at the border of the national park, whereas L. Fondococha is situated deep within the park itself. Any settlements located near the border of the park, as well as the closer proximity of the highway (implications discussed above), all result in higher flux rates of pollutants to the sediments of Llaviuco. This is particularly apparent as the flux rates of PAHs, especially LMW-PAHs and retene, are much more constant in Llaviuco, which would indicate that biomass burning close to the border of the park could be originating from permanent settlements. The exceptionally large factor increase in both Pb (57.1) and ΣCOMB-PAHs (19.4) (Table 5.4) clearly point towards the impact of the road on pollution deposition in L. Llaviuco. Lastly, surrounding L. Llaviuco is montane Andean forests (Hansen et al. 2003), which is subject to deforestation for firewood, and pastoral grassland (Colinvaux et al. 1997), which is subject to slash and burn techniques for grazing despite the parks restrictions (Sarmiento 2002). Furthermore, forests have a higher scavenging effect (due to a higher Leaf Area Index) and thus lakes located in forest ecosystems tend to have higher deposition rates than those located in grasslands (Daly and Wania 2005). L. Llaviuco is much more impacted by anthropogenic activities that produce organic pollutants and heavy metals than L. Fondococha.

**Influence of Fisheries.** Apart from combustion PAHs, average flux rate increases of heavy metals are remarkably higher in L. Llaviuco than they are for PACs (Table 5.4). From 1978 to 1998 L. Llaviuco housed a rainbow trout fishery where an estimated 15.6 million fish were raised in cages (Barros and Carrasco 2006). Monitoring of the lake found a deterioration in water quality which caused a change in the lakes' trophic state from mesotrophic to eutrophic over the course of two decades. Consequently, the fishery was banned in 1998 and L. Llaviuco restored itself to an oligo-mesotophic state by the 2000s. Two decades of fish farming is likely to leave a trace in the recorded heavy metal signal in the sediments of L. Llaviuco. Three options for increased heavy metal levels as a result of fish farming are considered, although with little additional information on the fish farming practices implemented in L. Llaviuco much is speculation. Firstly, antifoulants are used to prevent the settlement and growth of marine organisms on submerged structures, such as fish cages, and in the past have often contained zinc, copper, mercury, lead and arsenic (Chambers et al. 2006; Konstantinou and Albanis 2004). Commonly, antifoulant paints/coating

are copper or zinc based, but various heavy metals have been added to give marine/aquatic paints antifouling and anticorrosive properties. Fluxes of copper, zinc, lead and mercury in the sediments of L. Llaviuco could all be explained by the use of antifoulants on the fish cages in L. Llaviuco. However, levels of Cu, Zn and Pb were increasing already prior to the introduction of the fisheries, and levels steadily decline from their peak in 1978 (excluding the significant Cu peak in 1975, which is most likely an outlier). Hg, on the other hand, has more constant flux rates during the time the lake housed the fisheries, and could therefore be a likely candidate for antifoulants. Secondly, a further influencing factor would be the type of fishfeed used. If the feed was unregulated it may have contained traces of methyl mercury (NOAA). This would bioaccumulate in the fish and be released into the aquatic environment from unconsumed feed, metabolic products, feces and fish by-products. Lastly, elevated algal productivity associated with the eutrophication of L. Llaviuco during two decades of fish farming could have increased the Hg reservoir within the lake by producing a larger algal biomass containing more biologically-incorporated Hg (Outridge et al. 2005). The return of the lake to an oligo-mesotrophic state in the 2000s coincides with a decrease in Hg flux, suggesting that this may be a plausible explanation for increased Hg levels during the fish-farming decades.

**Catchment Processes.** The higher flux rates in L. Llaviuco compared to L. Fondococha could indicate that significant additional inputs of PACs, Hg and heavy metals are coming from riverine inputs. The catchment of L. Llaviuco is approximately 300 times the size of the lake basin (which is 142,512 $m^2$), and the Taitachugo river flowing into Llaviuco brings water which has passed through all of Cajas NP. As a consequence L. Llaviuco is impacted by all activities and processes occurring upstream. High mountain catchements often have only thin soils and sparse vegetation cover, which often means they are particularly sensitive to airborne pollutants as they are unable to act as a filter and prevent contaminants from entering the lake system (Vilanova et al. 2001). As the area around L. Llaviuco has been extensively deforested (Colinvaux et al. 1997) it is likely that pollutants deposited in the areas surround the lake are finding their way into the waters of L. Llaviuco. The watershed of a lake has been attributed as a significant source of Hg (Lamborg et al. 2002). For example, Swain et al. (1992) calculated that 20 – 60 % of the Hg load in the sediments of their lake originated from the catchment of the lake. Therefore, fluxes of Hg in L. Llaviuco and Fondococha are likely to be a combination of runoff and atmospheric flux. Calculating total Hg deposition since 1969 (Llaviuco) and 1967 (Fondococha) to 2014 shows that Llaviuco experienced 1517.4 ng $cm^2$ $yr^{-1}$ of Hg deposition, whereas only 135.83 ng $cm^2$ $yr^{-1}$ of Hg were deposited in L. Fondococha. This is a further indication that the catchment material of L. Llaviuco is most likely also polluted with Hg.

**Elevation and Precipitation.** It was hypothisised that the higher elevation lake, L. Fondococha at 4046 m, would scavenge more pollutants from the atmosphere as a result of higher precipitation rates/fog cover. From the literature (Daly and Wania 2005) it is known that pollutant deposition is favoured by low temperatures and high precipitation. Generally, air masses rising from the low lands cool and condense forming precipitation heavy clouds which cause precipitation rates to increase with elevation (Daly and Wania 2005). Average annual precipication data for the years 2002 – 2008 from eight meterological stations surround Cajas NP were analysed for the influence of elevation on precipitation rates. An increasing trend in precipitation rates with elevation was found, and the relationship between precipitation and elevation was found to be statistically significant. This should mean that L. Fondococha, situated 896 m higher, would have higher rates of pollutant deposition than L. Llaviuco, situated at 3150 m. This is clearly not the case. As we have no precipitation data from the precise locations and elevations of the lakes within Cajas NP itself

(the highest meterological station was at 3425 m), it is likely that micro-climates play a role in the depositional processes occurring in each lake. Additionally, temperature inversions, which can limit the vertical movement of airmasses along elevation gradients and cause contaminants become trapped during this time (Daly and Wania 2005), cannot be ruled out. The most plausible explanation, however, goes as follows. L. Llaviuco is situated just 17 km northwest of Cuenca, Ecuadors third largest city. L. Llaviuco is most likely influenced by easterly flowing air masses transporting pollutants from the city towards Cajas NP and, owing to its closer proximity to the city, pollutants are deposited/scavenged out of the atmosphere first and foremost on L. Llaviuco. As air masses rise they continue to deposit pollutants such that, as they reach higher elevations (L. Fondococha, 4046 m), the airmass contains a lighter pollutant load.

The influence of precipitation rates, temperature and elevation on wet and dry depositional processes in mountains cannot be ignored. Fog is a commom phenomenon in Cajas NP which sometimes experiences multiple days of constant fog cover. It has been described as a form of precipitation that is most efficient at scavenging certain pollutants. For example, OPAHs, AZAs and LMW-PAHs are known to be more water-soluble, and thus will scavenage and greater rates out of the atmosphere under the cover of fog. Wet deposition is generally more important for water-soluble (gas scavenging) and low-volatile (particle scavenging, HMW-PAHs) compounds. The relative importance and efficiency of wet deposition increases as temperatures decrease (Daly and Wania 2005). Dry deposition of gases also tends to be higher at lower temperatures, and because it is generally colder at higher elevations, this would enhance dry deposition of both particles and gases at higher altitudes. Yet, dry deposition is also strongly influenced by surface type. Higher rates of dry deposition have been linked to forested areas, thus areas below the treeline (such as L. Llaviuco) can experience higher rates of dry deposition than those further up. However, it must be said that dry deposition is a highly complex process and not so easily generalized. It is much more dependent on local conditions than wet deposition (Daly and Wania 2005). Morselli et al. (2003) found that dry deposition generally provides the greatest contribution to total heavy metal flux deposition as the preferred atmospheric scavenging process. Furthermore, pollutants associate faster with particles in the atmosphere (e.g. HMW-PAHs, heavy metals) at lower temperatures, and they are generally deposited at a faster rate than gases during dry desposition. Precipitation rates at 3150 m are still considered high, and most likely do not differ significantly between L. Llaviuco (3150 m) and L. Fondococha (4046 m). Given the high number of rainy days in Cajas NP, along with the high number of foggy days, it is likely that wet depositional processes play a more important role in both lakes in Cajas NP.

## 5.3 CLIMATE CHANGE

### 5.3.1 Climate Change in the Andes

Warming in the Andes is occurring at nearly twice the rate of the global average, making Andean societies among the most vulnerable globally in relation to the impacts of a changing climate. Warming is especially apparent on the impact of freshwater resources, for example through the shrinking of glaciers (Michelutti et al. 2015; Vuille et al. 2008, 2000). Glaciers and páramo act as critical buffers against highly seasonal precipitation by retaining much of the precipitation that falls at high elevations and releasing it gradually over time (Urrutia and Vuille 2009).

How warming will impact Andean lake systems, such as those in Cajas National Park which supply 60% of the drinking water to Ecuador's third largest city (Cuenca, population ca. 350,000), was

investigated by Michelutti et al. (2015). There have been many studies in this region that have demonstrated that the climate of the Andes has been highly dynamic over the Holocene and is greatly regulated by the Pacific Ocean (Bird et al. 2011; Hansen et al. 2003; Polissar et al. 2013; Rodbell et al. 1999; Urrutia and Vuille 2009). Michelutti et al. (2015) studied the impact that recent warming is having on Andean Lakes by looking at the the last several centuries of limnological (e.g. fossil diatom assemblages, chlorophyll production etc.) change from three lakes in Cajas National Park. They discovered that, since the 1970s, there has been an average increase in temperature of 1.15 °C, and that wind velocity has steadily decreased by over 40% since 2000, relative to the 1960s and 70s. The combined effect of increasing temperatres and decreasing winds resulted in a discernable ecological restructuring of the lakes in Cajas NP.

Rapid increase in diatom microfossil assemblages (*D. stelligera and Tabellaria flocculosa*) in the past ca. 50 years is attributed by Michelutti et al. (2015) to recent climate warming and reduced local wind speeds and is considered indicative of greater periods of water column stability and thermal stratification. Such fast rises in planktonic diatom taxa from near zero values to dominance is considered a key ecological change as it reveals physical restructuring of the water column, which in turn impacts multiple lake processes. For example, the climate-driven enhanced thermal stability of the water column lead to the inhibition of hypolimnetic nutrient upwelling to surface waters, thus decreasing the sediment signal of total lake production. Michelutti et al. (2015) also comment on the relationship between increased planktonic diatom taxa and elevation. According to climate model projections (Bradley et al. 2006), the scaling of temperature increases with elevation, thus the higher the altitude of the lake, the more impacted the lakes' ecological state will be by climate change. We can therefore expect that Laguna Fondococha, with its altitude of 4046 m, could be most impacted by a changing climate. At higher elevations in the Andes, Urrutia and Vuille (2009) projected that changes in precipitation with a changing climate will result in regions of both increase and decrease, but in general found that by the end of the 21$^{st}$ century enhanced monsoon precipitation would occur in the months of December, January, February, and a decrease in precipitation is projected for the months of June, July, August.

### 5.3.2 Implications for Pollution Deposition

There is a general lack of knowledge regarding the impact of climate change on pollutant behavior. Sadler et al. (2011) attempt to review the effects of changing climate on the behavior and fate of organic pollutants. Physical processes that are govered by the physiochemical properties of the pollutants are most likely to be impacted by changes in the environment, and the effect will vary. The temperature dependence of Henry's Law Constant (HLC) varies depending on the characteristics of the compound, but in general it is strongest with compounds that are polar. Increasing temperatures, suspended solids and dissolved organic matter are all parameters that impact HLC under climate change. The observed effect will depend on which factor comes into play in the environment under consideration.

In Cajas NP, where enhanced thermal stability of the lakes is occurring as a result of increasing temperatures, we see a decrease in nutrient upwelling (Michelutti et al. 2015). We can speculate that these changes will influence the depositional processes of OCs in the lake. These effect could be most apparent in terms of the sorption of PAHs and other OCs onto particulates in the water column as deposition in the lake occurs, as well as impacting those PACs that are most water soluble (e.g. OPAHs, AZAs). Increased water temperatures associated with climate change have

also been attributed to the association of heavy metals with particulates in that key parameters (ionic strength, pH etc.) are altered in a climate change scenario (Sadler et al. 2011).

A further influence, and possibly the most significant one, will be the impact of climate change on the global transport of chemicals. It is difficult to speculate on the effect climate change will have on organic pollutants sorbed to atmospheric particulates (Sadler et al. 2011). Several factors were identified by Panther et al. (1999) which are expected to increase atmospheric levels of PACs. Firstly, increased photolytic degradation in the summer, secondly, transport of pollutants to other sources, thirdly, removal of PACs via wet deposition and in-cloud scavenging mechanisms, and finally, the volatilization of LMW-PAHs as a result of higher temperatures.

In Cajas NP, we could speculate that the increasing temperatures stated by Michelutti et al. (2015) could lead to an increased loss of volatile PAHs from particulates. Furthermore, the decrease in wind velocity that Michelutti et al. (2015) found could also have an impact on the distribution and depositional patterns of pollutants in the region. Precipitation changes are difficult to project for the southern tropical Andes (Vuille et al. 2000) as a result of highly complex rainfall patterns spatially and temporally (Rollenbeck and Bendix 2011). However, any prevalence of cloud-free days (decreased precipitation) would be expected to lead to higher photodegradation of pollutants existing in the gaseous phase in the atmosphere, as well as decrease the importance of wet deposition and cloud-scavenging deposition mechanisms. Increased aridity would also cause an increase of particulates in the atmosphere (dust/dust storms) which would influence those HMW-PAHs and heavy metals which sorb most readily onto particles for atmospheric transport (Sadler et al. 2011). Morselli et al. (2003) found that dry deposition generally provides the greatest contribution to total heavy metal flux deposition, being the preferred atmospheric scavenging process. Less precipitation could thus lead to higher fluxes of heavy metal dry deposition from the atmosphere.

# CHAPTER 6: CONCLUSIONS AND OUTLOOK

## 6.1 CONCLUSIONS

The sediments from high altitude, remote mountain lakes in Cajas National Park proved to be valuable archives for the reconstruction of an anthropogenic pollution signal. To conclude the project the initial research questions will be addressed.

### 6.1.1 Validation of $^{210}$Pb Chronology

*Can OCs, PACs or Hg signals in the sediment cores be used as event markers to validate the $^{210}$Pb chronology?*

Common artificial chronostratigraphic markers, such as $^{137}$Cs, were not found at significant enough concentrations in the sediments of Cajas NP to be used as a proxy age indicator. For this reason, OCs, PACs or Hg, all known for their global distribution patterns, were measured with the expectation that a globally significant peak or initial increase could be identified. However, none of the legacy POPs, PAHs or Hg detected in the sediments followed global emission trends. Rather, regional influences seem to dominate any global fingerprint that may have been recorded. As the number of studies concerning pollution inventories in South America is limited, and in Ecuador non-existent, the uncertainty of using pollution peaks as independent event markers to constrain the $^{210}$Pb model was considered too high. Instead, a multi-model approach was followed which tested several different age-depth models in order to determine with a high degree of confidence the accuracy of the chronologies for each lake. All models tested displayed similar trends to a certain depth, thus the pollution inventories recorded in past ca. 70 years (L. Fondococha) and ca. 40 years (L. Llaviuco) can be considered accurate and not an artifact of dating.

### 6.1.2 Elevation and Precipitation

*Does elevation impact the depositional processes of PACs, Hg and heavy metals?*

Mountain cold trapping clearly plays a role in the Ecuadorian Andes. That there is definitive evidence of all forms of pollutants, organic and inorganic, in the sediments of L. Fondococha proves that this phenomenon is occurring in Cajas NP. Higher precipitation rates with higher elevation most likely influence the deposition of pollutants via wet deposition in the remote Laguna Fondococha. As this study has compared two high elevation lakes, one lower in elevation that the other yet clearly more polluted, the influence of mountain cold trapping of pollutants can be distorted. However, it is highly likely that is does occur, and that the exponentially higher pollutant levels in L. Llaviuco are a result of local anthropogenic activites, in-lake and catchment processes, as well as its closer proximity to the city of Cuenca.

### 6.1.3 Atmospheric Depositional Flux

*Does the depositional flux rate of atmospherically transported pollution in the lakes of Cajas National Park class them as pristine?*

PAC levels reported in L. Fondococha are in the low range of values found for remote high altitude lakes in the northern hemisphere, but within range of PAH levels found in other lakes from South America. For L. Fondococha, the main PAH found in the sediment was perylene, which forms from

the diagenesis of organic matter originating either from in-lake sources or terrigenous sources. The average fluxes of anthopogenic (post-1958) Hg within the sediment are higher than recorded fluxes for other remote areas of the world, such as Greenland and the Canadian Arctic, as well as fluxes measured in lake sediments in Brazil. However, the factor increase of > 3 found between pre and post industralisation in the core is on par with observed Hg depositions globally since pre-industrial times. Similarly, fluxes of Pb are much higher in L. Fondococha than they are in Brazil, while fluxes of Zn are similar and Cr is much lower. Thus it can be said that the anthropogenic signal found in the core lower than others but not insignificant. Nevertheless, the conclusion can be made that Laguna Fondococha is relatively pristine. L. Llaviuco, on the other hand, cannot be classed as pristine. It is severely polluted by Hg, Zn and Pb, moderately polluted by Cu and slightly polluted by Cr. With the exception of Cr, heavy metal and Hg concentrations in L. Llaviuco exceed concentrations recorded in Brazil and China by immense margins. Hg fluxes are > 40 times higher than in any other remote lake in industrial timescales. Fluxes of PAHs are also much higher than any other remote lake in South America by an order of magnitude of at least 2. Fluxes of PAHs in L. Llaviuco exceed even those of Lake Huguangyan Maar, located in an industrial region of China. Our results provide the first historical record of atmospheric fluxes of OPAH and AZA in lake sediments in South America.

### 6.1.4 Pollution Signal: Local, Regional, Global?

*Do the pollution inventories of PACs and Hg in southern hemisphere sediments follow global (northern hemisphere) patterns?*

The pollutants recorded in the sediments of L. Fondococha do not follow global trends found in European or North American Lakes. Rather, the the temporal trends in L. Fondococha represents the atmospheric deposition of PACs, Hg and metals on a regional to continental scale. It is concurrent with other PAC emission histories for South America, and follows the history of industrial activity, urbanization and petroleum exploration in Ecuador (Flores and Merrill 1991). L. Fondococha's remote location means that it is removed from influences other than long-range atmospheric input. L. Llaviuco shows indications of regional and national signals in the lake sediments, but influences on the lake seem to come more significantly from local sources. For example, we see increasing trends in the most recent sediments of L. Llaviuco in the profiles of retene and LMW-PAHs, which may be a result of more extensive grazing and consequent slash and burn techniques, and we also assume that two decades of fish farming within the lake have influenced the heavy metal signal recorded in the sediments. L. Llaviuco is clearly influenced by its closer proximity to settlements, roadways and human activity in general such that the local signal overwhelms any regional or continental fingerprint that may exist in the sediments.

### 6.1.5 Pollution Source Attribution

*Do the PACs concentration ratios (molecular diagnostic ratios) indicate the origin of an air mass?*

As with the lakes from the south central Chilean Andes, a main source of PAHs in the sediments from L. Fondococha and L. Llaviuco seem to originate from a non-combustion related source - perylene. However, an fossil fuel combustion PAH influence is progressively higher in recent times. Retene and LMW-PAHs clearly strongly influence the overall PAH profile and so it is reasonable to suggest that local biomass burning is contributing significantly to the overall PAH signal within the sediment of both lakes. It is clear from the molecular diagnostic ratios that in

most recent times the anthropogenic influence of PAHs (as seen from increases in HMW- and COMB-PAHs) has become increasingly more significant since the start of major industry in Ecuador and consequent population and vehicular growth. The fingerprint of Ecuador's economic and industrial history is evident from the molecular diagnostic ratios, especially from the depositional profiles of LMW-PAHs, which are markedly influenced by Ecuador's petrogenic emissions history.

### 6.1.6 Mining Signal

*Do the levels of Hg, Pb, Cu, Zn and Cr in the lake sediments indicate pollution from mining activities?*

Hg and heavy metal signals recorded in the sediments of L. Fondococha visibly follow Ecuadorian industrialisation in their onset and consequent progression in modern times, and is similarly in line with findings of trace metal concentrations in Brazilian lakes which show a factor increase > 2 for all metals since industrialization. In L. Fondococha, evidence of mining in the sediments prior to industrialisation is insignificant, and in L. Llaviuco we are not able to determine a mining influence as we do not reach background levels for any trace metals. It would seem that the lakes are not recording the signal of local mines surrounding the national park, but rather their depositional trends could be accredited to national/regional mining signals as a result of increased gold mining in the 1980s and the parallel increase we see in both cores for all heavy metal proxies at that time. We conclude that the dominant sources influencing Hg and heavy metals in the lake sediments is industrialization, petroleum exploration, population growth (urban activities) and increases in vehicular transport, but that the signal of the Ecuadorian gold rush in the 1980s is likely to be recorded in the sedimentary record of both lakes.

## 6.2 OUTLOOK

The results presented in this thesis provide the first long-term pollution inventory from a paleo-archive in Ecuador. Given the definitive and continuous rise of combustion PACs and heavy metals seen in the sediments of L. Fondococha it is considered imperative to conduct further studies on pollution trends in Ecuador, especially given that the overall economy of South America is flourishing and emissions are likely only to increase in the future. The highly polluted sediments of L. Llaviuco point towards the impact that anthropogenic activities within and surrounding Cajas NP are exerting on the supposedly pristine and natural environment of a national park. Further studies on pollutants within L. Llaviuco would be advisable in order to officially establish the severity of pollution levels. Furthermore, pollution proxies should be measured further downcore with the purpose of defining natural background levels for the lake.

Climate change has the potential to impact a variety of parameters which influence pollution distribution and depositional processes in the future. However, the effects are not simple or uniform, and climate change has implications for both short and long term behavior of pollutants at a region-specific level across all environmental media. Changes in the climate of the Andes will likely affect the processes influencing pollution transportation and deposition, and it would be logical to continue monitoring these effects in the long-term.

# REFERENCES

Albinet, A., E. Leoz-Garziandia, H. Budzinski, E. Villenave, and J. L. Jaffrezo. 2008. "Nitrated and Oxygenated Derivatives of Polycyclic Aromatic Hydrocarbons in the Ambient Air of Two French Alpine valleys. Part 1: Concentrations, Sources and Gas/Particle Partitioning." *Atmospheric Environment* 42(1):43–54.

Ammann, A. 2007. "Inductively Coupled Plasma Mass Spectrometry (ICP MS): A Versatile Tool." *Journal of Mass Spectrometry* 42(7):419–27.

Appleby, P. 2001. "Tracking Environmental Change Using Lake Sediments. Vol. 1 Basin Analysis Coring and Chronological Developments in Paleoenvironmental Research." In *Tracking Environmental Change Using Lake Sediments. Volume 1*: Basin A. Kluwer Academic Publishers, Dordrecht, The Netherlands.

Appleby, P. 2008. "Three Decades of Dating Recent Sediments by Fallout Radionuclides: A Review." *The Holocene* 18(1):83–93.

Appleby, P. and Oldfield, F. 1978. "The Calculation of Lead-210 Dates Assuming a Constant Rate of Supply of Unsupported 210Pb to the Sediment." *Catena* 5(1):1–8.

Arcusa, S. 2016. "Late Holocene Flood History and Tephrochronology using Lake Sediments from Cajas National Park, South Central Ecuador." *Master Thesis, University of Bern*.

Bailey, R. 2001. "Global Hexachlorobenzene Emissions." *Chemosphere* 43(2):167–82.

Bandowe, B. and Wilcke, W. 2010. "Analysis of Polycyclic Aromatic Hydrocarbons and their Oxygen-Containing Derivatives and Metabolites in Soils." *Journal of Environmental Quality* 39(4):1349–58.

Bandowe, B., Sobocka, J., Wilcke, W. 2011. "Oxygen-Containing Polycyclic Aromatic Hydrocarbons (OPAHs) in Urban Soils of Bratislava, Slovakia: Patterns, Relation to PAHs and Vertical Distribution." *Environmental Pollution* 159(2):539–49.

Bandowe, B., Srinivasan, S., Seelge, M., Sirocko, F., and Wilcke, W. 2014. "A 2600-Year Record of Past Polycyclic Aromatic Hydrocarbons (PAHs) Deposition at Holzmaar (Eifel, Germany)." *Palaeogeography, Palaeoclimatology, Palaeoecology* 401:111–21.

Barra, R., Popp, P., Quiroz, R., Hanns-Christian, T., Araneda, A., Bauer, C., Urrutia, R. 2006. "Polycyclic Aromatic Hydrocarbons Fluxes during the Past 50 Years Observed in Dated Sediment Cores from Andean Mountain Lakes in Central South Chile." *Ecotoxicology and Environmental Safety* 63(1):52–60.

Barros, S. and Carrasco, M. 2006. "Estudio Limnológico de la laguna Surocucho". *ETAPA-DGA*

Barros de Oliveira, S., Ruiz Pessenda, C., Teixeira Favaro, I., Babinski, M. 2012. "A 2400-Year Record of Trace Metal Loading in Lake Sediments of Lagoa Vermelha, Southeastern Brazil." *Journal of South American Earth Sciences* 33(1):1–7.

Berg, H. 2008. "Global Status of DDT and Its Alternatives for Use in Vector Control to Prevent Disease." *Environmental Health Perspectives* 117:575–90.

Biester, H., Richard B., Martinez-Cortizas, A., Engstrom, D. 2007. "Modeling the Past Atmospheric Deposition of Mercury Using Natural Archives." *Environmental Science and Technology* 41(14):4851–60.

Bignert, A. Olsson, M., Persson, W., Jensen, S., Zakrisson, S., Litzen, K., Eriksson, U., Häggberg, L., Alsberg, T. 1998. "Temporal Trends of Organochlorines in Northern Europe, 1967-1995. Relation to Global Fractionation, Leakage from Sediments and International Measures."

*Environmental Pollution* 99(2):177–98.

Bindler, R., Ingemar, R., Appleby, P., Anderson, J., Rose, N. 2001. "Mercury Accumulation Rates and Spatial Patterns in Lake Sediments from West Greenland: A Coast to Ice Margin Transect." *Environmental Science and Technology* 35(9):1736–41.

Binford, M. 1990. "Calculation and Uncertainty Analysis of 210Pb Dates for PIRLA Project Lake Sediment Cores." *Journal of Paleolimnology* 3:253–67.

Bird, B., Abbott, M., Vuille, M., Rodbell, D., Stansell, N., Rosenmeier, M. 2011. "A 2,300-Year-Long Annually Resolved Record of the South American Summer Monsoon from the Peruvian Andes." *Proceedings of the National Academy of Sciences of the United States of America* 108(21):8583–88.

Björklund, E., Nilsson, T., Bøwadt, S. 2000. "Pressurised Liquid Extraction of Persistent Organic Pollutants in Environmental Analysis." *Trends in Analytical Chemistry* 19(7):434–45.

Bleeker, E., Wiegman, S., de Voogt, P., Kraak, M., Leslie, H., de Haas, E., Admiraal, W. 2002. "Toxicity of Azaarenes." *Reviews Of Environmental Contamination And Toxicology* 173: 39 - 83.

Blumer, M. 1976. "Polycyclic Aromatic Compounds in Nature." *Scientific American* 234:35-45.

Boyle, J. 2001. "Redox Remobilization and the Heavy Metal Record in Lake Sediments: A Modelling Approach." *Journal of Paleolimnology* 26(4):423–31.

Boyle, J. 2001. "Inorganic Geochemical Methods in Paleolimnology." in *Tracking Environmental Change Using Lake Sediments.*, vol. 2, edited by W. M. Last & J. P. Smol. Kluwer Academic Publishers, Dordrecht, The Netherlands.

Bradley, R., Vuille, M., Diaz, H., Vergara, W. 2006. "Climate Change. Threats to Water Supplies in the Tropical Andes." *Science (New York, N.Y.)* 312(5781):1755–56.

Buggle, B. and M. Zech. 2015. "New Frontiers in the Molecular Based Reconstruction of Quaternary Paleovegetation from Loess and Paleosols." *Quaternary International* 1–8.

Buytaert, W., Deckers, J., Wyseure, G. 2006. "Description and Classification of Nonallophanic Andosols in South Ecuadorian Alpine Grasslands (Paramo)." *Geomorphology* 73(3-4):207–21.

Calamari, D., Bacci, E., Focardi, S., Gaggi, C., Morosini, M., Vighi, M. 1991. "Role of Plant Biomass in the Global Environmental Partitioning of Chlorinated Hydrocarbons." *Environmental Science & Technology* 25(8):1489–95.

Carroll, J. and Abraham, J. 1996. "Sediment Isotope Tomography (SIT) Model Version 1." *DOE/Grand Junction Projects Office* 70.

Cevallos Sierra, J. 2016. "Estimating Road Transport Fuel Consumption in Ecuador." *Energy Policy* 92:359–68.

Chambers, L., Stokes, K., Walsh, F., Wood, R. 2006. "Modern Approaches to Marine Antifouling Coatings." *Surface and Coatings Technology* 201(6):3642–52.

Cheng, H., Lin, T., Zhang, G., Liu, G., Zhang, W., Qi, S., Jones, K., Zhang, X. 2014. "DDTs and HCHs in Sediment Cores from the Tibetan Plateau." *Chemosphere* 94:183–89.

CODIGEM-BGS,1993. "Mapa Geológico del Ecuador, Escala 1:1,000,000" *CODIGEM and British Geological Survey Cooperative Program*, Quito.

Cohen, A. 2003. *Paleolimnology : The History and Evolution*. New York: Oxford University Press.

Colinvaux, P., Bush, M., Steinitz-Kannan, M., Miller, M. 1997. "Glacial and Postglacial Pollen Records from the Ecuadorian Andes and Amazon." *Quaternary Research* 48(1):69–78.

Cooke, C., Balcom, P., Biester, H., Wolfe, A. 2009. "Over Three Millennia of Mercury Pollution in the Peruvian Andes." *Proceedings of the National Academy of Sciences of the United States of America* 106(22):8830–34.

Cooke, C., Wolfe, A., Hobbs, W. 2009. "Lake-Sediment Geochemistry Reveals 1400 Years of Evolving Extractive Metallurgy at Cerro de Pasco, Peruvian Andes." *Geology* 37(11):1019–22.

Cooke, C., Abbott, M., Wolfe, A. 2008. "Late-Holocene Atmospheric Lead Deposition in the Peruvian and Bolivian Andes." *The Holocene* 18(2):353–59.

Daly, G., Lei, Y., Teixeira, C., Muir, D., Castillo, L., Wania, F. 2007. "Accumulation of Current-Use Pesticides in Neotropical Montane Forests." *Environmental Science & Technology* 41(4):1118–23.

Daly, G. and Wania, F. 2005. "Critical Review Organic Contaminants in Mountains." *Environmental Science & Technology* 39(2):385–98.

van Drooge, B., López, J., Fernández, P., Grimalt, J., Stuchlík, E. 2011. "Polycyclic Aromatic Hydrocarbons in Lake Sediments from the High Tatras." *Environmental Pollution* 159(5):1234–40.

ECOLAP & MAE, 2007. "Guía del Patrimonio de Áreas Naturales Protegidas del Ecuador." Quito.

Eichler, A., Gramlich, G., Kellerhals, T., Tobler, L., Schwikowski, M. 2015. "Pb Pollution from Leaded Gasoline in South America in the Context of a 2000-Year Metallurgical History." *Science Advances* 1(2):e1400196–e1400196.

ETAPA. 2012. "Informe de control de la Vía Cuenca – Molleturo – El Empalme."

Fernández, P., Vilanova, R., Martínez, C., Appleby, P., Grimalt, J. 2000. "The Historical Record of Atmospheric Pyrolytic Pollution over Europe Registered in the Sedimentary PAH from Remote Mountain Lakes." *Environmental Science & Technology* 34(10):1906–13.

Flores, E. 2013. "La ordenación de la red vial del cantón Cuenca". *Master Thesis.* (Cuenca, Ecuador): Universidad. de Cuenca.

Flores, E. and Merrill, T. 1991. "Growth and Structure of the Economy." P. 306 in *Ecuador: A country study*, edited by D. M. Hanratty. Library of Congress Cataloging-in-Publication Data.

Fraser, M., Cass, G., Simoneit, B., Rasmussen, R. 1998. "Air Quality Model Evaluation Data for Organics. 5. $C_6$-$C_{22}$ Nonpolar and Semipolar Aromatic Compounds." *Environmental Science & Technology* 32(12):1760–70.

Garrigues, P., E. Parlanti, R. Lapouyade, and J. Bellocq. 1988. "Distribution of Methylperylene Isomers in Selected Sediments." *Geochimica et Cosmochimica Acta* 52(4):901–7.

Gharbi, F. 2014. "Comment on the Article 'Multiple Dating of Varved Sediments from Lake Qazduny, Northern Poland: Toward an Improved Chronology for the Last 150 Years.'" *Quaternary Geochronology* 20:109–10.

Girón, R. and Peñaherrera, X. n.d. "National Park Route Guide." *ETAPA*.

Goldberg, E. 1963. "Geochronology with $^{210}$Pb Radioactive Dating." *International Atomic Energy Agency,* Vienna, 121-130.

González-Carrasco, V., Velasquez-Lopez, P., Olivero-Verbel, J., Pájaro-Castro, N. 2011. "Air Mercury Contamination in the Gold Mining Town of Portovelo, Ecuador." *Bulletin of Environmental Contamination and Toxicology* 87(3):250–53.

Grimalt, J., Fernandez, P., Berdie, L., Vilanova, R. 2001. "Selective Trapping of Organochlorine

Compounds in Mountain Lakes of Temperate Areas." *Environmental Science & Technology* 35(13):2690–97.

Grimalt, J., van Drooge, B., Ribes, A., Vilanova, R, Fernandez, P., Appleby, P. 2004. "Persistent Organochlorine Compounds in Soils and Sediments of European High Altitude Mountain Lakes." *Chemosphere* 54(10):1549–61.

Gschwend, P., Hites, R. 1981. "Fluxes of Polycyclic Aromatic Hydrocarbons to Marine and Lacustrine Sediments in the Northeastern United States." *Geochimica et Cosmochimica Acta* 45(12):2359–67.

von Gunten, L., Grosjean, M., Eggenberger, U., Grob, P., Urrutia, R., Morales, A. 2009. "Pollution and Eutrophication History AD 1800-2005 as Recorded in Sediments from Five Lakes in Central Chile." *Global and Planetary Change* 68(3):198–208.

Hall, M., Samaniego, P., Le Pennec, J., Johnson, J. 2008. "Ecuadorian Andes Volcanism: A Review of Late Pliocene to Present Activity." *Journal of Volcanology and Geothermal Research* 176(1):1–6.

Han, Y., Wei, C., Bandowe, B., Wilcke, W., Coa, J., Xu, B., Gao, S., Tie, X., Li, G., Jin, Z., An, Z. 2015. "Elemental Carbon and Polycyclic Aromatic Compounds in a 150-Year Sediment Core from Lake Qinghai, Tibetan Plateau, China: Influence of Regional and Local Sources and Transport Pathways." *Environmental Science & Technology* 49(7):4176–83.

Han, Y., Wei, C., Huang, R., Bandowe, B., Ho, S., Coa, J., Jin, Z., Xu, B., Goa, S., Tie, X., An, Z., Wilcke, W. 2016. "Reconstruction of Atmospheric Soot History in Inland Regions from Lake Sediments over the Past 150 Years." *Scientific Reports* 6:19151.

Hancock, G., Leslie, C., Everett, S., Tims, S., Brunskill, G., Haese, R. 2011. "Plutonium as a Chronomarker in Australian and New Zealand Sediments: A Comparison with (137)Cs." *Journal Of Environmental Radioactivity* 102(10):919–29.

Hancock, G., Edgington, D., Robbins, J., Smith, J., Brunskill, G., Pfitzner, J. 2002. "Workshop on Radiological Techniques in Sedimentation Studies: Methods and Applications." 19.

Hansen, B., Rodbell, D., Seltzer, G., Leon, B., Young, K., Abbott. 2003. "Late-Glacial and Holocene Vegetational History from Two Sites in the Western Cordillera of Southwestern Ecuador." *Palaeogeography, Palaeoclimatology, Palaeoecology* 194(1-3):79–108.

Heim, S., Schwarzenbauer, J., Kronimus, R., Littke, R., Woda, C., Mangini, A. 2004. "Geochronology of Anthropogenic Pollutants in Riparian Wetland Sediments of the Lippe River (Germany)." *Organic Geochemistry* 35:1409–25.

Heim, S. and Schwarzbauer, J. 2013. "Pollution History Revealed by Sedimentary Records: A Review." *Environmental Chemistry Letters* 11(3):255–70.

Hong, S., Barbante, C., Boutron, C., Gabrielli, P., Gaspari, V., Cescon, P., Thompson, L., Ferrari, C., Francou, B., Maurice-Bourgoin, L. 2004. "Atmospheric Heavy Metals in Tropical South America during the Past 22,000 Years Recorded in a High Altitude Ice Core from Sajama, Bolivia." *Journal Of Environmental Monitoring* 6(4):322–26.

Hudson, R., Gherini, S., Fitzgerald, W., Porcella, D. 1995. "Anthropogenic Influences on the Global Mercury Cycle: A Model-Based Analysis." in "Mercury as a Global Pollutant" Pg. 265–72 in *Water, Air, and Soil Pollution*, vol. 80.

Jensen, T. and Hites, R. 1983. "Aromatic Diesel Emissions as a Function of Engine Conditions." *Analytical Chemistry* 55(4):594–99.

Jones, K. and de Voogt, P. 1999. "Persistent Organic Pollutants ( POPs ): State of the Science." *Environmental Pollution* 100:209–21.

Konstantinou, I. and T. Albanis. 2004. "Worldwide Occurrence and Effects of Antifouling Paint Booster Biocides in the Aquatic Environment: A Review." *Environment International* 30(2):235–48.

Krishnaswamy, S., Lal, D., Martin, J., Meybeck, M. 1971. "Geochronology of Lake Sediments." *Earth and Planetary Science Letters* 11(1-5):407–14.

Lamborg, C., Fitzgerald, W., Damman, A., Benoit, J., Balcom, P., Engstrom, D. 2002. "Modern and Historic Atmospheric Mercury Fluxes in Both Hemispheres: Global and Regional Mercury Cycling Implications." *Global Biogeochemical Cycles* 16(4):51-1-51-11.

Lauscher, F. 1976. "Weltweite Typen Der Höhenabhängigkeit Des Niederschlags." *Wetter und Leben* 28:80–90.

Lei, D. and Wania, F. 2004. "Is Rain or Snow a More Efficient Scavenger of Organic Chemicals?" *Atmospheric Environment* 38(22):3557–71.

Lima, A., Eglinton, T., Reddy, C. 2003. "High-Resolution Record of Pyrogenic Polycyclic Aromatic Hydrocarbon Deposition during the 20th Century." *Environmental Science and Technology* 37(1):53–61.

Lima, A., Farrington, J., Reddy, C. 2005. "Combustion-Derived Polycyclic Aromatic Hydrocarbons in the Environment—A Review." *Environmental Forensics* 6(2):109–31.

Lindeberg, C., Bindler, R., Renberg, I., Emteryd, O., Karlsson, E., Anderson, N. 2006. "Natural Fluctuations of Mercury and Lead in Greenland Lake Sediments." *Environmental Science and Technology* 40(1):90–95.

Lockhart, W., Wilkinson, P., Billeck, B., Hunt, R., Wagemann, R., Brunskill, G. 1995. "Current and Historical Inputs of Mercury to High-Latitude Lakes in Canada and to Hudson Bay." *Water, Air, & Soil Pollution* 80(1-4):603–10.

Lockhart, W., Wilkinson, P., Billeck, B., Danell, R., Hunt, R., Brunskill, G., Delaronde, J., Lois, V. 1998. "Fluxes of Mercury to Lake Sediments in Central and Northern Canada Inferred from Dated Sediment Cores." *Biogeochemistry* 40(2-3):163–73.

Lockhart, W., Macdonald, R., Outridge, P., Wilkinson, O., DeLaronde, J., Rudd, J. 2000. "Tests of the Fidelity of Lake Sediment Core Records of Mercury Deposition to Known Histories of Mercury Contamination." *Science of the Total Environment* 260(1-3):171–80.

Lundstedt, S., Bandowe, B., Wilcke, W., Boll, E., Christensen, J., Vila, J., Grifoll, M., Faure, P., Biache, C., Lorgeoux, C., Larsson, M., Irgum, K., Ivarsson, P., Ricci, M. 2014. "First Intercomparison Study on the Analysis of Oxygenated Polycyclic Aromatic Hydrocarbons (Oxy-PAHs) and Nitrogen Heterocyclic Polycyclic Aromatic Compounds (N-PACs) in Contaminated Soil." *TrAC - Trends in Analytical Chemistry* 57:83–92.

Lundstedt, S., White, P., Lemieux, C., Lynes, K., Lambert, I., Öberg, L., Haglund, P., Tysklind, M. 2007. "Sources, Fate, and Toxic Hazards of Oxygenated Polycyclic Aromatic Hydrocarbons (PAHs) at PAH-Contaminated Sites." *Ambio* 36(6):475–85.

Mackay, D., Wania, F., Schroeder, W. 1995. "Prospects for Modeling the Behavior and Fate of Mercury, Globally and in Aquatic Systems." Pp. 941–50 in *Water, Air, and Soil Pollution* 80: 941 - 950.

Mackay, D., Shiu, W. 1981. "A Critical Review of Henry's Law Constants for Chemicals of Environmental Interest." *Journal of Physical and Chemical Reference Data* 10(4):1175–99.

MacKenzie, A., Hardie, S., Farmer, J., Eades, L., Pulford, I. 2011. "Analytical and Sampling Constraints in 210Pb Dating." *Science of the Total Environment* 409(7):1298–1304.

Mackey, E., Lindstrom, R., Murphy, K. 2010. "Certification of Three NIST Renewal Soil Standard

Reference Materials for Element Content : SRM 2709a San Joaquin Soil , SRM 2710a Montana Soil I , and SRM 2711a Montana Soil II NIST Special Publication 260-172 Certification of Three NIST Renewal Soil Sta." *National Institute of Standards and Technology Special Publication* 260–172.

Maliszewska-Kordybach, B. 1999. "Sources, Concentrations, Fate and Effects of Polycyclic Aromatic Hydrocarbons (PAHs) in the Environment. Part A: PAHs in Air." *Polish Journal of Environmental Studies* 8(3):131–36.

Malm, O. 1998. "Gold Mining as a Source of Mercury Exposure in the Brazilian Amazon." *Environmental research* 77(2):73–78.

Manoli, E., Kouras, A., Samara, C. 2004. "Profile Analysis of Ambient and Source Emitted Particle-Bound Polycyclic Aromatic Hydrocarbons from Three Sites in Northern Greece." *Chemosphere* 56(9):867–78.

McKinney, R., Pruell, R., Burgess, R. 1999. "Ratio of the Concentration of Anthraquinone to Anthracene in Coastal Marine Sediments." *Chemosphere* 38(10):2415–30.

van Metre, P., Mahler, B., Furlong, E. 2000. "Urban Sprawl Leaves Its PAH Signature." *Environmental Science and Technology* 34(19):4064–70.

Meyers, P. 1994. "Preservation of Elemental and Isotopic Source Identification of Sedimentary Organic Matter." *Chemical Geology* 114(3-4):289–302.

Meyers, P., Teranes, J. 2001. "Sediment Organic Matter." *Tracking Environmental Change Using Lake Sediments. Volume 2: Physical and Geochemical Methods* 2(1999):239–69.

Michelazzo, P., Fostier, A., Magarelli, G., Santos, J., Andrade De Carvalho, J. 2010. "Mercury Emissions from Forest Burning in Southern Amazon." *Geophysical Research Letters* 37(9):1–5.

Michelutti, N., Wolfe, A., Cooke, C., Hobbs, W., Vuille, M., Smol, J. 2015. "Climate Change Forces New Ecological States in Tropical Andean Lakes." *Plos One* 10(2):e0115338.

Monzier, M., Robin, C., Samaniego, P., Hall, M. 1999. "Sangay Volcano, Ecuador: Structural Development, Present Activity and Petrology." *Journal of Volcanology and Geothermal Research* 90(1-2):49–79.

Moore, J. 2006. "Azuay: A Site for Mining Expansion in Ecuador's South". Research Sites: Territory, Conflicts and Development in the Andes. *University of Manchester*.

Morán-Tejeda, E., Bazo, J., López-Moreno, J., Aguilar, E., Azorín-Molina, C., Sanchez-Lorenzo, A., Martínez, R., Nieto, J., Mejía, R., Martín-Hernández, N., Vicente-Serrano, S. 2016. "Climate Trends and Variability in Ecuador (1966-2011)." *International Journal of Climatology.*

Morselli, L., Olivieri, P., Brusori, B., Passarini, F. 2003. "Soluble and Insoluble Fractions of Heavy Metals in Wet and Dry Atmospheric Depositions in Bologna, Italy." *Environmental Pollution* 124(3):457–69.

Mostert, Maria M. R., Godwin A. Ayoko, and Serge Kokot. 2010. "Application of Chemometrics to Analysis of Soil Pollutants." *TrAC - Trends in Analytical Chemistry* 29(5):430–45.

Moy, C., Seltzer, G., Rodbell, D., Anderson, D. 2002. "Variability of El Nino/Southern Oscillation Activity at Millennial Timescales during the Holocene Epoch." *Letters To Nature* 420.

Muri, G., Wakeham, S., Rose, N. 2006. "Records of Atmospheric Delivery of Pyrolysis-Derived Pollutants in Recent Mountain Lake Sediments of the Julian Alps (NW Slovenia)." *Environmental Pollution* 139(3):461–68.

Nriagu, J. 1988. "A Silent Epidemic of Environmental Metal Poisoning?" *Environmental Pollution*

50(1-2):139–61.

Nriagu, J. 1994. “Mercury Pollution from the Past Mining of Gold and Silver in the Americas.” *Science of the Total Environment* 149(3):167–81.

Obrist, D., Moosmüller, H., Schürmann, R., Antony Chen, L., Kreidenweis, S. 2008. “Particulate-Phase and Gaseous Elemental Mercury Emissions during Biomass Combustion: Controlling Factors and Correlation with Particulate Matter Emissions.” *Environmental Science & Technology* 42(3):721–27.

Offenberg, J. and Baker, J. 2002. “Precipitation Scavenging of Polychlorinated Biphenyls and Polycyclic Aromatic Hydrocarbons along an Urban to over-Water Transect.” *Environmental Science & Technology* 36(17):3763–71.

Oldfield, F. and Appleby, P. 1984. “A Combined Radiometric and Mineral Magnetic Approach to Recent Geochronology in Lakes Affected by Catchment Disturbance and Sediment Redistribution.” *Chemical Geology* 44(1-3):67–83.

Outridge, P., Stern, G., Hamilton, P., Percival, J., McNeely, R., Lockhart, W. 2005. “Trace Metal Profiles in the Varved Sediment of an Arctic Lake.” *Geochimica et Cosmochimica Acta* 69(20):4881–94.

Pacyna, J. and Pacyna E. 2001. "An Assessment Of Global And Regional Emissions Of Trace Metals To The Atmosphere From Anthropogenic Sources Worldwide." *Environmental Reviews* 9 (4), 269 – 298.

Pacyna, E., Pacyna, J., Steenhuisen, F., Wilson, S. 2006. “Global Anthropogenic Mercury Emission Inventory for 2000.” *Atmospheric Environment* 40(22):4048–63.

Panther, B., Hooper, M., Tapper, N. 1999. “A Comparison of Air Particulate Matter and Associated Polycyclic Aromatic Hydrocarbons in Some Tropical and Temperate Urban Environments.” *Atmospheric Environment* 33(24-25):4087–99.

Pfeiffer, W. and Lacerda, L. 1988. "Mercury Inputs Into The Amazon Region, Brazil." *Environmental Technology Letters* 9, 325—330.

Pirrone, N., Hedgecock, I., Cinnirella, S., Sprovieri, F. 2010. “Overview of Major Processes and Mechanisms Affecting the Mercury Cycle on Different Spatial and Temporal Scales.” *Erca 9: From the Global Mercury Cycle to the Discoveries of Kuiper Belt Objects* 9:3–33.

Polissar, P., Abbott, M., Wolfe, A., Vuille, M., Bezada, M. 2013. “Synchronous Interhemispheric Holocene Climate Trends in the Tropical Andes.” *Proceedings of the National Academy of Sciences* 110(36):14551–56.

Putyrskaya, V., Klemt, E., Röllin, S., Astner, M., Sahli, H. 2015. “Dating of Sediments from Four Swiss Prealpine Lakes with 210Pb Determined by Gamma-Spectrometry: Progress and Problems.” *Journal of Environmental Radioactivity* 145:78–94.

Quiroz, R., Popp, P., Urrutia, R., Bauer, C., Araneda, A., Treutler, H., Barra, R. 2005. “PAH Fluxes in the Laja Lake of South Central Chile Andes over the Last 50 Years: Evidence from a Dated Sediment Core.” *Science of the Total Environment* 349(1-3):150–60.

R Development Core Team. 2006. "R: A Language And Environment For Statistical Computing." *R Foundation for Statistical Computing, Viena, Austria*. URL http://www.R-project.org

Ramsar Bureau. 2003. "Information Sheet on Ramsar Wetlands, Cajas National Park" *Wetlands International*.

Rapaport, R. and Eisenreich, S. 1988. "Historical Atmospheric Inputs of High Molecular Weight Chlorinated Hydrocarbons to Eastern North America." *Environmental Science & Technology*

22, 931 – 941.

Ravindra, K., Sokhi, R., van Grieken, R. 2008. "Atmospheric Polycyclic Aromatic Hydrocarbons: Source Attribution, Emission Factors and Regulation." *Atmospheric Environment* 42(13):2895–2921.

Reynaud, C., Jaillard, É., Lapierre, H., Mamberti, M., Mascle, G. 1999. "Oceanic Plateau and Island Arcs of Southwestern Ecuador: Their Place in the Geodynamic Evolution of Northwestern South America." *Tectonophysics* 307(3-4):235–54.

Richter, H. and Howard, J. 2000. "Formation of Polycyclic Aromatic Hydrocarbons and Their Growth to Soot—a Review of Chemical Reaction Pathways." *Progress in Energy and Combustion Science* 26(4-6):565–608.

Rodbell, D., Seltzer, G., Anderson, D., Abbott, M., Enfield, D., Newman, J. 1999. "A 15,000 Year Record of ENSO-Driven Alluviation in Southwestern Ecuador." *Science* 283(January):516–20.

Rollenbeck, R. and Bendix, J. 2011. "Rainfall Distribution in the Andes of Southern Ecuador Derived from Blending Weather Radar Data and Meteorological Field Observations." *Atmospheric Research* 99(2):277–89.

Rodríguez, S. 2008. "Plan de zonificación y manejo recreacional y turístico del Parque Nacional Cajas. (Cuenca, Ecuador): Empresa Municipal de Telecomunicaciones, Agua Potable, Alcantarillado y Saneamiento Ambiental de Cuenca".

Rose, N. and Rippey, B. 2002. "The Historical Record of PAH, PCB, Trace Metal and Fly-Ash Particle Deposition at a Remote Lake in North-West Scotland." *Environmental Pollution* 117(1):121–32.

Sadler, R., Gabric, A., Shaw, G., Shaw, E., Connell, D. 2011. "An Opinion on the Distribution and Behavior of Chemicals in Response to Climate Change, with Particular Reference to the Asia-Pacific Region." *Toxicological & Environmental Chemistry* 93(1):3–31.

Saenz Vera, C. 1953. "DDT in the Prevention of Plague in Ecuador." *Bulletin of the World Health Organization* 9(5):615–18.

Sander, K., Mira-Salama, D., Feuerbache, A. 2015. "The Cost of Air Pollution A Case Study for the City of Cuenca, Ecuador". *The World Bank.*

Sarmiento, F. 2002. "Anthropogenic Change in the Landscapes of Highland Ecuador." *Geographical Review* 92(2):213–34.

Schnurrenberger, D., Russell, J., Kelts, K. 2003. "Classification of Lacustrine Sediments Based on Sedimentary Components." *Journal of Paleolimnology* 141–54.

Schroeder, H. 1998. "Atmospheric Mercury - An Overview." Atmospheric Environment 32(5): 809 - 822.

Schubert, C. and Clapperton, C. 1990. "Quaternary Glaciations in the Northern Andes (Venezuela, Colombia and Ecuador)." *Quaternary Science Reviews* 9:123–35.

Silliman, J., Meyers, P., Eadie, B. 1998. "Perylene: An Indicator of Alteration Processes or Precursor Materials?" *Organic Geochemistry* 29(5-7 -7 pt 2):1737–44.

Silliman, J., Meyers, P., Eadie, B., Val Klump, J. 2001. "A Hypothesis for the Origin of Perylene Based on Its Low Abundance in Sediments of Green Bay, Wisconsin." *Chemical Geology* 177(3-4):309–22.

Slemr, F., Brunke, E., Ebinghaus, R., Kuss, J. 2011. "Worldwide Trend of Atmospheric Mercury since 1995." *Atmospheric Chemistry and Physics* 11(10):4779–87.

Smol, J. 2008. "Pollution of Lakes and Rivers: A Paleoenvironmental Perspective." *Book*, 2nd *Edition, Blackwell Publishing Ltd.*

Sprovieri, F., N. Pirrone, R. Ebinghaus, H. Kock, and A. Dommergue. 2010. "A Review of Worldwide Atmospheric Mercury Measurements." *Atmospheric Chemistry and Physics* 10(17):8245–65.

Sprovieri, F., Pirrone, N., Ebinghaus, R., Kock, H., Dommergue, A. 2010. "A Review of Worldwide Atmospheric Mercury Measurements." *Atmospheric Chemistry and Physics* 10(17):8245–65.

Streets, D., Devane, M., Lu, Z., Bond, T., Sunderland, E., Jacob, D. 2011. "All-Time Releases of Mercury to the Atmosphere from Human Activities." *Environmental Science & Technology* 45(24):10485–91.

Swain, B., Engstrom, D., Brigham, M., Henning, T., Brezonik, P. 1992. "Increasing Rates of Atmospheric Mercury Deposition in Midcontinental North America." *Science (New York, N.Y.)* 257(5071):784–87.

Tarras-Wahlberg, H. and Lane, S. 2003. "Suspended Sediment Yield and Metal Contamination in a River Catchment Affected by El Niño Events and Gold Mining Activities: The Puyango River Basin, Southern Ecuador." *Hydrological Processes* 17(15):3101–23.

Temporetti, P., Alonso, M., Baffico, G., Diaz, M., Lopez, W., Pedrozo, F., Vigliano, P. 2001. "Trophic State, Fish Community and Intensive Production of Salmonids in Alicura Reservoir (Patagonia, Argentina)." *Lakes and Reservoirs: Research and Management* 6(4):259–67.

Thomas, R. 2001. "Tutorial: A Beginner's Guide to ICP-MS." *Spectroscopy* 16(4):38–55.

Tobiszewski, M. and Namieśnik, J. 2012. "PAH Diagnostic Ratios for the Identification of Pollution Emission Sources." *Environmental Pollution* 162:110–19.

Tsapakis, M. and Stephanou, E. 2003. "Collection of Gas and Particle Semi-Volatile Organic Compounds: Use of an Oxidant Denuder to Minimize Polycyclic Aromatic Hydrocarbons Degradation during High-Volume Air Sampling." *Atmospheric Environment* 37(35):4935–44.

Tylmann, W., Bonk, A., Goslar, T., Wulf, S., Grosjean, M. 2016. "Calibrating $^{210}$Pb Dating Results with Varve Chronology and Independent Chronostratigraphic Markers: Problems and Implications. *Quaternary Geochronology* 32: 1 - 10.

Tylmann, W. 2014. "Reply to the Comment by F . Gharbi on ' Multiple Dating of Varved Sediments from Lake Q Azduny , Northern Poland : Toward an Improved Chronology for the Last 150 Years .'" *Quaternary Geochronology* 20:111–13.

Tylmann, W., Enters, D., Kinder, M., Moska, P., Ohlendorf, C., Poreba, G., Zolitschka, B. 2013. "Multiple Dating of Varved Sediments from Lake Lazduny, Northern Poland: Toward an Improved Chronology for the Last 150 Years." *Quaternary Geochronology* 15:98–107.

Urrutia, R., and Vuille, M. 2009. "Climate Change Projections for the Tropical Andes Using a Regional Climate Model: Temperature and Precipitation Simulations for the End of the 21st Century." *Journal of Geophysical Research* 114(D2):1–15.

Usenko, S., Landers, D.,. Appleby, P., Simonich, S. 2007. "Current and Historical Deposition of PBDEs, Pesticides, PCBs, and PAHs to Rocky Mountain National Park." *Environmental Science and Technology* 41(21):7235–41.

Velástegui, A. 2010. "Analisis Geospacial Y Estadistico Preliminar de La Actividad Minera En Los Paramos Del Ecuador." *PPA-EcoCiencia, Quito*, 1 - 38.

Vilanova, R., Fernández, P., Martínez, C., Grimalt, J. 2001. "Organochlorine Pollutants in Remote Mountain Lake Waters." *Journal of Environmental Quality* 30(4):1286–95.

Vione, D., Barra, S., Gennaro, G., Rienzo, M., Gilardoni, S., Perrone, M., Pozzoli, L. 2004. "Polycyclic

Aromatic Hydrocarbons in the Atmosphere: Monitoring, Sources, Sinks and Fate. II: Sinks and Fate." *Annali di Chimica* 94(4):257–68.

Vuille, M., Francou, B., Wagnon, P., Juen, I., Kaser, G., Mark, B., Bradley, R. 2008. "Climate Change and Tropical Andean Glaciers: Past, Present and Future." *Earth-Science Reviews* 89(3-4):79–96.

Vuille, M., Bradley, R., Keimig, F. 2000. "Climate Variability in the Andes of Ecuador and Its Relation to Tropical Pacific and Atlantic Sea Surface Temperature Anomalies." *Journal of Climate* 13(14):2520–35.

Wakeham, S., Schaffner, C., Giger, W. 1980. "Poly Cyclic Aromatic Hydrocarbons in Recent Lake Sediments-II. Compounds Derived from Biogenic Precursors during Early Diagenesis." *Geochimica et Cosmochimica Acta* 44(3):415–29.

Wania, F., and Mackay, D. 1993. "Global Fractionation and Cold Condensation of Low Volatility Organochlorine Compounds in Polar Regions." *Ambio* 22(1):10–18.

Wania, F. and Westgate, J. 2008. "On the Mechanism of Mountain Cold-Trapping of Organic Chemicals." *Environmental Science & Technology* 42(24):9092–98.

Warren, N., Allan, I., Carter, J., House, W., Parker, A. 2003. "Pesticides and Other Micro-Organic Contaminants in Freshwater Sedimentary Environments - A Review." *Applied Geochemistry* 18(2):159–94.

Weber, J., Halsall, C., Muir, D., Teixeira, C., Small, J., Solomon, K., Hermanson, M., Hung, H., Bindleman, T. 2010. "Endosulfan, a Global Pesticide: A Review of Its Fate in the Environment and Occurrence in the Arctic." *Science of the Total Environment* 408(15):2966–84.

Whiteman, C. 2000. "Mountain Meteorology: Fundamentals and Applications." *Oxford University Press.*

Whiteman, D., Bian, X., Zhong, S. 1999. "Wintertime Evolution of the Temperature Inversion in the Colorado Plateau Basin." *Journal of Applied Meteorology and Climatology* 38(8):1103–17.

Wilcke, W. 2007. "Global Patterns of Polycyclic Aromatic Hydrocarbons ( PAHs ) in Soil." *Geoderma* 141:157–66.

Wilcke, W., Bandowe, B., Lueso, M., Ruppenthal, M., del Valle, H., Oelmannm, Y. 2014. "Polycyclic Aromatic Hydrocarbons (PAHs) and Their Polar Derivatives (Oxygenated PAHs, Azaarenes) in Soils along a Climosequence in Argentina." *Science of the Total Environment* 473-474:317–25.

World Bank. 1987. "Ecuador: Emergency Petroleum Reconstruction Project, Loan and Project Summary." *World Bank April 1987.*

Yan, B., Abrajano, T., Bopp, R., Chaky, D., Benedict, L., Chillrud, S. 2005. "Molecular Tracers of Saturated and Polycyclic Aromatic Hydrocarbon Inputs into Central Park Lake, New York City." *Environmental Science & Technology* 39(18):7012–19.

Yunker, M., Macdonald, R., Vingarzan, R., Mitchelld, R., Goyettee, D., Sylvestrec, S. 2002. "PAHs in the Fraser River Basin: a Critical Appraisal of PAH Ratio as Indicators of PAH Source and Composition." *Organic Geochemistry* 33:489–515.

Yunker, M., McLaughlin, F., Fowler, M., Fowler, B. 2014. "Source Apportionment of the Hydrocarbon Background in Sediment Cores from Hecate Strait, a Pristine Sea on the West Coast of British Columbia, Canada." *Organic Geochemistry* 76:235–58.

Zan, F., Huo, S., Xi, B., Su, J., Li, X., Zhang, J., Yeager, K. 2011. "A 100 Year Sedimentary Record of Heavy Metal Pollution in a Shallow Eutrophic Lake, Lake Chaohu, China." *Journal of Environmental Monitoring* 13(10):2788.

**ONLINE RESOURCES**

ARCOM. National Mining Authority. Available at: http://geo.controlminero.gob.ec:1026/geo_visor/ (accessed on 10.4.16)

CIA. 2014. The World Factbook 2013 – 2014. Available at: https://www.cia.gov/library/publications/the-world-factbook/geos/ec.html (accessed on 15.03.16)

Environmental Justice Atlas. 2014. Available at: https://ejatlas.org/conflict/international-minerals-corporation-imc-in-molleturo-ecuador (accessed on 24.01.16)

Lieber, Don. 2013. 10 Most Toxic Ingredients Used In Coal, Oil And Gas Production. Available at: http://ecowatch.com/2013/12/09/10-toxic-ingredients-used-in-coal-oil-gas-production/ (accessed on 14.5.16)

Nations Encyclopedia. 2016. Available at: http://www.nationsencyclopedia.com/economies/Americas/Ecuador.html (accessed on 10.04.16)

NOAA (National Oceanic and Atmospheric Administration). Fisheries, Feeds for Aquaculture. Available at: http://www.nmfs.noaa.gov/aquaculture/faqs/faq_feeds.html (accessed on 12.04.16)

Parque Nacional Cajas. 2009. Available at: http://www.parque-nacional-cajas.org/sp.html (accessed on 14.3.2016)

Stockholm Convention. Protecting human health and the environment from persistent organic pollutants (UNEP). Available at: http://chm.pops.int/default.aspx (accessed on 20.01.2016)

US-EPA. 2007. Available at: https://www.epa.gov/sites/production/files/2015-12/documents/3545a.pdf (acessed on 13.04.16)

World Development Indicators (World Bank). Available at: http://data.worldbank.org/data-catalog/world-development-indicators (accessed on 3.17.16)

# APPENDIX

## Annex 1: METHODS

*Table A.1.1. List of target PAHs, deuterium-labelled PAHs, retention time (minutes), monitored ion (MI) and qualifier ion (QI) used for measurements. Each group of PAHs is quantified relative to the deuterium-labelled PAH before it.*

| Name of PAH | **Abbreviation** | **RT(min)** | **MI** | **Q1** |
|---|---|---|---|---|
| **Naphthalene-D8** | **NAPH-D8** | 7.775 | 136 | 137 |
| 1,2,3,4-Tetrahydronaphthalene | 1,2,3,4-THNAPH | 7.509 | 104 | 132 |
| Naphthalene | NAPH | 7.815 | 128 | 127 |
| 2-Methylnaphthalene | 2-MNAPH | 9.153 | 142 | 141 |
| 1-Methylnapthalene | 1-MNAPH | 9.380 | 142 | 141 |
| Biphenyl | BP | 10.076 | 154 | 153 |
| 1,3-Dimethylnaphthalene | 1,3-DMNAPH | 10.573 | 156 | 141 |
| **Acenaphthene-D10** | **ACEN-D10** | 11.393 | 164 | 162 |
| Acenaphthylene | ACENY | 10.982 | 152 | 151 |
| Acenaphthene | ACEN | 11.474 | 153 | 154 |
| Fluorene | FLUO | 12.960 | 166 | 165 |
| **Phenanthrene-D10** | **PHEN-D10** | 16.200 | 188 | 189 |
| Phenanthrene | PHEN | 16.281 | 178 | 179 |
| Anthracene | ANTH | 16.453 | 178 | 179 |
| Cyclopenta | CYCLOPENTADEF | 18.702 | 190 | 189 |
| 2-Methylphenanthrene | 2-MPHEN | 18.840 | 192 | 191 |
| 3,6-Dimethylphenanthrene | 3,6-DMPHEN | 20.285 | 206 | 205 |
| Pyrene-D10 | **PYR-D10** | 22.052 | 212 | 213 |
| Fluoranthene | FLUA | 21.217 | 202 | 200 |
| Pyrene | PYR | 22.120 | 202 | 200 |
| Retene | RETENE | 23.908 | 219 | 234 |
| **Chrysene-D12** | **CHRY-D12** | 28.691 | 240 | 241 |
| Benzo[a]anthracene | B(A)A | 28.598 | 228 | 226 |
| Chrysene | CHRY+TRY | 28.598 | 228 | 226 |
| **Perylene-D12** | **PERY-D12** | 37.469 | 264 | 265 |
| Benzo[b+j+k]fluoranthene | B(BJK) | 35.721 | 525 | 253 |
| Benzo[e]pyrene | B(E)P | 36.928 | 252 | 253 |
| Benzo[a]pyrene | B(A)P | 37.159 | 252 | 253 |
| Perylene | PERY | 37.574 | 252 | 253 |
| **Benzo[ghi]perylene-D12** | **B(GHI)-D12** | 42.764 | 288 | 289 |
| Indeno[1,2,3-cd]pyrene | IND | 41.974 | 276 | 274 |
| Dibenz[a,h]anthracene | DIBE | 42.169 | 278 | 279 |
| Benzo[ghi]perylene | B(GHI) | 42.847 | 276 | 277 |
| Coronene | COR | 48.602 | 300 | 150 |

*Table A.1.2. List of target AZAs and OPAHs, deuterium-labelled AZAs/OPAHs, retention time (minutes), monitored ion (MI) and qualifier ion (QI) used for measurements. Each group of PAHs is quantified relative to the deuterium-labelled PAH before it.*

| **AZAs** | **Abbreviation** | **RT (min)** | **MI** | **QI** |
|---|---|---|---|---|
| **Carbazole-D8** | **CBZ-D8** | **28.167** | **175** | **146** |
| Quinoline | QUI | 11.715 | 129 | 102 |
| Benzo[h]quinoline | BQI | 26.972 | 179 | 151 |
| Acridine | ACR | 27.281 | 179 | 151 |
| Carbazole | CBZ | 28.246 | 167 | 139 |
| **OPAHs** | **Abbreviation** | **RT (min)** | **MI** | **QI** |
| **Benzophenone-$D_5$** | **BP-D5** | **22.431** | **187** | **105** |
| 1-Indanone | 1-INDA | 12.892 | 132 | 104 |
| 1,4-Naphthoquinone | 1,4-NQ | 16.361 | 158 | 102 |
| 1-Naphthaldehyde | 1-NLD | 18.719 | 156 | 128 |
| 2-Biphenylcarboxaldehyde | 2-BPCD | 22.253 | 181 | 152 |
| 1-Acenaphthenone | 1-ACENone | 23.312 | 168 | 140 |
| 9-Fluorenone | 9-FLO | 25.628 | 180 | 152 |
| 1,2-Acenaphthenequinone | 1,2-ACQ | 29.034 | 126 | 182 |
| **9,10-Anthraquinone-$D_8$** | **9,10-ANQ-D8** | **31.126** | **216** | **188** |
| 9,10-Anthracenedione | 9,10-ANQ | 32.221 | 208 | 180 |
| 1,8-Naphthalic anhydride | 1,8-NAA | 32.528 | 154 | 126 |
| 4H-Cyclopenta[d,e,f]phenanthrene-4-one | CPHENone | 32.727 | 204 | 176 |
| Fluoranthene-D10 | FLUA-D10 | 32.974 | 212 | 213 |
| 2-Methyl-9,10-anthracenedione | 2-MANQ | 34.108 | 222 | 165 |
| 1,4-Anthraquinone | 1,4-ANQ | 32.273 | 208 | 153 |
| Benzo[a]fluorenone | B(A)FLUone | 41.086 | 230 | 202 |
| 7H-Benz[d,e]anthracene-7-one | BANTone | 43.363 | 230 | 202 |
| Benzo[a]anthracene-7,12-dione | 7,12-B(A)Dione | 44.419 | 258 | 230 |
| 5,12-Naphthacenedione | 5,12-NACQ | 45.132 | 258 | 230 |
| 6H-Benzo[c,d]pyrene-6-one | BPYRone | 46.392 | 254 | 226 |

*Table A.1.3. List of target OCs, deuterium-labelled POPs, retention time (minutes), monitored ion (MI) and qualifier ion (QI) used for measurements. Each group of OCs is quantified relative to the deuterium-labelled OCsbefore it.*

| Organochlorines | RT (min) | MI | QI |
|---|---|---|---|
| **Alpha-HCH-D6** | 17.74 | 224 | 181/112 |
| Alpha-HCH | 17.94 | 181 | 183/219 |
| Hexachlorobenzene | 18.32 | 284 | 286 |
| Beta-HCH | 19.47 | 181 | 183/219 |
| Gamma-HCH | 19.77 | 181 | 183/219 |
| Delta-HCH | 21.12 | 181 | 183/219 |
| Heptachlor | 23.81 | 100 | 272/274 |
| Aldrin | 25.72 | 263 | 91/66 |
| Heptachlor-endo-epoxide | 28.37 | 81 | 183/185 |
| **Fluranthene-D10** | 27.96 | 212 | 213 |
| Cis-Chlordane | 29.50 | 373 | 375/377 |
| **Endosulfan-D4** | 29.92 | 237 | 199/172/207 |
| Alpha-Endosulfan | 30.15 | 195 | 241/277 |
| Trans-Chlordane | 30.42 | 373 | 375/377 |
| Dieldrin | 31.67 | 79 | 263/108 |
| 4,4‘-DDE | 32.05 | 246 | 176/248 |
| Endrin | 32.82 | 263 | 81/281 |
| Beta-Endosulfan | 33.43 | 195 | 159/241 |
| 4,4’-DDD | 34.45 | 235 | 237/165 |
| Endrin-aldehyde | 34.58 | 67 | 250/345 |
| Endosulfan-sulfate | 35.98 | 272 | 229/274 |
| **4,4‘-DDT-D8** | 36.39 | 243 | 173/245 |
| 4,4‘-DDT | 36.56 | 235 | 165/237 |
| Endrin-ketone | 38.43 | 67 | 317 |
| Methoxychlor | 39.76 | 227 | |

*Table A.1.4 PAC compound physicochemical properties*

| Group | Compound Name | Abbreviation | Molecular Weight (g/mol) | Vapour Pressure (Pa, 25°C) | Water Solubility (mg/L) |
|---|---|---|---|---|---|
| LMW-PAHs | Naphthalene | NAPH | 128.17 | 32.8 | 142.1 |
| | 2-Methylnaphthalene | 2-MNAPH | 142.19 | 5.386 | 41.42 |
| | 1-Methylnaphthalene | 1-MNAPH | 142.19 | 4.6 | 40.62 |
| | Biphenyl | BP | 154.2 | 4.906 | 27.35 |
| | 1,3-Dimethylnaphthalene | 1,3-DMNAPH | 156.23 | 0.9986 | 11.96 |
| | Acenaphthylene | ACENY | 152.19 | 1.8 | 2.487 |
| | Acenaphthene | ACEN | 154.2 | 0.1667 | 2.534 |
| | Fluorene | FLUO | 166.21 | 0.172 | 1.339 |
| | Phenanthrene | PHEN | 178.22 | 0.044 | 0.677 |
| | Anthracene | ANTH | 178.22 | 0.00576 | 0.6905 |
| | 1-Methylphenanthrene | 1-MNAPH | 192.25 | 0.0002893 | 0.1706 |
| | 3,6-Dimethylphenanthrene | 3,6-DMPHEN | 206.28 | 0.00101 | 0.07133 |
| HMW-PAHs | 4H-Cyclopenta[d,e,f]phenanthrene | CPHEN | 190.25 | 0.00198 | 0.4456 |
| | Fluoanthene | FLUA | 202.26 | 0.0004173 | 0.1297 |
| | Pyrene | PYR | 202 | 4.59E-05 | 0.2249 |
| | Benzo[a]anthracene | B(A)A | 228.3 | 3.63E-05 | 0.02907 |
| | Chrysene + Triphenylene | CHRY+TRY | 228.3 | 2.08E-07 | 0.02635 |
| | Benzo [b+j+k] fluoanthene | B(BJK) | 252.3 | 3.32E-06 | 0.02065 |
| | Benzo[e]pyrene | B(E)P | 252 | 2.59E-06 | 0.00564 |
| | Benzo[a]pyrene | B(A)P | 252.3 | 1.31E-07 | 0.01038 |
| | Indeno [1,2,3-cd] pyrene | IND | 276 | 1.67E-08 | 0.002491 |
| | Dibenzo[ah]anthracene | DIBE | 278.4 | 1.85E-09 | 0.003304 |
| | Benzo[ghi]perylene | B(GHI) | 276 | 1.31E-08 | 0.002842 |
| | Coronene | COR | 300.4 | 1.14E-11 | 0.0002834 |
| Bio-PAHs | Retene | RET | 234.34 | 0.000352 | 0.00848 |
| | Perylene | PERY | 252.3 | 1.79E-07 | 0.008195 |
| AZAs | Quinoline | QUI | 129.15 | 7.186 | 1711 |
| | Benzo[h]quinoline | BQI | 179.21 | 0.01813 | 5.075 |
| | Acridine | ACR | 179.21 | 0.003453 | 5.383 |
| | Carbazole | CBZ | 167.2 | 5.41E-05 | 3.274 |
| OPAHs | 1-Indanone | 1-INDA | 132.16 | 3.56 | 1427 |
| | 1,4-Naphthoquinone | 1,4-NQ | 158.16 | 0.02253 | 2417 |
| | 1-Naphthaldehyde | 1-NLD | 156.19 | 0.3333 | 244.2 |
| | 2-Biphenylcarboxaldehyde | 2-BPCD | 182.22 | | |
| | 9-Fluorenone | 9-FLO | 180.21 | 0.007626 | 3.737 |
| | 1,2-Acenaphthylenequinone | 1,2-ACQ | 182.18 | 4.53E-05 | 90.14 |
| | 9,10-Anthraquinone | 9,10-ANQ | 208.22 | 5.11E-06 | 3.923 |
| | 1,8-Naphthalic anhydride | 1,8-NAA | 198.18 | 5.49E-05 | 5.878 |
| | 4H-Cyclopenta[def]phenanthrenone | CPHENone | 204.23 | 0.000356 | 0.9438 |
| | 2-Methylanthracene-9,10-dione | 2-MANQ | 222.25 | 0.0001164 | 1.234 |
| | Benzo[a]fluorenone | B(A)FLUone | 230.27 | 5.16E-05 | 0.2164 |
| | 7H-Benz[de]anthracene-7-one | BANTone | 230.27 | 2.95E-05 | 0.1837 |
| | Benz[a]anthracene-7,12-dione | 7,12-B(A)Dione | 258.28 | 5.17E-06 | 0.2885 |
| | Naphthacene-5,12-dione | 5,12-NACQ | 258.28 | 4.67E-06 | 0.2277 |
| | 6H-Benzo[cd]pyrene-6-one | BPYRone | 254.29 | 2.01E-06 | 0.05027 |

## Annex 2: $^{210}$Pb MODELS

*Fig A.2.1. Comparision of the CIC model and CRS model with and without missing inventory calculations (both CRS models have corrected with projected surface activity) for L. Fondococha.*

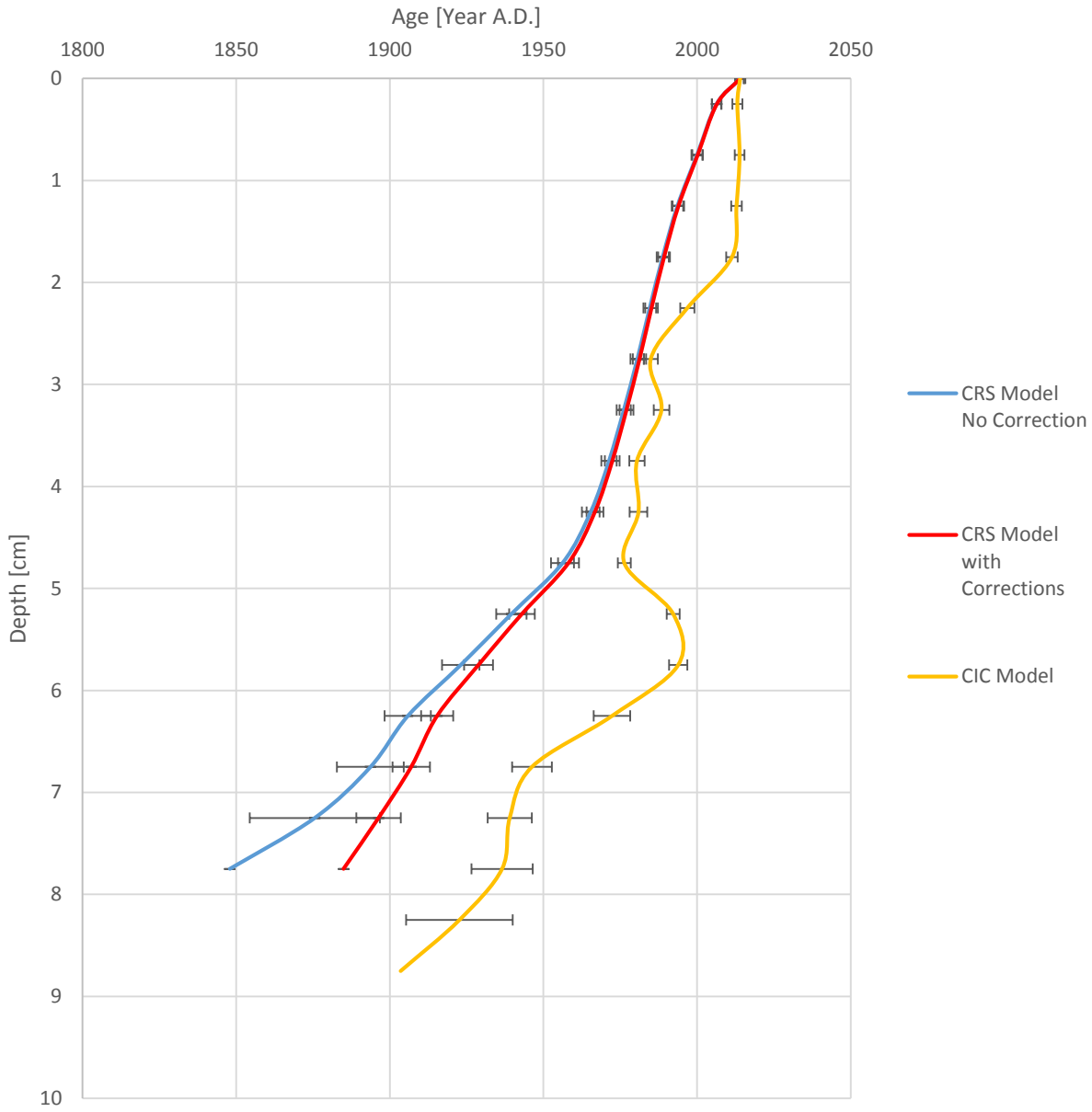

*Fig A.2.2. Comparision of the CIC model and CRS model with and without missing inventory calculations for L. Llaviuco. The CRS model that Michelutti et al. (2015) calculated for L. Llaviuco is also included for comparison.*

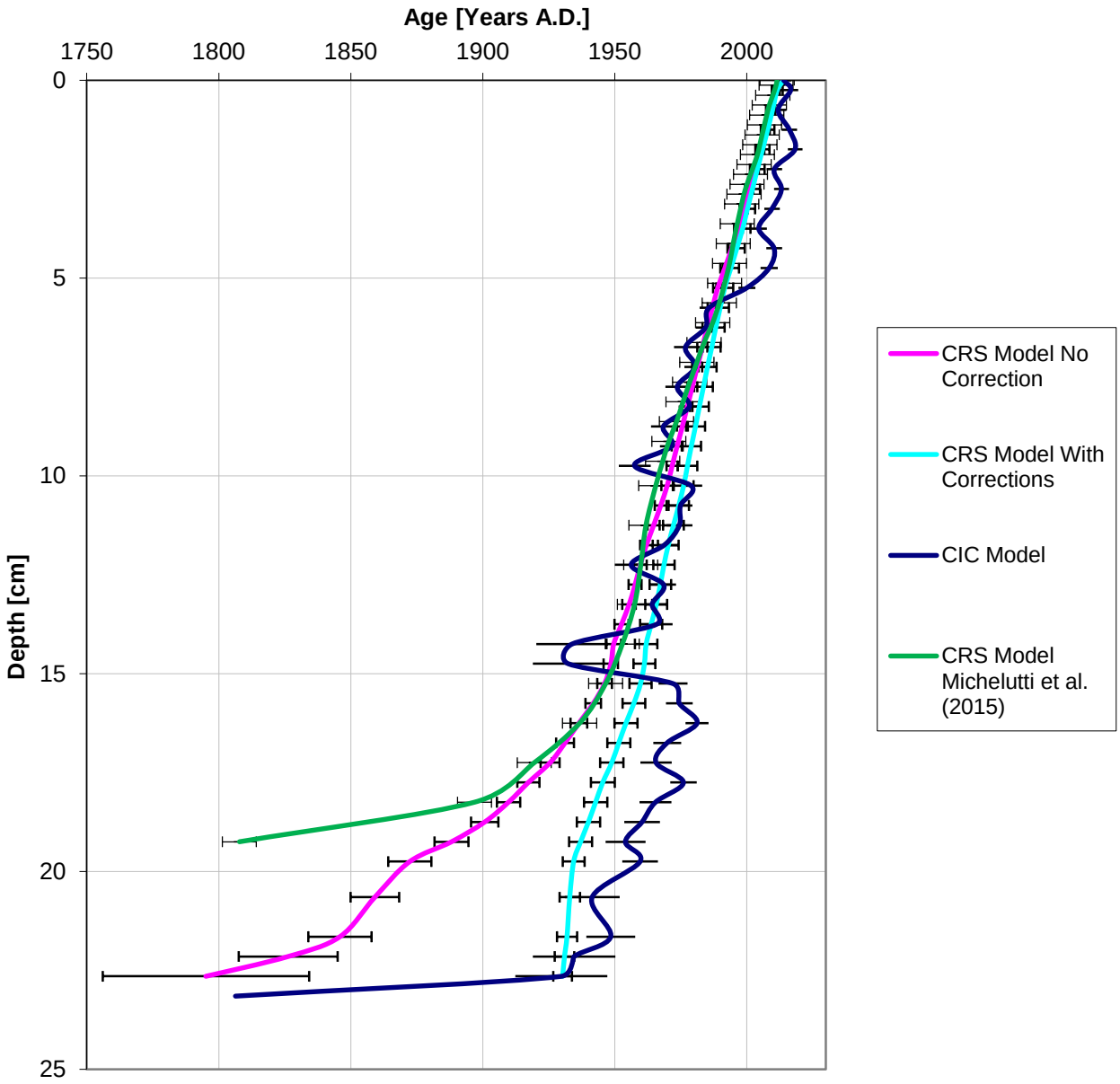

## Annex 3: RESULTS

*Table A.3.1 Persistent Organic Pollutant Concentrations in L. Fondococha*

| Laguna Fondococha | | Compound Concentration [ng g$^{-1}$] | | | |
|---|---|---|---|---|---|
| **Mid Point (cm)** | **Year** | **Hexachlorobenzene** | **Beta-HCH** | **Dieldrin** | **Endrin** |
| 0 | 2014 | 0.02 | | 0.16 | |
| 0.25 | 2006 | 0.01 | | 0.08 | |
| 0.75 | 2000 | 0.03 | | 0.43 | 0.31 |
| 1.25 | 1994 | 0.03 | | 0.52 | 0.50 |
| 1.75 | 1989 | 0.01 | 0.72 | 0.36 | 0.33 |
| 2.25 | 1985 | 0.03 | | 0.54 | 0.44 |
| 2.75 | 1981 | 0.04 | 0.11 | 0.28 | 0.29 |
| 3.25 | 1977 | 0.03 | 0.21 | 0.24 | 0.22 |
| 3.75 | 1972 | 0.02 | 1.79 | 0.35 | |
| 4.25 | 1967 | 0.02 | | 0.66 | |
| 4.75 | 1958 | 0.03 | 0.78 | 0.60 | |
| 5.25 | 1943 | | 0.91 | 0.72 | 0.51 |
| 5.75 | 1929 | 0.01 | | 0.67 | 0.54 |
| 6.25 | 1915 | 0.01 | | 1.06 | 0.73 |
| 6.75 | 1907 | | | | |
| 7.25 | 1896 | | | | |
| 7.75 | 1885 | 0.01 | | | |

*Table A.3.2 Persistent Organic Pollutant concentrations in L. Llaviuco. Past 1998 no Methoxychlor was detected in any samples.*

| Laguna Llaviuco | | [ng g$^{-1}$] |
|---|---|---|
| **Mid Point (cm)** | **Year** | **Methoxychlor** |
| 0 | 2014 | |
| 0.35 | 2010 | 22.37 |
| 0.95 | 2008 | 20.51 |
| 1.45 | 2006 | 36.40 |
| 1.95 | 2004 | 33.76 |
| 2.45 | 2003 | 87.09 |
| 2.95 | 2001 | 42.28 |
| 3.45 | 2000 | 21.34 |
| 3.95 | 1998 | 10.36 |
| 4.45 | 1996 | |
| 4.95 | 1994 | |
| 5.45 | 1993 | |
| 5.95 | 1991 | |
| 6.45 | 1990 | |
| 6.95 | 1988 | |
| 7.45 | 1986 | |
| ... | .... | |

*Table A.3.3. Total organic carbon and C/N ratio values for Laguna Llaviuco and Fondococha*

| LLAVIUCO | | | FONDOCOCHA | | |
|---|---|---|---|---|---|
| **Depth (cm)** | **C [%]** | **C/N Ratio** | **Depth (cm)** | **C [%]** | **C/N Ratio** |
| 0-0 - 0.0 | 11.00 | 12.78 | 0.0 - 0.5 | 11.79 | 14.66 |
| 0.0 - 0.7 | 9.26 | 12.69 | 0.5 - 1.0 | 12.31 | 14.42 |
| 0.7 - 1.2 | 9.79 | 12.64 | 1.0 - 1.5 | 12.12 | 13.95 |
| 1.2 - 1.7 | 10.38 | 12.84 | 1.5 - 2.0 | 11.12 | 13.50 |
| 1.7 - 2.2 | 10.02 | 12.77 | 2.0 - 2.5 | 10.08 | 13.26 |
| 2.2 - 2.7 | 10.32 | 12.96 | 2.5 - 3.0 | 9.06 | 12.94 |
| 2.7 - 3.2 | 10.18 | 13.11 | 3.0 - 3.5 | 8.89 | 12.77 |
| 3.2 - 3.7 | 9.34 | 12.40 | 3.5 - 4.0 | 8.71 | 12.86 |
| 3.7 - 4.2 | 9.67 | 12.24 | 4.0 - 4.5 | 8.97 | 12.89 |
| 4.2 - 4.7 | 9.23 | 12.58 | 4.5 - 5.0 | 8.97 | 12.70 |
| 4.7 - 5.2 | 8.63 | 12.60 | 5.0 - 5.5 | 9.13 | 12.84 |
| 5.2 - 5.7 | 8.03 | 12.64 | 5.5 - 6.0 | 8.57 | 13.07 |
| 5.7 - 6.2 | 8.07 | 12.64 | 6.0 - 6.5 | 9.57 | 13.28 |
| 6.2 - 6.7 | 8.21 | 12.58 | 6.5 - 7.0 | 8.89 | 12.71 |
| 6.7 - 7.2 | 8.31 | 12.66 | 7.0 - 7.5 | 8.35 | 12.95 |
| 7.2 - 7.7 | 8.27 | 12.60 | 7.5 - 8.0 | 8.35 | 13.31 |
| 7.7 - 8.2 | 8.22 | 12.69 | 8.0 - 8.5 | 9.11 | 12.84 |
| 8.2 - 8.7 | 8.26 | 12.58 | 8.5 - 9.0 | 7.08 | 13.00 |
| 8.7 - 9.2 | 8.07 | 12.58 | 9.0 - 9.5 | 5.03 | 12.86 |
| 9.2 - 9.7 | 8.22 | 12.67 | 9.5 - 10.0 | 7.88 | 12.81 |
| 9.7 - 10.4 | 7.46 | 12.88 | 10.0 - 10.5 | 7.86 | 12.73 |
| 10.4 - 10.9 | 8.32 | 12.66 | 10.5 - 11.3 | 7.19 | 12.56 |
| 10.9 - 11.4 | 8.42 | 12.68 | 11.3 - 11.8 | 8.04 | 12.84 |
| 11.4 - 11.9 | 8.30 | 12.82 | 11.8 - 12.5 | 8.02 | 12.76 |
| 11.9 - 12.4 | 8.16 | 12.99 | | | |
| 12.4 - 12.9 | 8.10 | 13.01 | | | |
| 12.9 - 13.4 | 8.43 | 12.82 | | | |
| 13.4 - 14.3 | 8.07 | 13.07 | | | |

*Table A.3.4.. Displaying the depth (cm), age (years A.D.), mass accumulation rate (g cm² yr⁻¹) and the fluxes (ng cm² yr⁻¹) for the ∑PAHs (no PERY), retene, perylene, ∑LMW-PAHs, ∑COMB-PAHs, ∑OPAHs and ∑AZAs for Laguna Fondococha.*

| Laguna Fondococha | | | CRS Model | | FLUX [ng cm-2 yr-1] | | | | | | |
|---|---|---|---|---|---|---|---|---|---|---|---|
| Depth (cm) | | Mid Point (cm) | MAR (g cm2 yr-1) | Year | ∑PAHs (no PERY) | Retene | Perylene | ∑LMW | ∑COMB-PAHs | ∑AZAs | ∑OPAHs |
| 0 | 0 | 0 | 0.017 | 2014 | 2.74 | 0.09 | 4.22 | 0.76 | 0.32 | 0.06 | 0.65 |
| 0.0 | 0.5 | 0.25 | 0.017 | 2006 | 2.74 | 0.09 | 4.22 | 0.76 | 0.32 | 0.06 | 0.65 |
| 0.5 | 1.0 | 0.75 | 0.016 | 2000 | 4.16 | 0.08 | 3.77 | 1.02 | 0.36 | 0.05 | 0.64 |
| 1.0 | 1.5 | 1.25 | 0.014 | 1994 | 4.50 | 0.12 | 4.24 | 1.14 | 0.27 | 0.05 | 0.88 |
| 1.5 | 2.0 | 1.75 | 0.019 | 1989 | 7.00 | 0.19 | 10.68 | 2.19 | 0.31 | 0.07 | 1.39 |
| 2.0 | 2.5 | 2.25 | 0.025 | 1985 | 4.86 | 0.12 | 25.31 | 1.41 | 0.30 | 0.10 | 1.32 |
| 2.5 | 3.0 | 2.75 | 0.020 | 1981 | 8.62 | 0.17 | 23.40 | 3.58 | 0.22 | 0.09 | 1.28 |
| 3.0 | 3.5 | 3.25 | 0.022 | 1977 | 3.97 | 0.15 | 24.57 | 1.20 | 0.26 | 0.06 | 1.12 |
| 3.5 | 4.0 | 3.75 | 0.019 | 1972 | 3.01 | 0.09 | 21.34 | 0.85 | 0.25 | 0.07 | 0.98 |
| 4.0 | 4.5 | 4.25 | 0.018 | 1967 | 2.82 | 0.05 | 21.31 | 0.84 | 0.25 | 0.07 | 0.90 |
| 4.5 | 5.0 | 4.75 | 0.008 | 1958 | 1.56 | 0.04 | 11.27 | 0.49 | 0.10 | 0.03 | 0.50 |
| 5.0 | 5.5 | 5.25 | 0.005 | 1943 | 1.24 | 0.03 | 6.49 | 0.37 | 0.07 | 0.03 | 0.28 |
| 5.5 | 6.0 | 5.75 | 0.006 | 1929 | 1.02 | 0.03 | 10.24 | 0.32 | 0.05 | 0.03 | 0.28 |
| 6.0 | 6.5 | 6.25 | 0.009 | 1915 | 1.34 | 0.04 | 19.64 | 0.38 | 0.06 | 0.04 | 0.38 |
| 6.5 | 7.0 | 6.75 | 0.009 | 1907 | 3.76 | 0.05 | 19.20 | 1.27 | 0.04 | 0.04 | 0.43 |
| 7.0 | 7.5 | 7.25 | 0.007 | 1896 | 1.35 | 0.04 | 12.64 | 0.38 | 0.02 | 0.03 | 0.34 |
| 7.5 | 8.0 | 7.75 | 0.008 | 1885 | 2.76 | 0.04 | 16.15 | 0.79 | 0.03 | 0.04 | 0.40 |
| | | | | **Average:** | 3.38 | 0.08 | 14.04 | 1.04 | 0.19 | 0.05 | 0.73 |

*Table A.3.5. Displaying the depth (cm), age (years A.D.), mass accumulation rate (g cm² yr⁻¹) and the fluxes (ng cm² yr⁻¹) for the ∑PAHs (no PERY), retene, perylene, ∑LMW-PAHs, ∑COMB-PAHs, ∑OPAHs and ∑AZAs for Laguna Llaviuco.*

| Laguna Llaviuco | | CRS Model | | FLUX (ng cm² yr⁻¹) | | | | | | |
|---|---|---|---|---|---|---|---|---|---|---|
| **Depth (cm)** | **Mid Point (cm)** | **Year** | **MAR (g cm² yr⁻¹)** | **∑PAHs (no PERY)** | **Retene** | **Perylene** | **∑LMW-PAHs** | **∑COMB-PAHs** | **∑OPAHs** | **∑AZAs** |
| 0.0-0.0 | 0 | 2014 | 0.078 | 25.70 | 1.83 | 11.26 | 8.86 | 5.91 | 5.29 | 0.35 |
| 0.0-0.7 | 0.35 | 2010 | 0.085 | 31.51 | 0.43 | 8.29 | 3.77 | 5.39 | 5.29 | 0.35 |
| 0.7-1.2 | 0.95 | 2008 | 0.090 | 19.55 | 0.42 | 7.14 | 6.07 | 5.67 | 5.36 | 0.37 |
| 1.2-1.7 | 1.45 | 2006 | 0.096 | 45.77 | 0.84 | 7.40 | 7.36 | 6.69 | 6.68 | 0.49 |
| 1.7-2.2 | 1.95 | 2004 | 0.101 | 20.05 | 0.59 | 7.67 | 6.69 | 6.34 | 6.26 | 0.41 |
| 2.2-2.7 | 2.45 | 2003 | 0.104 | 33.65 | 0.58 | 8.00 | 9.49 | 6.86 | 5.99 | 0.46 |
| 2.7-3.2 | 2.95 | 2001 | 0.109 | 33.17 | 0.51 | 12.09 | 9.39 | 6.50 | 5.79 | 0.40 |
| 3.2-3.7 | 3.45 | 2000 | 0.112 | 36.73 | 0.72 | 16.21 | 8.48 | 6.61 | 6.12 | 0.34 |
| 3.7-4.2 | 3.95 | 1998 | 0.117 | 29.88 | 0.71 | 18.46 | 8.34 | 6.74 | 5.62 | 0.38 |
| 4.2-4.7 | 4.45 | 1996 | 0.122 | 52.51 | 0.73 | 26.28 | 11.70 | 7.20 | 6.26 | 0.43 |
| 4.7-5.2 | 4.95 | 1994 | 0.128 | 33.15 | 0.97 | 22.53 | 8.31 | 5.39 | 5.62 | 0.40 |
| 5.2-5.7 | 5.45 | 1993 | 0.130 | 22.50 | 0.73 | 15.99 | 7.08 | 4.37 | 5.98 | 0.41 |
| 5.7-6.2 | 5.95 | 1991 | 0.135 | 31.79 | 0.80 | 15.62 | 8.18 | 4.64 | 6.04 | 0.44 |
| 6.2-6.7 | 6.45 | 1990 | 0.138 | 35.91 | 0.73 | 17.17 | 9.74 | 5.26 | 5.29 | 0.46 |
| 6.7-7.2 | 6.95 | 1988 | 0.143 | 38.26 | 0.92 | 18.89 | 13.02 | 5.26 | 6.84 | 0.42 |
| 7.2-7.7 | 7.45 | 1986 | 0.149 | 30.97 | 1.04 | 17.34 | 8.74 | 5.40 | 6.15 | 0.49 |
| 7.7-8.2 | 7.95 | 1984 | 0.154 | 28.06 | 1.42 | 19.06 | 8.47 | 6.39 | 7.91 | 0.57 |
| 8.2-8.7 | 8.45 | 1983 | 0.157 | 20.35 | 1.11 | 21.22 | 7.24 | 5.55 | 8.18 | 0.78 |
| 8.7-9.2 | 8.95 | 1981 | 0.162 | 22.12 | 1.03 | 20.13 | 7.80 | 5.58 | 8.08 | 0.70 |
| 9.2-9.7 | 9.45 | 1980 | 0.165 | 26.81 | 0.92 | 23.48 | 10.01 | 6.09 | 8.25 | 0.77 |
| 9.7-10.4 | 10.05 | 1978 | 0.170 | 28.32 | 0.67 | 19.43 | 10.35 | 5.58 | 6.72 | 0.65 |
| 10.4-10.9 | 10.65 | 1976 | 0.162 | 19.52 | 0.89 | 20.19 | 7.01 | 5.31 | 7.70 | 0.75 |
| 10.9-11.4 | 11.15 | 1975 | 0.158 | 24.55 | 0.92 | 20.87 | 9.05 | 5.46 | 7.25 | 0.70 |
| 11.4-11.9 | 11.65 | 1974 | 0.154 | 21.72 | 0.72 | 17.31 | 6.89 | 4.91 | 6.97 | 0.60 |
| 11.9-12.4 | 12.15 | 1973 | 0.150 | 46.58 | 0.86 | 17.63 | 6.15 | 4.46 | 6.66 | 0.75 |
| 12.4-12.9 | 12.65 | 1972 | 0.146 | 22.71 | 0.84 | 16.69 | 6.42 | 4.54 | 6.11 | 0.56 |
| 12.9-13.4 | 13.15 | 1970 | 0.138 | 17.40 | 0.64 | 15.35 | 5.31 | 3.96 | 5.38 | 0.57 |
| 13.4-14.3 | 13.85 | 1969 | 0.134 | 16.37 | 0.74 | 18.34 | 5.28 | 3.98 | 5.60 | 0.54 |
| | | | **Average:** | 29.13 | 0.83 | 16.43 | 8.04 | 5.57 | 6.22 | 0.51 |

*Table A.3.6. Displaying the depth (cm), age (years A.D.), mass accumulation rate (g cm² yr⁻¹) and the fluxes (ng cm² yr⁻¹) for mercury (Hg), copper (Cu), zinc (Zn), lead (Pb) and chromium (Cr) for Laguna Fondococha.*

| Laguna Fondococha | | CRS Model | | FLUX [ng cm-2 yr-1] | | | | |
|---|---|---|---|---|---|---|---|---|
| **Depth (cm)** | **Mid-Point (cm)** | **MAR (g cm2 yr-1)** | **Year** | **Mercury** | **Copper** | **Zinc** | **Lead** | **Chromium** |
| 0 - 0 | 0 | 0.017 | 2014 | 2.61 | 719.73 | 1306.02 | 398.72 | 268.38 |
| 0 - 0.5 | 0.25 | 0.017 | 2006 | 3.01 | 435.39 | 1181.89 | 403.92 | 260.63 |
| 0.5 - 1.0 | 0.75 | 0.016 | 2000 | 3.00 | 384.23 | 1151.49 | 423.30 | 219.40 |
| 1.0 - 1.5 | 1.25 | 0.014 | 1994 | 2.39 | 319.66 | 1041.24 | 356.41 | 200.78 |
| 1.5 - 2.0 | 1.75 | 0.019 | 1989 | 3.01 | 520.62 | 1400.31 | 447.05 | 273.52 |
| 2.0 - 2.5 | 2.25 | 0.025 | 1985 | 4.17 | 486.87 | 1672.31 | 501.86 | 323.89 |
| 2.5 - 3.0 | 2.75 | 0.020 | 1981 | 2.49 | 402.14 | 1459.78 | 436.67 | 280.98 |
| 3.0 - 3.5 | 3.25 | 0.022 | 1977 | 2.90 | 455.79 | 1580.76 | 475.45 | 301.19 |
| 3.5 - 4.0 | 3.75 | 0.019 | 1972 | 2.74 | 375.16 | 1362.44 | 393.31 | 261.82 |
| 4.0 - 4.5 | 4.25 | 0.018 | 1967 | 2.60 | 382.96 | 1299.68 | 358.28 | 254.32 |
| 4.5 - 5.0 | 4.75 | 0.008 | 1958 | 1.15 | 180.93 | 624.28 | 165.27 | 121.29 |
| 5.0 - 5.5 | 5.25 | 0.005 | 1943 | 0.72 | 99.43 | 329.37 | 97.65 | 67.72 |
| 5.5 - 6.0 | 5.75 | 0.006 | 1929 | 0.71 | 134.90 | 487.74 | 155.81 | 97.35 |
| 6.0 - 6.5 | 6.25 | 0.009 | 1915 | 1.11 | 236.42 | 785.35 | 227.70 | 154.17 |
| 6.5 - 7.0 | 6.75 | 0.009 | 1907 | 0.88 | 228.38 | 751.40 | 211.57 | 146.23 |
| 7.0 - 7.5 | 7.3 | 0.007 | 1896 | 0.68 | 156.26 | 541.94 | 173.52 | 108.87 |
| 7.5 - 8.0 | 7.85 | 0.008 | 1885 | 0.84 | 188.50 | 624.94 | 170.55 | 130.23 |
| | | | **Average:** | 2.06 | 335.73 | 1035.35 | 317.47 | 204.16 |

*Table A.3.7. Displaying the depth (cm), age (years A.D.), mass accumulation rate (g cm² yr⁻¹) and the fluxes (ng cm² yr⁻¹) for mercury (Hg), copper (Cu), zinc (Zn), lead (Pb) and chromium (Cr) for Laguna Llaviuco.*

| Laguna Llaviuco | | CRS Model | | FLUX (ng cm-2 yr-1) | | | | |
|---|---|---|---|---|---|---|---|---|
| **Depth (cm)** | **Mid Point (cm)** | **Year** | **MAR (g cm-2 yr-1)** | **Mercury** | **Copper** | **Zinc** | **Lead** | **Chromium** |
| 0.0-0.0 | 0 | 2014 | 0.078 | 20.85 | 4283.02 | 24661.19 | 12690.72 | 3434.39 |
| 0.0-0.7 | 0.35 | 2010 | 0.085 | 25.50 | 6122.86 | 27375.37 | 13429.13 | 3807.51 |
| 0.7-1.2 | 0.95 | 2008 | 0.090 | 23.88 | 4246.36 | 24436.56 | 11424.27 | 3874.24 |
| 1.2-1.7 | 1.45 | 2006 | 0.096 | 21.13 | 4427.51 | 24029.24 | 10677.65 | 4041.45 |
| 1.7-2.2 | 1.95 | 2004 | 0.101 | 20.58 | 4221.49 | 23701.03 | 10524.05 | 3880.00 |
| 2.2-2.7 | 2.45 | 2003 | 0.104 | 26.36 | 5043.45 | 26254.54 | 12018.89 | 4320.23 |
| 2.7-3.2 | 2.95 | 2001 | 0.109 | 29.03 | 4870.74 | 30743.11 | 14506.41 | 4367.45 |
| 3.2-3.7 | 3.45 | 2000 | 0.112 | 36.23 | 5967.58 | 36231.47 | 19005.85 | 5249.83 |
| 3.7-4.2 | 3.95 | 1998 | 0.117 | 32.34 | 5765.14 | 38887.05 | 19672.84 | 5280.57 |
| 4.2-4.7 | 4.45 | 1996 | 0.122 | 32.91 | 7086.63 | 37440.14 | 19696.50 | 5104.02 |
| 4.7-5.2 | 4.95 | 1994 | 0.128 | 33.53 | 7738.35 | 48967.25 | 28178.48 | 5985.81 |
| 5.2-5.7 | 5.45 | 1993 | 0.130 | 30.96 | 7734.85 | 47754.18 | 26623.64 | 6128.31 |
| 5.7-6.2 | 5.95 | 1991 | 0.135 | 34.79 | 7623.88 | 47514.81 | 27017.11 | 6060.93 |
| 6.2-6.7 | 6.45 | 1990 | 0.138 | 35.71 | 7897.61 | 50146.65 | 28160.85 | 6269.59 |
| 6.7-7.2 | 6.95 | 1988 | 0.143 | 42.24 | 8614.68 | 53167.72 | 30029.14 | 6466.80 |
| 7.2-7.7 | 7.45 | 1986 | 0.149 | 38.03 | 9101.61 | 54211.41 | 31518.68 | 6323.28 |
| 7.7-8.2 | 7.95 | 1984 | 0.154 | 44.58 | 9497.10 | 57043.70 | 33270.57 | 6358.16 |
| 8.2-8.7 | 8.45 | 1983 | 0.157 | 44.98 | 10771.47 | 61287.39 | 36860.05 | 6746.24 |
| 8.7-9.2 | 8.95 | 1981 | 0.162 | 44.07 | 11089.31 | 64578.02 | 36905.75 | 7202.83 |
| 9.2-9.7 | 9.45 | 1980 | 0.165 | 48.18 | 10603.53 | 63582.47 | 36052.36 | 8276.84 |
| 9.7-10.4 | 10.05 | 1978 | 0.170 | 48.02 | 12022.94 | 72739.18 | 46179.36 | 8032.00 |
| 10.4-10.9 | 10.65 | 1976 | 0.162 | 37.15 | 9665.64 | 57460.03 | 30744.80 | 7121.14 |
| 10.9-11.4 | 11.15 | 1975 | 0.158 | 40.12 | 19229.33 | 53382.47 | 27863.51 | 6993.33 |
| 11.4-11.9 | 11.65 | 1974 | 0.154 | 32.78 | 7590.93 | 47280.54 | 24483.38 | 6972.72 |
| 11.9-12.4 | 12.15 | 1973 | 0.150 | 28.46 | 6200.05 | 38744.22 | 20155.35 | 5562.02 |
| 12.4-12.9 | 12.65 | 1972 | 0.146 | 31.61 | 6859.33 | 44904.11 | 22209.21 | 6257.58 |
| 12.9-13.4 | 13.15 | 1970 | 0.138 | 28.62 | 6729.44 | 41325.08 | 20768.20 | 6101.76 |
| 13.4-14.3 | 13.85 | 1969 | 0.134 | 31.62 | 6399.99 | 39557.89 | 19817.64 | 5865.50 |
| | | | **Average:** | 33.72 | 7764.46 | 44193.10 | 23945.87 | 5788.73 |

*Table A.3.8. PAH, OPAH and AZA molecular diagnostic ratios for L. Fondococha. The ratio trend depicts the trend of the molecular diagnostic ratios from 1969 (right side) to 2014 (left side). Increases in ratios show the trend line going up, decreasing ratios and the trend line dips down.*

| Year | ΣLMW-PAHs/ΣHMW-PAH | ΣCOMB-PAHs/ΣParent-PAHs | Naphthalene/2-MethylNaphthalene | Naphthalene/1-MethylNaphthalene | Naphthalene/1,3-DimethylNaphthalene | Phenanthrene/1-Methylphenanthrene | ΣOPAHs/ΣPAHs | Σ4AZAs/ΣParent-PAHs |
|---|---|---|---|---|---|---|---|---|
| 2014 | 0.8 | 0.19 | 9.3 | 10.4 | 4.6 | 3.6 | 0.24 | 0.03 |
| 2006 | 0.8 | 0.19 | 9.3 | 10.4 | 4.6 | 3.6 | 0.24 | 0.03 |
| 2000 | 1.2 | 0.19 | 2.4 | 1.8 | 1.8 | 0.4 | 0.15 | 0.02 |
| 1994 | 1.2 | 0.13 | 3.2 | 2.8 | 2.2 | 0.7 | 0.20 | 0.02 |
| 1989 | 1.8 | 0.09 | 2.8 | 2.2 | 1.9 | 1.2 | 0.20 | 0.02 |
| 1985 | 1.6 | 0.13 | 2.5 | 2.2 | 2.2 | 0.5 | 0.27 | 0.04 |
| 1981 | 2.5 | 0.04 | 2.9 | 2.0 | 1.2 | 2.6 | 0.15 | 0.02 |
| 1977 | 1.6 | 0.14 | 3.0 | 2.4 | 1.9 | 1.0 | 0.28 | 0.03 |
| 1972 | 1.4 | 0.17 | 3.8 | 2.6 | 2.8 | 0.5 | 0.33 | 0.05 |
| 1967 | 1.1 | 0.16 | 4.0 | 3.5 | 3.5 | 0.9 | 0.32 | 0.04 |
| 1958 | 1.4 | 0.12 | 4.1 | 3.6 | 3.3 | 1.2 | 0.32 | 0.04 |
| 1943 | 1.6 | 0.12 | 2.8 | 2.1 | 2.1 | 0.6 | 0.22 | 0.05 |
| 1929 | 2.1 | 0.10 | 3.3 | 2.4 | 2.1 | 0.5 | 0.28 | 0.06 |
| 1915 | 1.9 | 0.11 | 3.0 | 2.3 | 2.6 | 0.3 | 0.29 | 0.07 |
| 1907 | 6.9 | 0.03 | 2.4 | 1.8 | 2.3 | 0.2 | 0.12 | 0.03 |
| 1896 | 4.1 | 0.05 | 2.2 | 1.6 | 2.1 | 0.2 | 0.25 | 0.06 |
| 1885 | 5.2 | 0.03 | 2.0 | 1.5 | 1.7 | 0.2 | 0.14 | 0.04 |
| **RATIO TREND** (2014 - 1885) |  | 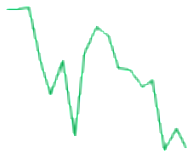 | 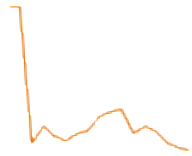 | 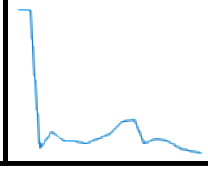 | 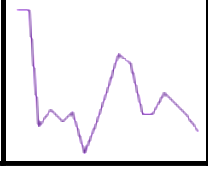 | 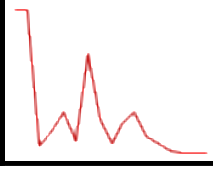 | 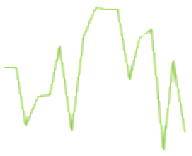 | 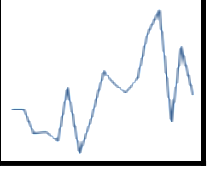 |

*Table A.3.9. PAH, OPAH and AZA molecular diagnostic ratios for L. Llaviuco. The ratio trend depicts the trend of the molecular diagnostic ratios from 1969 (right side) to 2014 (left side). Increases in ratios show the trend line going up, decreasing ratios and the trend line dips down*

| Year | ΣLMW-PAHs/ΣHMW-PAH | ΣCOMB-PAHs/ΣParent-PAHs | Naphthalene/2-MethylNaphthalene | Naphthalene/1-MethylNaphthalene | Naphthalene/1,3-DimethylNaphthalene | ΣOPAHs/ΣPAHs | Σ4AZAs/ΣParent-PAHs |
|---|---|---|---|---|---|---|---|
| 2014 | 1.2 | 0.36 | 0.0 | 0.0 | 0.0 | 0.00 | 0.00 |
| 2010 | 0.6 | 0.51 | 1.0 | 0.5 | 0.7 | 0.50 | 0.03 |
| 2008 | 0.9 | 0.43 | 0.0 | 0.0 | 3.5 | 0.41 | 0.03 |
| 2006 | 0.8 | 0.42 | 1.2 | 0.6 | 0.8 | 0.41 | 0.03 |
| 2004 | 0.8 | 0.43 | 0.0 | 0.0 | 8.4 | 0.43 | 0.03 |
| 2003 | 1.1 | 0.38 | 5.8 | 3.0 | 2.0 | 0.33 | 0.03 |
| 2001 | 1.2 | 0.38 | 5.6 | 3.4 | 1.9 | 0.34 | 0.02 |
| 2000 | 1.0 | 0.40 | 3.6 | 2.3 | 1.4 | 0.37 | 0.02 |
| 1998 | 1.0 | 0.41 | 9.0 | 4.2 | 1.6 | 0.34 | 0.02 |
| 1996 | 1.3 | 0.35 | 2.3 | 1.5 | 1.0 | 0.31 | 0.02 |
| 1994 | 1.2 | 0.35 | 2.6 | 1.5 | 1.0 | 0.37 | 0.03 |
| 1993 | 1.3 | 0.34 | 6.0 | 3.7 | 1.5 | 0.47 | 0.03 |
| 1991 | 1.4 | 0.33 | 2.7 | 1.8 | 1.0 | 0.43 | 0.03 |
| 1990 | 1.5 | 0.32 | 3.4 | 2.0 | 1.3 | 0.32 | 0.03 |
| 1988 | 1.9 | 0.26 | 3.4 | 2.2 | 1.5 | 0.34 | 0.02 |
| 1986 | 1.3 | 0.35 | 3.7 | 2.2 | 1.2 | 0.40 | 0.03 |
| 1984 | 1.0 | 0.38 | 7.0 | 3.1 | 1.8 | 0.47 | 0.03 |
| 1983 | 1.0 | 0.38 | 12.9 | 6.1 | 4.6 | 0.56 | 0.05 |
| 1981 | 1.1 | 0.37 | 10.1 | 5.1 | 3.0 | 0.53 | 0.05 |
| 1980 | 1.3 | 0.35 | 7.3 | 3.6 | 2.7 | 0.47 | 0.04 |
| 1978 | 1.4 | 0.31 | 4.3 | 2.7 | 1.8 | 0.38 | 0.04 |
| 1976 | 1.0 | 0.38 | 8.4 | 4.5 | 3.2 | 0.55 | 0.05 |
| 1975 | 1.3 | 0.34 | 6.5 | 3.8 | 2.4 | 0.45 | 0.04 |
| 1974 | 1.1 | 0.37 | 4.7 | 3.0 | 1.9 | 0.53 | 0.05 |
| 1973 | 1.1 | 0.37 | 0.6 | 0.4 | 0.5 | 0.56 | 0.06 |
| 1972 | 1.1 | 0.37 | 3.1 | 2.2 | 1.5 | 0.49 | 0.05 |
| 1970 | 1.0 | 0.38 | 6.8 | 3.5 | 1.4 | 0.52 | 0.05 |
| 1969 | 1.0 | 0.38 | 4.8 | 2.7 | 2.3 | 0.53 | 0.05 |
| **RATIO TREND** (2014 - 1969) | 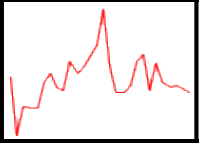 | 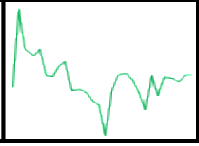 | 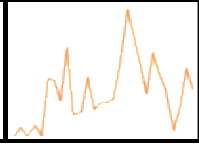 | 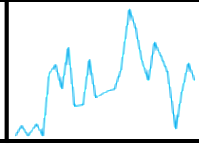 | 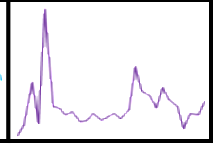 | 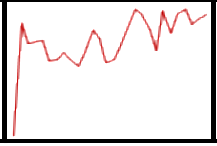 | 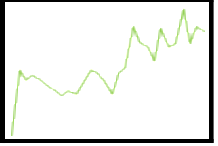 |

## Annex 4: STATISTICS

*Table A.4.1. Contribution of the % of different elements and PAHs to each of the 7 principle components (PCs) with eigenvalue > 1 in all depths (n = 17) using PCA. Largest contributions are highlighted in red for PC 1 and blue for PC2 for L. Fondococha.*

| | PC1 | PC2 | PC3 | PC4 | PC5 | PC6 | PC7 |
|---|---|---|---|---|---|---|---|
| **Hg** | 2.52 | 0.54 | 1.70 | 0.01 | 0.03 | 0.96 | 1.60 |
| **Al** | 2.28 | 0.30 | 1.92 | 3.12 | 0.00 | 2.35 | 3.75 |
| **V** | 2.87 | 0.16 | 1.70 | 0.98 | 1.10 | 0.97 | 0.01 |
| **Cr** | 2.52 | 0.12 | 1.74 | 1.08 | 5.09 | 0.39 | 0.23 |
| **Mn** | 2.25 | 0.36 | 0.00 | 0.38 | 0.60 | 1.61 | 0.37 |
| **Fe** | 1.44 | 0.63 | 3.23 | 0.09 | 2.25 | 7.59 | 13.28 |
| **Co** | 3.06 | 0.06 | 0.00 | 1.59 | 0.17 | 0.05 | 1.97 |
| **Ni** | 3.02 | 0.02 | 0.56 | 0.70 | 2.19 | 0.02 | 1.43 |
| **Cu** | 0.00 | 0.46 | 5.19 | 5.66 | 6.56 | 3.37 | 5.83 |
| **Zn** | 2.85 | 0.07 | 0.69 | 0.20 | 0.14 | 5.20 | 5.52 |
| **As** | 0.05 | 0.29 | 12.59 | 0.19 | 0.83 | 9.34 | 2.46 |
| **Ag** | 0.90 | 0.03 | 9.15 | 4.04 | 1.23 | 0.37 | 0.05 |
| **Cs** | 3.07 | 0.10 | 0.07 | 0.81 | 1.96 | 2.01 | 0.56 |
| **La** | 3.54 | 0.01 | 0.01 | 0.10 | 0.72 | 0.06 | 0.02 |
| **Pr** | 3.54 | 0.00 | 0.05 | 0.14 | 0.56 | 0.00 | 0.17 |
| **Nd** | 3.54 | 0.00 | 0.06 | 0.08 | 0.52 | 0.00 | 0.26 |
| **Sm** | 3.57 | 0.00 | 0.09 | 0.07 | 0.29 | 0.01 | 0.18 |
| **Eu** | 3.51 | 0.01 | 0.11 | 0.21 | 0.30 | 0.00 | 0.91 |
| **Gd** | 3.57 | 0.01 | 0.00 | 0.05 | 0.57 | 0.03 | 0.04 |
| **Ho** | 3.54 | 0.00 | 0.03 | 0.07 | 0.54 | 0.00 | 0.47 |
| **Er** | 3.52 | 0.00 | 0.01 | 0.10 | 0.33 | 0.12 | 1.58 |
| **Tm** | 3.53 | 0.00 | 0.05 | 0.00 | 0.51 | 0.02 | 0.80 |
| **Yb** | 3.13 | 0.09 | 0.19 | 0.31 | 0.04 | 0.15 | 5.10 |
| **Lu** | 3.42 | 0.00 | 0.36 | 0.02 | 1.56 | 0.13 | 0.04 |
| **Tl** | 3.19 | 0.20 | 0.31 | 0.39 | 0.14 | 0.45 | 3.22 |
| **Pb** | 0.38 | 0.06 | 10.82 | 0.49 | 7.47 | 0.60 | 2.59 |
| **Th** | 2.08 | 0.31 | 0.43 | 3.71 | 0.56 | 10.42 | 3.82 |
| **U** | 3.05 | 0.01 | 0.97 | 0.13 | 1.07 | 0.01 | 4.52 |
| **NAPH** | 1.69 | 2.73 | 1.28 | 0.63 | 2.55 | 0.25 | 0.09 |
| **2-MNAPH** | 1.99 | 2.19 | 0.88 | 0.71 | 2.99 | 0.29 | 1.80 |
| **1-MNAPH** | 1.98 | 2.20 | 0.67 | 0.67 | 3.73 | 0.36 | 2.08 |
| **BP** | 0.77 | 3.33 | 5.04 | 1.03 | 0.22 | 0.62 | 0.95 |
| **1,3-DMNAPH** | 1.12 | 4.84 | 0.43 | 0.02 | 1.12 | 0.91 | 2.88 |
| **ACEN** | 0.03 | 5.83 | 1.45 | 4.07 | 0.28 | 0.37 | 0.56 |
| **FLUO** | 0.17 | 7.57 | 0.00 | 0.02 | 0.30 | 0.23 | 0.16 |
| **PHEN** | 0.21 | 6.34 | 0.35 | 2.55 | 1.51 | 0.16 | 0.46 |
| **ANTH** | 0.05 | 5.36 | 1.82 | 4.82 | 0.18 | 0.16 | 0.36 |
| **3,6-DMPHEN** | 0.13 | 5.64 | 1.07 | 0.28 | 1.68 | 2.30 | 0.25 |
| **CPHEN** | 0.20 | 4.37 | 2.18 | 5.94 | 1.09 | 0.34 | 0.01 |
| **FLUA** | 0.33 | 5.17 | 1.10 | 4.68 | 0.11 | 0.76 | 0.90 |
| **PYR** | 0.66 | 4.04 | 0.12 | 7.03 | 0.23 | 0.00 | 0.83 |
| **RET** | 0.00 | 4.79 | 3.08 | 0.59 | 1.47 | 0.46 | 0.24 |
| **B(A)A** | 2.06 | 1.87 | 0.16 | 1.92 | 0.23 | 0.38 | 4.31 |
| **CHRY** | 2.17 | 2.37 | 0.01 | 0.24 | 0.30 | 2.20 | 3.92 |
| **B(BJK)** | 2.55 | 0.20 | 0.66 | 0.30 | 2.32 | 1.34 | 8.06 |
| **B(E)P** | 0.32 | 0.64 | 7.10 | 3.70 | 10.04 | 0.05 | 0.99 |
| **B(A)P** | 0.34 | 0.59 | 7.23 | 3.65 | 9.53 | 0.33 | 0.79 |
| **PERY** | 2.60 | 0.08 | 3.55 | 0.36 | 0.09 | 0.28 | 2.01 |
| **B(GHI)** | 2.59 | 0.02 | 3.26 | 0.01 | 1.37 | 0.62 | 0.73 |
| **CBZ** | 1.02 | 1.85 | 1.13 | 2.07 | 5.32 | 1.69 | 0.88 |
| **1-INDA** | 0.89 | 0.01 | 0.13 | 11.58 | 0.49 | 0.02 | 0.58 |
| **9-FLO** | 0.51 | 5.13 | 2.00 | 0.99 | 0.55 | 0.01 | 1.12 |
| **9,10-ANQ** | 0.24 | 4.79 | 0.47 | 5.04 | 0.22 | 5.24 | 0.04 |
| **CPHENone** | 0.00 | 6.54 | 0.57 | 0.07 | 0.01 | 0.67 | 0.05 |
| **B(A)FLUone** | 0.49 | 5.99 | 0.48 | 0.15 | 2.07 | 0.87 | 2.09 |
| **BANTone** | 0.03 | 1.23 | 1.07 | 8.95 | 7.87 | 11.71 | 2.07 |
| **7,12-B(A)A** | 0.95 | 0.45 | 0.73 | 3.21 | 4.80 | 21.14 | 0.02 |

*Fig A.4.1. Biplot of PC1 and 2 for L. Fondococha showing the contribution (%) of the variance of different metals (Cu, Zn, Pb, Cr, Hg), C and C/N and PAHs, OPAHs, AZAs.*

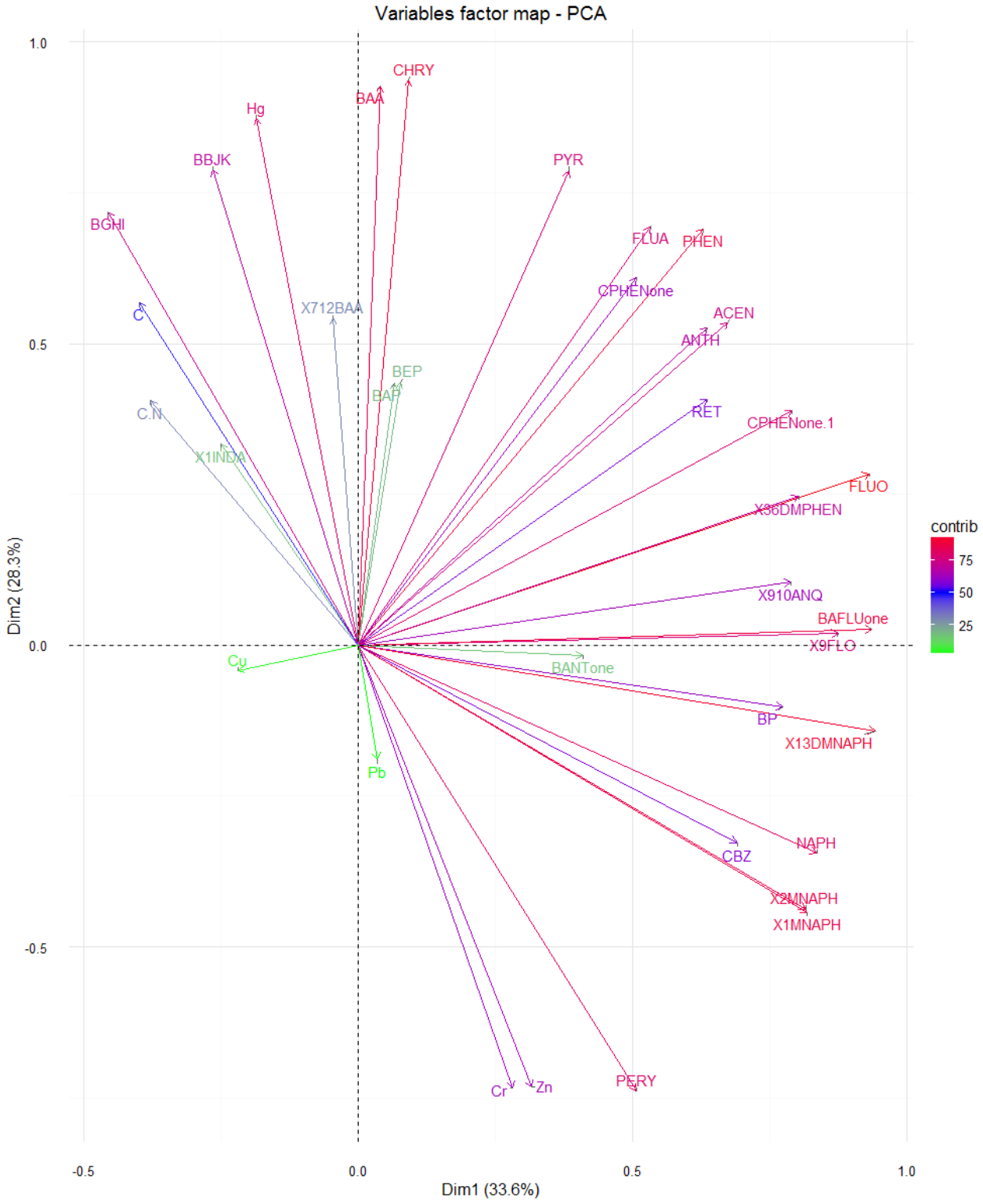

*Fig A.4.2. Biplots of PC2 + 3 and PC3 + 4 showing pollutant group distribution of ∑OPAHs, ∑LMW-PAHs, ∑HMW-PAHs, ∑AZAs, ∑COMB-PAHs, Cu, Pb, Hg, Zn, Cr, retene, perylene, C and the C/N ratio for L. Llaviuco from a PCA.*

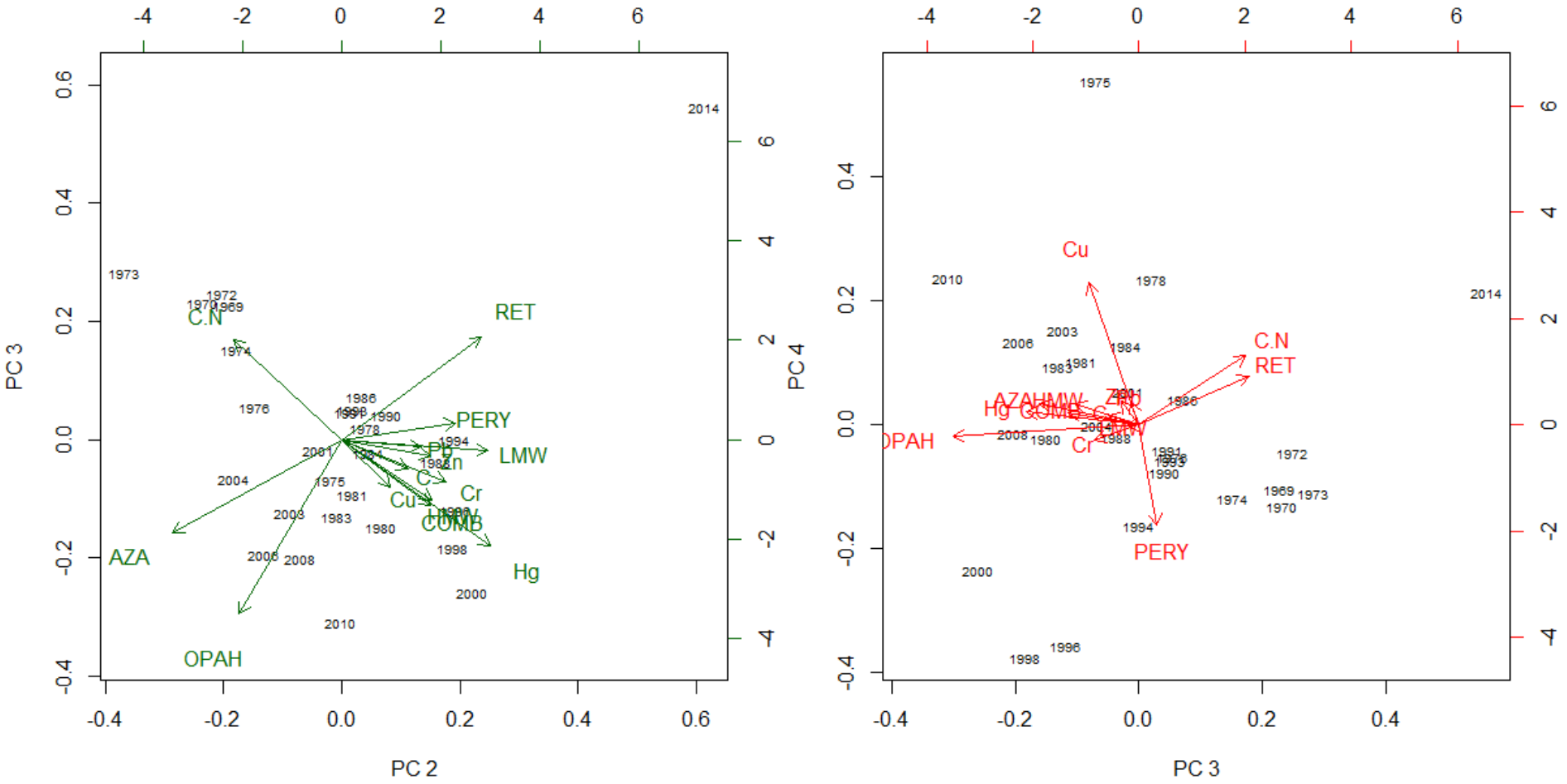

# DECLARATION OF CONSENT

On the basis of Article 28 Para. 2 of the RSL 05 phil. –nat.

Name, First Name: Fränkl, Lea Alina

Matriculation Number: 09-753-666

Study Programme: Masters in Climate Science

Bachelor ☐ Master ☐ Dissertation ☐

Thesis Title: A 20th Century Pollution History Reconstruction using Lake Sediments from Cajas National Park, South Central Ecuador

Thesis Supervisor: Prof. Dr. Martin Grosjean

I hereby declare that the submitted thesis is my own work and that I have not used any sources other than those stated. I have indicated the adoption of quotations as well as thoughts taken from other authors made in the text. In accordance with academic rules and ethical conduct I have fully cited and referenced all material and results that are not original to this work. I am aware that on the basis of Article 36 Paragraph 1 Letter o of the University Act of 5 September, 1996, the Senate is entitled to deny the title awarded on the basis of this work if proven otherwise. I hereby grant inspection of my thesis.

…….. ……..

Place, Date Signature